Novel (Advanced) Oxidation and Disinfection Processes based on Reactions of Free Available Chlorine or Hydrogen Peroxide with Unconventional Activating Agents: Superoxide Radical and Non-Ferrous/Non-Cuprous Metal(loid) Oxide Catalysts

Sin-Yi Liou

A dissertation
submitted in partial fulfillment of the
requirements for the degree of

Doctor of Philosophy

University of Washington
2023

Reading Committee:
Michael Dodd, Chair
Gregory Korshin
Edward Kolodziej
Jessica Ray

Program Authorized to Offer Degree:
Civil and Environmental Engineering

University of Washington

Abstract

Novel (Advanced) Oxidation and Disinfection Processes based on Reactions of Free Available Chlorine or Hydrogen Peroxide with Unconventional Activating Agents: Superoxide Radical and Non-Ferrous/Non-Cuprous Metal(loid) Oxide Catalysts

Sin-Yi Liou

Chair of the Supervisory Committee:
Michael Dodd
Civil and Environmental Engineering

Advanced oxidation processes (AOPs) are a suite of physical/chemical treatment processes that are increasingly investigated and applied to enhance attenuation of trace organic contaminants in water and wastewater treatment and reuse, through in situ generation of hydroxyl radical ($HO^{\bullet}$) and various other radical or reactive oxidant species. The most prevalent AOPs are typically driven by using UV light and/or ozone (O_3) to convert (or "activate") hydrogen peroxide (H_2O_2) or free available chlorine (FAC) to $HO^{\bullet}$ and other more reactive oxidants, and often require specialized capital- and energy-intensive infrastructure (e.g., arrays of low- or medium-pressure Hg vapor lamps, or ozone generators), or are constrained by mass-transfer, hydrodynamics, and/or spatial heterogeneity in light transmission. As potential alternatives to such "conventional" AOP approaches, several novel reaction systems were

investigated in this work, in which FAC or H_2O_2 were "activated" using several unconventional agents, including the superoxide radical ($O_2^{\bullet-}$) and a suite of non-ferrous/non-cuprous metal(loid) oxides (MeOx). MeOx minerals studied in this work included amorphous zirconium oxide (a-ZrO_2), monoclinic zirconium oxide (m-ZrO_2), cerium oxide (CeO_2), titanium oxide (TiO_2), aluminum oxide (Al_2O_3), and silicon oxide (SiO_2). The reaction of $O_2^{\bullet-}$ with FAC ($O_2^{\bullet-}$/FAC) was found capable of effectively generating $HO^{\bullet}$ as well as various reactive chlorine species (RCS), including chlorine monoxide radical ($ClO^{\bullet}$), chlorine radical ($Cl^{\bullet}$), and dichloride radical ($Cl_2^{\bullet-}$) with exposure levels comparable to many commonly applied AOPs such as UV/H_2O_2, O_3/H_2O_2, and UV/FAC under representative water treatment and reuse conditions. Direct formation of halogen-containing disinfection byproducts (DBPs) during $O_2^{\bullet-}$/FAC treatment was found to be minimal. The reactions of MeOx species with H_2O_2 (MeOx/H_2O_2) or FAC (MeOx/FAC) were (tentatively) found to be capable of (catalytically) generating the reactive oxidant species singlet oxygen ($^1O_2$) and/or superoxide ($O_2^{\bullet-}$) in aqueous phase and/or on the MeOx mineral surfaces, and limited amounts of $HO^{\bullet}$ radical, as identified by multiple radical probes and radical scavengers. FAC-containing systems also appear to generate reactive chlorine species (potentially including $Cl^{\bullet}$ and $ClO^{\bullet}$). Due to their tendency to generate more selective oxidants ($^1O_2$, $ClO^{\bullet}$) in favor of less selective/stronger oxidants ($HO^{\bullet}$, $Cl^{\bullet}$), the MeOx/H_2O_2 and MeOx/FAC reactions appear less useful as advanced oxidation processes, but could be quite effective as targeted oxidation processes (consistent with observations obtained using the $^1O_2$ probe furfuryl alcohol). Several MeOx/H_2O_2 and MeOx/FAC reactions were also investigated as the basis for potential (advanced) disinfection processes, using two commonly-employed surrogates of water-borne pathogens, *Bacillus subtilis* endospores and MS2 bacteriophage. Limited effectiveness was observed toward the highly disinfection-resistant *B. subtilis*

endospores, whereas the CeO_2/H_2O_2 and m-ZrO_2/H_2O_2 reactions were each found to be quite effective toward MS2, which is known to be sensitive to $^1O_2$ (where MS2 was stable toward MeOx or H_2O_2 alone). In addition to contaminant oxidation and disinfection, several of the MeOx minerals could provide substantial ancillary benefits as (i) adsorbents (e.g., a-ZrO_2 is highly effective for adsorption of phosphate, as well as of MS2), or (ii) oxidant quenchers, where a-ZrO_2 and CeO_2 in particular were found to be especially capable of rapidly and catalytically decomposing H_2O_2 and FAC. This latter benefit could prove especially advantageous in post-processing of waters treated using conventional AOPs (which frequently require removal of H_2O_2) or of chlorinated (waste)waters from which removal of FAC is desired prior to use or discharge (e.g., point-of-use consumption or discharge of wastewater to natural receiving waters). Findings reported in this study provide a promising foundation for further examination of a wide array of potential applications of $O_2^{\bullet-}$/FAC, MeOx/H_2O_2, and MeOx/FAC treatment for mitigating organic contaminants and microbial pathogens (via inactivation and/or adsorption), as well as for rapid, sustained removal of residual H_2O_2 or FAC during or following (waste)water treatment when desirable.

ACKNOWLEDGEMENTS

First and foremost, I would like to express my deepest gratitude to my advisor Prof. Michael Dodd for his patient guidance, encouragement and excellent advice throughout my Ph.D. study for not only research but also life here at the University of Washington. His constant support and experienced feedback help made this work successful, and also made me become a better scientist in many aspects. I am very thankful to have had this experience working with him in the past years.

I would also like to thank Prof. Gregory Korshin, Prof. Edward Kolodziej, Prof. Jessica Ray for serving as my committee members, and Prof. James Gawel as the graduate school representative. Their valuable input and suggestions greatly strengthen and help complete this dissertation.

I am thankful to my lab members, Huan He and Tessora Young for training me during my first and second year. Those memories with your accompanies in the lab will never been forgotten; also thanks to Jennifer Hooper, Chu-Ching Lin, Minju Lee, Younggun Yoon, Yegyun Choi, Chaoqun Tan and Mika Emoto for being helpful in the lab. A special thanks goes to Prof. Chu-Ching Lin for his great contributions and feedbacks on the microbial experiments. I would also like to thank my other fellow at UW CEE: Nina Zhao, Ximin Hu, Zhenyu Tian, Bolun Wang, Aminda Cheney-Irgens, Samuel Walters, Po-An Chen, Chenyang Zhang, Ivette Pinochet Troncoso, Fanny Okaikue-Woodi, Jessica Steigerwald, Alanna Hildebrandt for supporting me and building a friendly community in More Hall 3rd floor environmental engineering labs.

I appreciate those who have helped train me in the laboratories and research centers. I would like to give thanks to the lab managers, Sean Yeung, Virginia Engel and Songlin Wang,

for their wonderful technical support and maintenance on instrument; to Dale Whittington and Scott Edgar for training me on the LC-MS/MS; to Phillip Cox and Michael Pomfret for training on the SEM and BET; to Kristine Parra for training on the ICP-MS, and Tatyana Galenko for teaching me to use the particle size analyzer. I would also like to thank to Prof. Karl Linden and Emma Payne from the University of Colorado for providing their KrCl lamp, through which I was able to generate some interesting experimental data.

I would also like to express my gratitude to Mr. Chao-Yao and Mrs. Maria Lee Koh, as well as Mr. Paul Bao-Ho and Mrs. Meiyea Liao for their generous donations to UW. It was truly my pleasure to be awarded by these fellowships created by them which allowed me to pursue knowledge in a more profound level of study in environmental engineering, and was able to make contributions to water safety and human health through my research here.

I also thanks to my friends in Taiwan and those who are currently also pursuing Ph.D. in the United States for encouraging me all the time even though we were not able to meet each other often. Lastly and most importantly, I would like to give many thanks to my family and our cat for their unconditional love, support and encouragement when I went through those difficult times. I would never have completed my Ph.D. study and become the person who I am today without this wonderful family.

Contents

List of Figures

List of Tables

Chapter 1. INTRODUCTION

1.1 Overview

In recent decades, tremendous attention has been directed towards the development and application of advanced oxidation processes (AOPs) for degradation of trace organic contaminants during (waste)water treatment and reuse (Lee et al., 2020; Miklos et al., 2018; O'Shea and Dionysiou, 2012; von Gunten, 2018). Such AOPs comprise a wide variety of approaches, including UV irradiation+hydrogen peroxide (UV/H_2O_2), UV+free available chlorine (UV/FAC, with FAC comprising predominantly hypochlorous acid, HOCl, and its conjugate base hypochlorite, OCl^-), UV+monochloramine (UV/NH_2Cl), UV+ozone (UV/O_3), O_3+H_2O_2 (O_3/H_2O_2), (photo-)Fenton and (photo-)Fenton-like processes, radiolysis, sonolysis, various semiconductor photocatalysis processes, and an array of persulfate-based processes (Lee et al., 2020; Li et al., 2020; Miklos et al., 2018; O'Shea and Dionysiou, 2012; von Gunten, 2018). In all of these approaches, hydroxyl radical ($HO^{\bullet}$) is a key (and often *the* key) oxidant responsible for contaminant oxidation, with $HO^{\bullet}$ reacting non-selectively and having high second-order rate constants for reactions with most organic and many inorganic contaminants.

While many of the AOPs noted can yield highly effective contaminant degradation, they often require specialized capital- and energy-intensive infrastructure; for example, arrays of low- or medium-pressure Hg vapor lamps for UV-driven processes, or – in the case of O_3-driven processes – high-capacity O_3 generators – often accompanied by extensive equipment for liquid- or gas-phase O_2 handling and/or purification and post-treatment O_3 destruction (Miklos et al., 2018; Oturan and Aaron, 2014; Rakness, 2005; Stefan, 2017). Many such AOPs are also subject to various physical-chemical constraints on process efficiency; for example, hydrodynamics and spatial heterogeneity in light intensity in the case of UV-driven processes, hydrodynamics and mass-transfer limitations on gas-phase O_3 dissolution into solution for O_3-driven processes,

mass-transfer limitations on contaminant transport to interfacial reactive sites for heterogeneous photocatalysis processes, and low pH requirements in the case of many (photo)Fenton and (photo)Fenton-like approaches (Oturan and Aaron, 2014; Rakness, 2005; Stefan, 2017).

For a process to improve upon the suite of available AOP options, desirable attributes would include the potential to operate with minimal additional infrastructure, low cost and energy consumption, homogeneous reaction chemistry or at least minimal mass-transfer limitations, and high efficiency at circumneutral pH. In light of the discussion above, this study is dedicated to developing several innovative AOPs that could fulfill these desirable traits or deal with some of the challenges.

1.2 Scientific Background

1.2.1 Advanced Oxidation Processes (AOPs)

In recent decades, trace organic contaminants (TrOCs), including pharmaceuticals, herbicides, pesticides, industrial chemicals, nanomaterials, etc., have been widely detected in aquatic environments (Huerta-Fontela et al., 2010). Since conventional physical and biological treatment procedures oftentimes, can only partially remove these substances, making them remain in the drinking water supplies or wastewater treatment plant effluents, and thus there are raising concerns of these TrOCs in (waster)water treatments nowadays.

Advanced oxidation processes (AOPs) are technologies that have been widely applied as an effective attenuation option for TrOCs removal due to their effective abilities of oxidation. AOPs are chemical procedures that can generate in situ strongly oxidizing species, in which hydroxyl radical ($HO^{\bullet}$) is the one constitute the majority of AOPs. There are also processes

favoring some other oxidizing species, such as sulfate- and chlorine-based radicals. Common classification of AOPs include ozone-based (e.g., O_3/H_2O_2, O_3/catalyst), UV-based (e.g., UV/H_2O_2, UV/O_3, UV/peroxydisulfate, UV/chlorine), electrochemical, catalytic (e.g., Fenton, photo-Fenton, UV/catalyst) and physical processes (e.g., ultrasound, microwave, plasma, electron beam) (Miklos et al., 2018; Oturan and Aaron, 2014; von Sonntag and von Gunten, 2012).

(i) O_3-based AOPs

Ozone has long been used as an oxidant and disinfectant in water treatment. As an oxidant, it is very selective and attacks primarily electron-rich functional groups like double bonds, amines, and activated aromatic rings. $HO^{\bullet}$ can be formed from the direct reaction of O_3 with hydroxide ions, and from side reactions with organic matter (mainly phenol and amine functional groups) (Buffle and von Gunten, 2006). Many O_3-based AOPs have been widely investigated (Merényi et al., 2010a; Merényi et al., 2010b), among which O_3/H_2O_2 is a well-established process in drinking water treatment and water reuse applications (Pisarenko et al., 2012).

(ii) UV-based AOPs

UV-based AOPs comprise processes based on UV irradiation and the combination of UV with different radical promoters. The UV sources usually consist of either low- or medium-pressure mercury lamps with mono- or polychromatic emission spectra. UV light emitting diode (LED) light sources with specific wavelength distributions have also been proposed recently (Song et al., 2016). The most frequently applied UV-based AOP is the combinations with H_2O_2 (to form $HO^{\bullet}$), persulfate (to form $HO^{\bullet}$ and $SO_4^{\bullet-}$) and chlorine (to form $HO^{\bullet}$ and reactive

chlorine species) (Miklos et al., 2018; Oturan and Aaron, 2014). Full scale of such applications have been established for potable water reuse and surface water treatment (Audenaert et al., 2011; Kruithof et al., 2007).

(iii) Other AOPs (electrochemical, catalytic and physical)

Electrochemical AOPs, despite are relatively new technologies, have been considerably performed at both the bench-scale and pilot-scale studies. In recent years, development of various stable electrode materials allows efficient generation of high yields of $OH^{\bullet}$ (Chaplin, 2014).

Catalytic AOPs, including the Fenton process and processes involved photo-active catalysts (typically irradiated by UV and visible light from 180 to 400 nm), were intensively studied over the last decades (Dong et al., 2015). The Fenton process has been established in several industrial full-scale applications (Bae et al., 2015). Other commonly applied processes are the homogeneous photo-Fenton reaction and the heterogeneous photocatalysis of semiconductor TiO_2 (Oturan and Aaron, 2014; Simonsen et al., 2010).

Electrical discharge and plasma reactors can generate major reactive species of $OH^{\bullet}$, atomic hydrogen, and O_3 (Hijosa-Valsero et al., 2014; Jiang et al., 2014; Locke et al., 2006). Sonication of water by ultrasound (20-500 kHz) can lead to destruction of water contaminants due to the formation of highly reactive radicals and thermal decomposition (Pétrier et al., 2007; Torres et al., 2008). The application of highly energetic radiation in the microwave range (300 MH-300 GHz) has also been investigated for the oxidation of micropollutants in water treatment, while usually applied in combination with H_2O_2 or catalysts to assist in TrOCs destruction (Han et al., 2004; Zhihui et al., 2005).

1.2.2 Free Available Chorine (FAC)

Free available chlorine (FAC), also known as free chlorine, is the sum of hypochlorous acid (HOCl) and its conjugated base hypochlorite (OCl^-). It is the most widely utilized drinking water disinfectant worldwide. Nowadays, ~99% and 75% of drinking water and wastewater treatment facilities in the United States are using some type of chlorine disinfection process (Jacangelo and Trussell, 2002; Leong et al., 2008; USEPA, 2009; 1999). Free chlorine is typically introduced to water as chlorine gas (Cl_2), sodium hypochlorite solution (NaOCl), or solid calcium hypochlorite ($Ca(OCl)_2$); each will ultimately form $HOCl/OCl^-$ in aqueous solution. HOCl is a weak acid that can dissociates into OCl^- and hydrogen ion (H^+) according to the following equation:

$$HOCl \leftrightarrow H^+ + OCl^- \qquad pK_a = 7.5 \text{ (Morris, 1966)} \qquad (1.1)$$

(i) Chlorination versus microorganism inactivation

Commercial available sodium hypochlorite solution normally sits at a alkaline pH around 11 to 13, in which all available chlorine is in a form of OCl^-. The OCl^- ion is a relatively poor disinfectant because of its inability to diffuse through the cell wall of microorganisms. Since it is negatively charged, it is electrostatically repelled from the cell walls which are also negatively charged. Conversely, HOCl is the more effective one in terms of disinfection than OCl^-, primarily because the uncharged HOCl is more easy to penetrate cell walls. Chlorine usually can cause significant injury to harmful pathogens during water treatment via cell permeability dislocation, nucleic acid damage and enzyme injury. In brief, HOCl oxidizes sulfhydryl groups, harms iron-sulfur centers, deactivates nutrient transport, hinders cell respiration, and deteriorates the capacity of cells to keep a sufficient adenylate energy charge to stay viable. However, there

are still microorganisms that are resistant to chlorination and cannot be inactivated effectively, such as some protozoan cysts (*G. lamblia, E. histolytica, Naegleria gruberi*) and parasite oocysts (*Cryptosporidium parvum*) (Ghernaout, 2017).

(ii) Chlorination versus organic and inorganic contaminants

Chlorine can oxidize organic contaminants via three pathways: (i) oxidation reactions, (ii) addition reactions to unsaturated bonds, (iii) electrophilic substitution reactions at nucleophilic sites. However, from a kinetic point of view, usually only electrophilic attack is considered significant. Although it has been shown that numerous organic micropollutants can be transformed by chlorine during water treatment processes, its reactivity sometimes is low to certain compounds, and can only make minor modifications in the parent compound structure. As a result, second-order rate constants for chlorination can vary over 10 orders of magnitude (i.e., 0.1–10^9 $M^{-1}s^{-1}$). This is because that chlorine reactivity is limited to particular sites (mainly amines, reduced sulfur moieties or activated aromatic systems). In the case of inorganic compounds, fast reactions with ammonia, halides (Br^- and I^-), SO_3^{2-}, CN^-, NO_2^-, As(III) and Fe(II) with chlorine are reported (10^3 –10^9 $M^{-1}s^{-1}$), whereas low chlorine reaction rates with Mn(II) were shown (Deborde and Von Gunten, 2008).

1.2.3 Superoxide ($O_2^{\bullet-}$)

The superoxide radical anion ($O_2^{\bullet-}$) is involved in a variety of biochemical reactions in living systems. The generation of $O_2^{\bullet-}$ has been reported in many enzyme-catalyzed reactions involved in respiration and biological oxidation. $O_2^{\bullet-}$ can act both as a reductant and as an oxidant. Biologically, $O_2^{\bullet-}$ can be generated from two major sources, the mitochondrial respiratory chain and phagocytic nicotinamide adenine dinucleotide phosphate oxidase (NADPH

oxidase) (Babior, 1984; Klebanoff, 1975; Segal, 2008). It has a acid-base dissociation constant (p*K*a) of 4.8 (eq 1.2), so it is mainly exist in the form of $O_2^{\bullet-}$ under most environmental conditions.

$$HO_2^{\bullet} \leftrightarrow H^+ + O_2^{\bullet-} \qquad pK_a = 4.8 \text{ (Bielski et al., 1985)} \qquad (1.2)$$

From an engineering perspective, $O_2^{\bullet-}$ has seldom been studied because of the difficulty of generating and maintaining $O_2^{\bullet-}$ in a stable state. This is perhaps mainly due to the instability of $O_2^{\bullet-}$ and $HO_2^{\bullet}$ under circumneutral pH conditions, on account of their rapid disproportionation to H_2O_2 and its conjugate base hydroperoxide (HO_2^-) in aqueous solution (eqs 1.3-1.5).

$$HO_2^{\bullet} + HO_2^{\bullet} \rightarrow H_2O_2 + O_2 \qquad k_{1.3} = 8.3\times10^5\ M^{-1}s^{-1} \text{ (Bielski et al., 1985)} \qquad (1.3)$$

$$HO_2^{\bullet} + O_2^{\bullet-} \rightarrow HO_2^- + O_2 \qquad k_{1.4} = 9.7\times10^7\ M^{-1}s^{-1} \text{ (Bielski et al., 1985)} \qquad (1.4)$$

$$O_2^{\bullet-} + O_2^{\bullet-} \rightarrow O_2^{2-} + O_2 \qquad k_{1.5} < 3.5\times10^{-1}\ M^{-1}s^{-1} \text{ (Bielski, 1978)} \qquad (1.5)$$

As evident from eqs 1.3-1.5, the apparent kinetics of $HO_2^{\bullet}/O_2^{\bullet-}$ disproportionation depend strongly on pH, where this pH dependence can be described by eq 1.6,

$$k_{app,HO_2^{\bullet}/O_2^{\bullet-},DP} = k_{10}\left(\alpha_{HO_2^{\bullet}}\right)^2 + k_{11}\alpha_{HO_2^{\bullet}}\alpha_{O_2^{\bullet-}} = k_{10}\left(\frac{[H^+]}{[H^+]+K_{a,HO_2^{\bullet}}}\right)^2 + k_{11}\left(\frac{[H^+]}{[H^+]+K_{a,HO_2^{\bullet}}}\right)\left(\frac{K_{a,HO_2^{\bullet}}}{[H^+]+K_{a,HO_2^{\bullet}}}\right) \qquad (1.6)$$

with $k_{app,HO_2^{\bullet}/O_2^{\bullet-},DP}$ representing the pH-dependent apparent second-order rate constant for the overall disproportionation reaction.

Numerous options for $O_2^{\bullet-}$ preparation have been reported, including electrochemical, enzymatic, sonolytic, radiolytic, and photochemical methods, as well as dissolution of $O_2^{\bullet-}$ salts (typically potassium superoxide, KO_2) (Hayyan et al., 2016). Although many of these require

specialized equipment and/or organic solvents or additives that would hinder use of the resulting stock solutions in an AOP, certain photochemical approaches and KO_2 dissolution can yield high-μM to mM $O_2^{\bullet-}$ concentrations in fully aqueous solution at pH≥11 (Heller and Croot, 2011; Holroyd and Bielski, 1978).

1.2.4 Superoxide/Hypochlorous Acid Reactions

The $O_2^{\bullet-}$/FAC reaction has long been recognized as a potential source of $HO^{\bullet}$ in biological systems (Candeias et al., 1993; Long and Bielski, 1980), and has recently been identified as an important driver of radical pathways in the oxidation of phenols and hydroquinones by FAC (Rodríguez and von Gunten, 2020) and in a newly-reported approach to photocatalytic FAC activation (Cheng et al., 2020), it has otherwise received relatively little attention as a possible basis for an AOP. The reaction involves generation of $HO^{\bullet}$ from the homogeneous, aqueous-phase reaction of superoxide radical ($O_2^{\bullet-}$) with hypochlorous acid (HOCl) (eq 1.7) (Candeias et al., 1993; Long and Bielski, 1980).

$$HOCl + O_2^{\bullet-} \rightarrow Cl^- + HO^{\bullet} + O_2 \qquad k_{1.7} = 7.5\times10^6\ M^{-1}s^{-1}\ \text{(Long and Bielski, 1980)} \quad (1.7)$$

As indicated by eq 1.7, the reaction occurs specifically between HOCl and $O_2^{\bullet-}$, while the reactions of $HO_2^{\bullet}$ with HOCl and OCl^-, and of $O_2^{\bullet-}$ with OCl^-, are negligible in comparison to eq 1.7) (Long and Bielski, 1980). The apparent kinetics for the reaction of $HO_2^{\bullet}/O_2^{\bullet-}$ (comprising the sum of $O_2^{\bullet-}$ and its conjugate acid, hydroperoxyl, $HO_2^{\bullet}$) with FAC (hereafter referred to as the $O_2^{\bullet-}$/FAC reaction for convenience) therefore depend strongly on pH. This pH dependence can be described by eq 1.8,

$$k_{\text{app},O_2^{\bullet-}/\text{FAC}} = k_1 \alpha_{O_2^{\bullet-}} \alpha_{\text{HOCl}} = k_1 \left(\frac{K_{\text{a,HO}_2^\bullet}}{[\text{H}^+] + K_{\text{a,HO}_2^\bullet}} \right) \left(\frac{[\text{H}^+]}{[\text{H}^+] + K_{\text{a,HOCl}}} \right) \quad (1.8)$$

where $k_{\text{app},O_2^{\bullet-}/\text{FAC}}$ represents the pH-dependent apparent second-order rate constant for the $O_2^{\bullet-}$ /FAC reaction, and at 25°C, and $K_{\text{a,HO2}\bullet} = 10^{-4.8}$ (Bielski et al., 1985) and $K_{\text{a,HOCl}} = 10^{-7.5}$ (Morris, 1966) represent the acid-base dissociation constants for the equilibria $HO_2^\bullet \rightleftarrows H^+ + O_2^{\bullet-}$ and $HOCl \rightleftarrows H^+ + OCl^-$, respectively. As shown in Figure 1.1, the theoretical $k_{\text{app},O_2^{\bullet-}/\text{FAC}}$ increases from 2.4 $M^{-1}s^{-1}$ at pH 14 to a maximum of 6.9×10^6 $M^{-1}s^{-1}$ at pH 6.2, with rate constants in excess of 10^6 $M^{-1}s^{-1}$ from pH 6-8 (Long and Bielski, 1980).

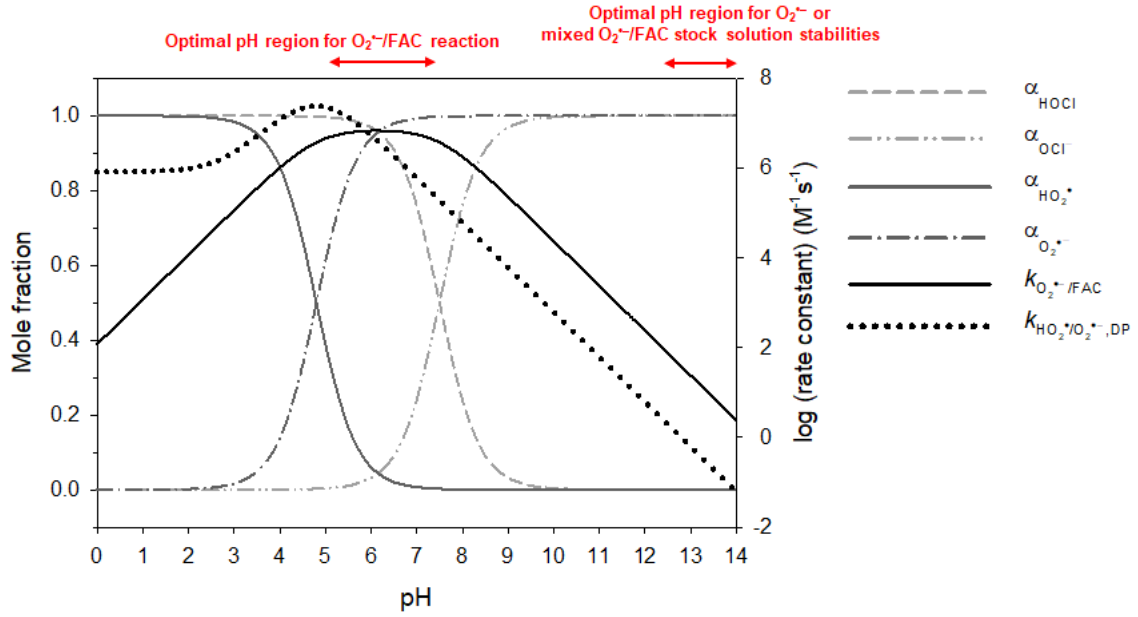

Figure 1.1. Acid-base speciation of $HO_2^\bullet/O_2^{\bullet-}$ and $HOCl/OCl^-$, and theoretical apparent rate constants (k_{app}) for the $O_2^{\bullet-}$/FAC reaction and the $HO_2^\bullet/O_2^{\bullet-}$ disproportionation reaction (based on $K_{\text{a,HO2}\bullet} = 10^{-4.8}$, $K_{\text{a,HOCl}} = 10^{-7.5}$, eq 1.6, and eq 1.8, respectively). Adopted from (Liou and Dodd, 2021).

As shown in Figure 1.1, eqs 1.3-1.5 lead to extremely rapid decay of $HO_2^\bullet/O_2^{\bullet-}$ at circumneutral pH (Bielski et al., 1985). However, as apparent from eqs 1.5-1.6, stability of

$HO_2^{\bullet}/O_2^{\bullet-}$ increases significantly with increasing pH (Figure 1.1), so that aqueous $O_2^{\bullet-}$ stock solutions with lifetimes of several minutes or longer can be prepared at pH>12 and then dosed to FAC-containing waters at lower pH – opening the door to their use in harnessing eq 1.7 for contaminant oxidation. The low value of $k_{app,O_2^{\bullet-}/FAC}$ at pH>12 (Figure 1.1) affords the added possibility of premixing alkaline $O_2^{\bullet-}$/FAC solutions that can then be "activated" by dosing to lower-pH waters (effectively providing "stock solutions" of $HO^{\bullet}$ and RCS).

In addition to $HO^{\bullet}$, the $O_2^{\bullet-}$/FAC reaction may lead to the formation of various reactive chlorine species (RCS), including chlorine monoxide radical ($ClO^{\bullet}$), hydroxidochlorate radical ($HOCl^{\bullet-}$), chlorine radical ($Cl^{\bullet}$), and dichloride radical ($Cl_2^{\bullet-}$) (eqs 1.9-1.15). These RCS can also contribute substantially to degradation of organic contaminants, especially those containing electron-rich functional groups (Fang et al., 2014; Kong et al., 2018; Lei et al., 2019; Sun et al., 2016).

$HOCl + HO^{\bullet} \rightarrow ClO^{\bullet} + H_2O$ $k_{1.9} = 1.2\times10^9\ M^{-1}s^{-1}$ (Bulman et al., 2019) (1.9)

$OCl^- + HO^{\bullet} \rightarrow ClO^{\bullet} + OH^-$ $k_{1.10} = 6.4\times10^9\ M^{-1}s^{-1}$ (Bulman et al., 2019) (1.10)

$HO^{\bullet} + Cl^- \rightleftarrows HOCl^{\bullet-}$ $k_{1.11f} = 4.3\times10^9\ M^{-1}s^{-1}$ (Jayson et al., 1973) (1.11)

$k_{1.11r} = 6.1\times10^9\ s^{-1}$ (Jayson et al., 1973)

$HOCl^{\bullet-} + H^+ \rightleftarrows Cl^{\bullet} + H_2O$ $k_{1.12f} = 2.1\times10^{10}\ M^{-1}s^{-1}$ (Jayson et al., 1973) (1.12)

$k_{1.12r} = 4.5\times10^3\ M^{-1}s^{-1}$ (Buxton et al., 2000)

$Cl^{\bullet} + HOCl \rightarrow H^+ + Cl^- + ClO^{\bullet}$ $k_{1.13} = 3.0\times10^9\ M^{-1}s^{-1}$ (Kläning and Wolff, 1985) (1.13)

$Cl^{\bullet} + ClO^- \rightarrow Cl^- + ClO^{\bullet}$ $k_{1.14} = 8.2\times10^9\ M^{-1}s^{-1}$ (Kläning and Wolff, 1985) (1.14)

$Cl^{\bullet} + Cl^{-} \rightleftarrows Cl_2^{\bullet-}$ $k_{1.15f} = 6.5\times10^9\ M^{-1}s^{-1}$ (Kläning and Wolff, 1985) (1.15)

$k_{1.15r} = 1.1\times10^5\ s^{-1}$ (Jayson et al., 1973)

1.2.5 Metal(loid) Oxides for Reactive Radical/Species Generation

Photogenerated reactive oxygen species (ROS), including $HO^{\bullet}$, $O_2^{\bullet-}$, and singlet oxygen ($^1O_2$), were found to be produced during the UV irradiation of various metal or metalloid oxides, including TiO_2, CuO, ZnO, ZrO_2, V_2O_3, CeO_2, Fe_2O_3, Al_2O_3 and SiO_2 (Bedilo et al., 2005; Li et al., 2012; Nosaka and Nosaka, 2016; Wang et al., 2017). It has also been reported that various organic contaminants in water can be oxidized effectively by $HO^{\bullet}$ radical produced during the photolysis of H_2O_2 in the presence of aqueous iron species or Fe oxides (Emilio et al., 2002; He et al., 2002; Kwan and Voelker, 2002; Ravikumar and Gurol, 1994). Destruction of harmful organic compounds by these oxidation techniques is gaining widespread attention as an AOP.

Formation of ROS on crystalline zirconia (ZrO_2) and many other metal oxides via reactions with H_2O_2 has been studied in recent years. The surface-catalyzed decomposition of H_2O_2 basically follows the mechanism depicted in eqs 1.16-1.18. The initial step of the catalytic decomposition of H_2O_2 on metal oxide surfaces has been proposed to be the homolytic cleavage of the O−O bond in H_2O_2 to form two $HO^{\bullet}$, or can be expressed by its reactions on the surface catalytically active site (S_{CA}) as shown in eqs. 1.19-1.22 (Fidalgo et al., 2016; Lousada et al., 2015; Lousada et al., 2012; Lousada et al., 2013a; Lousada et al., 2013b; Yang and Jonsson, 2015). Formation of $HO^{\bullet}$ was confirmed by using radical scavengers like tris(hydroxymethyl)aminomethane (Tris) and methanol (MeOH) with both scavengers yield formaldehyde upon hydrogen abstraction, or by using probe that can yield detectable $HO^{\bullet}$-mediated fluorescent product (Fidalgo et al., 2016; Lousada et al., 2013a; Maier et al., 2019;

Yang and Jonsson, 2014). EPR/ESR measurements also revealed the presence of $HO_2^{\bullet}$, $O_2^{\bullet-}$, and peroxyl radical species on the surface of different oxides. These normally short-lived and reactive species had become long-lived due to the stabilization imparted by their adsorption onto the oxide surface by means of interactions of the formed radicals with the oxide lattice (Anpo et al., 1999; Bahnemann and Hoffmann, 1987).

$H_2O_{2\,(ads)} + \rightarrow 2HO^{\bullet}_{\,(ads)}$ (Fidalgo et al., 2016) (1.16)

$H_2O_{2\,(ads)} + HO^{\bullet}_{\,(ads)} \rightarrow H_2O_{\,(ads)} + HO_2^{\bullet}{}_{\,(ads)}$ (Fidalgo et al., 2016) (1.17)

$2HO_2^{\bullet}{}_{\,(ads)} \rightarrow H_2O_2 + O_2$ (Fidalgo et al., 2016) (1.18)

$H_2O_{2\,(ads)} + S_{CA} \rightarrow H_2O_{\,(ads)} + HO^{\bullet}_{\,(ads)} + S_{CA}^{\bullet}$ (Lousada et al., 2013a) (1.19)

$H_2O_{2\,(ads)} + HO^{\bullet}_{\,(ads)} \rightarrow H_2O_{\,(ads)} + HO_2^{\bullet}{}_{\,(ads)}$ (Lousada et al., 2013a) (1.20)

$H_2O_{2\,(ads)} + S_{CA}^{\bullet} \rightarrow HO_2^{\bullet}{}_{\,(ads)} + S_{CA}H$ (Lousada et al., 2013a) (1.21)

where SCAH represents $H^{\bullet}$ bound onto the $S_{CA}^{\bullet}$ site. Another possible reaction pathway for H_2O_2 at the surface is:

$2H_2O_{2\,(SCA)} \rightarrow 2HO_2^{\bullet}{}_{(SCA)} + 2H^{\bullet}_{\,(SCA)} \rightarrow 2HO_2^{\bullet}{}_{(SCA)} + H_{2\,(g)}$ (Lousada et al., 2013a) (1.22)

where the state S_{CA} denotes that the corresponding species is adsorbed onto the surface catalytically active site.

Sobanska et al. examined the formation of ROS ($HO^{\bullet}$, $O_2^{\bullet-}$, and O_2^{2-}) via reactions of amorphous ZrO_2 with H_2O_2. Decomposition of H_2O_2 can go through two basic pathways, referred to as peroxidase-like activity and catalase-like activity (similar to enzymatic abatement of H_2O_2 in biological systems), as described in eqs 1.23-1.25. The former has the characteristic

feature of ROS formation as intermediate. A plausible mechanism of this reaction, $\equiv Zr^{+}-HO_2^{-}$ (surf) + H_2O_2 (aq) → $HO^{\bullet}$ (aq) + $\equiv Zr^{+} - O_2^{\bullet-}$ (surf) + H_2O, was proposed. In contrast, the latter does not involve explicit ROS formation with H_2O_2 directly decomposed to O_2 (Sobańska et al., 2017). Peroxidase-like activity, forming $HO^{\bullet}$ and $O_2^{\bullet-}$, was dominant at low pH ≤ 5.3, while catalase-like activity dominant at higher pH ranges (Sobańska et al., 2017). They concluded that unlike the amorphous gel, crystalline zirconia exhibits only weak activity in the production of the $HO^{\bullet}$ and $O_2^{\bullet-}$ radicals, and a different mechanism is involved.

Activity of peroxidase (Sobańska et al., 2017)*:*

$$H_2O_2 + e^{-} + H^{+} \rightarrow HO^{\bullet} + H_2O, \text{ followed by} \quad (1.23)$$

$$HO^{\bullet} + e^{-} + H^{+} \rightarrow H_2O \quad (1.24)$$

Activity of catalase (Sobańska et al., 2017)*:*

$$H_2O_2 \rightarrow H_2O + 1/2O_2 \quad (1.25)$$

These kind of reactions occur both on oxides in their highest oxidation state, or on oxides that can be oxidized to higher oxidation states. In the latter case, oxidation and catalytic decomposition are competing reactions. Therefore, there are a wide variety of reaction pathways possible because of the differences in the properties of the oxides. For example, the oxidation of ferrous oxide by H_2O_2 occurs with the formation of the ferric cation, which is also highly reactive toward H_2O_2, leading to a chain process (Lin and Gurol, 1998). However, no higher oxidation states exist for the cations in oxides such as CeO_2 or ZrO_2, and thus other mechanisms for H_2O_2 decomposition must occur in these systems. It was also demonstrated that the possible existence of such chemical species is a factor that depends on the solution pH. Kinetic studies on

these systems have shown that for the catalytic decomposition of H_2O_2 on different metal oxide surfaces similar activation energies are involved, while the pre-exponential factors differ widely. Consequently, the rate constants differ substantially depending on the types of oxides (Hiroki and LaVerne, 2005). This indicates that different surface processes might be involved in the reactions of H_2O_2 with the different metal oxides.

1.2.6 Microorganism Inactivation by MeOx and MeOx/H_2O_2

The use of metal and metal oxide nanoparticles has been widely studied for their antimicrobial effects against pathogens, including bacteria, fungi parasites and viruses via generation of ROS (Abo-zeid and Williams, 2020; Gold et al., 2018; Khezerlou et al., 2018; Pachaiappan et al., 2021). UV irradiation of some MeOx like TiO_2 and ZnO was also found to generate $O_2^{\bullet-}$, $HO^{\bullet}$ and H_2O_2, causing cell membrane damage and in turn inhibiting the growth of cells or leading to their death. H_2O_2 can subsequently transformed into more $HO^{\bullet}$ for killing microorganisms (Khezerlou et al., 2018). Giannakis and Fernández et al. reported efficient inactivation of MS2 bacteriophage and *E. coli* (more than 2-log of inactivation within 1 hour) under treatments of various Fe oxide-mediated photo-Fenton processes in the presence of H_2O_2, including FeO, Fe_2O_3, Fe_3O_4, $FeSO_4$ and $Fe_2(SO_4)_3$ (Fernández et al., 2020; Giannakis et al., 2017). Similar MS2 inactivation was also proposed by Nieto-Juarez et al. in Fe/H_2O_2 and Cu/H_2O_2 systems. The inactivation involves (1) the adsorption of Cu ions or Fe colloids onto the virus, and (2) the production of $OH^{\bullet}$ from virus-associated Cu, or of ferryl species (major) and $OH^{\bullet}$ (minor) from virus-associated iron colloids. These reactive species generated can cause MS2 inactivation. However, in the Fe/H_2O_2 system under sunlight, $OH^{\bullet}$ become a more dominant contributor than ferryl ions (Nieto-Juarez et al., 2010). Kohn et al. reported that MS2 bacteriophage can be inactivated primarily by singlet oxygen ($^1O_2$) produced via sunlight-

mediated excitation of natural organic matter (NOM) in surface waters (Kohn et al., 2007; Kohn and Nelson, 2007).

1.3 Objectives

Advanced oxidation processes (AOPs) are a suite of technology that have been widely applied for effective attenuation of trace organic contaminants due to their abilities of driving efficient chemical oxidation since traditional chemical disinfection approaches may not always be effective to micropollutant removal. However, the most prevalent AOPs are typically driven by using UV light and/or ozone (O_3) to convert (or "activate") hydrogen peroxide (H_2O_2) or free available chlorine (FAC) to $HO^{\bullet}$ and other more reactive oxidants, and often require specialized capital- and energy-intensive infrastructure (e.g., arrays of low- or medium-pressure Hg vapor lamps, or ozone generators), or are constrained by mass-transfer, hydrodynamics, and/or spatial heterogeneity in light transmission. On the basis of earlier reports suggesting potential for radical generation, three non-photochemical/non-ozone based reaction systems using novel FAC and H_2O_2 activating agents, including (a) superoxide with free available chlorine ($O_2^{\bullet-}$/FAC), (b) metal(loid) oxides with hydrogen peroxide (MeOx/H_2O_2), and (c) metal(loid) oxides with free available chlorine (MeOx/FAC) were investigated systematically and comprehensively. MeOx minerals studied in this work include amorphous zirconium oxide (a-ZrO_2), monoclinic zirconium oxide (m-ZrO_2), cerium oxide (CeO_2), titanium oxide (TiO_2), aluminum oxide (Al_2O_3), and silicon oxide (SiO_2).

Primary goals of this research are to (i) elucidate the reaction mechanisms and reaction kinetics, and to identify reactive/radical species generated in each of the reaction system, (ii) examine the treatment effectiveness of these novel processes in organic contaminant removal and

microorganism inactivation under different reaction conditions, and finally (iii) evaluate potential of implementation of these processes as novel AOPs or of other applications in (waste)water treatment.

1.4 References for Chapter 1

Abo-zeid, Y. and Williams, G.R., 2020. The potential anti-infective applications of metal oxide nanoparticles: A systematic review. *Wiley Interdisciplinary Reviews: Nanomedicine and Nanobiotechnology* 12(2), e1592.

Anpo, M., Che, M., Fubini, B., Garrone, E., Giamello, E. and Paganini, M.C., 1999. Generation of superoxide ions at oxide surfaces. *Topics in Catalysis* 8(3), 189. 10.1023/A:1019117328935

Audenaert, W.T.M., Vermeersch, Y., Van Hulle, S.W.H., Dejans, P., Dumoulin, A. and Nopens, I., 2011. Application of a mechanistic UV/hydrogen peroxide model at full-scale: Sensitivity analysis, calibration and performance evaluation. *Chemical Engineering Journal* 171(1), 113-126. https://doi.org/10.1016/j.cej.2011.03.071

Babior, B.M., 1984. The respiratory burst of phagocytes. *The Journal of clinical investigation* 73(3), 599-601. 10.1172/JCI111249

Bae, W., Won, H., Hwang, B., de Toledo, R.A., Chung, J., Kwon, K. and Shim, H., 2015. Characterization of refractory matters in dyeing wastewater during a full-scale Fenton process following pure-oxygen activated sludge treatment. *Journal of Hazardous Materials* 287, 421-428.

Bahnemann, D. and Hoffmann, M. (1987) Stabilization of free-radical intermediates on metal-oxide semiconductor surfaces pp. C463-C463, ELECTROCHEMICAL SOC INC 10 SOUTH MAIN STREET, PENNINGTON, NJ 08534.

Bedilo, A.F., Plotnikov, M.A., Mezentseva, N.V., Volodin, A.M., Zhidomirov, G.M., Rybkin, I.M. and Klabunde, K.J., 2005. Superoxide radical anions on the surface of zirconia and sulfated zirconia: formation mechanisms, properties and structure. *Physical Chemistry Chemical Physics* 7(16), 3059-3069. 10.1039/B504262C

Bielski, B.H.J., 1978. Reevaluation of the spectral and kinetic properties of HO_2 and $O_2^{\bullet-}$ free radicals. *Photochemistry and Photobiology* 28(4-5), 645-649. 10.1111/j.1751-1097.1978.tb06986.x

Bielski, B.H.J., Cabelli, D.E., Arudi, R.L. and Ross, A.B., 1985. Reactivity of $HO_2/O_2^{\bullet-}$ radicals in aqueous solution. *Journal of Physical and Chemical Reference Data* 14(4), 1041-1100. 10.1063/1.555739

Buffle, M.-O. and von Gunten, U., 2006. Phenols and Amine Induced HO• Generation During the Initial Phase of Natural Water Ozonation. *Environmental Science & Technology* 40(9), 3057-3063. 10.1021/es052020c

Bulman, D.M., Mezyk, S.P. and Remucal, C.K., 2019. The impact of pH and irradiation wavelength on the production of reactive oxidants during chlorine photolysis. *Environmental Science & Technology* 53(8), 4450-4459. 10.1021/acs.est.8b07225

Buxton, G.V., Bydder, M., Arthur Salmon, G. and Williams, J.E., 2000. The reactivity of chlorine atoms in aqueous solution. Part III. The reactions of $Cl^{\bullet}$ with solutes. *Physical Chemistry Chemical Physics* 2(2), 237-245. 10.1039/A907133D

Candeias, L.P., Patel, K.B., Stratford, M.R.L. and Wardman, P., 1993. Free hydroxyl radicals are formed on reaction between the neutrophil-derived species superoxide anion and hypochlorous acid. *FEBS Letters* 333(1-2), 151-153. 10.1016/0014-5793(93)80394-a

Chaplin, B.P., 2014. Critical review of electrochemical advanced oxidation processes for water treatment applications. *Environmental Science: Processes & Impacts* 16(6), 1182-1203.

Cheng, Z., Ling, L., Wu, Z., Fang, J., Westerhoff, P. and Shang, C., 2020. Novel visible light-driven photocatalytic chlorine activation process for carbamazepine degradation in drinking water. *Environmental Science & Technology* 54(18), 11584-11593. 10.1021/acs.est.0c03170

Deborde, M. and Von Gunten, U., 2008. Reactions of chlorine with inorganic and organic compounds during water treatment—kinetics and mechanisms: a critical review. *Water research* 42(1-2), 13-51.

Dong, S., Feng, J., Fan, M., Pi, Y., Hu, L., Han, X., Liu, M., Sun, J. and Sun, J., 2015. Recent developments in heterogeneous photocatalytic water treatment using visible light-responsive photocatalysts: a review. *Rsc Advances* 5(19), 14610-14630.

Emilio, C.A., Jardim, W.F., Litter, M.I. and Mansilla, H.D., 2002. EDTA destruction using the solar ferrioxalate advanced oxidation technology (AOT): Comparison with solar photo-Fenton treatment. *Journal of Photochemistry and Photobiology A: Chemistry* 151(1), 121-127. https://doi.org/10.1016/S1010-6030(02)00173-9

Fang, J., Fu, Y. and Shang, C., 2014. The roles of reactive species in micropollutant degradation in the UV/free chlorine system. *Environmental Science & Technology* 48(3), 1859-1868. 10.1021/es4036094

Fernández, L., González-Rodríguez, J., Gamallo, M., Vargas-Osorio, Z., Vázquez-Vázquez, C., Piñeiro, Y., Rivas, J., Feijoo, G. and Moreira, M.T., 2020. Iron oxide-mediated photo-Fenton catalysis in the inactivation of enteric bacteria present in wastewater effluents at neutral pH. *Environmental Pollution* 266, 115181. https://doi.org/10.1016/j.envpol.2020.115181

Fidalgo, A.B., Dahlgren, B., Brinck, T. and Jonsson, M., 2016. Surface Reactions of H2O2, H2, and O2 in Aqueous Systems Containing ZrO2. *The Journal of Physical Chemistry C* 120(3), 1609-1614. 10.1021/acs.jpcc.5b10491

Ghernaout, D., 2017. Water Treatment Chlorination: An Updated Mechanistic Insight Review. 2, 125-138.

Giannakis, S., Liu, S., Carratalà, A., Rtimi, S., Amiri, M.T., Bensimon, M. and Pulgarin, C., 2017. Iron oxide-mediated semiconductor photocatalysis vs. heterogeneous photo-Fenton treatment of viruses in wastewater. Impact of the oxide particle size. *Journal of hazardous materials* 339, 223-231.

Gold, K., Slay, B., Knackstedt, M. and Gaharwar, A.K., 2018. Antimicrobial activity of metal and metal-oxide based nanoparticles. *Advanced Therapeutics* 1(3), 1700033.

Han, D.-H., Cha, S.-Y. and Yang, H.-Y., 2004. Improvement of oxidative decomposition of aqueous phenol by microwave irradiation in UV/H2O2 process and kinetic study. *Water Research* 38(11), 2782-2790.

Hayyan, M., Hashim, M.A. and AlNashef, I.M., 2016. Superoxide ion: generation and chemical implications. *Chemical Reviews* 116(5), 3029-3085.

He, J., Ma, W., He, J., Zhao, J. and Yu, J.C., 2002. Photooxidation of azo dye in aqueous dispersions of H2O2/α-FeOOH. *Applied Catalysis B: Environmental* 39(3), 211-220. https://doi.org/10.1016/S0926-3373(02)00085-1

Heller, M.I. and Croot, P.L., 2011. Superoxide decay as a probe for speciation changes during dust dissolution in Tropical Atlantic surface waters near Cape Verde. *Marine Chemistry* 126(1-4), 37-55. 10.1016/j.marchem.2011.03.006

Hijosa-Valsero, M., Molina, R. and Bayona, J.M., 2014. Assessment of a dielectric barrier discharge plasma reactor at atmospheric pressure for the removal of bisphenol A and tributyltin. *Environmental technology* 35(11), 1418-1426.

Hiroki, A. and LaVerne, J.A., 2005. Decomposition of hydrogen peroxide at water−ceramic oxide interfaces. *The Journal of Physical Chemistry B* 109(8), 3364-3370. 10.1021/jp046405d

Holroyd, R.A. and Bielski, B.H.J., 1978. Photochemical generation of superoxide radicals in aqueous solutions. *Journal of the American Chemical Society* 100(18), 5796-5800. 10.1021/ja00486a034

Huerta-Fontela, M., Galceran, M.T. and Ventura, F., 2010. Fast liquid chromatography–quadrupole-linear ion trap mass spectrometry for the analysis of pharmaceuticals and hormones in water resources. *Journal of Chromatography A* 1217(25), 4212-4222. https://doi.org/10.1016/j.chroma.2009.11.007

Jacangelo, J.G. and Trussell, R.R., 2002. International report: water and wastewater disinfection - trends, issues and practices. *Water Science & Technology: Water Supply* 2, 147-157.

Jayson, G.G., Parsons, B.J. and Swallow, A.J., 1973. Some simple, highly reactive, inorganic chlorine derivatives in aqueous solution. Their formation using pulses of radiation and their role in the mechanism of the Fricke dosimeter. *Journal of the Chemical Society, Faraday Transactions 1* 69(0), 1597-1607. 10.1039/F19736901597

Jiang, B., Zheng, J., Qiu, S., Wu, M., Zhang, Q., Yan, Z. and Xue, Q., 2014. Review on electrical discharge plasma technology for wastewater remediation. *Chemical Engineering Journal* 236, 348-368.

Khezerlou, A., Alizadeh-Sani, M., Azizi-Lalabadi, M. and Ehsani, A., 2018. Nanoparticles and their antimicrobial properties against pathogens including bacteria, fungi, parasites and viruses. *Microbial pathogenesis* 123, 505-526.

Kläning, U.K. and Wolff, T., 1985. Laser flash photolysis of HClO, ClO^-, HBrO, and BrO^- in aqueous solution. Reactions of $Cl^\bullet$ and $Br^\bullet$ atoms. *Berichte der Bunsengesellschaft für physikalische Chemie* 89(3), 243-245. 10.1002/bbpc.19850890309

Klebanoff, S.J. (1975) Antimicrobial mechanisms in neutrophilic polymorphonuclear leukocytes, pp. 117-142.

Kohn, T., Grandbois, M., McNeill, K. and Nelson, K.L., 2007. Association with Natural Organic Matter Enhances the Sunlight-Mediated Inactivation of MS2 Coliphage by Singlet Oxygen. *Environmental Science & Technology* 41(13), 4626-4632. 10.1021/es070295h

Kohn, T. and Nelson, K.L., 2007. Sunlight-mediated inactivation of MS2 coliphage via exogenous singlet oxygen produced by sensitizers in natural waters. *Environmental science & technology* 41(1), 192-197.

Kong, X., Wu, Z., Ren, Z., Guo, K., Hou, S., Hua, Z., Li, X. and Fang, J., 2018. Degradation of lipid regulators by the UV/chlorine process: Radical mechanisms, chlorine oxide radical ($ClO^{\bullet}$)-mediated transformation pathways and toxicity changes. *Water Research* 137, 242-250. https://doi.org/10.1016/j.watres.2018.03.004

Kruithof, J.C., Kamp, P.C. and Martijn, B.J., 2007. UV/H2O2 treatment: A practical solution for organic contaminant control and primary disinfection. *Ozone: Science and Engineering* 29(4), 273-280.

Kwan, W.P. and Voelker, B.M., 2002. Decomposition of hydrogen peroxide and organic compounds in the presence of dissolved iron and ferrihydrite. *Environmental Science & Technology* 36(7), 1467-1476. 10.1021/es011109p

Lee, J., von Gunten, U. and Kim, J.-H., 2020. Persulfate-based advanced oxidation: critical assessment of opportunities and roadblocks. *Environmental Science & Technology* 54(6), 3064-3081. 10.1021/acs.est.9b07082

Lei, Y., Cheng, S., Luo, N., Yang, X. and An, T., 2019. Rate constants and mechanisms of the reactions of $Cl^{\bullet}$ and $Cl_2^{\bullet-}$ with trace organic contaminants. *Environmental Science & Technology* 53(19), 11170-11182. 10.1021/acs.est.9b02462

Leong, L.Y.C., Kuo, J. and Tang, C.-C. (2008) Disinfection of wastewater effluent ; Comparison of alternative technologies, IWA Publishing, London.

Li, S., Ao, X., Li, C., Lu, Z., Cao, W., Wu, F., Liu, S. and Sun, W., 2020. Insight into PPCP degradation by UV/NH_2Cl and comparison with UV/NaClO: Kinetics, reaction mechanism, and DBP formation. *Water Research* 182, 115967. https://doi.org/10.1016/j.watres.2020.115967

Li, Y., Zhang, W., Niu, J. and Chen, Y., 2012. Mechanism of photogenerated reactive oxygen species and correlation with the antibacterial properties of engineered metal-oxide nanoparticles. *ACS Nano* 6(6), 5164-5173. 10.1021/nn300934k

Lin, S.-S. and Gurol, M.D., 1998. Catalytic decomposition of hydrogen peroxide on iron oxide: kinetics, mechanism, and implications. *Environmental Science & Technology* 32(10), 1417-1423. 10.1021/es970648k

Liou, S.-Y. and Dodd, M.C., 2021. Evaluation of hydroxyl radical and reactive chlorine species generation from the superoxide/hypochlorous acid reaction as the basis for a novel advanced oxidation process. *Water Research* 200, 117142.

Locke, B., Sato, M., Sunka, P., Hoffmann, M. and Chang, J.-S., 2006. Electrohydraulic discharge and nonthermal plasma for water treatment. *Industrial & engineering chemistry research* 45(3), 882-905.

Long, C.A. and Bielski, B.H.J., 1980. Rate of reaction of superoxide radical with chloride-containing species. *The Journal of Physical Chemistry* 84(5), 555-557. 10.1021/j100442a023

Lousada, C.M., Brinck, T. and Jonsson, M., 2015. Application of reactivity descriptors to the catalytic decomposition of hydrogen peroxide at oxide surfaces. *Computational and Theoretical Chemistry* 1070, 108-116.

Lousada, C.M., Johansson, A.J., Brinck, T. and Jonsson, M., 2012. Mechanism of H2O2 decomposition on transition metal oxide surfaces. *The Journal of Physical Chemistry C* 116(17), 9533-9543. 10.1021/jp300255h

Lousada, C.M., LaVerne, J.A. and Jonsson, M., 2013a. Enhanced hydrogen formation during the catalytic decomposition of H2O2 on metal oxide surfaces in the presence of HO radical scavengers. *Physical Chemistry Chemical Physics* 15(30), 12674-12679. 10.1039/C3CP51616D

Lousada, C.M., Yang, M., Nilsson, K. and Jonsson, M., 2013b. Catalytic decomposition of hydrogen peroxide on transition metal and lanthanide oxides. *Journal of Molecular Catalysis A: Chemical* 379, 178-184. https://doi.org/10.1016/j.molcata.2013.08.017

Maier, A.C., Iglebaek, E.H. and Jonsson, M., 2019. Confirming the formation of hydroxyl radicals in the catalytic decomposition of H2O2 on metal oxides using coumarin as a probe. *ChemCatChem* 11(22), 5435-5438. https://doi.org/10.1002/cctc.201901316

Merényi, G., Lind, J., Naumov, S. and Sonntag, C.v., 2010a. Reaction of Ozone with Hydrogen Peroxide (Peroxone Process): A Revision of Current Mechanistic Concepts Based on Thermokinetic and Quantum-Chemical Considerations. *Environmental Science & Technology* 44(9), 3505-3507. 10.1021/es100277d

Merényi, G., Lind, J., Naumov, S. and von Sonntag, C., 2010b. The Reaction of Ozone with the Hydroxide Ion: Mechanistic Considerations Based on Thermokinetic and Quantum Chemical Calculations and the Role of HO_4^- in Superoxide Dismutation. *Chemistry – A European Journal* 16(4), 1372-1377. https://doi.org/10.1002/chem.200802539

Miklos, D.B., Remy, C., Jekel, M., Linden, K.G., Drewes, J.E. and Hübner, U., 2018. Evaluation of advanced oxidation processes for water and wastewater treatment–A critical review. *Water Research* 139, 118-131.

Morris, J.C., 1966. The acid ionization constant of HOCl from 5 to 35°. *The Journal of Physical Chemistry* 70(12), 3798-3805. 10.1021/j100884a007

Nieto-Juarez, J.I., Pierzchła, K., Sienkiewicz, A. and Kohn, T., 2010. Inactivation of MS2 coliphage in Fenton and Fenton-like systems: role of transition metals, hydrogen peroxide and sunlight. *Environmental Science & Technology* 44(9), 3351-3356. 10.1021/es903739f

Nosaka, Y. and Nosaka, A., 2016. Understanding hydroxyl radical (•OH) generation processes in photocatalysis. *ACS Energy Letters* 1(2), 356-359. 10.1021/acsenergylett.6b00174

O'Shea, K.E. and Dionysiou, D.D., 2012. Advanced oxidation processes for water treatment. *The Journal of Physical Chemistry Letters* 3(15), 2112-2113. 10.1021/jz300929x

Oturan, M. and Aaron, J.-J., 2014. Advanced oxidation processes in water/wastewater treatment: principles and applications. A review. *Critical Reviews in Environmental Science and Technology* 44. 10.1080/10643389.2013.829765

Pachaiappan, R., Rajendran, S., Show, P.L., Manavalan, K. and Naushad, M., 2021. Metal/metal oxide nanocomposites for bactericidal effect: A review. *Chemosphere* 272, 128607.

Pétrier, C., Combet, E. and Mason, T., 2007. Oxygen-induced concurrent ultrasonic degradation of volatile and non-volatile aromatic compounds. *Ultrasonics sonochemistry* 14(2), 117-121.

Pisarenko, A.N., Stanford, B.D., Yan, D., Gerrity, D. and Snyder, S.A., 2012. Effects of ozone and ozone/peroxide on trace organic contaminants and NDMA in drinking water and water reuse applications. *Water Research* 46(2), 316-326. https://doi.org/10.1016/j.watres.2011.10.021

Rakness, K.L., 2005. Ozone in Drinking Water Treatment: Process Design, Operation, and Optimization, American Water Works Association (AWWA).

Ravikumar, J.X. and Gurol, M.D., 1994. Chemical oxidation of chlorinated organics by hydrogen peroxide in the presence of sand. *Environmental science & technology* 28(3), 394-400.

Rodríguez, E.M. and von Gunten, U., 2020. Generation of hydroxyl radical during chlorination of hydroxyphenols and natural organic matter extracts. *Water Research* 177, 115691. https://doi.org/10.1016/j.watres.2020.115691

Segal, A.W., 2008. The function of the NADPH oxidase of phagocytes and its relationship to other NOXs in plants, invertebrates, and mammals. *The international journal of biochemistry & cell biology* 40(4), 604-618. 10.1016/j.biocel.2007.10.003

Simonsen, M.E., Muff, J., Bennedsen, L.R., Kowalski, K.P. and Søgaard, E.G., 2010. Photocatalytic bleaching of p-nitrosodimethylaniline and a comparison to the performance of other AOP technologies. *Journal of Photochemistry and Photobiology A: Chemistry* 216(2), 244-249. https://doi.org/10.1016/j.jphotochem.2010.07.008

Sobańska, K., Pietrzyk, P. and Sojka, Z., 2017. Generation of reactive oxygen species via electroprotic interaction of H2O2 with ZrO2 gel: ionic sponge effect and pH-switchable peroxidase-and catalase-like activity. *ACS Catalysis* 7(4), 2935-2947.

Song, K., Mohseni, M. and Taghipour, F., 2016. Application of ultraviolet light-emitting diodes (UV-LEDs) for water disinfection: A review. *Water research* 94, 341-349.

Stefan, M.I., 2017. Advanced Oxidation Processes for Water Treatment: Fundamentals and Applications, IWA Publishing.

Sun, P., Lee, W.-N., Zhang, R. and Huang, C.-H., 2016. Degradation of DEET and caffeine under UV/chlorine and simulated sunlight/chlorine conditions. *Environmental Science & Technology* 50(24), 13265-13273. 10.1021/acs.est.6b02287

Torres, R.A., Nieto, J.I., Combet, E., Pétrier, C. and Pulgarin, C., 2008. Influence of TiO2 concentration on the synergistic effect between photocatalysis and high-frequency ultrasound for organic pollutant mineralization in water. *Applied Catalysis B: Environmental* 80(1-2), 168-175.

USEPA (2009) 2006 Community Water System Survey. Volume II: Detailed Tables and Survey Methodology.

USEPA (1999) Alternative Disinfectants and Oxidants Guidance Manual.

von Gunten, U., 2018. Oxidation processes in water treatment: are we on track? *Environmental science & technology* 52(9), 5062-5075.

von Sonntag, C. and von Gunten, U., 2012. Chemistry of Ozone in Water and Wastewater Treatment: From Basic Principles to Applications, IWA Publishing, London.

Wang, D., Zhao, L., Ma, H., Zhang, H. and Guo, L.-H., 2017. Quantitative analysis of reactive oxygen species photogenerated on metal oxide nanoparticles and their bacteria toxicity: The role of superoxide radicals. *Environmental Science & Technology* 51(17), 10137-10145. 10.1021/acs.est.7b00473

Yang, M. and Jonsson, M., 2014. Evaluation of the O2 and pH effects on probes for surface bound hydroxyl radicals. *The Journal of Physical Chemistry C* 118(15), 7971-7979. 10.1021/jp412571p

Yang, M. and Jonsson, M., 2015. Surface reactivity of hydroxyl radicals formed upon catalytic decomposition of H2O2 on ZrO2. *Journal of Molecular Catalysis A: Chemical* 400, 49-55.

Zhihui, A., Peng, Y. and Xiaohua, L., 2005. Degradation of 4-chlorophenol by microwave irradiation enhanced advanced oxidation processes. *Chemosphere* 60(6), 824-827.

Chapter 2. SUPEROXIDE/HYPOCHLOROUS ACID REACTION, FORMATION OF REACTIVE RADICAL SPECIES, DEGRADATION OF ORGANIC CONTAMINANTS, AND FORMATION OF DISINFECTION BYPRODUCTS

2.1 Introduction

The present work aims to examine $O_2^{\bullet-}$/FAC reaction chemistry and highlights the potential for its application in (waste)water treatment by: (i) developing experimental procedures enabling manipulation of the $O_2^{\bullet-}$/FAC reaction via controlled blending of aqueous $O_2^{\bullet-}$ and FAC stock solutions, (ii) quantifying molar yields of $HO^{\bullet}$ and cumulative in situ exposures ($\int_0^t [\text{radical}]\,dt$) for $HO^{\bullet}$ and RCS from the $O_2^{\bullet-}$/FAC reaction, (iii) evaluating approaches for optimizing organic contaminant degradation via the $O_2^{\bullet-}$/FAC reaction under various conditions and in various water matrixes (including natural waters), and (iv) quantifying impacts of $O_2^{\bullet-}$/FAC treatment on formation of regulated organic and inorganic disinfection byproducts (DBPs).

2.2 Materials and Methods

2.2.1 Chemicals

All stock solutions of general reagents were prepared in Milli-Q ultrapure water with resistivity ≥ 18.2 MΩ•cm. FAC stock solutions were prepared by diluting a commercial aqueous NaOCl stock (available chlorine, 4.00-4.99% w/w, Sigma-Aldrich) in Milli-Q water, and standardized spectrophotometrically at 292 nm (ε_{OCl^-} = 350 $M^{-1}cm^{-1}$) (Hand and Margerum, 1983). H_2O_2 stock solutions were prepared by diluting a commercial aqueous H_2O_2 stock (31.7% w/w, Fisher) in Milli-Q water, and standardized spectrophotometrically at 240 nm ($\varepsilon_{H2O2/HO2^-}$ = 38 $M^{-1}cm^{-1}$) (Morgan et al., 1988). The reverse osmosis isolate of Suwannee River natural organic matter (SRNOM) was obtained from the International Humic Substance Society (IHSS). SRNOM aqueous stock solutions were prepared by dissolving 20 mg of SRNOM isolate in 100 mL of 1mM NaOH with mixing for 30 min. A sufficient amount of sulfuric acid was then added

to lower the pH to 7, and the solution was filtered through a 400°C-baked Whatman GF/F glass fiber filter (nominal pore size ~0.7 μm). The resulting SRNOM stock solution was stored in the dark at 4 °C prior to use. Natural surface waters samples were collected from (i) a Local Reservoir that serves as a regional drinking water source, and (ii) the exit of Lake Washington at the Montlake Cut near the University of Washington. The water samples were collected in glass bottles and stored at 4 °C prior to vacuum filtration through a 0.45 μm polyethersulfone membrane (SterliTech). Dissolved organic carbon (DOC) concentrations in SRNOM stock solutions and natural water samples were determined using a Shimadzu TOC-L high-temperature catalytic combustion analyzer. Additional details on natural water characteristics are provided in Table A1. Prior to use in experiments, all natural water samples were buffered with 50mM phosphate at pH 7. Chemicals obtained from commercial suppliers were typically of ≥98% purity, and were used without further purification (see Table 2.1 for a list of chemicals with suppliers and purities).

Table 2.1. Chemical suppliers and purities[a]

Chemical	Manufacturer	Purity/Specification	Purpose
NaOH (high-purity)	Alfa Aesar	≥ 99.99%	$O_2^{\bullet-}$ stability tests
EDTA	Sigma-Aldrich	≥ 99%	$O_2^{\bullet-}$ stability tests
FAC	Sigma-Aldrich	4.00-4.99% w/w	$O_2^{\bullet-}$/FAC treatment
H_2O_2	Fisher	31.7%	$O_2^{\bullet-}$/FAC treatment
KO_2	Sigma-Aldrich	42.4-47.4% O_2	$O_2^{\bullet-}$/FAC treatment
NaOH (regular)	Sigma-Aldrich	≥ 98%	$O_2^{\bullet-}$/FAC treatment
H_2SO_4	Sigma-Aldrich	95-98%	$O_2^{\bullet-}$/FAC treatment
NB	Sigma-Aldrich	≥ 99%	probe compound
BA	Alfa Aesar	99%	probe compound
DMB	Sigma-Aldrich	99%	probe compound
pCBA	Sigma-Aldrich	99%	probe compound
NaH_2PO_4	Sigma-Aldrich	≥ 99%	buffer
Na_2HPO_4	Sigma-Aldrich	≥ 99%	buffer
H_3BO_3	Sigma-Aldrich	≥ 99.5%	buffer
$Na_2S_2O_3$	Sigma-Aldrich	≥ 99.99%	quenching reagent for FAC
catalase from bovine liver	Sigma-Aldrich	10,000-40,000 units/mL	quenching reagent for H_2O_2

KI	Sigma-Aldrich	≥ 99%	Allen reagent
$(NH_4)_6Mo_7O_{24} \cdot 4H_2O$	Alfa Aesar	99%	Allen reagent
KHP	Alfa Aesar	99%	Allen reagent, DOC standard
ABTS	Fluka	≥ 99%	ClO_2 measurement
formaldehyde	Sigma-Aldrich	37%	formaldehyde experiments
t-BuOH	Sigma-Aldrich	≥ 99%	formaldehyde experiments, radical scavenger
acetylacetone	Sigma-Aldrich	≥ 99%	Hantzsch reagent
CH_3COONH_4	EMD	≥ 98%	Hantzsch reagent
CH_3COOH	Fisher	100%	Hantzsch reagent
TPA	TCI	≥ 99%	$HO^{\bullet}$ indicator
NaCl	Sigma-Aldrich	≥ 99.5%	halide analyses
NaBr	Sigma-Aldrich	≥ 99%	halide analyses
$NaBrO_3$	Sigma-Aldrich	≥ 99%	oxyhalide analyses
$NaClO_2$	Sigma-Aldrich	80%	oxyhalide analyses
$NaClO_3$	Sigma-Aldrich	≥ 99%	oxyhalide analyses
$NaClO_4$	EMD	98-102%	oxyhalide analyses
$Ba(OH)_2 \cdot 8H_2O$	Sigma-Aldrich	≥ 98%	halide/oxyhalide sample pretreatment
Na_2SO_4	Fisher	100.2%	THM/HAA analyses
MTBE	Sigma-Aldrich	99.9%	THM/HAA analyses
CF	EMD	99.8%	THM/HAA analyses
MCAA	Supelco	99.9%	THM/HAA analyses
DCAA	Supelco	97.9%	THM/HAA analyses
TCAA	Supelco	99.9%	THM/HAA analyses
H_3PO_4	Macron	85%	HPLC mobile phase
MeOH	Sigma-Aldrich	≥ 99.9%	HPLC mobile phase
Acetonitrile (LC-MS)	Thermo Scientific	99.9%	HPLC mobile phase
Acetonitrile	Fisher	≥ 99.9%	HPLC mobile phase
Water (LC-MS)	Merk	100%	HPLC mobile phase
methylamine	Sigma-Aldrich	40%	HPLC mobile phase
$^{35}Cl^{18}O_4^-$	ICON stable isotopes	95 Atom% ^{18}O	internal standard
$^{35}Cl^{18}O_3^-$	EURL-SRM	n.a.	internal standard
$^{81}Br^{18}O_3^-$	ICON stable isotopes	95 Atom% ^{18}O	internal standard
1,2,3-TCP	Sigma-Aldrich	99%	internal standard
2,3-DBP	Sigma-Aldrich	98%	internal standard

[a] Adopted from (Liou and Dodd, 2021).

2.2.2 Superoxide Stock Preparation

All $O_2^{\bullet-}$ stock solutions were prepared in Milli-Q ultrapure water with resistivity 18.2 MΩ•cm, with the exception of a limited number of KO_2 stock solutions prepared in molecular grade water (Corning, molecular grade water, MT-46-000-CM). Stock solutions were prepared by three methods: (a) Dissolution of KO_2 solids, (b) UV irradiation of alkaline H_2O_2/HO_2^-, or (c) O_3 treatment of alkaline H_2O_2/HO_2^-. Most aqueous $O_2^{\bullet-}$ stock solutions used in this work were prepared by dissolution of potassium dioxide (KO_2) solids (powder form) in aqueous NaOH solutions.

(i) KO_2 dissolution in 0.1 and 1M NaOH (NaOH solutions added to KO_2 solids)

Desired masses of KO_2 were weighed and placed in 20 mL amber borosilicate glass vials, NaOH solution (0.1 or 1 M) was rapidly poured into the vials, and the vials were shaken immediately after NaOH addition to ensure full dissolution of KO_2 solids. The pH values of 0.1 and 1M NaOH solutions were 13.0 and 13.9, respectively, at room temperature (22±2 °C), as confirmed by direct measurement for 0.1M NaOH, and calculated using Visual MINTEQ with correction for ionic strength/activity via the Brønsted-Guggenheim-Scatchard implementation of specific ion interaction theory for 1M NaOH (direct pH measurement at the latter NaOH concentration proved problematic due to apparent elevated sensitivity of the electrode to sodium error at >0.1M NaOH).

KO_2 was dissolved in NaOH solutions prepared in Milli-Q water at initial concentrations ranging from 0.5 to 10 mM, yielding $HO_2^{\bullet}/O_2^{\bullet-}$ concentrations ranging from ~0.07-2.1 mM (as well as H_2O_2/HO_2^- at similar levels) in the resulting stock solutions (Figure 2.1). As expected, higher initial KO_2 concentrations led to higher initial $[HO_2^{\bullet}/O_2^{\bullet-}]_0$ in stock solutions. However,

$[HO_2^{\bullet}/O_2^{\bullet-}]_0$ was always markedly lower than the concentrations of KO_2 dissolved (Figure 2.1), presumably due to the presence of very high localized concentrations of $HO_2^{\bullet}/O_2^{\bullet-}$ (with concomitant rapid disproportionation to H_2O_2/HO_2^- via eqs 1.3-1.5, and/or direct reactions with H_2O_2/HO_2^- via eqs 2.1-2.3) during dissolution of the KO_2 solids, even with rapid mixing.

$$HO_2^{\bullet} + H_2O_2 \rightarrow HO^{\bullet} + H_2O + O_2 \qquad k_{2.1} = 10^{-2} \text{ to } 5\ M^{-1}s^{-1} \text{ (Ross et al., 1998)} \qquad (2.1)$$

$$O_2^{\bullet-} + H_2O_2 \rightarrow HO^{\bullet} + OH^- + O_2 \qquad k_{2.2} = 10^{-4} \text{ to } 2.3\ M^{-1}s^{-1} \text{ (Ross et al., 1998)} \qquad (2.2)$$

$$O_2^{\bullet-} + HO_2^- \rightarrow O_2 + H_2O_2 \qquad k_{2.3} < 2\ M^{-1}s^{-1} \text{ (Ross et al., 1998)} \qquad (2.3)$$

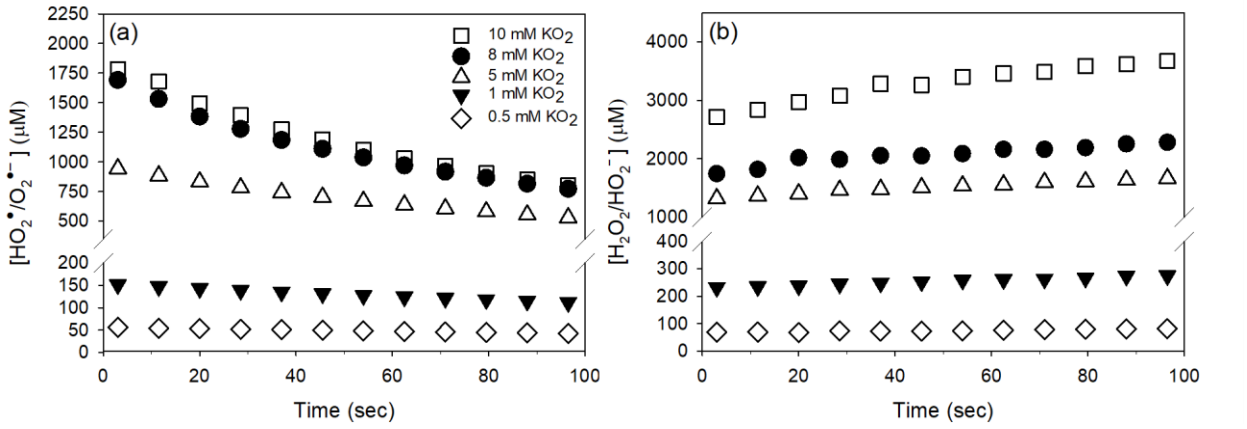

Figure 2.1. (a) $[HO_2^{\bullet}/O_2^{\bullet-}]$ and (b) $[H_2O_2/HO_2^-]$ in $O_2^{\bullet-}$ stock solutions prepared from dissolution of KO_2 in 1M NaOH at pH 13.9, using Milli-Q water and NaOH (≥98%, Sigma-Aldrich). Adopted from (Liou and Dodd, 2021).

(ii) UV irradiation of alkaline H_2O_2/HO_2^-

The photolysis of H_2O_2 (pK_a = 11.6 (Black and Hayon, 1970)) and its conjugate base, hydroperoxide (HO_2^-) proceeds via eqs 2.4-2.5 (Baxendale and Wilson, 1957; Glaze et al., 1987),

$$H_2O_2 \xrightarrow{h\nu} HO^{\bullet} + HO^{\bullet} \qquad (2.4)$$

$$HO_2^- \xrightarrow{h\nu} HO^\bullet + O^{\bullet-} \quad (2.5)$$

where in the presence of excess H_2O_2/HO_2^- (comprising the sum of H_2O_2 and HO_2^-), subsequent reactions of $HO^\bullet$ and its conjugate base, oxide radical ($O^{\bullet-}$) (pK_a = 11.9 (Buxton et al., 1988)), with H_2O_2/HO_2^- can lead to formation of $O_2^{\bullet-}$ (eqs 2.6-2.9).

$$HO^\bullet + H_2O_2 \rightarrow H_2O + O_2^{\bullet-} + H^+ \qquad k_{2.6} = 2.7 \times 10^7\ M^{-1}s^{-1} \text{ (Christensen et al., 1982)} \quad (2.6)$$

$$O^{\bullet-} + H_2O_2 \rightarrow OH^- + O_2^{\bullet-} + H^+ \qquad k_{2.7} \leq 5 \times 10^8\ M^{-1}s^{-1} \text{ (Christensen et al., 1982)} \quad (2.7)$$

$$HO^\bullet + HO_2^- \rightarrow H_2O + O_2^{\bullet-} \qquad k_{2.8} = 7.5 \times 10^9\ M^{-1}s^{-1} \text{ (Christensen et al., 1982)} \quad (2.8)$$

$$O^{\bullet-} + HO_2^- \rightarrow OH^- + O_2^{\bullet-} \qquad k_{2.9} = 4 \times 10^8\ M^{-1}s^{-1} \text{ (Buxton et al., 1988)} \quad (2.9)$$

Under circumneutral pH conditions, rapid disproportionation of $HO_2^\bullet$ and $O_2^{\bullet-}$ (eqs 1.3-1.4) prevents their buildup in solution; however, under strongly alkaline conditions (pH > 12), $O_2^{\bullet-}$ can accumulate. Consistent with this, $O_2^{\bullet-}$ has been reported as a product in the photolysis of HO_2^- (Allen and Bielski, 1980; Behar and Czapski, 1970; Bielski and Cabelli, 1995; Lunak and Sedlak, 1992). In this work, $O_2^{\bullet-}$ was in turn generated by using a 5W low-pressure (LP) Hg lamp (Pen-Ray 11SC-1, UVP) equipped with an 18mA AC power supply (Pen-Ray 11SC-1, UVP) to irradiate alkaline solutions of H_2O_2/HO_2^-. The Hg lamp, which emits monochromatic ultraviolet (UV) light (λ = 254 nm), was housed in a metal shield with a rectangular opening of 0.48 cm × 3.81 cm (see Figure 2.2). Irradiations were initiated by placing a 1-cm quartz cuvette containing 0.05M or 0.0316M NaOH and H_2O_2/HO_2^- at various initial concentrations in the path of the emitted light. The cuvette was place ~4 mm away from the outer surface of the lamp for irradiations, with the contents continuously stirred by a magnetic stir bar at 200 rpm. At pre-

defined times, the quartz cuvette was removed from the light and samples were collected for spectrophotometric analyses of [$HO_2^{\bullet}/O_2^{\bullet-}$] and [$H_2O_2/HO_2^-$].

Irradiation at initial concentrations of H_2O_2/HO_2^- ranging from 5-20 mM resulted in the buildup of $HO_2^{\bullet}/O_2^{\bullet-}$ over 3-5 minutes to maximal $HO_2^{\bullet}/O_2^{\bullet-}$ concentrations of ~1mM and ~0.5mM in 0.1M NaOH (pH13.0), 0.05M NaOH (pH 12.7) and 0.0316M NaOH (pH 12.5) solutions, respectively (Figure 2.3), with higher $[H_2O_2/HO_2^-]_0$ yielding higher [$HO_2^{\bullet}/O_2^{\bullet-}$] (consistent with eqs 2.4-2.9). These values are comparable to or in excess of the highest $O_2^{\bullet-}$ concentrations (~400 μM) reported when using vacuum-UV photolysis of oxygenated aqueous ethanol and/or formate solutions, or UV photolysis of mixture of ketones with alcohols (Bielski and Gebicki, 1982; Holroyd and Bielski, 1978; McDowell et al., 1983). $O_2^{\bullet-}$/FAC treatments using UV-derived $O_2^{\bullet-}$ stocks were described later in Chapter 3.

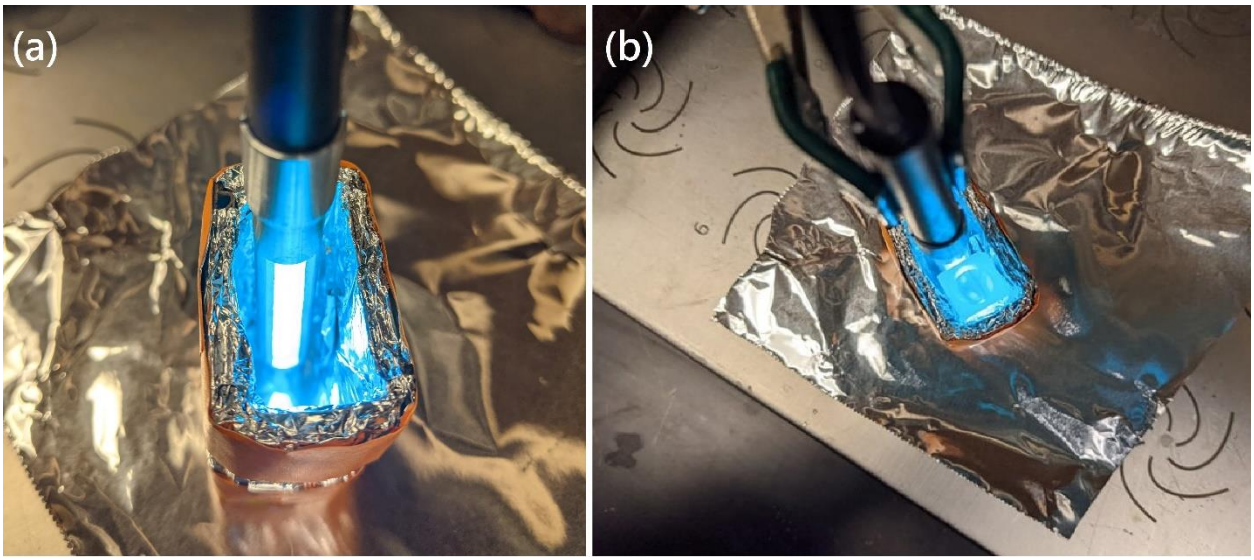

Figure 2.2. Setup for UV photolysis of alkaline H_2O_2/HO_2^- solutions for $O_2^{\bullet-}$ stock preparation. (a) Low-pressure Hg lamp housed in metal shield. (b) UV reactor setup with quartz cuvette in place on a magnetic stirrer. Adopted from (Liou and Dodd, 2021).

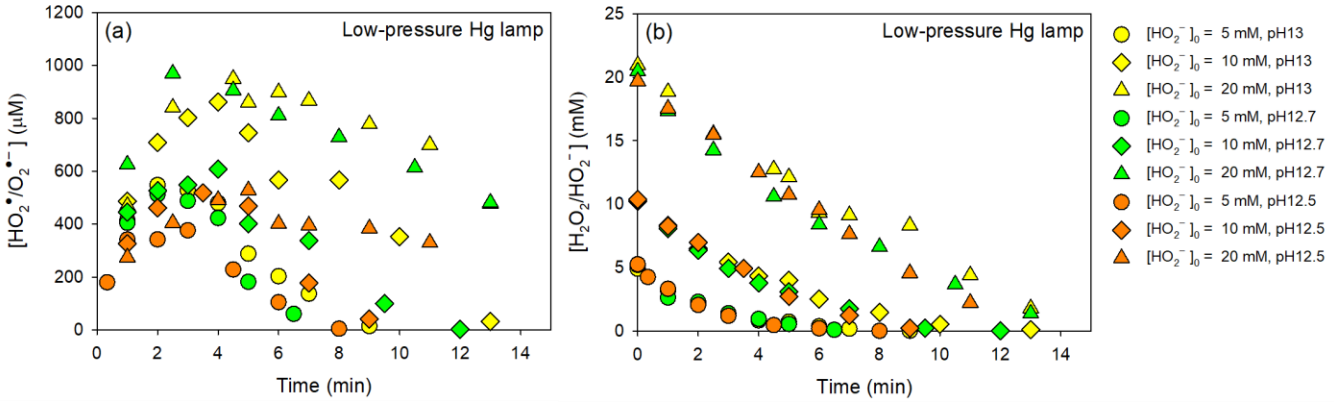

Figure 2.3. Evolution of (a) [$HO_2^{\bullet}/O_2^{\bullet-}$] and (b) [$H_2O_2/HO_2^-$] during continuous photolysis of H_2O_2/HO_2^- in 0.1, 0.05 or 0.0316M NaOH solutions at pH 13.0, 12.7 or 12.5, using a 5W low-pressure Hg vapor lamp. H_2O_2/HO_2^- solutions were prepared using Milli-Q water and NaOH (≥98%, Sigma-Aldrich). Adopted from (Liou and Dodd, 2021).

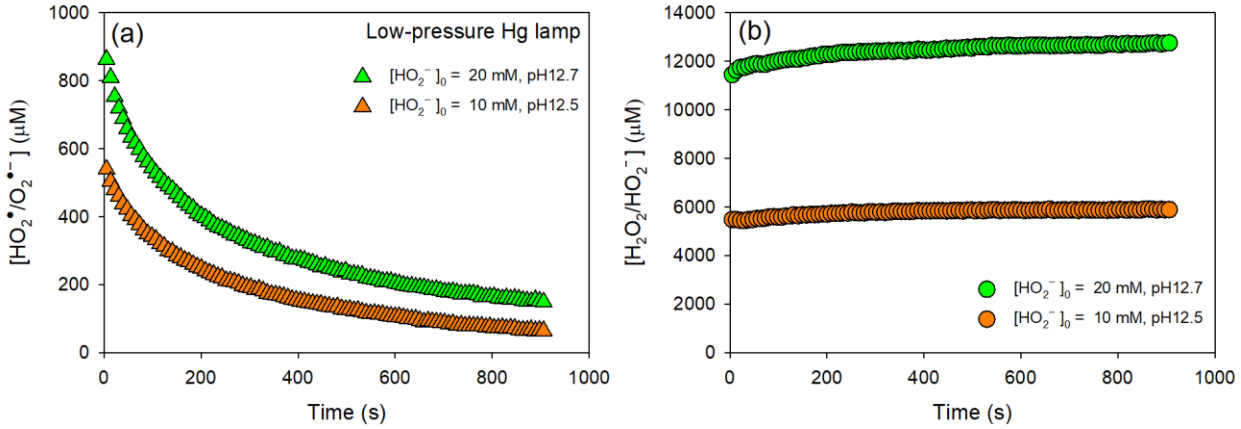

Figure 2.4. Decay of $HO_2^{\bullet}/O_2^{\bullet-}$, following removal of irradiated solutions of H_2O_2/HO_2^-in 0.05M or 0.0316M NaOH (pH 12.7 or 12.5) from the UV light source (a 5W low-pressure Hg vapor lamp). H_2O_2/HO_2^- solutions were prepared using Milli-Q water and NaOH (≥98%, Sigma-Aldrich). Adopted from (Liou and Dodd, 2021).

(iii) O_3 treatment of alkaline H_2O_2/HO_2^-

Under conditions of excess H_2O_2/HO_2^- at alkaline pH, O_3 is rapidly consumed by HO_2^- to yield $O_2^{\bullet-}$ and $HO^{\bullet}$ by way of a multi-step reaction now understood to proceed through an adduct HO_5^- (eq 2.10) (von Sonntag and von Gunten, 2012), with scavenging of $HO^{\bullet}$ by H_2O_2/HO_2^- leading to further $O_2^{\bullet-}$ (eqs 2.6-2.9). In this process, rapid reaction of O_3 with $O_2^{\bullet-}$ to yield $O_3^{\bullet-}$

(and subsequently, $O^{\bullet-}$, which in equilibrium with $HO^{\bullet}$, will in turn be scavenged by H_2O_2/HO_2^- through eqs 2.6-2.9) will to some extent self-limit $O_2^{\bullet-}$ accumulation (eqs 2.11-2.12).

$$O_3 + HO_2^- \rightarrow\rightarrow O_2^{\bullet-} + HO^{\bullet} + O_2 \qquad k_{2.10} = 2.8 \times 10^6\ M^{-1}s^{-1}\ \text{(Staehelin and Hoigne, 1982)} \quad (2.10)$$

$$O_3 + O_2^{\bullet-} \rightarrow O_2 + O_3^{\bullet-} \qquad k_{2.11} = 1.6 \times 10^9\ M^{-1}s^{-1}\ \text{(Buehler et al., 1984)} \quad (2.11)$$

$$O_3^{\bullet-} \rightarrow O^{\bullet-} + O_2 \qquad k_{2.12} = 2.8 \times 10^3\ s^{-1}\ \text{(Elliot and McCracken, 1989)} \quad (2.12)$$

In this work, aqueous O_3 stock solutions were prepared by bubbling gas-phase O_3 produced by a high-output, air-cooled, corona-discharge ozone generator (IN USA) through an ice-chilled Erlenmeyer flask of Milli-Q water until stable concentrations were reached (typically after 1 hr). O_3 concentrations obtained in the stock solutions typically reached ~1.1-1.2 mM, and were measured spectrophotometrically at 260 nm ($\varepsilon = 3150\ M^{-1}cm^{-1}$ (Hoigné, 1998)). Four mL volumes of O_3 stock solution were transferred by gas-tight glass syringe (either manually or with a syringe pump) into amber borosilicate glass vessels containing 4 mL of 1M NaOH amended with $[H_2O_2/HO_2^-]_0 = 1.2$ mM under constant stirring, allowed to react for 40 s, and then sampled for analyses of $HO_2^{\bullet}/O_2^{\bullet-}$ and H_2O_2/HO_2^-.

O_3 treatment of alkaline H_2O_2/HO_2^- under in situ conditions of pH ~13.6, $[H_2O_2/HO_2^-]_0$ = 0.6 mM, and $[O_3]_0 = 0.575$ mM resulted in the buildup of $HO_2^{\bullet}/O_2^{\bullet-}$ over 30 s to maximal concentrations ranging from 0.02-0.06 mM (Figure 2.5). Higher $HO_2^{\bullet}/O_2^{\bullet-}$ levels were observed when using a syringe pump to slowly meter the rate of O_3 addition to alkaline H_2O_2/HO_2^- solutions instead of dosing rapidly by manual injection. This effect was likely due to a lowering of O_3 concentrations present in solution at a given instant, with consequent minimization of the consumption of $O_2^{\bullet-}$ generated in eq 2.10 by subsequent reaction with O_3 (eq 2.11). $O_2^{\bullet-}$ stocks

generated by O_3 treatment of alkaline H_2O_2/HO_2^- were not used for $O_2^{\bullet-}$/FAC treatment due to the relatively low $[HO_2^{\bullet}/O_2^{\bullet-}]_{stock}$ levels resulting from this approach (Figure 2.5).

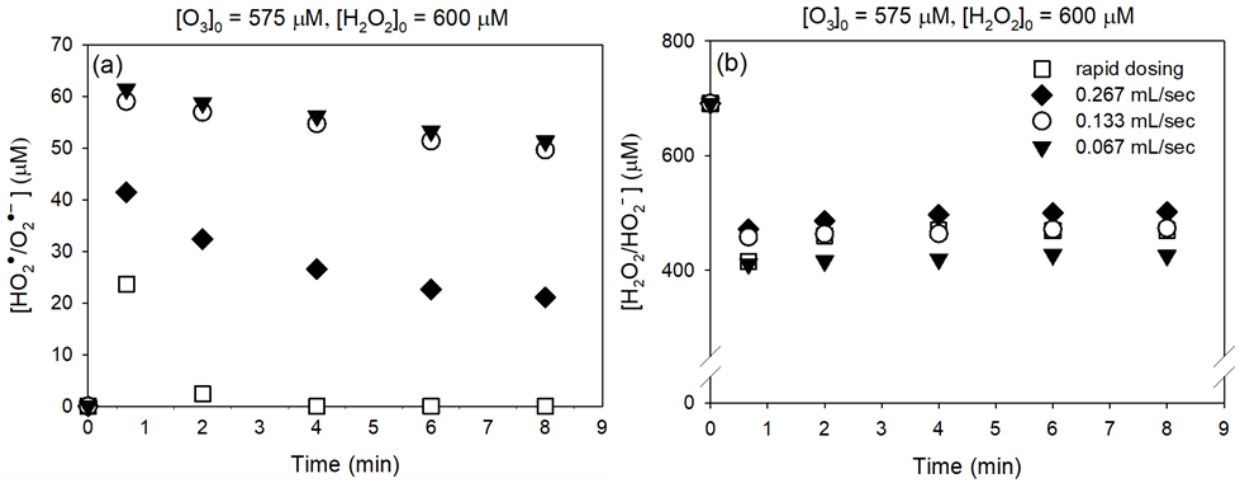

Figure 2.5. Evolution of (a) $[HO_2^{\bullet}/O_2^{\bullet-}]_0$ and (b) $[H_2O_2/HO_2^-]_0$ following reaction of $[O_3]_0$ = 575 μM with $[H_2O_2/HO_2^-]_0$ = 600 μM, in 0.5M NaOH at a calculated pH of 13.6 (obtained using VisualMINTEQ to correct for ionic strength, with activity coefficients determined from the Brønsted-Guggenheim-Scatchard implementation of specific ion interaction theory). As noted in the legend, O_3 was dosed to the alkaline H_2O_2/HO_2^- solutions either manually in a single, rapid injection, or by syringe pump at flow rates of 0.067, 0.133, or 0.267 mL/min. Alkaline H_2O_2/HO_2^- solutions were prepared using Milli-Q water and high-purity NaOH (99.99%, metals basis, Alfa Aesar). Adopted from (Liou and Dodd, 2021).

2.2.3 $O_2^{\bullet-}$/FAC Treatment Procedures

(i) KO_2-derived $O_2^{\bullet-}$ stocks used for treatment

KO_2-derived $O_2^{\bullet-}$ stocks in 1M NaOH were typically prepared to contain $[HO_2^{\bullet}/O_2^{\bullet-}]_{stock}$ ~ 1000 μM at the time of dosing to receiving solutions. Due to $HO_2^{\bullet}/O_2^{\bullet-}$ disproportionation (eqs 1.3-1.4), such stocks inevitably also contained H_2O_2/HO_2^-, typically at concentrations of $[H_2O_2/HO_2^-]_{stock}$ ~ 3500 μM. The stocks were dosed to receiving solutions at dilution factors ranging from 1:50 to 1:5 (stock volume added : final receiving solution volume) yielding in situ $[HO_2^{\bullet}/O_2^{\bullet-}]$ ~ 20-200 μM, and $[H_2O_2/HO_2^-]$ ~ 70-700 μM in the $O_2^{\bullet-}$/FAC-treated receiving

solutions. KO_2-derived $O_2^{\bullet-}$ stocks in 0.05M NaOH were typically prepared to contain $[HO_2^{\bullet}/O_2^{\bullet-}]_{stock}$ ~ 2000 μM and $[H_2O_2/HO_2^-]_{stock}$ ~ 6000 μM, and dosed to receiving solutions at dilution factors from 1:40 to 1:10 – yielding in situ $[HO_2^{\bullet}/O_2^{\bullet-}]$ ~ 50-200 μM and $[H_2O_2/HO_2^-]$ ~ 150-600 μM in the $O_2^{\bullet-}$/FAC-treated receiving solutions.

(ii) $O_2^{\bullet-}$/FAC treatment experiments

$O_2^{\bullet-}$/FAC treatment experiments were undertaken by either (i) dosing various volumes of alkaline $O_2^{\bullet-}$ stocks to 5mM or 50mM, phosphate- or borate-buffered solutions (pH 7-10) containing FAC and radical probes or in some cases *tert*-butanol (*t*-BuOH) (hereafter referred to as ***postmix*** treatment), or (ii) premixing alkaline $O_2^{\bullet-}$ with alkaline FAC, and then dosing various volumes of premixed alkaline $O_2^{\bullet-}$/FAC stocks to 5mM or 50mM pH 7 phosphate-buffered solutions or natural waters containing radical probes or other additives (e.g., H_2O_2, Suwannee River natural organic matter (SRNOM), or bromide) (hereafter referred to as ***premix*** treatment). $O_2^{\bullet-}$ stocks for postmix-dosing and $O_2^{\bullet-}$/FAC stocks for premix-dosing were generally prepared in 0.1M or 1M NaOH to stabilize $O_2^{\bullet-}$ and FAC, in accord with the slow kinetics of $O_2^{\bullet-}$ disproportionation and the $O_2^{\bullet-}$/FAC reaction at pH≥13 (Figure 1.1). $O_2^{\bullet-}$ and premixed $O_2^{\bullet-}$/FAC stocks were utilized as soon as possible after preparation (typically within 0.5-5 minutes) to minimize reactant losses before dosing to receiving solutions.

$O_2^{\bullet-}$ or $O_2^{\bullet-}$/FAC stocks were dosed into receiving solutions simultaneously with a stoichiometric amount of H_2SO_4 to neutralize OH^- and ensure the desired in situ pH (typically 7, with selected experiments at 8, 9, and 10) in receiving solutions. All $O_2^{\bullet-}$, $O_2^{\bullet-}$/FAC, and H_2SO_4 additions were conducted under rapid mixing, with receiving solutions agitated using PTFE-coated magnetic stir bars. All initial concentrations of *t*-BuOH, radical probes, $HO_2^{\bullet}/O_2^{\bullet-}$,

H_2O_2/HO_2^-, FAC, or other solution constituents reported herein were the initial values in solution after dosing all reactants (accounting for dilution due to blending reactants). Many experiments were conducted using a single dose of $O_2^{\bullet-}$ or premixed $O_2^{\bullet-}$/FAC stocks (henceforth referred to as ***single-dose*** or ***single-dosing*** experiments). In a number of experiments, a given receiving solution was repeatedly dosed with $O_2^{\bullet-}$ or premixed $O_2^{\bullet-}$/FAC stocks at fixed concentrations and stoichiometric ratios, with samples collected for analyses of probe compounds and other analytes after each dosing step (henceforth referred to as ***multiple-dose*** or ***multiple-dosing*** experiments).

(iii) H_2O_2/HO_2^- removal

Following addition of $O_2^{\bullet-}$ or premixed $O_2^{\bullet-}$/FAC stocks to receiving solutions, solutions were allowed to sit for at least 10 minutes to ensure completion of reactions. Any FAC not consumed directly by $O_2^{\bullet-}$ was consumed subsequently by excess H_2O_2/HO_2^- originating from the $O_2^{\bullet-}$ stock solution, via eq 2.13,

$$HOCl + HO_2^- \rightarrow H_2O + Cl^- + {}^1O_2 \qquad k_{2.13} = 4.4 \times 10^7\ M^{-1}s^{-1}\ \text{(Held et al., 1978)} \tag{2.13}$$

with an apparent $k_{app,\left(H_2O_2/HO_2^-\right)/FAC} = 8.4 \times 10^2\ M^{-1}s^{-1}$ at pH 7 (corresponding to $t_{1/2,\left(H_2O_2/HO_2^-\right)/FAC} \sim$ 12 s at $[H_2O_2/HO_2^-]_0 = 100\ \mu M$) (Figure S2.1b), as confirmed using DPD colorimetry (see Section 2.2.4).

Note that the reaction of FAC with H_2O_2/HO_2^- is too slow to compete directly with the $O_2^{\bullet-}$/FAC reaction upon $O_2^{\bullet-}$ or $O_2^{\bullet-}$/FAC dosing to receiving solutions at circumneutral pH (Figure S2.1b). Residual H_2O_2/HO_2^- in treated solutions was typically quenched using purified catalase from bovine liver (with thymol removed by repeated washing and centrifugation in phosphate buffer) prior to analyses of probe compounds and/or oxyhalides, and prior to

subsequent re-dosing with $O_2^{\bullet-}$ or premixed $O_2^{\bullet-}$/FAC stocks in multiple-dosing experiments. A catalase concentration of ≥5 units/mL was selected for H_2O_2/HO_2^- quenching (based on measurements of catalase-driven H_2O_2 decay here) to ensure complete H_2O_2/HO_2^- removal within 15 min. In selected experiments, residual H_2O_2/HO_2^- concentrations after $O_2^{\bullet-}$/FAC treatment were quenched by addition of excess FAC instead of catalase. Dosed FAC concentrations were selected to yield residual [FAC] values (after H_2O_2/HO_2^- consumption) based on stoichiometric requirements for re-dosing with $O_2^{\bullet-}$ stocks (for use in multiple-dosing experiments).

(iv) THM/HAA experiments

In experiments undertaken to examine THM and HAA formation during $O_2^{\bullet-}$/FAC treatment and post-chlorination of $O_2^{\bullet-}$/FAC treated samples, catalase was used to remove H_2O_2/HO_2^- from solutions following $O_2^{\bullet-}$/FAC dosing (or after each $O_2^{\bullet-}$/FAC dosing step in multiple-dosing experiments), with sub-samples collected directly afterward for THM, HAA, and probe compound analyses. Then, the solutions were dosed with a target $[FAC]_0$ = 8 $mgCl_2/L$, to assess impacts of $O_2^{\bullet-}$/FAC treatment on formation of THMs and HAAs from SRNOM during post-chlorination. After FAC dosing, samples were allowed to react in the dark for times sufficient to reach a cumulative FAC exposure ($\int_0^t [\mathrm{FAC}]\,dt$, hereafter referred to as CT_{FAC}) of 400 $mgCl_2/L \bullet min$, and finally quenched with $Na_2S_2O_3$ to prepare samples for subsequent THM and HAA analyses. Dosed $Na_2S_2O_3$ concentrations were selected to be in ≥10-fold molar excess of [FAC]. Catalase addition after $O_2^{\bullet-}$/FAC treatment was estimated to introduce no more than ~0.06 mgC/L of DOC into solutions, and was included in controls subjected to treatment with

FAC alone at the same levels as used in $O_2^{\bullet-}$/FAC treatment experiments, to ensure that THM and HAA measurements were not biased by the presence of catalase.

2.2.4 Analytical Methods

Full details of methods used for measurements of pH, $HO_2^{\bullet}/O_2^{\bullet-}$, H_2O_2/HO_2^-, oxyhalides, trihalomethanes (THMs), and haloacetic acids (HAAs); and for identification and quantification of $HO^{\bullet}$ and RCS during $O_2^{\bullet-}$/FAC treatment are provided below.

(i) pH measurements

All pH measurements were performed using an Orion 5 Star meter with Orion ROSS Ultra pH electrode, with pH adjustment using NaOH or H_2SO_4. Unless otherwise specified, solutions were prepared and experiments conducted at room temperature (22±2 °C).

(ii) Measurement of $HO_2^{\bullet}/O_2^{\bullet-}$ and/or H_2O_2/HO_2^- in stock and reaction (receiving) solutions

(a) UV spectrophotometry ($HO_2^{\bullet}/O_2^{\bullet-}$ and H_2O_2/HO_2^-)

The molar absorption coefficients of $HO_2^{\bullet}$, $O_2^{\bullet-}$, and H_2O_2 at 240 and 260 nm have been reported as $e_{HO_2^{\bullet},240nm}$ = 1260 $M^{-1}cm^{-1}$ and $e_{HO_2^{\bullet},260nm}$ = 540 $M^{-1}cm^{-1}$, $e_{O_2^{\bullet-},240nm}$ = 2345 $M^{-1}cm^{-1}$ and $e_{O_2^{\bullet-},260nm}$ = 1940 $M^{-1}cm^{-1}$, and $e_{H_2O_2,240nm}$ = 38 $M^{-1}cm^{-1}$ and $e_{H_2O_2,260nm}$ = 13 $M^{-1}cm^{-1}$, respectively (Bielski and Allen, 1977; Bielski et al., 1985; Czapski and Bielski, 1993; Morgan et al., 1988). Because some uncertainty exists as to the corresponding coefficients for HO_2^- (Czapski and Bielski, 1993; Morgan et al., 1988), they were determined here by measurement of HO_2^- absorbance in 1M NaOH solutions dosed with [H_2O_2/HO_2^-] = 0.5, 1, 2, 3 and 5 mM and corrected by subtraction of background OH^- absorbance (as measured in 1M NaOH solutions

lacking H_2O_2/HO_2^-), yielding $\varepsilon_{HO_2^-,240nm}$ = 346 $M^{-1}cm^{-1}$ and $\varepsilon_{HO_2^-,260nm}$ = 188 $M^{-1}cm^{-1}$. These values are in general agreement with those reported in several studies by Bielski et al. (Bielski and Allen, 1977; Bielski and Cabelli, 1995; Czapski and Bielski, 1993).

From the preceding, effective molar absorption coefficients $\varepsilon_{HO_2^\bullet/O_2^{\bullet-},\lambda}$ for $HO_2^\bullet/O_2^{\bullet-}$ and $\varepsilon_{H_2O_2/HO_2^-,\lambda}$ for H_2O_2/HO_2^- were calculated at λ= 240 and 260 nm for a given pH by eqs 2.14-2.15,

$$\varepsilon_{HO_2^\bullet/O_2^{\bullet-},\lambda} = a_{HO_2^\bullet}\varepsilon_{HO_2^\bullet,\lambda} + a_{O_2^{\bullet-}}\varepsilon_{O_2^{\bullet-},\lambda} = \left(\frac{[H^+]}{[H^+]+K_{a,HO_2^\bullet}}\right)\varepsilon_{HO_2^\bullet,\lambda} + \left(\frac{K_{a,HO_2^\bullet}}{[H^+]+K_{a,HO_2^\bullet}}\right)\varepsilon_{O_2^{\bullet-},\lambda} \quad (2.14)$$

$$\varepsilon_{H_2O_2/HO_2^-,\lambda} = a_{H_2O_2}\varepsilon_{H_2O_2,\lambda} + a_{HO_2^-}\varepsilon_{HO_2^-,\lambda} = \left(\frac{[H^+]}{[H^+]+K_{a,H_2O_2}}\right)\varepsilon_{H_2O_2,\lambda} + \left(\frac{K_{a,H_2O_2}}{[H^+]+K_{a,H_2O_2}}\right)\varepsilon_{HO_2^-,\lambda} \quad (2.15)$$

The resulting values of $\varepsilon_{HO_2^\bullet/O_2^{\bullet-},\lambda}$ and $\varepsilon_{H_2O_2/HO_2^-,\lambda}$ were then used in combination with real-time 240 and 260 nm absorbances, $Abs_{total,240nm}$ and $Abs_{total,260nm}$ (measured simultaneously with a Shimadzu UV-2700 spectrophotometer) to calculate $HO_2^\bullet/O_2^{\bullet-}$ and H_2O_2/HO_2^- concentrations in stock solutions by simultaneously solving eqs 2.16-2.17 via Cramer's Rule (with l = 1 cm) (Schreiber and Mitch, 2005; Shores, 2018).

$$Abs_{total,240nm} = \varepsilon_{HO_2^\bullet/O_2^{\bullet-},240nm}\times[HO_2^\bullet/O_2^{\bullet-}]\times l + \varepsilon_{H_2O_2/HO_2^-,240nm}\times[H_2O_2/HO_2^-]\times l \quad (2.16)$$

$$Abs_{total,260nm} = \varepsilon_{HO_2^\bullet/O_2^{\bullet-},260nm}\times[HO_2^\bullet/O_2^{\bullet-}]\times l + \varepsilon_{H_2O_2/HO_2^-,260nm}\times[H_2O_2/HO_2^-]\times l \quad (2.17)$$

(b) Allen reagent (H_2O_2/HO_2^-)

The potassium iodide/potassium hydrogen phthalate/molybdate reagent described by Allen et al. (Allen et al., 1952) was used to measure H_2O_2/HO_2^- concentrations in selected stock solutions as a check on the accuracy of the Cramer's rule method (Figure 2.6), as well as in reaction solutions during multiple-dosing experiments.

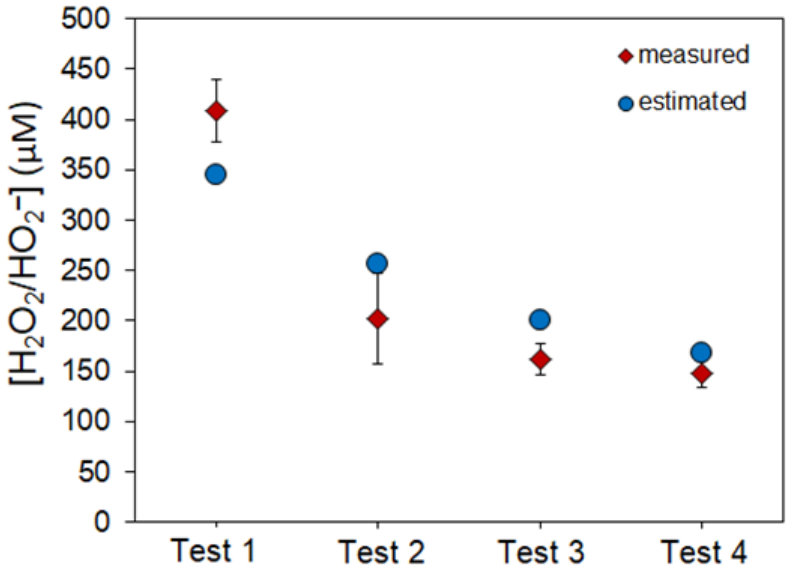

Figure 2.6. Comparison of $[H_2O_2/HO_2^-]$ measurements obtained using the Allen reagent method with $[H_2O_2/HO_2^-]$ measurements obtained using the UV spectrophotometry/Cramer's rule method (eqs 2.16-2.17) for the same solutions. Adopted from (Liou and Dodd, 2021).

(iii) Identification and quantification of HO• and RCS

(a) Probe compound methods (HO• and RCS exposures)

Because of the extremely rapid kinetics of the $O_2^{\bullet-}$/FAC reaction and associated secondary radical reactions at circumneutral pH, radical generation and consequent degradation of probe compounds occur in a brief pulse, within 0.1-0.4 s of mixing $O_2^{\bullet-}$ and FAC stock solutions at circumneutral pH in either postmix or premix experiments (Figure 1.1, eqs 1.7-1.15). As a consequence of the non-steady state nature of this process (with concomitant $HO_2^{\bullet}/O_2^{\bullet-}$ and

FAC decay resulting in continuous variation in radical levels over the course of the $O_2^{\bullet-}$ and FAC reaction), it is not possible to determine steady-state radical concentrations applicable over the entire course of the reaction timescale, as one might in a UV/H_2O_2 or UV/FAC process. Instead, the probe compounds nitrobenzene (NB), benzoic acid (BA), and 1,4-dimethoxybenzene (DMB) were utilized together to quantify cumulative in situ exposures ($\int_0^t [\text{radical}]\, dt$) for HO$^\bullet$, Cl$^\bullet$, ClO$^\bullet$, and/or $Cl_2^{\bullet-}$ during $O_2^{\bullet-}$/FAC treatment (see Section 2.2.5 for details). Exposures for ClO$^\bullet$ and/or $Cl_2^{\bullet-}$ could not be separated, due to the lack of an available probe selective for only one of these species, and so are considered here in terms of a single aggregate term for ClO$^\bullet$/$Cl_2^{\bullet-}$ exposure. *para*-Chlorobenzoic acid (pCBA) was used for semi-quantitative assessment of variations in radical exposures with varying $O_2^{\bullet-}$/FAC treatment conditions.

Concentrations of NB, BA, DMB, and pCBA in samples were all analyzed (after quenching residual H_2O_2/HO_2^- with catalase, or residual FAC with $Na_2S_2O_3$ in 10-fold molar excess of [FAC]) using a Dionex UltiMate 3000 HPLC coupled with a diode array detector. NB, BA, and DMB separations were performed together on a Supelco Ascentis C18 column (150 × 2.1 mm, 3 μm), using an isocratic mobile phase comprising 50% 100mM H_3PO_4 (A) and 50% methanol (B), while pCBA was analyzed in separate experiments using an isocratic mobile phase comprising 65% 100mM H_3PO_4 (A) and 35% acetonitrile (B). In all cases, a 20μL injection volume and 0.25 mL/min flow rate were used.

(b) Terephthalate (HO$^\bullet$ identification)

Reaction of terephthalate (TPA) with HO$^\bullet$ ($k_{HO^\bullet,TPA}$ = (3.3-4.4)×10^9 $M^{-1}s^{-1}$) produces highly fluorescent hydroxyterephthalate (hTPA), which exhibits two excitation/emission maxima at 240 nm/425 nm and 310 nm/425 nm (Charbouillot et al., 2011; Fang et al., 1996; Page et al.,

2010). Formation of hTPA was used as a qualitative and semi-quantitative diagnostic measurement for confirmation of $HO^{\bullet}$ generation in $O_2^{\bullet-}$/FAC treated solutions. Excitation-emission matrixes (EEM) were collected for samples (after quenching residual H_2O_2/HO_2^- with catalase, or residual FAC with $Na_2S_2O_3$ in 10-fold molar excess of [FAC]) at excitation wavelengths from 200-400 nm (5 nm increments) and emission wavelengths from 247.0-824.6 nm (~4.5 nm increments), using a 1 × 1 cm quartz cuvette on a Horiba Aqualog Fluorometer. The EEM data were post-processed using Aqualog software to correct for inner filter effects, and for Raman and Rayleigh-scattering, with blanks collected for Milli-Q water.

(c) Hantzsch reagent ($HO^{\bullet}$ yields)

t-BuOH reacts with $HO^{\bullet}$ ($k_{HO^{\bullet},t\text{-BuOH}} = 6.0\times10^8\ M^{-1}s^{-1}$) to generate formaldehyde as a predominant stable product (Buxton et al., 1988; Schuchmann and Von Sonntag, 1979). Formation of formaldehyde was used as a qualitative and quantitative diagnostic measurement of $HO^{\bullet}$ yields in $O_2^{\bullet-}$/FAC treated solutions. Formaldehyde was quantified in samples (after quenching residual H_2O_2/HO_2^- with catalase) by means of the Hantzsch reaction,(Nash, 1953) wherein the product diacetyldihydrolutidine (DDL) was detected at 412 nm (ε = 8,000 $M^{-1}cm^{-1}$) using the Shimadzu UV-2700 spectrophotometer noted above. Calibrations were performed using formaldehyde standards prepared in Milli-Q water (Figure 2.7).

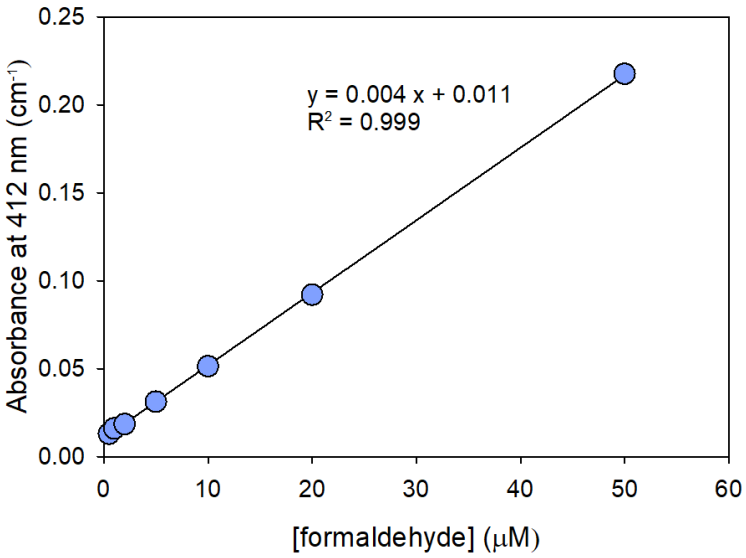

Figure 2.7. Calibration curve obtained by derivatization of formaldehyde standards with the Hantzsch reagent. Calibration standards were prepared by adding $[formaldehyde]_0$ = 0.5-50 μM into Milli-Q water, allowing 2 h at 22±2 °C for reaction to form the product diacetyldihydrolutidine, and measurement of absorbance at 412 nm. Adopted from (Liou and Dodd, 2021).

(iv) DPD and ABTS colorimetry

Colorimetric methods employing *N*,*N*-diethyl-*p*-phenylenediamine (DPD) and 2,2-azino-bis(3-ethylvenzothiazoline-6-sulfonate (ABTS) were used to quantify FAC and chlorine dioxide (ClO_2) concentrations, respectively, in selected samples following $O_2^{\bullet-}$/FAC treatment (APHA/AWWA/WEF, 2005; Pinkernell et al., 2000).

(v) Measurement of oxyhalides, chloride, THMs, and HAAs

(a) Non-suppressed ion chromatography with electrospray ionization and tandem mass spectrometry (NS-IC-MS/MS) (oxyhalides)

Chlorite (ClO_2^-), chlorate (ClO_3^-), perchlorate (ClO_4^-), and bromate (BrO_3^-) were analyzed using a Shimadzu LC-20 HPLC coupled with an API 4000 QTRAP linear ion trap with

hybrid triple-quadrupole mass spectrometer (AB Sciex), with quantification using ^{18}O-labelled internal standards ($^{35}Cl^{18}O_4^-$, $^{35}Cl^{18}O_3^-$, and $^{81}Br^{18}O_3^-$). Separations were performed on a 2×250 nm Dionex IonPac AS16 column (9 μm particle size, 2000 Å pore size), using a 100 μL injection volume and isocratic mobile phase comprising 20% 1 M aqueous methylamine (A) and 80% acetonitrile (B) at a flow rate of 0.25 mL/min. Full method details are available elsewhere (Young et al., 2020).

Immediately after experiments, phosphate and sulfate in treated samples were removed by $Ba(OH)_2$ treatment and sedimentation of $Ba_3(PO4)_2$ and $BaSO_4$ precipitates via centrifugation at 14000 rpm for 10 min (to avoid interference in NS-IC-MS/MS analyses (Young et al., 2020)). Supernatants were collected and diluted 7-fold for analyses. Recoveries of 95-105% were achieved for all oxyhalides. Samples were stored at 4 ºC until analyses within 24 h.

(b) Ion chromatography with conductivity detection (chloride)

Background chloride concentrations in FAC stocks and chloride concentrations formed during $O_2^{\bullet-}$/FAC treatment were measured using a Dionex ICS-3000 ion chromatograph equipped with a conductivity detector, with 100 μL injection volumes. Separations were performed with the AS16 column noted above, using a gradient method with varying concentrations of aqueous potassium hydroxide at a flow rate of 0.25 mL/min.

(c) Liquid-liquid extraction/esterification with gas chromatography-electron capture detection (GC-ECD) (THMs and HAAs)

Ten mL of $Na_2S_2O_3$-treated samples were acidified to pH < 2 by 98% H_2SO_4. Then ~4 g of sodium sulfate was added to samples to increase ionic strength, and THMs and protonated HAAs were extracted into 2 mL of MTBE amended with internal standards (100 μg/L 1,2,3-

trichloropropane and 2,3-dibromopropanoic acid) via vortex. Then 2 mL of the supernatant MTBE layer containing THMs and HAAs was transferred into a conical-bottom borosilicate glass vial, and amended with 0.5 mL of methanol acidified with 10% H_2SO_4. The MTBE extract was then heated at 50 °C for 2 h in order to esterify the HAAs. After cooling, 2 mL of saturated aqueous sodium bicarbonate was added into the esterified extract to neutralize excess acid, and the MTBE supernatant was transferred into autosampler vials for analysis by GC-ECD on a Shimadzu GC-2010 system, with separation on a 30 m × 0.25 mm × 1.0 μm HP-1MS column, in accord with EPA Method 552.2 (Hodgeson, 1995).

2.2.5 Determination of Cumulative in situ Radical Exposures

Nitrobenzene (NB) is reported to react rapidly only with hydroxyl radical ($HO^{\bullet}$) (of the radicals relevant to the $O_2^{\bullet-}$/FAC reaction) (Buxton et al., 1988; Nowell and Hoigné, 1992; Watts and Linden, 2007), while benzoic acid (BA) reacts rapidly with $HO^{\bullet}$ and chlorine radical ($Cl^{\bullet}$) (Buxton et al., 1988; Mártire et al., 2001), and 1,4-dimethoxybenzene (DMB) reacts rapidly with $HO^{\bullet}$, $Cl^{\bullet}$, chlorine monoxide radical ($ClO^{\bullet}$), and likely also dichloride radical ($Cl_2^{\bullet-}$) (Alfassi et al., 1988; Alfassi et al., 1989; O'Neill et al., 1975). The rate constants for reactions of $ClO^{\bullet}$ and $Cl_2^{\bullet-}$ with BA are each at least three orders of magnitude smaller than reported or predicted for their reaction with DMB (Alfassi et al., 1988; Hasegawa and Neta, 1978), and thus are neglected here. In situ exposures for $HO^{\bullet}$ and $Cl^{\bullet}$, and an aggregate exposure value for $ClO^{\bullet}$ and $Cl_2^{\bullet-}$, were calculated from probe compound losses measured during $O_2^{\bullet-}$/FAC treatment according to the following sets of equations (eqs 2.18-2.26):

HO• exposure

$$-\frac{d[\mathrm{NB}]}{dt} = k_{\mathrm{HO}^\bullet,\mathrm{NB}}[\mathrm{NB}][\mathrm{HO}^\bullet] \tag{2.18}$$

$$\int_0^t \frac{d[\mathrm{NB}]}{[\mathrm{NB}]} = \ln\left(\frac{[\mathrm{NB}]}{[\mathrm{NB}]_0}\right) = -k_{\mathrm{HO}^\bullet,\mathrm{NB}}\int_0^t [\mathrm{HO}^\bullet]\,dt \tag{2.19}$$

$$\mathrm{HO}^\bullet\text{exposure} = \int_0^t [\mathrm{HO}^\bullet]\,dt = \frac{\ln\left(\frac{[\mathrm{NB}]}{[\mathrm{NB}]_0}\right)}{-k_{\mathrm{HO}^\bullet,\mathrm{NB}}} \tag{2.20}$$

Cl• exposure

$$-\frac{d[\mathrm{BA}]}{dt} = k_{\mathrm{HO}^\bullet,\mathrm{BA}}[\mathrm{BA}][\mathrm{HO}^\bullet] + k_{\mathrm{Cl}^\bullet,\mathrm{BA}}[\mathrm{BA}][\mathrm{Cl}^\bullet] \tag{2.21}$$

$$\int_0^t \frac{d[\mathrm{BA}]}{[\mathrm{BA}]} = \ln\left(\frac{[\mathrm{BA}]}{[\mathrm{BA}]_0}\right) = -k_{\mathrm{HO}^\bullet,\mathrm{BA}}\int_0^t [\mathrm{HO}^\bullet]\,dt - k_{\mathrm{Cl}^\bullet,\mathrm{BA}}\int_0^t [\mathrm{Cl}^\bullet]\,dt \tag{2.22}$$

$$\mathrm{Cl}^\bullet\text{exposure} = \int_0^t [\mathrm{Cl}^\bullet]\,dt = \frac{\ln\left(\frac{[\mathrm{BA}]}{[\mathrm{BA}]_0}\right) + k_{\mathrm{HO}^\bullet,\mathrm{BA}}\int_0^t [\mathrm{HO}^\bullet]\,dt}{-k_{\mathrm{Cl}^\bullet,\mathrm{BA}}} \tag{2.23}$$

Aggregate $ClO^{\bullet}/Cl_2^{\bullet-}$ exposure

$$-\frac{d[\mathrm{DMB}]}{dt} = k_{\mathrm{HO}^{\bullet},\mathrm{DMB}}[\mathrm{DMB}][\mathrm{HO}^{\bullet}] + k_{\mathrm{Cl}^{\bullet},\mathrm{DMB}}[\mathrm{DMB}][\mathrm{Cl}^{\bullet}] + k_{\mathrm{ClO}^{\bullet},\mathrm{DMB}}[\mathrm{DMB}][\mathrm{ClO}^{\bullet}] + k_{\mathrm{Cl_2}^{\bullet-},\mathrm{DMB}}[\mathrm{DMB}][\mathrm{Cl_2}^{\bullet-}] \quad (2.24)$$

$$\begin{aligned}
&\int_0^t \frac{d[\mathrm{DMB}]}{[\mathrm{DMB}]} = \ln\left(\frac{[\mathrm{DMB}]}{[\mathrm{DMB}]_0}\right) \\
&= -k_{\mathrm{HO}^{\bullet},\mathrm{DMB}}\int_0^t [\mathrm{HO}^{\bullet}]dt - k_{\mathrm{Cl}^{\bullet},\mathrm{DMB}}\int_0^t [\mathrm{Cl}^{\bullet}]dt - k_{\mathrm{ClO}^{\bullet},\mathrm{DMB}}\int_0^t [\mathrm{ClO}^{\bullet}]dt - k_{\mathrm{Cl_2}^{\bullet-},\mathrm{DMB}}\int_0^t [\mathrm{Cl_2}^{\bullet-}]dt \\
&= -k_{\mathrm{HO}^{\bullet},\mathrm{DMB}}\int_0^t [\mathrm{HO}^{\bullet}]dt - k_{\mathrm{Cl}^{\bullet},\mathrm{DMB}}\int_0^t [\mathrm{Cl}^{\bullet}]dt - k_{\mathrm{ClO}^{\bullet},\mathrm{DMB}}\int_0^t [\mathrm{ClO}^{\bullet}]dt - 0.41k_{\mathrm{ClO}^{\bullet},\mathrm{DMB}}\int_0^t [\mathrm{Cl_2}^{\bullet-}]dt \\
&= -k_{\mathrm{HO}^{\bullet},\mathrm{DMB}}\int_0^t [\mathrm{HO}^{\bullet}]dt - k_{\mathrm{Cl}^{\bullet},\mathrm{DMB}}\int_0^t [\mathrm{Cl}^{\bullet}]dt - k_{\mathrm{ClO}^{\bullet},\mathrm{DMB}}\left(\int_0^t [\mathrm{ClO}^{\bullet}]dt + 0.41\int_0^t [\mathrm{Cl_2}^{\bullet-}]dt\right)
\end{aligned} \quad (2.25)$$

$$\left(\int_0^t [\mathrm{ClO}^{\bullet}]dt + 0.41\int_0^t [\mathrm{Cl_2}^{\bullet-}]dt\right) = \text{Aggregate } \mathrm{ClO}^{\bullet}/\mathrm{Cl_2}^{\bullet-} \text{ exposure, or} \int_0^t [\mathrm{ClO}^{\bullet}/\mathrm{Cl_2}^{\bullet-}]dt =$$

$$= \frac{\ln\left(\frac{[\mathrm{DMB}]}{[\mathrm{DMB}]_0}\right) + k_{\mathrm{HO}^{\bullet},\mathrm{DMB}}\int_0^t [\mathrm{HO}^{\bullet}]dt + k_{\mathrm{Cl}^{\bullet},\mathrm{DMB}}\int_0^t [\mathrm{Cl}^{\bullet}]dt}{-k_{\mathrm{ClO}^{\bullet},\mathrm{DMB}}} \quad (2.26)$$

where $k_{\mathrm{HO}^{\bullet},i}$, $k_{\mathrm{Cl}^{\bullet},i}$, $k_{\mathrm{ClO}^{\bullet},i}$, and $k_{\mathrm{Cl_2}^{\bullet-},i}$ represent the second-order rate constants for reactions of $HO^{\bullet}$, $Cl^{\bullet}$, $ClO^{\bullet}$, and $Cl_2^{\bullet-}$ with probe compound *i*; and $[i]_0$ and $[i]$ represent the concentrations of *i* before and after $O_2^{\bullet-}$/FAC treatment, respectively.

$k_{\mathrm{HO}^{\bullet},\mathrm{NB}}$, $k_{\mathrm{HO}^{\bullet},\mathrm{BA}}$ and $k_{\mathrm{HO}^{\bullet},\mathrm{DMB}}$ have been reported as 3.9×10^9 $M^{-1}s^{-1}$ (Buxton et al., 1988), 5.9×10^9 $M^{-1}s^{-1}$ (for the benzoate ion) (Buxton et al., 1988), and 7.0×10^9 $M^{-1}s^{-1}$ (O'Neill et al., 1975), respectively. $k_{\mathrm{Cl}^{\bullet},\mathrm{BA}}$ and $k_{\mathrm{Cl}^{\bullet},\mathrm{DMB}}$ have each been reported as 1.8×10^{10} $M^{-1}s^{-1}$ (Alfassi et al., 1989; Mártire et al., 2001), and $k_{\mathrm{ClO}^{\bullet},\mathrm{DMB}}$ has been reported as 2.1×10^9 $M^{-1}s^{-1}$ (Alfassi et al., 1988). The second-order rate constant for reaction of $Cl_2^{\bullet-}$ with DMB was not found in the literature; therefore, it was estimated as described in Text S2.1, yielding a value of $k_{\mathrm{Cl_2}^{\bullet-},\mathrm{DMB}}$ = 8.6×10^8 $M^{-1}s^{-1}$.

Because values of $\int_0^t \left[ClO^{\bullet} \right] dt$ and $0.41 \int_0^t \left[Cl_2^{\bullet -} \right] dt$ could not be independently determined, their sums $\left(\int_0^t \left[ClO^{\bullet} \right] dt + 0.41 \int_0^t \left[Cl_2^{\bullet -} \right] dt \right)$ are reported together here as aggregate values abbreviated as $\int_0^t \left[ClO^{\bullet}/Cl_2^{\bullet -} \right] dt$, and were calculated by means of eq 2.26.

2.3 Results and Discussion

2.3.1 Preparation and Stabilities of Superoxide Stock Solutions

Rates of $HO_2^{\bullet}/O_2^{\bullet -}$ decay in aqueous stock solutions were proportional to $[HO_2^{\bullet}/O_2^{\bullet -}]_0$, consistent with the second-order kinetics of $HO_2^{\bullet}/O_2^{\bullet -}$ disproportionation (eqs 1.3-1.4 and 1.6) (Table 2.2), with slower decay kinetics (i.e., higher $HO_2^{\bullet}/O_2^{\bullet -}$ stability) observed in solutions at lower $[HO_2^{\bullet}/O_2^{\bullet -}]_0$. Overall, $HO_2^{\bullet}/O_2^{\bullet -}$ decay kinetics were much faster than predicted based on theoretical values of $k_{app,HO_2^{\bullet}/O_2^{\bullet -},DP}$ calculated using eq 1.6 (Figure 1.1, Table 2.2). For instance at pH 13 and 13.9, $k_{app,HO_2^{\bullet}/O_2^{\bullet -},DP}$ values of 0.61 and 0.077 $M^{-1}s^{-1}$ were calculated from eq 1.6, corresponding to theoretical half-times, $t_{1/2,HO_2^{\bullet}/O_2^{\bullet -},DP}$, of 14 and 110 min, respectively, at a representative concentration of $[HO_2^{\bullet}/O_2^{\bullet -}]_0$ = 2 mM. In comparison, typical values of $t_{1/2,obs,HO_2^{\bullet}/O_2^{\bullet -}}$ ~ 15 and 60 s were measured here in 10 mM KO_2 stocks prepared at pH 13 and 13.9, respectively.

Our empirical half-life for $O_2^{\bullet -}$ stock is much shorter than theoretical value, which might be due to unideal mixing during stock preparation, impurities, trace metals, high background H_2O_2 concentrations, and/or high background carbonate concentrations. Trace transition metals (e.g., Fe, Cu) and various organic substances (e.g., quinones, ascorbate) are known to directly

scavenge $HO_2^{\bullet}/O_2^{\bullet-}$ and/or catalyze Fenton-type reactions that contribute to decreased $O_2^{\bullet-}$ stability in aqueous solution (Bielski and Cabelli, 1995; Bielski et al., 1985). To investigate whether the presence of such impurities may have been responsible for the decreased $O_2^{\bullet-}$ stabilities, and to assess options for improving $O_2^{\bullet-}$ stabilities, KO_2 stocks were also prepared by: (i) amending NaOH solutions used for stock preparation with 0.1-10 mM of ethylenediaminetetraacetate (EDTA) as a chelating agent (Oviedo and Rodríguez, 2003), (ii) using higher-purity NaOH (99.99%, metals basis), (iii) using molecular grade water in place of Milli-Q water, (iv) acid-washing glassware used for experiments, (v) using plastic (polypropylene) instead of glass vessels, and (vi) thermostating at 5 °C. A summary of experimental $t_{1/2,obs,HO_2^{\bullet}/O_2^{\bullet-}}$ values determined under these conditions is provided in Table 2.3. No consistent positive or negative effects on $HO_2^{\bullet}/O_2^{\bullet-}$ stabilities were observed for usage of high-purity NaOH, acid-washing of glassware, or usage of polypropylene vessels. Moderate (up to ~2-fold) improvements in $HO_2^{\bullet}/O_2^{\bullet-}$ stability were observed when lowering stock solution temperatures to 5 °C, or when adding EDTA or using molecular grade water. The effects of EDTA and molecular grade water indicate that the presence of trace metals and/or organic impurities in the Milli-Q water used for stock solutions may have been partly responsible for discrepancies in theoretical and experimental $HO_2^{\bullet}/O_2^{\bullet-}$ decay kinetics. Although use of EDTA would be undesirable for AOPs, use of chelating agents with low $HO^{\bullet}$-reactivities (e.g., polyphosphates) and/or higher-purity water (e.g., molecular grade or distilled water) for $O_2^{\bullet-}$ stock preparation could provide options for improving $O_2^{\bullet-}$ yields and/or stabilities.

As shown in Tables 2.2 and 2.3, preparation of $O_2^{\bullet-}$ stocks by addition of KO_2 solids to 0.05M NaOH solutions (pH12.7) under rapid stirring led to considerable improvements in $HO_2^{\bullet}/O_2^{\bullet-}$ stability – likely by suppressing disproportionation of $HO_2^{\bullet}/O_2^{\bullet-}$ (eqs 1.3-1.4) through

a reduction in the localized concentrations of KO_2 solids during dissolution. However, kinetics of $HO_2^{\bullet}/O_2^{\bullet-}$ decay in stock solutions prepared in this manner were still faster than expected based on theoretical values of $k_{app,HO_2^{\bullet}/O_2^{\bullet-},DP}$ and $t_{1/2,HO_2^{\bullet}/O_2^{\bullet-},DP}$ (Table 2.2).

$HO_2^{\bullet}/O_2^{\bullet-}$ may also be consumed in direct reactions with H_2O_2/HO_2^- (eqs 2.1-2.3), where a range of values have been reported for the relevant rate constants (Ross et al., 1998). Although the kinetics of these reactions are slow, levels of H_2O_2/HO_2^- present in stock solutions (up to ~5 mM) are high enough to yield estimated half-times from eqs 2.1-2.3 near those observed experimentally. For example, at pH 13.9 – assuming $[H_2O_2/HO_2^-]_0$ = 5 mM (present as HO_2^-), a maximum value of $k_{2.3}$ = 2 $M^{-1}s^{-1}$, and that $HO_2^{\bullet}/O_2^{\bullet-}$ is present as $O_2^{\bullet-}$ – the $t_{1/2}$ for second-order decay of $O_2^{\bullet-}$ would be ~100 s, compared to experimental $t_{1/2,obs,HO_2^{\bullet}/O_2^{\bullet-}}$ values ~60 s. Thus, the proportion of $HO_2^{\bullet}/O_2^{\bullet-}$ decay not attributable to trace metals or organic impurities may have been due to the presence of high levels of H_2O_2/HO_2^- in stock solutions. This highlights that approaches for suppressing formation of H_2O_2/HO_2^- may represent an additional route to improving yields and stabilities of $O_2^{\bullet-}$ in stock solutions.

Table 2.2. Comparison of observed and theoretical $HO_2^{\bullet}/O_2^{\bullet-}$ decay kinetics in KO_2 stocks[a]

Condition	$[HO_2^{\bullet}/O_2^{\bullet-}]_0$ (mM)	$[H_2O_2/HO_2^-]_0$ (mM)	Experimental	Theoretical[b]	
			$t_{1/2,obs,HO_2^{\bullet}/O_2^{\bullet-}}$ (s)	$k_{app,HO_2^{\bullet}/O_2^{\bullet-},DP}$ ($M^{-1}s^{-1}$)	$t_{1/2,HO_2^{\bullet}/O_2^{\bullet-},DP}$ (s)
pH13.9 (adding NaOH solutions to KO_2 solids; see Section 2.2.2)					
10 mM KO_2	2.10 ± 0.11	3.35 ± 0.14	55	0.077 (pH13.9)	6.18×10^3
8 mM KO_2	1.84 ± 0.17	2.27 ± 0.34	72		7.05×10^3
5 mM KO_2	0.92 ± 0.05	1.62 ± 0.13	107		1.41×10^4
1 mM KO_2	0.14 ± 0.02	0.35 ± 0.04	244		9.27×10^4
0.5 mM KO_2	0.07 ± 0.01	0.11 ± 0.02	286		1.85×10^5
pH13.0 (adding NaOH solutions to KO_2 solids; Section 2.2.2)					
10 mM KO_2	3.21 ± 0.31	3.36 ± 0.12	15	0.612 (pH13.0)	5.09×10^2
8 mM KO_2	2.37 ± 0.52	2.53 ± 0.11	21		6.89×10^2
5 mM KO_2	1.39 ± 0.20	1.45 ± 0.05	33		1.22×10^3
pH12.7 (refined preparation procedure; adding KO_2 solids to NaOH solutions; see Section 3.2.1)					
20 mM KO_2	2.72 ± 0.11	6.07 ± 0.44	86	1.220 (pH12.7)	3.62×10^2

[a] Error bars represent one standard deviation about the mean of duplicate measurements. [b] Theoretical apparent rate constants ($k_{app,HO_2^{\bullet}/O_2^{\bullet-},DP}$) and half-times ($t_{1/2,HO_2^{\bullet}/O_2^{\bullet-},DP}$) for $HO_2^{\bullet}/O_2^{\bullet-}$ disproportionation were calculated according to eq 1.13 (Bielski et al., 1985)**.** Adopted from (Liou and Dodd, 2021).

Table 2.3. Summary of observed $HO_2^{\bullet}/O_2^{\bullet-}$ decay kinetics in KO_2 stocks prepared under various conditions[a]

Container	Temp.[b]	Solvent	Note[c]	pH	$[KO_2]_0$ (mM)	$[O_2^{\bullet-}]_0$ (mM)	$t_{1/2,obs,HO_2^{\bullet}/O_2^{\bullet-}}$ (s)
Glass	Room	1 M NaOH (≥ 98 %)	Milli-Q	13.9	10	2.10 ± 0.11	55
Glass	Room	1 M NaOH (≥ 98 %)	Milli-Q	13.9	8	1.84 ± 0.17	72
Glass	Room	1 M NaOH (≥ 98 %)	Milli-Q	13.9	5	0.92 ± 0.05	107
Glass	Room	1 M NaOH (≥ 98 %)	Milli-Q	13.9	1	0.14 ± 0.02	244
Glass	Room	1 M NaOH (≥ 98 %)	Milli-Q	13.9	0.5	0.07 ± 0.01	286
Glass	Room	0.1 M NaOH (≥ 98 %)	Milli-Q	13.0	10	3.21 ± 0.31	15
Glass	Room	0.1 M NaOH (≥ 98 %)	Milli-Q	13.0	8	2.37 ± 0.52	21
Glass	Room	0.1 M NaOH (≥ 98 %)	Milli-Q	13.0	5	1.39 ± 0.20	33
Glass	Room	0.05 M NaOH (≥ 98 %) (refined preparation procedure; see Text S2)	Milli-Q	12.7	20	2.72 ± 0.11	86
Glass	Room	1 M NaOH (≥ 98 %)	Milli-Q	13.9	10	2.50	68
Glass (acid-washed)	Room	1 M NaOH (≥ 98 %)	Milli-Q	13.9	10	2.17	71

Polypropylene	Room	1 M NaOH (≥ 98 %)	Milli-Q	13.9	10	2.31	69
Glass	Room	1 M NaOH (≥ 99.99 %)	Milli-Q	13.9	10	1.96	82
Glass (acid-washed)	Room	1 M NaOH (≥ 99.99 %)	Milli-Q	13.9	10	2.13	66
Polypropylene	Room	1 M NaOH (≥ 99.99 %)	Milli-Q	13.9	10	2.39	62
Glass	Room	1 M NaOH (≥ 99.99 %) 0.1 mM EDTA	Milli-Q	13.9	10	2.41	80
Glass	Room	1 M NaOH (≥ 99.99 %) 0.5 mM EDTA	Milli-Q	13.9	10	2.67	75
Glass	Room	1 M NaOH (≥ 99.99 %) 1 mM EDTA	Milli-Q	13.9	10	2.38	86
Glass	Room	1 M NaOH (≥ 99.99 %) 5 mM EDTA	Milli-Q	13.9	10	2.34	89
Glass	Room	1 M NaOH (≥ 99.99 %) 10 mM EDTA	Milli-Q	13.9	10	1.96	105
Glass (acid-washed)	Room	1 M NaOH (≥ 99.99 %) 10 mM EDTA	Milli-Q	13.9	10	2.14	93

Polypropylene	Room	1 M NaOH (≥ 99.99 %) 10 mM EDTA	Milli-Q	13.9	10	2.71	81
Glass	Room	1 M NaOH (≥ 99.99 %)	MG water	13.9	10	1.87	94
Glass (acid-washed)	Room	1 M NaOH (≥ 99.99 %)	MG water	13.9	10	1.78	66
Polypropylene	Room	1 M NaOH (≥ 99.99 %)	MG water	13.9	10	2.27	71
Glass	Room	1 M NaOH (≥ 99.99 %) 1 mM EDTA	MG water	13.9	10	2.58	81
Glass	Room	1 M NaOH (≥ 99.99 %) 10 mM EDTA	MG water	13.9	10	2.29	101
Glass (acid-washed)	Room	1 M NaOH (≥ 99.99 %) 10 mM EDTA	MG water	13.9	10	2.03	110
Polypropylene	Room	1 M NaOH (≥ 99.99 %) 10 mM EDTA	MG water	13.9	10	2.40	93
Glass	5 °C	1 M NaOH (≥ 99.99 %)	Milli-Q	14.5[d]	10	2.11	104
Glass	5 °C	1 M NaOH (≥ 99.99 %) 1 mM EDTA	Milli-Q	14.5[d]	10	2.27	131

Glass	5 °C	1 M NaOH (≥ 99.99 %) 10 mM EDTA	Milli-Q	14.5[d]	10	2.54	133
Glass	5 °C	1 M NaOH (≥ 99.99 %)	MG water	14.5[d]	10	2.02	115
Glass	5 °C	1 M NaOH (≥ 99.99 %) 1 mM EDTA	MG water	14.5[d]	10	2.47	131
Glass	5 °C	1 M NaOH (≥ 99.99 %) 10 mM EDTA	MG water	14.5[d]	10	2.13	174

[a] Error bars represent one standard deviation about the mean of duplicate measurements. [b] "Room" represents room temperature (22±2 °C) without specific control; "5 °C" experiments were conducted with thermostating at 5 °C via refrigerated circulating bath. [c] MG = molecular grade. [d] pH values for "5 °C" experiments were calculated using VisualMINTEQ to correct for ionic strength and temperature, with activity coefficients determined using the Brønsted-Guggenheim-Scatchard implementation of specific ion interaction theory, consistent with room temperature experiments. Adopted from (Liou and Dodd, 2021).

2.3.2 Confirmation of Radical Formation from the $O_2^{\bullet-}$/FAC Reaction

(i) Probe compound degradation

pH 7, 50mM phosphate buffer solutions containing 1 μM nitrobenzene (NB), benzoic acid (BA), 1,4-dimethoxybenzene (DMB), and/or *para*-chlorobenzoic acid (pCBA) were subjected to single-dose postmix $O_2^{\bullet-}$/FAC treatment with increasing $[HO_2^{\bullet}/O_2^{\bullet-}]_0$ (20, 50, 100, 200 μM) and $[FAC]_0$ (10, 25, 50, 100 μM) at a fixed 2:1 molar $[HO_2^{\bullet}/O_2^{\bullet-}]_0/[FAC]_0$ ratio. NB reacts rapidly only with $HO^{\bullet}$ (of the radicals relevant to the $O_2^{\bullet-}$/FAC reaction) (Buxton et al., 1988; Nowell and Hoigné, 1992; Watts and Linden, 2007), while BA reacts rapidly with $HO^{\bullet}$ and $Cl^{\bullet}$ (Buxton et al., 1988; Mártire et al., 2001), and DMB reacts rapidly with $HO^{\bullet}$, $Cl^{\bullet}$, $ClO^{\bullet}$, and likely also $Cl_2^{\bullet-}$ (Alfassi et al., 1988; Alfassi et al., 1989; O'Neill et al., 1975). $HO^{\bullet}$ exposures were measured based on NB degradation during treatment, and RCS exposures estimated based on degradation of BA and DMB, according to procedures described in Section 2.2.5. pCBA – which reacts rapidly with $HO^{\bullet}$ (Neta and Dorfman, 1968) and presumably also $Cl^{\bullet}$, considering its structural similarity to BA (though no rate constant appears to be available for this reaction) – was used as a non-specific radical probe in some preliminary experiments.

As shown in Figure 2.8, increasing probe losses were observed when jointly increasing $[HO_2^{\bullet}/O_2^{\bullet-}]_0$ and $[FAC]_0$. In contrast, none of the probes were degraded in solutions treated separately with $HO_2^{\bullet}/O_2^{\bullet-}$ or FAC, confirming that probe degradation was not due to direct reactions with $HO_2^{\bullet}/O_2^{\bullet-}$ or FAC. Direct reactions with H_2O_2/HO_2^- could also be ruled out on the basis of the treatments with $HO_2^{\bullet}/O_2^{\bullet-}$ in the absence of FAC, as $O_2^{\bullet-}$ stocks also contained H_2O_2/HO_2^- at levels yielding $[H_2O_2/HO_2^-]_0$ = 70-700 μM in the receiving solutions (Figure 2.8). Furthermore, no probe losses were observed in the presence of FAC dosed with $[H_2O_2/HO_2^-]_0$ =

250 μM (Figure 2.8), confirming probe degradation during $O_2^{\bullet-}$/FAC treatment was not due to singlet oxygen ($^1O_2$) generated from reaction of FAC with H_2O_2/HO_2^- (eq 2.13) . Finally, no probe losses were observed during postmix $O_2^{\bullet-}$/FAC treatment in the presence of 50mM *t*-BuOH – which was sufficient to yield ≥93% scavenging of HO$^\bullet$ and, as a consequence, block the formation of RCS (since in this system RCS are secondary radicals generated from HO$^\bullet$ via eqs 1.9-1.15, which would have been precluded due to scavenging of HO$^\bullet$ by *t*-BuOH) (Figure 2.8, Text S2.2). Thus, probe degradation during $O_2^{\bullet-}$/FAC treatment could be attributed to HO$^\bullet$ and/or RCS.

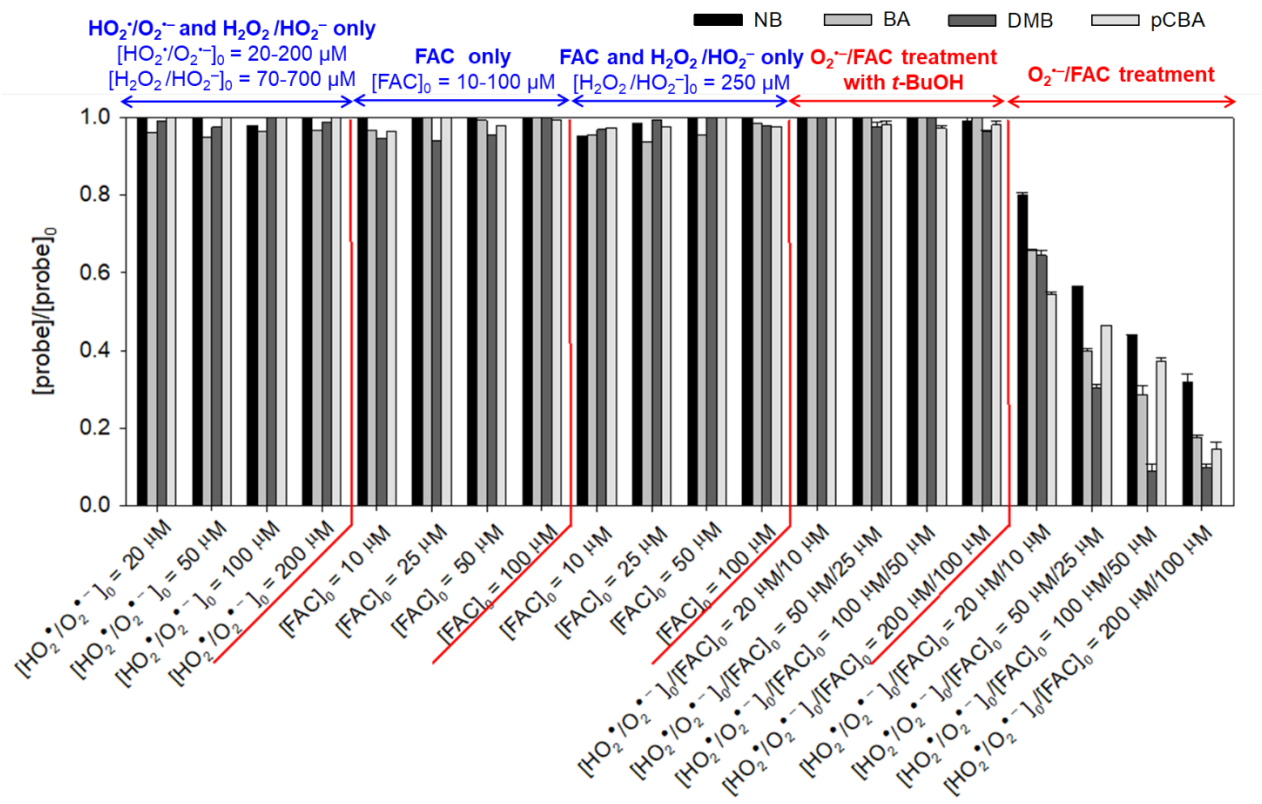

Figure 2.8. Effects of various control treatments and $O_2^{\bullet-}$/FAC treatments on probe compound concentrations in pH 7, 50mM phosphate buffer containing [NB, BA, DMB]$_0$ = 1 μM or [pCBA]$_0$ = 1 μM. Solutions were subjected to (from left to right on graph): (i) $HO_2^{\bullet}/O_2^{\bullet-}$ and H_2O_2/HO_2^- only treatment (by single-dose addition of $[HO_2^{\bullet}/O_2^{\bullet-}]_0$ = 20-200 μM; noting that $O_2^{\bullet-}$ stocks also contained H_2O_2/HO_2^-, due to $HO_2^{\bullet}/O_2^{\bullet-}$ disproportionation), (ii) FAC only treatment (by single-dose addition of [FAC]$_0$ = 10-100 μM), (iii) FAC and H_2O_2/HO_2^- only treatment (by single-dose addition first of [FAC]$_0$ = 10-100 μM and then of $[H_2O_2/HO_2^-]_0$ = 250 μM), (iv) $O_2^{\bullet-}$/FAC treatment with *t*-BuOH (by single-dose, postmix addition of $[HO_2^{\bullet}/O_2^{\bullet-}]_0$ = 20-200 μM to [FAC]$_0$ = 10-100 μM in the presence of [*t*-BuOH]$_0$ = 50 mM), or (v) $O_2^{\bullet-}$/FAC treatment (by single-dose, postmix addition of $[HO_2^{\bullet}/O_2^{\bullet-}]_0$ = 20-200 μM to [FAC]$_0$ = 10-100 μM). $HO_2^{\bullet}/O_2^{\bullet-}$ and H_2O_2/HO_2^- only, FAC only, and FAC and H_2O_2/HO_2^- only control treatments were evaluated in single experiments, whereas $O_2^{\bullet-}$/FAC treatment experiments (with and without *t*-BuOH) were conducted in duplicate. Error bars represent one standard deviation about the mean of duplicate measurements. Adopted from (Liou and Dodd, 2021).

Degradation of the $HO^{\bullet}$-selective probe NB during $O_2^{\bullet-}$/FAC treatment, in conjunction with the lack of NB or other probe degradation during $O_2^{\bullet-}$/FAC treatment in the presence of *t*-BuOH, point to $HO^{\bullet}$ as a key driver of probe degradation under the conditions evaluated, consistent with eq 1.1. However, trends in NB, BA, and DMB degradation indicate that RCS also play an important role (as discussed in Section 2.3.4 and Section 2.2.5 and Text S2.3), consistent with eqs 1.9-1.15.

(ii) hydroxy-Terephthalate (hTPA) formation from terephthalate (TPA)

TPA is well known to yield hTPA upon reaction with $HO^{\bullet}$ (Page et al., 2010). When dosed with increasing $[HO_2^{\bullet}/O_2^{\bullet-}]_0$ during single-dose postmix treatment, solutions containing $[TPA]_0$ = 10 μM and $[FAC]_0$ = 100 μM at pH 7 yielded increasing hTPA levels (Figure 2.9). In contrast, hTPA formation was not observed in such solutions without $HO_2^{\bullet}/O_2^{\bullet-}$ addition (Figure 2.9), or in FAC-free controls treated with $[HO_2^{\bullet}/O_2^{\bullet-}]_0$ = 25 μM (also including $[H_2O_2/HO_2^{-}]_0$ = 200 μM) (data not shown). These observations further highlight the role of $HO^{\bullet}$ as a key oxidant during $O_2^{\bullet-}$/FAC treatment.

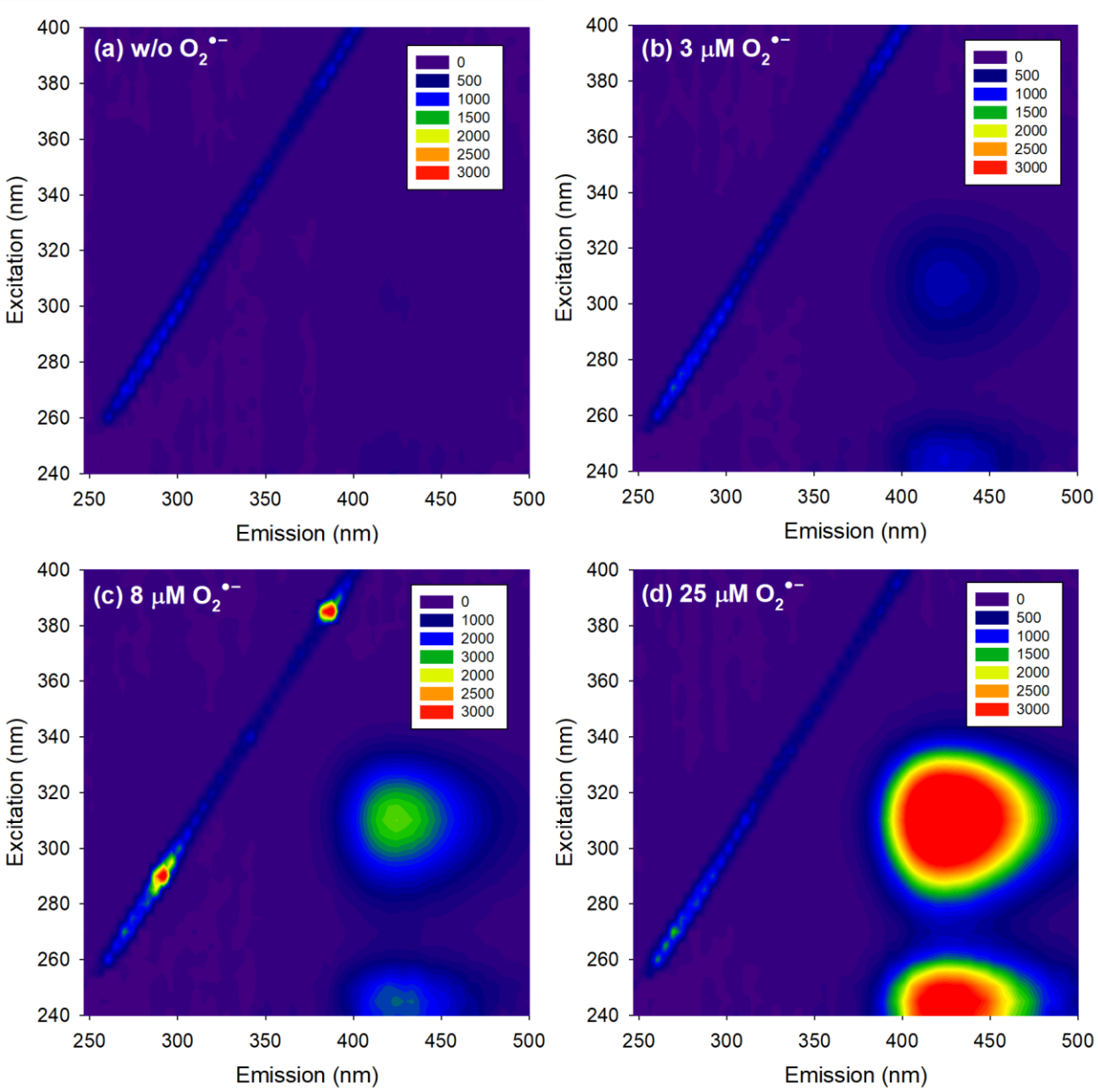

Figure 2.9. Fluorescence excitation-emission matrixes obtained for solutions of pH 7, 50mM phosphate buffer containing $[TPA]_0$ = 10 μM and $[FAC]_0$ = 50 μM following single-dose postmix $O_2^{\bullet-}$/FAC treatment at (a) $[HO_2^{\bullet}/O_2^{\bullet-}]_0$ = 0 μM, (b) $[HO_2^{\bullet}/O_2^{\bullet-}]_0$ = 3 μM, (c) $[HO_2^{\bullet}/O_2^{\bullet-}]_0$ = 8 μM, and (d) $[HO_2^{\bullet}/O_2^{\bullet-}]_0$ = 25 μM. FAC only control treatments were conducted with exposure times of 30 minutes following addition of FAC, whereas $O_2^{\bullet-}$/FAC treatment experiments were conducted as described in Section 2.2. Adopted from (Liou and Dodd, 2021).

(iii) Formaldehyde generation from t-BuOH

The reaction of *t*-BuOH with HO$^{\bullet}$ to yield formaldehyde can be used as a means of quantifying HO$^{\bullet}$ yields in various oxidation processes (Flyunt et al., 2003; Schuchmann and Von Sonntag, 1979). When dosed with increasing $[HO_2^{\bullet}/O_2^{\bullet-}]_0$ during single-dose postmix treatment, solutions containing $[t\text{-BuOH}]_0$ = 50 mM and $[FAC]_0$ = 50, 100, or 250 μM at pH 7 yielded increasing formaldehyde levels at $[HO_2^{\bullet}/O_2^{\bullet-}]_0/[FAC]_0$ below 1, with formaldehyde levels plateauing as $[HO_2^{\bullet}/O_2^{\bullet-}]_0/[FAC]_0$ exceeded 1 (Figure 2.10). This likely reflects increasing conversion of $[FAC]_0$ to HO$^{\bullet}$ at sub-stoichiometric $[HO_2^{\bullet}/O_2^{\bullet-}]_0$, with full conversion of $[FAC]_0$ (and maximum HO$^{\bullet}$ yield) reached at stoichiometric or higher concentrations of $[HO_2^{\bullet}/O_2^{\bullet-}]_0$ (i.e., at $[HO_2^{\bullet}/O_2^{\bullet-}]_0/[FAC]_0 \geq 1$). Note that contributions of RCS to formaldehyde formation can be neglected, as HO$^{\bullet}$ is the precursor of the RCS, and its scavenging by *t*-BuOH would have precluded RCS formation via eqs 1.9-1.15.

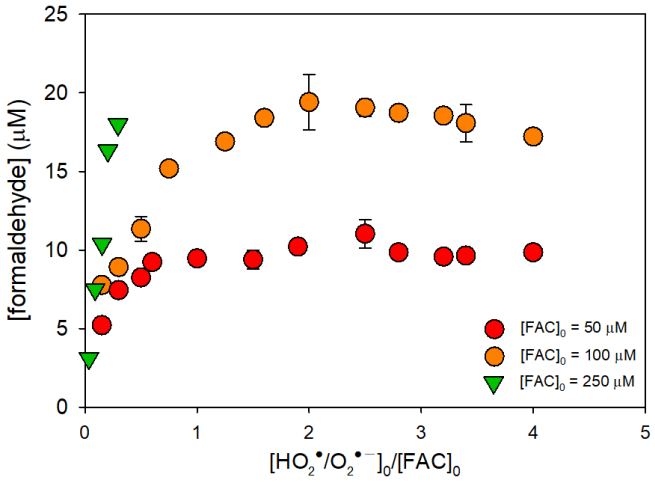

Figure 2.10. Formaldehyde concentrations formed in solutions of pH 7, 50mM phosphate buffer containing $[t\text{-BuOH}]_0$ = 50 mM and $[FAC]_0$ = 50, 100, or 250 μM following single-dose postmix $O_2^{\bullet-}$/FAC treatment with increasing concentrations of $[HO_2^{\bullet}/O_2^{\bullet-}]_0$. All concentrations were background-corrected for low formaldehyde concentrations (<2 μM) observed in controls subjected to $HO_2^{\bullet}/O_2^{\bullet-}$ and H_2O_2/HO_2^- only, FAC only, and H_2O_2/HO_2^- only treatments – apparently arising as impurities from *t*-BuOH stocks, phosphate salts, and/or Hantzsch method reagents. Error bars represent one standard deviation about the mean of duplicate measurements. Adopted from (Liou and Dodd, 2021).

In these experiments, $[t\text{-BuOH}]_0$ = 50 mM would have been sufficient to scavenge ≥90% of $HO^{\bullet}$, except at the highest $[HO_2^{\bullet}/O_2^{\bullet-}]_0$ applied (at which $f(HO^{\bullet})$ – the fraction of total generated $HO^{\bullet}$ scavenged by *t*-BuOH – would have been equal to 0.88) (Figure 2.10, Text S2.2). Based on a reported molar yield of ~25% for formaldehyde formation from reaction of $HO^{\bullet}$ with *t*-BuOH (Flyunt et al., 2003; Schuchmann and Von Sonntag, 1979), and an apparent plateau value of ~0.2 mol formaldehyde formed/mol FAC consumed in Figure 2.10, an estimated yield of ~0.8 mol $HO^{\bullet}$ formed/mol FAC consumed was obtained for the $O_2^{\bullet-}$/FAC reaction under the conditions applied here. This is lower than the theoretical yield of 1 mol $HO^{\bullet}$/mol FAC (eq 1.7), and may represent an underestimate due to (a) uncertainties in formaldehyde yield from *t*-BuOH in the presence of oxidants other than $HO^{\bullet}$ (Flyunt et al., 2003), and/or (b) inhibition of formaldehyde formation by reaction of excess $HO_2^{\bullet}/O_2^{\bullet-}$ with the primary peroxyl radical formed in reaction of $HO^{\bullet}$ with *t*-BuOH (Schuchmann and Von Sonntag, 1979).

2.3.3 Effects of pH

Little variation in pCBA degradation was observed during $O_2^{\bullet-}$/FAC treatment at pH 7, 8, 9, and 10 (Figure 2.11). The small apparent decrease in pCBA degradation at pH>7 may have been attributable to (a) an increase in $k_{app,HO_2^{\bullet}/O_2^{\bullet-},DP}$ relative to $k_{app,O_2^{\bullet-}/FAC}$ – leading to increased loss of $HO_2^{\bullet}/O_2^{\bullet-}$ via disproportionation (eqs 1.3-1.4), and/or (b) a shift in speciation from HOCl to OCl^- (pK_a = 7.5 (Morris, 1966)) – leading to increased scavenging of $HO^{\bullet}$ by the latter (eqs 1.9-1.10). Although subsequent discussion focuses on $O_2^{\bullet-}$/FAC treatment at pH 7, these findings indicate comparable effectiveness could be achievable at other pH values.

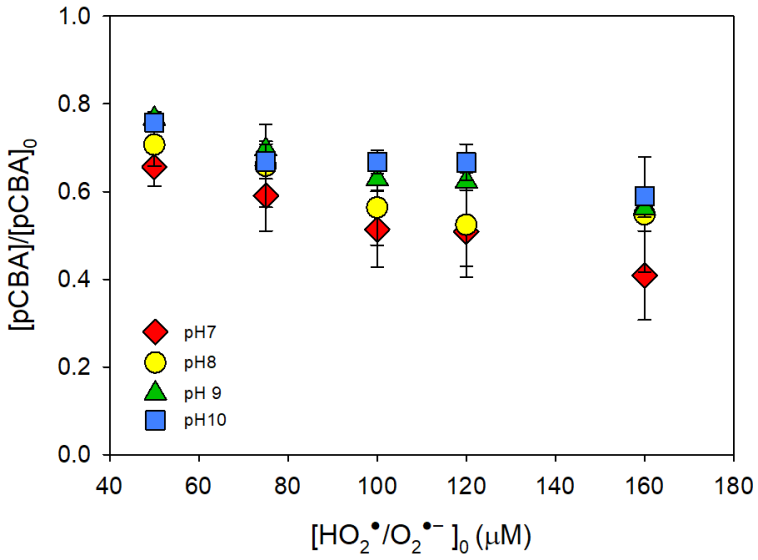

Figure 2.11. pCBA concentrations resulting from single-dose postmix $O_2^{\bullet-}$/FAC treatment of solutions containing $[pCBA]_0$ = 1 μM and $[FAC]_0$ = 200 μM with $[HO_2^{\bullet}/O_2^{\bullet-}]_0$ = 50-160 μM at pH 7, 8, 9, and 10, with pH buffering provided by 50mM phosphate (pH 7 and 8) or borate (pH 9 and 10). Error bars represent one standard deviation about the mean of duplicate measurements. Adopted from (Liou and Dodd, 2021).

2.3.4 Effects of $[HO_2^{\bullet}/O_2^{\bullet-}]_0/[FAC]_0$ and Absolute Values of $[HO_2^{\bullet}/O_2^{\bullet-}]_0$ and $[FAC]_0$

Due to (a) the dependence of $HO^{\bullet}$ yield on $[HO_2^{\bullet}/O_2^{\bullet-}]_0$ and $[FAC]_0$, and (b) the rapid reactions of $HO^{\bullet}$ with FAC and $HO_2^{\bullet}/O_2^{\bullet-}$ (eqs 1.9-1.10 and 2.27-2.28, respectively),

$$HO^{\bullet} + HO_2^{\bullet} \rightarrow H_2O + O_2 \qquad k_{2.27} = 7.1\times10^{9}\ M^{-1}s^{-1}\ \text{(Sehested et al., 1968)} \quad (2.27)$$

$$HO^{\bullet} + O_2^{\bullet-} \rightarrow OH^{-} + O_2 \qquad k_{2.28} = 1.0\times10^{10}\ M^{-1}s^{-1}\ \text{(Sehested et al., 1968)} \quad (2.28)$$

both *relative* and *absolute* concentrations of $[HO_2^{\bullet}/O_2^{\bullet-}]_0$ and $[FAC]_0$ may influence probe degradation and radical exposures, $\int_0^t [\text{radical}]\,dt$, during $O_2^{\bullet-}$/FAC treatment. NB, BA, DMB, and pCBA degradation were in turn evaluated over a range of $[HO_2^{\bullet}/O_2^{\bullet-}]_0$ and $[FAC]_0$ at

$[HO_2^{\bullet}/O_2^{\bullet-}]_0/[FAC]_0$ ranging from 0.2-7.5, in order to evaluate resulting variations in $\int_0^t [\text{radical}]\,dt$ and identify optimal $O_2^{\bullet-}$/FAC treatment conditions.

As shown in Figures 2.12 and 2.13, in single-dose postmix experiments, the extents of NB, BA, DMB, and pCBA degradation, expressed here as change in probe compound concentration normalized to initial probe compound concentration, or $\Delta[\text{probe}]/[\text{probe}]_0$ (where probe = NB, BA, DMB, or pCBA), increased with increasing $[HO_2^{\bullet}/O_2^{\bullet-}]_0/[FAC]_0$ up to maxima at $[HO_2^{\bullet}/O_2^{\bullet-}]_0/[FAC]_0 \sim 2$, beyond which $\Delta[\text{probe}]/[\text{probe}]_0$ decreased with increasing $[HO_2^{\bullet}/O_2^{\bullet-}]_0/[FAC]_0$. Furthermore, when holding $[HO_2^{\bullet}/O_2^{\bullet-}]_0/[FAC]_0$ fixed at 2, $\Delta[\text{probe}]/[\text{probe}]_0$ generally increased as $[HO_2^{\bullet}/O_2^{\bullet-}]_0$ and $[FAC]_0$ were increased in tandem up to ~200 and 100 μM, respectively, beyond which further increases in $[HO_2^{\bullet}/O_2^{\bullet-}]_0$ and $[FAC]_0$ appeared to yield diminishing improvement. The observed maximal levels of $\Delta[\text{probe}]/[\text{probe}]_0$ for single-dosing of $[HO_2^{\bullet}/O_2^{\bullet-}]_0$ = 200 μM and $[FAC]_0$ = 100 μM translated to calculated exposures of ~2-3×10^{-10} M×s for both $\int_0^t [HO^{\bullet}]\,dt$ and $\int_0^t [ClO^{\bullet}/Cl_2^{\bullet-}]\,dt$, and ~$10^{-11}$ M×s for $\int_0^t [Cl^{\bullet}]\,dt$, though with wider ranges apparent for $ClO^{\bullet}/Cl_2^{\bullet-}$ and $Cl^{\bullet}$ – due in part to greater uncertainties in the small changes in probe concentrations from which these latter exposures were determined. Furthermore, it is important to note that the values of $\int_0^t [\text{radical}]\,dt$ determined here do not account for uncertainties associated with the rate constants used in their determination (see Section 2.2.5 for rate constants), as the lack of reported error bounds for most of the associated rate constants precludes quantification of such uncertainties. They are thus most appropriately interpreted as estimates, rather than exact values of $\int_0^t [\text{radical}]\,dt$. Details

regarding uncertainties in calculating radical exposures are discussed thoroughly in the Supporting Information Text S2.4.

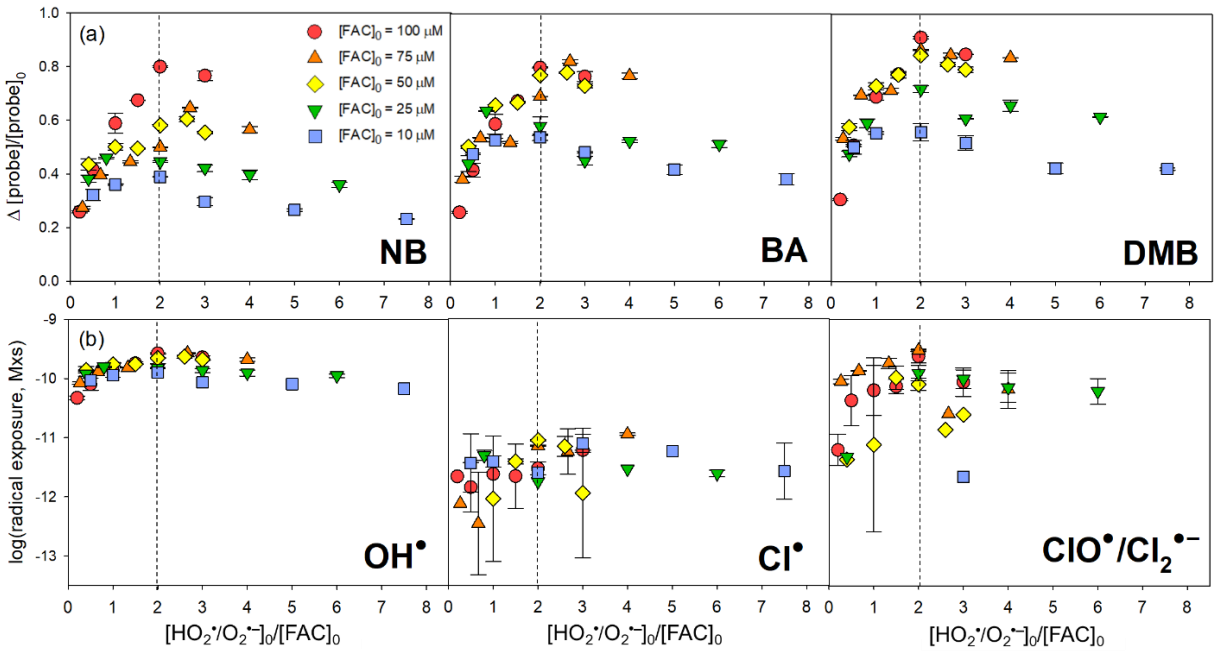

Figure 2.12. Effects of $[HO_2^{\bullet}/O_2^{\bullet-}]_0$, $[FAC]_0$, and $[HO_2^{\bullet}/O_2^{\bullet-}]_0/[FAC]_0$ ratio on (a) extent of probe compound degradation ($\Delta[probe]/[probe]_0$), and (b) in situ radical exposures ($\int_0^t [radical]\,dt$), during single-dose, post-mix $O_2^{\bullet-}$/FAC treatment of pH 7, 50mM phosphate buffer containing [NB, BA, DMB]$_0$ = 1 μM. Solutions were treated with variable concentrations of $[HO_2^{\bullet}/O_2^{\bullet-}]_0$ = 5-300 μM and $[FAC]_0$ = 10-100 μM. Error bars represent one standard deviation about the mean of duplicate measurements. Adopted from (Liou and Dodd, 2021).

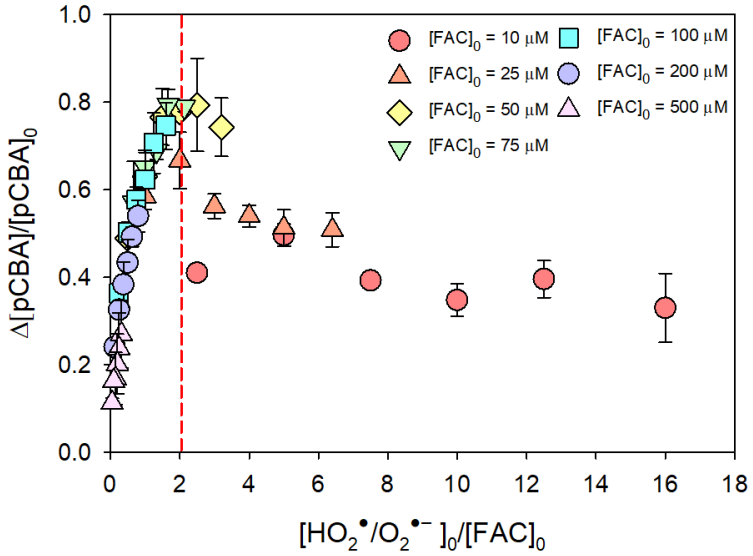

Figure 2.13. Effects of $[HO_2^{\bullet}/O_2^{\bullet-}]_0$, $[FAC]_0$, and $[HO_2^{\bullet}/O_2^{\bullet-}]_0/[FAC]_0$ ratio on extent of pCBA degradation ($\Delta[pCBA]/[pCBA]_0$) during single-dose, postmix $O_2^{\bullet-}$/FAC treatment of pH 7, 50mM phosphate buffer containing $[pCBA]_0$ = 1 μM. Solutions were treated with variable concentrations of $[HO_2^{\bullet}/O_2^{\bullet-}]_0$ = 25-160 μM and $[FAC]_0$ = 10-500 μM. Error bars represent one standard deviation about the mean of duplicate measurements. Adopted from (Liou and Dodd, 2021).

Similar to HO• *yields*, HO• *exposures* (and $\Delta[probe]/[probe]_0$) increased with increasing $[HO_2^{\bullet}/O_2^{\bullet-}]_0/[FAC]_0$ up to a maximum. However, maximal HO• exposures and $\Delta[probe]/[probe]_0$ were observed at $[HO_2^{\bullet}/O_2^{\bullet-}]_0/[FAC]_0 \sim 2$, rather than at $[HO_2^{\bullet}/O_2^{\bullet-}]_0/[FAC]_0 \sim 1$ as in the case HO• *yields*. This likely reflects a combination of increasing FAC conversion to HO• via eq 1.7 as $[HO_2^{\bullet}/O_2^{\bullet-}]_0$ is increased, coupled with consumption of $HO_2^{\bullet}/O_2^{\bullet-}$ by HO• (eqs 2.27-2.28). Without the presence of 50mM *t*-BuOH to block eqs 2.27-2.28 (as in the yield measurements), they would divert available $HO_2^{\bullet}/O_2^{\bullet-}$ away from eq 1.7 – in turn raising the $[HO_2^{\bullet}/O_2^{\bullet-}]_0/[FAC]_0$ ratio required for full conversion of FAC by $HO_2^{\bullet}/O_2^{\bullet}$. The observed decrease in HO• exposures and $\Delta[probe]/[probe]_0$ at $[HO_2^{\bullet}/O_2^{\bullet-}]_0/[FAC]_0 \geq 2$ likely reflects increasing scavenging of HO• by excess $HO_2^{\bullet}/O_2^{\bullet-}$ via eqs 2.27-2.28 as $[HO_2^{\bullet}/O_2^{\bullet-}]_0/[FAC]_0$ is further increased beyond the optimum ratio. The observed trends in $ClO^{\bullet}/Cl_2^{\bullet-}$ and Cl• exposures vs $[HO_2^{\bullet}/O_2^{\bullet-}]_0/[FAC]_0$ (Figure 2.12) can be similarly explained, as each RCS ultimately originates from HO•, via eqs

1.9-1.15. Based on these findings, a ratio of $[HO_2^{\bullet}/O_2^{\bullet-}]_0/[FAC]_0 = 2$ was selected for use in most subsequent experiments.

In addition to the $HO^{\bullet}$ and RCS exposure optimum at $[HO_2^{\bullet}/O_2^{\bullet-}]_0/[FAC]_0 \sim 2$, and the general increase in $HO^{\bullet}$ exposure with increasing $[HO_2^{\bullet}/O_2^{\bullet-}]_0$ and $[FAC]_0$ at fixed $[HO_2^{\bullet}/O_2^{\bullet-}]_0/[FAC]_0$, it is noteworthy that $ClO^{\bullet}/Cl_2^{\bullet-}$ exposures and their relative contributions to degradation of the $ClO^{\bullet}/Cl_2^{\bullet-}$–reactive probe DMB generally increased with increasing $[FAC]_0$ up to an apparent maximum at $[FAC]_0 \sim 75$ μM (Figures 2.12 and 2.14). This is likely attributable to increasing formation of $ClO^{\bullet}$ and/or $Cl_2^{\bullet-}$ via eqs 1.9-1.15 with increasing $[FAC]_0$ (and associated background $[Cl^-]_0$ in FAC stocks) up to ~75 μM, beyond which disproportionation of $ClO^{\bullet}$ and/or $Cl_2^{\bullet-}$ (eqs 2.29-2.30) may predominate.

$$ClO^{\bullet} + ClO^{\bullet} \xrightarrow{H_2O} ClO_2^- + OCl^- + 2H^+ \qquad k_{2.29} = 2.5\times10^9\ M^{-1}s^{-1}\ \text{(Kläning and Wolff, 1985)} \qquad (2.29)$$

$$Cl_2^{\bullet-} + Cl_2^{\bullet-} \rightarrow Cl_2 + 2Cl^- \qquad k_{2.30} = 3.5\times10^9\ M^{-1}s^{-1}\ \text{(Yu, 2004)} \qquad (2.30)$$

The increasing importance of $ClO^{\bullet}/Cl_2^{\bullet-}$ relative to $HO^{\bullet}$ at higher $[FAC]_0$, and potential formation of ClO_2^- (a regulated DBP) via eq 2.29, suggest that there may be benefit to implementing $O_2^{\bullet-}$/FAC treatment at lower $[FAC]_0$ if possible (as discussed in Section 2.3.6).

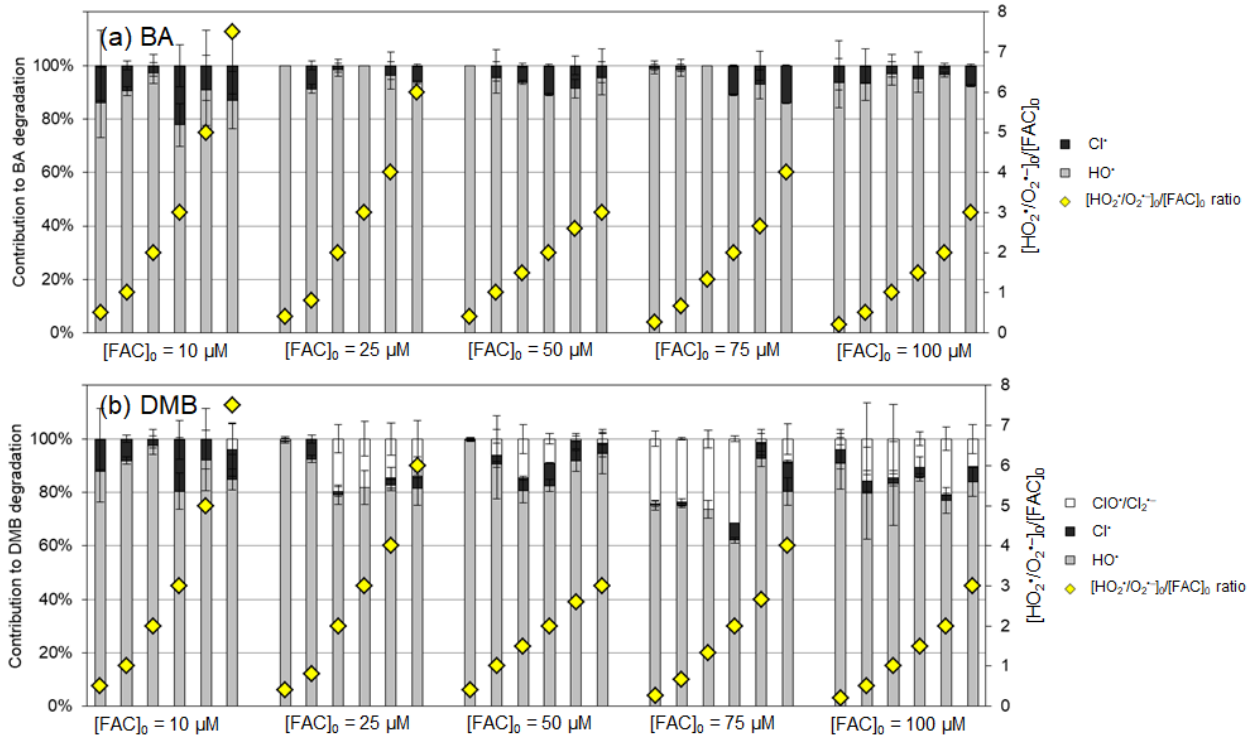

Figure 2.14. Effects of $[HO_2^{\bullet}/O_2^{\bullet-}]_0$, $[FAC]_0$, and $[HO_2^{\bullet}/O_2^{\bullet-}]_0/[FAC]_0$ ratios on fractional contributions of $HO^{\bullet}$ and $Cl^{\bullet}$ to BA degradation, and of $HO^{\bullet}$, $Cl^{\bullet}$, $ClO^{\bullet}/Cl_2^{\bullet-}$ to DMB degradation, during single-dose postmix $O_2^{\bullet-}$/FAC treatment of pH 7 phosphate-buffered solutions containing $[NB, BA, DMB]_0$ = 1 µM. Solutions were treated with variable concentrations of $[HO_2^{\bullet}/O_2^{\bullet-}]_0$ = 5-300 µM and $[FAC]_0$ = 10-100 µM. Error bars represent one standard deviation about the mean of duplicate measurements. Adopted from (Liou and Dodd, 2021).

2.3.5 Postmix versus Premix Dosing of $O_2^{\bullet-}$ and FAC

All results discussed to this point were obtained by adding alkaline $O_2^{\bullet-}$ stocks to buffered receiving solutions containing probes and FAC (postmix dosing). As noted in Section 2.2.3, it is also possible to prepare relatively stable ($t_{1/2,O2^{\bullet-},FAC}$ > 60 s) premixed $O_2^{\bullet-}$ and FAC stocks at pH>12. This can simplify $O_2^{\bullet-}$/FAC treatment by enabling addition of premixed $O_2^{\bullet-}$/FAC to receiving solutions as a single stock, with rapid conversion of the stock to $HO^{\bullet}$ and RCS at the lower pH of the receiving solution (premix dosing). This has the added benefit of preventing heterogeneities in $[HO_2^{\bullet}/O_2^{\bullet-}]_0/[FAC]_0$ that may result from non-ideal mixing of separate $O_2^{\bullet-}$ and FAC solutions during postmix dosing. A comparison of results for postmix and

premix dosing at $[HO_2^{\bullet}/O_2^{\bullet-}]_0/[FAC]_0$ = (200 μM)/(100 μM) is shown in Figure 2.15 (see the two groups of measurements designated by red 1×100 μM labels). As apparent from the figure, postmix and premix dosing yielded similar radical exposures and $\Delta[probe]/[probe]_0$, confirming the utility of the premix dosing approach.

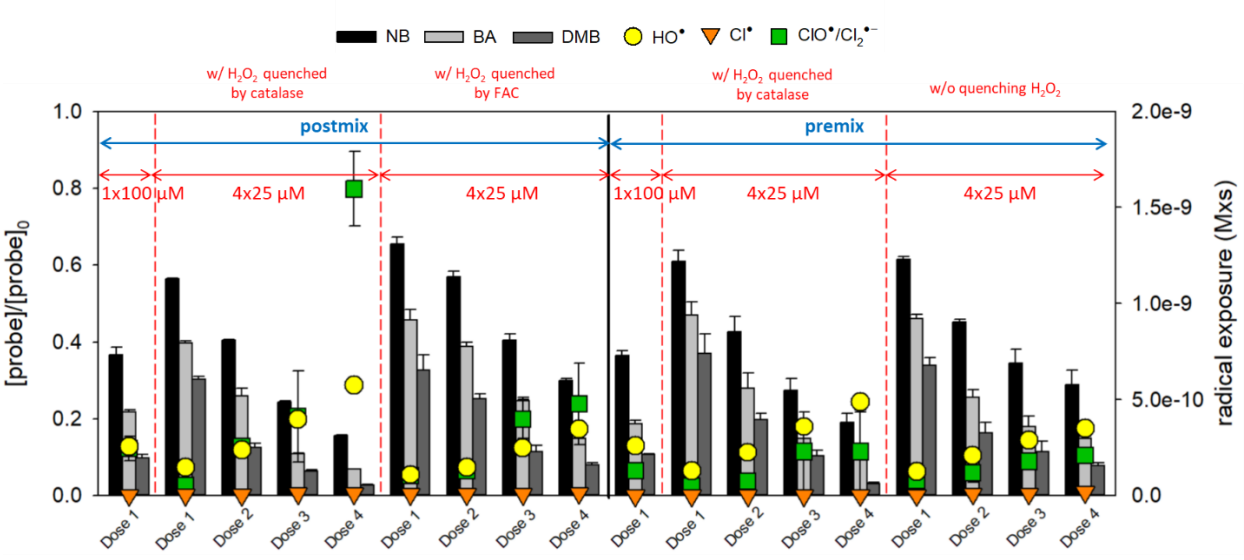

Figure 2.15. Probe compound concentrations and in situ radical exposures ($\int_0^t [\text{radical}]\,dt$) resulting from multiple-dose postmix and premix $O_2^{\bullet-}$/FAC treatment of pH 7, 50mM phosphate buffer containing $[NB, BA, DMB]_0$ = 1 μM, with or without removal of residual H_2O_2/HO_2^-, where H_2O_2/HO_2^- removal was achieved by either catalase or FAC treatment after each $O_2^{\bullet-}$ or $O_2^{\bullet-}$/FAC dose. When using FAC to remove H_2O_2/HO_2^-, residual H_2O_2/HO_2^- concentrations were first measured by the Allen reagent method, after which sufficient FAC was added to scavenge all H_2O_2/HO_2^- and leave the desired [FAC] residual in solution for the following $O_2^{\bullet-}$ dose. Experiments were undertaken by dosing $[HO_2^{\bullet}/O_2^{\bullet-}]_0/[FAC]_0$ = (50 μM)/(25 μM) four times (4×25 μM). Error bars represent one standard deviation about the mean of duplicate measurements. Adopted from (Liou and Dodd, 2021).

2.3.6 Single-dose versus Multiple-dose $O_2^{\bullet-}$/FAC Treatment

As noted in Section 2.3.4, increased radical exposures and contaminant degradation may be achievable by implementing $O_2^{\bullet-}$/FAC treatment at lower $[FAC]_0$ and $[HO_2^{\bullet}/O_2^{\bullet-}]_0$, due to consequent decreases in $HO^{\bullet}$ scavenging by FAC (eqs 1.9-1.10) and by H_2O_2/HO_2^- (eqs 2.6-2.9)

associated with $O_2^{\bullet-}$ stocks. This may also lead to decreased $HO^{\bullet}$ scavenging by $HO_2^{\bullet}/O_2^{\bullet-}$ (eqs 2.27-2.28). One means of undertaking such an approach is to dose $O_2^{\bullet-}$ and FAC repeatedly (or continuously) at lower concentrations (*multiple-dosing*), rather than once at higher concentrations (*single-dosing*). To investigate this, $\Delta[probe]/[probe]_0$ and radical exposures were measured when applying $O_2^{\bullet-}$ and FAC via several *multiple-dose* postmix treatment approaches: (a) twice at $[HO_2^{\bullet}/O_2^{\bullet-}]_0/[FAC]_0$ = (100 μM)/(50 μM) (henceforth designated as 2×50 μM, with the 50 μM referring to applied $[FAC]_0$), (b) four times at $[HO_2^{\bullet}/O_2^{\bullet-}]_0/[FAC]_0$ = (50 μM)/(25 μM) (i.e., 4×25 μM), and (c) ten times at $[HO_2^{\bullet}/O_2^{\bullet-}]_0/[FAC]_0$ = (20 μM)/(10 μM) (i.e., 10×10 μM). Receiving solutions were treated with catalase after each $O_2^{\bullet-}$ dosing step to completely remove H_2O_2/HO_2^- derived from $O_2^{\bullet-}$ stocks, and FAC was then added into the receiving solutions for the subsequent step. Without H_2O_2/HO_2^- quenching beforehand, FAC added to the receiving solutions would have first been consumed via the direct reaction with H_2O_2/HO_2^- (eq 2.13). The removal of residual H_2O_2/HO_2^- between $O_2^{\bullet-}$ dosing steps was thus necessary to enable the use of postmix $O_2^{\bullet-}$ dosing, which requires the presence of FAC in receiving solutions prior to $O_2^{\bullet-}$ addition.

Measurements obtained from these multiple-dose postmix treatments were then compared to measurements obtained when applying $O_2^{\bullet-}$ and FAC via *single-dose* postmix treatment at $[HO_2^{\bullet}/O_2^{\bullet-}]_0/[FAC]_0$ = (200 μM)/(100 μM) (i.e., 1×100 μM). In all four cases, the total (cumulative) levels of $[HO_2^{\bullet}/O_2^{\bullet-}]_{0,tot}$ and $[FAC]_{0,tot}$ applied summed to 200 μM and 100 μM, respectively.

As shown in Figure 2.16, increased $\int_0^t \left[HO^{\bullet}\right] dt$ and $\Delta[probe]/[probe]_0$ were observed when applying lower $[HO_2^{\bullet}/O_2^{\bullet-}]_0$ and $[FAC]_0$ in multiple doses to achieve the same cumulative

$[HO_2^{\bullet}/O_2^{\bullet-}]_{0,tot}$ and $[FAC]_{0,tot}$ levels as in a single dose. In general, higher $\int_0^t [HO^{\bullet}]dt$ and $\Delta[probe]/[probe]_0$ were observed at lower $[HO_2^{\bullet}/O_2^{\bullet-}]_0$ and $[FAC]_0$, with $\int_0^t [HO^{\bullet}]dt$ and $\Delta[probe]/[probe]_0$ for the single- and multiple-dosing approaches ranked in the order 10×10 μM ~ 4×25 μM > 2×50 μM > 1×100 μM (Figures 16 and 17). The effects of multiple-dosing on $\int_0^t [ClO^{\bullet}/Cl_2^{\bullet-}]dt$ and $\int_0^t [Cl^{\bullet}]dt$ were less clear, due to higher uncertainties associated with these values (Figure 2.16).

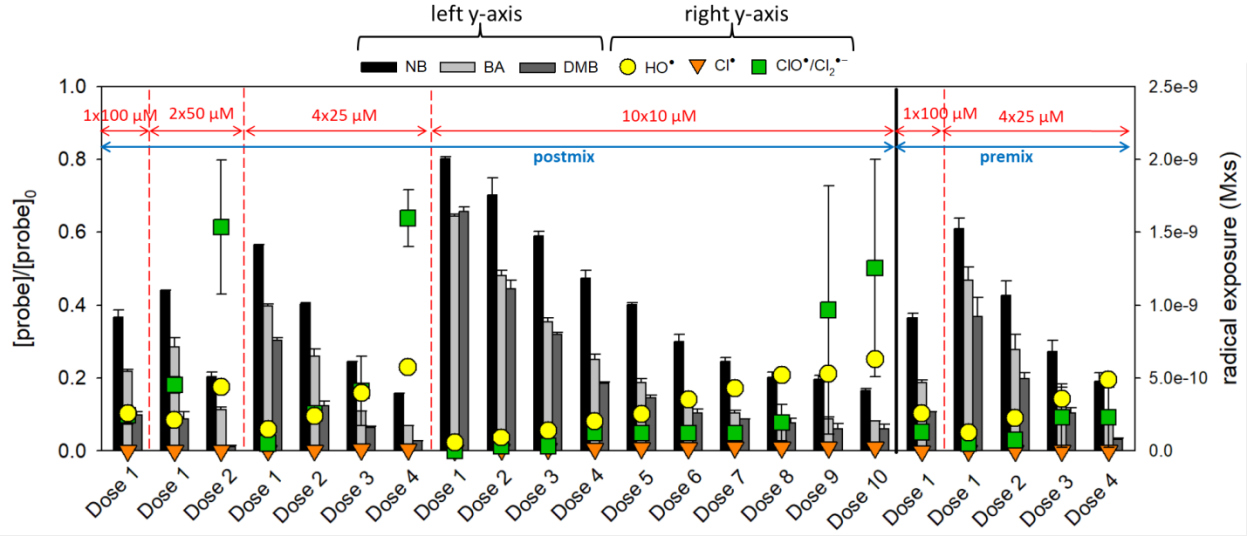

Figure 2.16. Probe compound concentrations and in situ radical exposures ($\int_0^t [radical]dt$) resulting from single- and multiple-dose postmix and premix $O_2^{\bullet-}$/FAC treatment of pH 7, 50mM phosphate buffer containing [NB, BA, DMB]$_0$ = 1 μM, with removal of residual H_2O_2/HO_2^- by catalase after each dosing step in multiple-dose experiments. Single-dose experiments were undertaken by dosing $[HO_2^{\bullet}/O_2^{\bullet-}]_0/[FAC]_0$ = (200 μM)/(100 μM) once (1×100 μM), and multiple-dose experiments by dosing $[HO_2^{\bullet}/O_2^{\bullet-}]_0/[FAC]_0$ = (100 μM)/(50 μM) twice (2×50 μM), $[HO_2^{\bullet}/O_2^{\bullet-}]_0/[FAC]_0$ = (50 μM)/(25 μM) four times (4×25 μM), or $[HO_2^{\bullet}/O_2^{\bullet-}]_0/[FAC]_0$ = (20 μM)/(10 μM) ten times (10×10 μM). Error bars represent one standard deviation about the mean of duplicate measurements. Adopted from (Liou and Dodd, 2021).

It is important to note that the use of catalase as a H_2O_2/HO_2^- quenching agent is not likely to be practical for water/wastewater treatment. As a more practical alternative, the removal

of H_2O_2/HO_2^- can also be achieved simply by reaction with excess FAC. To investigate this, further multiple-dose postmix experiments were undertaken in which FAC was added to receiving solutions between $O_2^{\bullet-}$ dosing steps at concentration sufficient to consume all H_2O_2/HO_2^-, while also leaving a desired level of FAC residual for subsequent reactions with $O_2^{\bullet-}$. Analogous results were obtained when applying 4×25 μM multiple-dose postmix treatment with H_2O_2/HO_2^- quenched by FAC instead of catalase after each dosing step (eq 2.13), though $\int_0^t \left[HO^\bullet\right] dt$ and $\Delta[\text{probe}]/[\text{probe}]_0$ levels were somewhat lower than when using catalase for H_2O_2/HO_2^- quenching (Figure 2.16). This may reflect the presence of higher levels of background $HO^\bullet$ scavengers (e.g., Cl^-; eqs 1.11-1.15) originating from FAC stocks – due to use of elevated FAC concentrations to quench H_2O_2/HO_2^-. Experiments using pCBA as a probe and FAC to quench H_2O_2/HO_2^- yielded similar results (Figure 2.17).

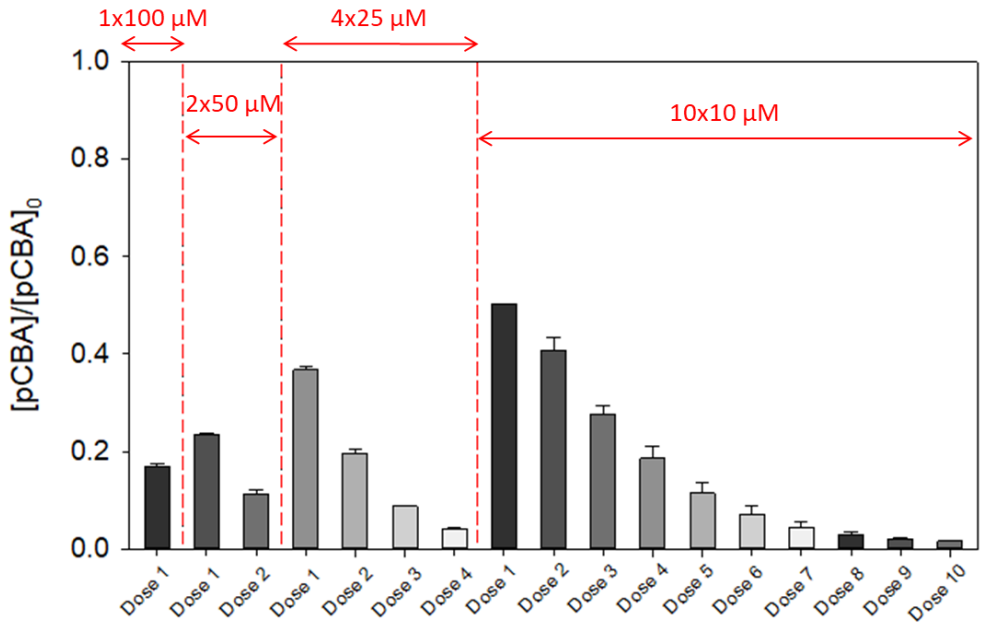

Figure 2.17. pCBA concentrations resulting from single- and multiple-dose postmix $O_2^{\bullet-}$/FAC treatment of pH 7, 50mM phosphate buffer containing $[pCBA]_0$ = 1 µM, with removal of residual H_2O_2/HO_2^- by FAC treatment after each $O_2^{\bullet-}$ dose. For removal of H_2O_2/HO_2^-, residual H_2O_2/HO_2^- concentrations were first measured by the Allen reagent method, after which sufficient FAC was added to scavenge all H_2O_2 and leave the desired [FAC] residual in solution for the following $O_2^{\bullet-}$ dose. Single-dose experiments were undertaken by dosing $[HO_2^{\bullet}/O_2^{\bullet-}]_0/[FAC]_0$ = (200 µM)/(100 µM) once (1×100 µM), and multiple-dose experiments by dosing $[HO_2^{\bullet}/O_2^{\bullet-}]_0/[FAC]_0$ = (100 µM)/(50 µM) twice (2×50 µM), $[HO_2^{\bullet}/O_2^{\bullet-}]_0/[FAC]_0$ = (50 µM)/(25 µM) four times (4×25 µM), or $[HO_2^{\bullet}/O_2^{\bullet-}]_0/[FAC]_0$ = (20 µM)/(10 µM) ten times (10×10 µM). Error bars represent one standard deviation about the mean of duplicate measurements. Adopted from (Liou and Dodd, 2021).

Additional experiments were undertaken to investigate the use of premixed $O_2^{\bullet-}$/FAC stocks in multiple-dosing approaches. As observed for postmix treatment, 4×25 µM multiple-dose premix treatment yielded increased $\int_0^t [HO^{\bullet}]\,dt$ and $\Delta[probe]/[probe]_0$ compared to 1×100 µM single-dose premix treatment when H_2O_2/HO_2^- was quenched with catalase after each dosing step (Figure 2.16). However, lower $\int_0^t [HO^{\bullet}]\,dt$ and $\Delta[probe]/[probe]_0$ were observed when H_2O_2/HO_2^- was not quenched after each dosing step (Figure 2.16), likely due to $HO^{\bullet}$ scavenging by H_2O_2/HO_2^-, as discussed in more detail below.

2.3.7 Effects of $[H_2O_2/HO_2^-]_0$

Due to $HO_2^\bullet/O_2^{\bullet-}$ disproportionation (eqs 1.3-1.4), $[H_2O_2/HO_2^-]$ was always present in $O_2^{\bullet-}$ stocks. As H_2O_2/HO_2^- can scavenge $HO^\bullet$ (eqs 2.6-2.9) and RCS (eqs 2.31-2.32), it may in turn lower $HO^\bullet$ and RCS exposures during $O_2^{\bullet-}$/FAC treatment.

$$Cl^\bullet + H_2O_2 \rightarrow HO_2^\bullet + Cl^- + H^+ \qquad k_{2.31} = 2 \times 10^9\ M^{-1}s^{-1}\ \text{(Yu, 2004)} \qquad (2.31)$$

$$Cl_2^{\bullet-} + H_2O_2 \rightarrow HO_2^\bullet + 2Cl^- + H^+ \qquad k_{2.32} \sim 10^5\text{-}10^6\ M^{-1}s^{-1}\ \text{(Yu, 2004)} \qquad (2.32)$$

To investigate this, probe degradation was examined during premix dosing of $[HO_2^\bullet/O_2^{\bullet-}]_0/[FAC]_0$ = (200 μM)/(100 μM) to phosphate buffer pre-amended with varying $[H_2O_2/HO_2^-]_0$. Measured $HO^\bullet$ and $ClO^\bullet/Cl_2^{\bullet-}$ exposures were then examined versus total in situ concentrations, $[H_2O_2/HO_2^-]_{0,tot}$, comprising the sum of pre-amended $[H_2O_2/HO_2^-]_0$ plus $[H_2O_2/HO_2^-]_0$ derived from the $O_2^{\bullet-}$/FAC stock ($Cl^\bullet$ exposures were not included in this comparison, due to their large uncertainties). As shown in Figure 2.18, $HO^\bullet$ and $ClO^\bullet/Cl_2^{\bullet-}$ exposures decreased linearly with increasing $[H_2O_2/HO_2^-]_{0,tot}$, with a nearly constant ratio of $\int_0^t \left[HO^\bullet\right] dt \Big/ \int_0^t \left[ClO^\bullet/Cl_2^{\bullet-}\right] dt$ ~ 3.6-3.7 maintained over the range of $[H_2O_2/HO_2^-]_{0,tot}$ investigated. Extrapolation of the regression lines for $\int_0^t \left[HO^\bullet\right] dt$ and $\int_0^t \left[ClO^\bullet/Cl_2^{\bullet-}\right] dt$ to $[H_2O_2/HO_2^-]_{0,tot} = 0$ indicates that in the absence of H_2O_2/HO_2^-, the $HO^\bullet$ and $ClO^\bullet/Cl_2^{\bullet-}$ exposures would be ~10-20% higher than at the lowest $[H_2O_2/HO_2^-]_{0,tot}$ investigated (i.e., $[H_2O_2/HO_2^-]_{0,tot}$ ~ 700 μM, which represents H_2O_2/HO_2^- originating solely from the $O_2^{\bullet-}$ stock). These findings suggest that (a) minimizing H_2O_2/HO_2^- formation within $O_2^{\bullet-}$ stocks (which could also lead to improved stability of $O_2^{\bullet-}$), and/or (b) undertaking $O_2^{\bullet-}$/FAC treatment at lower

total $[HO_2^{\bullet}/O_2^{\bullet-}]_0$, may enable further increases in $HO^{\bullet}$ and RCS exposures and contaminant degradation.

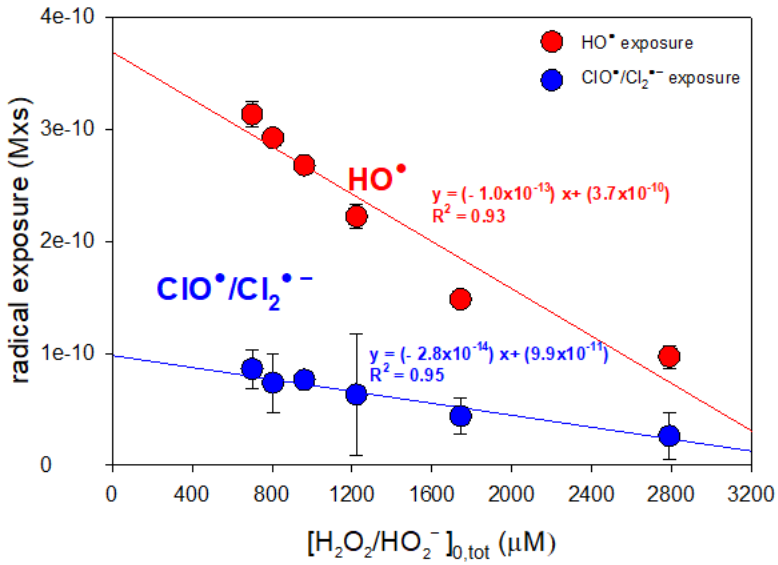

Figure 2.18. In situ $HO^{\bullet}$ and $ClO^{\bullet}/Cl_2^{\bullet-}$ exposures ($\int_0^t [HO^{\bullet}]dt$ and $\int_0^t [ClO/Cl_2^{\bullet-}]dt$) resulting from single-dose premix $O_2^{\bullet-}$/FAC treatment of pH 7, 50mM phosphate-buffered solutions pre-amended with $[H_2O_2/HO_2^-]_0$ = 0-2100 μM and [NB, BA, DMB]$_0$ = 1 μM, at $[HO_2^{\bullet}/O_2^{\bullet-}]_0$/[FAC]$_0$ = (200 μM)/(100 μM). Error bars represent one standard deviation about the mean of duplicate measurements. The x-axis represents $[H_2O_2/HO_2^-]_{0,tot}$, which is the sum of pre-amended $[H_2O_2/HO_2^-]_0$ and $[H_2O_2/HO_2^-]_0$ from the KO_2 stock. The solid lines were obtained by linear least squares regressions of the $\int_0^t [HO^{\bullet}]dt$ and $\int_0^t [ClO/Cl_2^{\bullet-}]dt$ values obtained for each sample versus $[H_2O_2/HO_2^-]_{0,tot}$. Adopted from (Liou and Dodd, 2021).

2.3.8 Effects of Dissolved Organic Matter (DOM) and Application to Natural Waters

To investigate the influence of DOM on $HO^{\bullet}$ and RCS exposures, probe degradation was examined by premix dosing of $O_2^{\bullet-}$/FAC to (a) phosphate buffer amended with varying concentrations of SRNOM, and (b) two natural water samples collected from a Local Reservoir and Lake Washington (see Table S2.4 for key water quality parameters). As shown in Figure

2.19, radical exposures and $\Delta[probe]/[probe]_0$ were greater at higher $[HO_2^{\bullet}/O_2^{\bullet-}]_0$ and $[FAC]_0$, but inhibited by increasing DOC concentrations. This is consistent with the anticipated scavenging of $HO^{\bullet}$, $Cl^{\bullet}$, $ClO^{\bullet}$, and $Cl_2^{\bullet-}$ by DOM (Brigante et al., 2014; Fang et al., 2014; Lei et al., 2019; Rosario-Ortiz et al., 2008; Westerhoff et al., 2007; Wu et al., 2017). Contributions of phosphate species to scavenging were negligible (Text S2.5). Nevertheless, these findings demonstrate that relatively high $HO^{\bullet}$ and RCS exposures and contaminant degradation can still be achieved over DOC concentration ranges representative of drinking waters and potable reuse. Wastewaters usually contain more DOM and transition metals, which can scavenge radicals and lower the treatment efficiency.

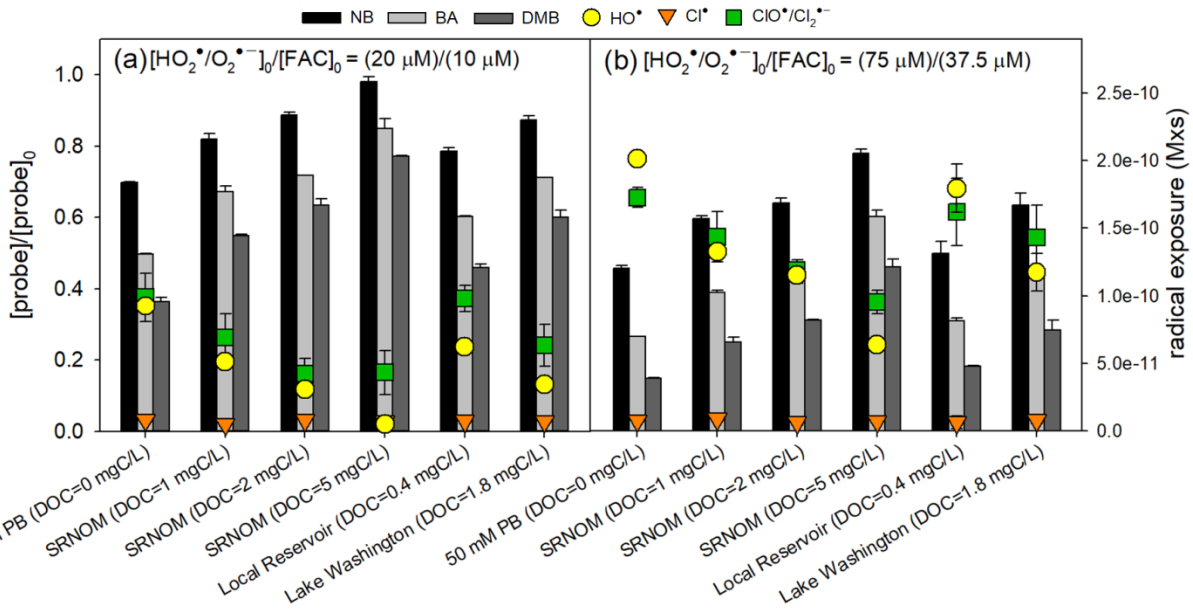

Figure 2.19. Probe compound concentrations and in situ radical exposures ($\int_0^t [\text{radical}]\,dt$) resulting from single-dose premix $O_2^{\bullet-}$/FAC treatment of SRNOM-amended pH 7, 50mM phosphate buffer or 50mM phosphate-buffered natural water samples containing [NB, BA, DMB]$_0$ = 1 μM at (a) $[HO_2^{\bullet}/O_2^{\bullet-}]_0/[FAC]_0$ = (20 μM)/(10 μM) or (b) $[HO_2^{\bullet}/O_2^{\bullet-}]_0/[FAC]_0$ = (75 μM)/(37.5 μM). Error bars represent one standard deviation about the mean of duplicate measurements. Note: Concentrations of DOC and other solution constituents listed here are the values in solution after dilution with all reagents. Adopted from (Liou and Dodd, 2021).

2.3.9 Disinfection Byproduct Formation

(i) Oxyhalides

ClO_2^-, ClO_3^-, ClO_4^-, and BrO_3^- were monitored in solutions containing 200 μgBr^-/L during single- and multiple-dose postmix and premix $O_2^{\bullet-}$/FAC treatment. As shown in Figure 2.20, only ClO_2^- and ClO_3^- were formed in treated samples at concentrations above limits of quantification, and at no more than ~25 μg/L – far below the maximum contaminant levels (MCLs) and health reference levels (HRLs) for ClO_2^- and ClO_3^- (note that concentrations in Figure 2.20a have been corrected for background levels in FAC stocks) (USEPA, 2016; 2020). Relatively little difference was observed whether using postmix or premix treatment. Mass balances on concentrations of Cl^- formed in these samples confirmed that nearly all (>99.6%) of the FAC applied during $O_2^{\bullet-}$/FAC treatment under these conditions reacts to Cl^-, and that only traces of FAC are consumed via oxidation to higher oxidation states. This is further supported by the absence of detectable ClO_2 in $O_2^{\bullet-}$/FAC treated solutions, which would be expected if substantial proportions of FAC were oxidized to ClO_2^- or higher states (Alfassi et al., 1988).

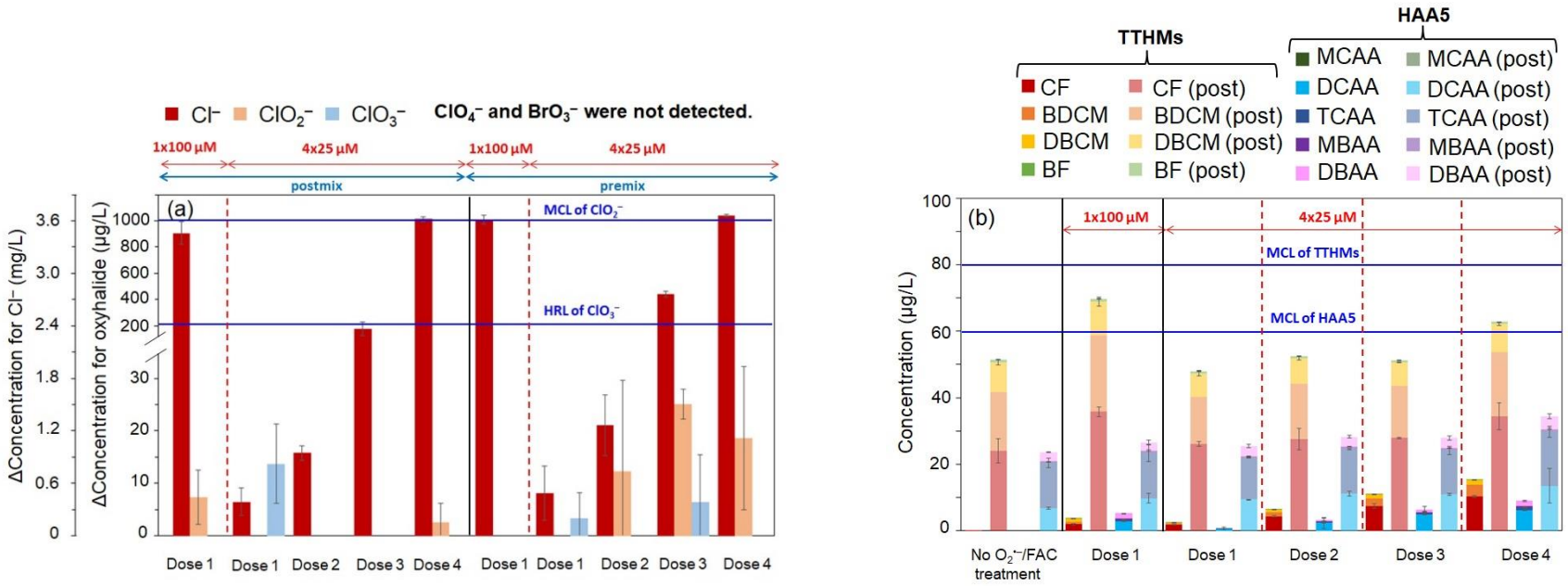

Figure 2.20. Concentrations of (a) oxyhalides and (b) THMs and HAAs resulting from single- and multiple-dose postmix and/or premix $O_2^{\bullet-}$/FAC treatment. Oxyhalide formation experiments used alkaline $O_2^{\bullet-}$ stocks prepared from KO_2 in 0.1M NaOH (pH 13.0), with $O_2^{\bullet-}$/FAC treatment either by adding $O_2^{\bullet-}$ to 5-mM, pH 7 phosphate buffer containing $[FAC]_0$ = 25 or 100 µM and $[Br^-]_0$ = 200 µg/L (postmix), or by premixing alkaline $O_2^{\bullet-}$ with alkaline FAC (pH 13.0) and then adding the premixed $O_2^{\bullet-}$/FAC stock to 5-mM, pH 7 phosphate buffer containing $[Br^-]_0$ = 200 µg/L (premix). ΔConcentration = $Concentration_{meas.}$ – $Concentration_{stock}$, where $Concentration_{meas.}$ represents measured in situ concentration, and $Concentration_{stock}$ represents background in situ concentration attributable to FAC stock (determined from controls prepared without $O_2^{\bullet-}$/FAC treatment). THM/HAA formation experiments used alkaline $O_2^{\bullet-}$ stocks prepared from KO_2 in 1M NaOH (pH 13.9), with $O_2^{\bullet-}$/FAC treatment by premixing alkaline $O_2^{\bullet-}$ with alkaline FAC (pH 13.9) and then adding the premixed $O_2^{\bullet-}$/FAC stock to 50-mM, pH 7 phosphate buffer solutions containing 2 mgC/L of DOC (from SRNOM) and $[Br^-]_0$ = 200 µg/L. $O_2^{\bullet-}$/FAC-treated solutions were post-chlorinated at $[FAC]_0$ = 8 $mgCl_2$/L and allowed to react to CT_{FAC} = 400 $mgCl_2$/L•min. Single-dose experiments were undertaken by dosing $[HO_2^{\bullet}/O_2^{\bullet-}]_0/[FAC]_0$ = (200 µM)/(100 µM) once (1×100 µM), and multiple-dose experiments by dosing $[HO_2^{\bullet}/O_2^{\bullet-}]_0/[FAC]_0$ = (50 µM)/(25 µM) four times (4×25 µM). Residual H_2O_2/HO_2^- was removed by catalase after each $O_2^{\bullet-}$ or $O_2^{\bullet-}$/FAC dose, and residual FAC removed by excess $Na_2S_2O_3$ following post-chlorination. Error bars represent one std. dev. about the mean of duplicate measurements. HRL (health reference level) and MCL (maximum contaminant level) values are from the USEPA (USEPA, 2016; 2020). Samples for organic DBPs were collected before and after post-chlorination. "(post)" in the legend for (b) indicates that samples were post-chlorinated after $O_2^{\bullet-}$/FAC treatment.

(ii) THMs and HAAs

Formation of THMs and HAAs was monitored in solutions containing 2 mgC/L of SRNOM and 200 μgBr$^-$/L during (a) single- and multiple-dose premix $O_2^{\bullet-}$/FAC treatment, and (b) following post-chlorination of the $O_2^{\bullet-}$/FAC-treated samples to CT_{FAC} = 400 mgCl_2/L•min. All $O_2^{\bullet-}$/FAC-treated samples were separated into two sub-volumes: one for direct THM/HAA analyses, and the other for THM/HAA analyses after post-chlorination. Results from these experiments, in addition to a control sample subjected to chlorination alone for comparison, are shown in Figure 2.20. Single- and multiple-dose $O_2^{\bullet-}$/FAC treatment led to limited direct formation of TTHM or HAA5 (no more than ~5-15 μg/L in either case).

Following post-chlorination of $O_2^{\bullet-}$/FAC-treated samples, concentrations reached ~60-70 μg/L for TTHMs, and ~25-35 μg/L for HAA5; compared to 52(±7) μg/L for TTHMs and 24(±2) μg/L for HAA5 in control samples subjected to chlorination alone (Figure 2.20). Notably, THM/HAA levels generated *during* multiple-dose $O_2^{\bullet-}$/FAC treatment were higher than observed *during* single-dose treatment, with increasing levels formed during each dosing step in the multiple-dose experiments. This is consistent with the higher overall HO$^\bullet$ and RCS exposures observed during multiple- versus single-dose treatment (Figures 2.15 and 2.16), and may be due in part to direct DOM halogenation by RCS, as reported in prior work on FAC-based AOPs (Bulman and Remucal, 2020; Young et al., 2018). In contrast, higher TTHM levels *following post-chlorination* were observed in samples initially subjected to single-dose $O_2^{\bullet-}$/FAC treatment. This latter observation may reflect a net *increase* of FAC-reactive THM precursor moieties in DOM (e.g., via HO$^\bullet$- and/or RCS-driven hydroxylation of aromatic moieties) when subjected to the HO$^\bullet$ and RCS exposures prevailing during single-dose treatment; whereas the higher HO$^\bullet$ and RCS exposures prevailing during multiple-dose treatment may have led to more

extensive DOM processing and a net *decrease* in FAC-reactive precursor moieties (e.g., via $HO^{\bullet}$- and/or RCS-driven degradation of aromatic moieties via ring opening), as reported for various AOPs (Ike et al., 2019a; Ike et al., 2019b). Although neither TTHM nor HAA5 levels exceeded USEPA MCLs (USEPA, 2020), these findings indicate the potential for increased THM/HAA formation in $O_2^{\bullet-}$/FAC treatment, particularly following post-chlorination, and should be investigated further as part of continued research into potential applications of this approach for advanced oxidation.

Measurements of oxyhalide, THM, and HAA formation show that direct production of regulated DBPs is likely to be minimal during $O_2^{\bullet-}$/FAC treatment. Although $O_2^{\bullet-}$/FAC treatment does appear to lead to increased THM and HAA formation during post-chlorination (as might be the case if $O_2^{\bullet-}$/FAC treatment is applied for pre-oxidation of water that is then subjected to FAC treatment for disinfection or distribution system residual maintenance), this appears to be a trait shared by nearly all AOPs (Ike et al., 2019a; Ike et al., 2019b), and may be manageable by minimizing post-treatment FAC exposures, or by limiting treatment applications to waters containing low DOC concentrations. Future investigations will be needed to evaluate potential impacts of $O_2^{\bullet-}$/FAC treatment on unregulated DBPs (in particular, certain classes of nitrogenous and carbonaceous DBPs now increasingly recognized for their potential health risk) (Prasse et al., 2018; Richardson and Plewa, 2020).

2.3.10 Potential of $O_2^{\bullet-}$/FAC Application as an AOP

This work highlights the potential for applying the $O_2^{\bullet-}$/FAC reaction (eq 1.7) as the basis for a novel, non-photochemical approach to advanced oxidation, with the capability to rapidly generate high $HO^{\bullet}$ and RCS levels for organic contaminant degradation at circumneutral pH and

under homogenous conditions. The $HO^{\bullet}$ and RCS exposures achieved during $O_2^{\bullet-}$/FAC treatment (up to ~5×10^{-10} M×s for $HO^{\bullet}$, ~10^{-9} M×s for $ClO^{\bullet}/Cl_2^{\bullet-}$, and ~$10^{-11}$ M×s for $Cl^{\bullet}$) are comparable to or higher than those observed in several of the AOPs most commonly applied in (waste)water treatment and reuse, including UV/H_2O_2 (~10^{-12}-10^{-10} M×s for $HO^{\bullet}$) (Miklos et al., 2018a; Rosario-Ortiz et al., 2010; Rosenfeldt and Linden, 2007; Rosenfeldt et al., 2006), O_3/H_2O_2 (~10^{-12} - 10^{-10} M×s for $HO^{\bullet}$) (Acero and Von Gunten, 2001; Bourgin et al., 2017; Lee et al., 2017; Rosenfeldt et al., 2006), and UV/FAC (~10^{-11}-10^{-10}, ~10^{-10}, ~10^{-12}, and ~10^{-11} M×s for $HO^{\bullet}$, $ClO^{\bullet}$, $Cl_2^{\bullet-}$, and $Cl^{\bullet}$, respectively) (Bulman et al., 2019; Chuang et al., 2017; Kong et al., 2018).

By preparing and standardizing aqueous $O_2^{\bullet-}$ stocks under conditions of enhanced $HO_2^{\bullet}/O_2^{\bullet-}$ stability (pH>12), they can be easily handled and dosed to receiving solutions already containing FAC. This provides the option of utilizing $O_2^{\bullet-}$/FAC treatment as a means of generating a nearly instantaneous pulse (or multiple pulses) of $HO^{\bullet}$ and RCS in a post-oxidation process following pre-exposure to FAC for disinfection or pre-oxidation, in much the same way that O_3/H_2O_2 can be used to convert residual O_3 to $HO^{\bullet}$ following a prior period of O_3 exposure for disinfection or pre-oxidation. Alternatively, pre-mixing of alkaline $O_2^{\bullet-}$ and FAC provides a unique option in which a combined $O_2^{\bullet-}$/FAC stock can be added directly to a water at circumneutral pH to generate a pulse of $HO^{\bullet}$ and RCS for advanced oxidation; with the pre-mixed $O_2^{\bullet-}$/FAC stock effectively serving as a ready-made $HO^{\bullet}$ and RCS stock. The use of such a pre-mixing approach also presents the opportunity to apply $O_2^{\bullet-}$/FAC treatment without subjecting a water to pre-chlorination (with potential benefits for minimizing halogenated organic DBP formation), and may enable application to waters containing high levels of matrix constituents that would normally prevent maintenance of an FAC residual (e.g., NH_4^+/NH_3).

2.4 Summary and Potential Practical Implications

- This work shows that moderately stable aqueous $O_2^{\bullet-}$ stocks ($t_{1/2}$ ~ minutes) prepared by several approaches at pH>12 can be either (i) directly added to aqueous FAC at circumneutral pH, or (ii) premixed with alkaline FAC and acidified to pH 7, to effectively degrade various organic probe compounds (NB, BA, DMB, and pCBA) via in situ generated $HO^{\bullet}$ and RCS (including $ClO^{\bullet}$, $Cl^{\bullet}$, and/or $Cl_2^{\bullet-}$).
- $O_2^{\bullet-}$/FAC treatment results in the production of ~0.8 mol $HO^{\bullet}$/mol FAC consumed and can generate $HO^{\bullet}$ and RCS exposures reaching ~5×10^{-10} and ~10^{-9} M×s, respectively, at pH 7 – on par with or higher than for many of the AOPs currently in use in (waste)water treatment (including UV/H_2O_2, O_3/H_2O_2, and UV/FAC).
- $O_2^{\bullet-}$/FAC treatment can be applied effectively in natural waters and SRNOM-amended phosphate buffer containing up to 5 mgC/L of DOC, though efficiency decreases with increasing DOC, due to scavenging of $HO^{\bullet}$ and RCS by DOM.
- Direct formation of halogen-containing DBPs – including chlorite, chlorate, bromate, perchlorate, THMs, and HAAs *during* $O_2^{\bullet-}$/FAC treatment is minimal, though THM and HAA formation was found to be moderately enhanced during *post-chlorination* of $O_2^{\bullet-}$/FAC-treated solutions.
- The findings reported here provide a foundation for further examining potential applications of $O_2^{\bullet-}$/FAC treatment. Additional work is needed to more fully evaluate opportunities for optimizing various aspects of this process – in particular, with respect to approaches for producing and stabilizing $O_2^{\bullet-}$ stocks, chemical usage and costs, implementation at scale, and predicting and monitoring process performance.

- This process could provide a beneficial addition to the range of available AOPs due to its high radical exposures, simplicity, rapid time-scales, potential for on-site $O_2^{\bullet-}$ generation, and widespread accessibility of FAC and other reagents.

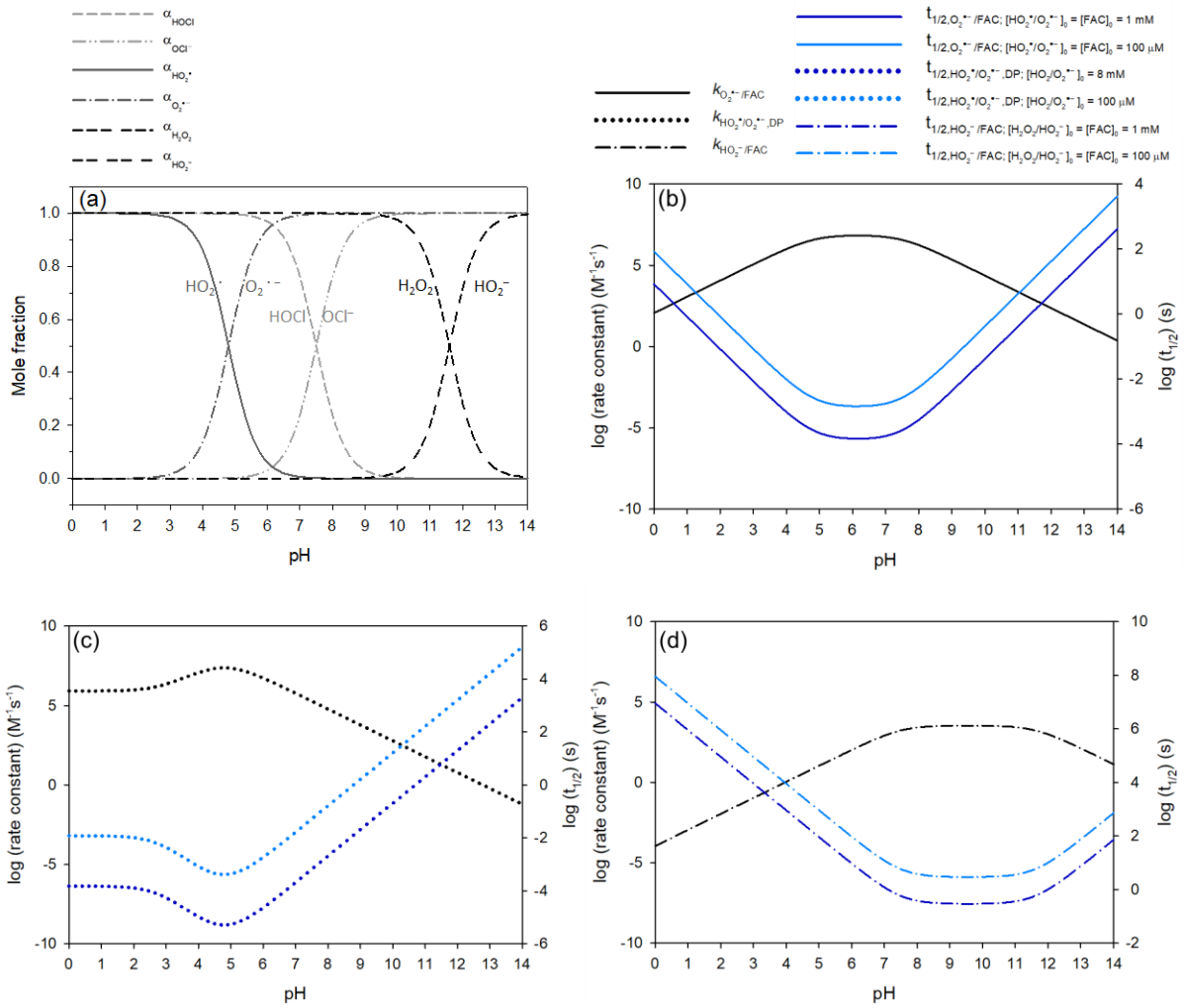

Figure S2.1. (a) Acid-base speciation of $HO_2^{\bullet}/O_2^{\bullet-}$, H_2O_2/HO_2^-, and $HOCl/OCl^-$, and theoretical apparent rate constants (k_{app}) and half-times ($t_{1/2}$) for the (b) $O_2^{\bullet-}$/FAC reaction, (c) $HO_2^{\bullet}/O_2^{\bullet-}$ disproportionation reaction, and (d) HO_2^-/FAC reaction (based, respectively on eqs 1.6, 1.8, and $k_{app,HO_2^-/FAC} = k_{S13}\alpha_{HO_2^-}\alpha_{HOCl} = k_1\left(\frac{K_{a,H_2O_2}}{[H^+]+K_{a,H_2O_2}}\right)\left(\frac{[H^+]}{[H^+]+K_{a,HOCl}}\right)$). Values of $t_{1/2,HO2\bullet/O2\bullet-,DP}$ were calculated for $[HO_2^{\bullet}/O_2^{\bullet-}]_0$ = 8 mM (a typical concentration of $O_2^{\bullet-}$ stock solutions) and $[HO_2^{\bullet}/O_2^{\bullet-}]_0$ = 100 μM (a typical in situ concentration in $O_2^{\bullet-}$/FAC treatment experiments), values of $t_{1/2,O2\bullet-/FAC}$ were calculated for $[HO_2^{\bullet}/O_2^{\bullet-}]_0 = [FAC]_0$ = 1 mM (typical of concentrations in premixed $O_2^{\bullet-}$/FAC stock solutions) and $[HO_2^{\bullet}/O_2^{\bullet-}]_0 = [FAC]_0$ = 100 μM (near typical in situ concentrations in $O_2^{\bullet-}$/FAC treatment experiments), and values of $t_{1/2,HO2-/FAC}$ were calculated for $[H_2O_2/HO_2^-]_0 = [FAC]_0$ = 1 mM (typical of concentrations in premixed $O_2^{\bullet-}$/FAC stock solutions) and $[H_2O_2/HO_2^-]_0 = [FAC]_0$ = 100 μM (near typical in situ concentrations in $O_2^{\bullet-}$/FAC treatment experiments). Equimolar $[HO_2^{\bullet}/O_2^{\bullet-}]_0$, $[H_2O_2/HO_2^-]_0$, and $[FAC]_0$ values were assumed to simplify calculation and graphical depiction of $t_{1/2,O2\bullet-/FAC}$ and $t_{1/2,HO2-/FAC}$ values. Adopted from (Liou and Dodd, 2021).

Text S2.1. Estimation of reaction rate constant for $k_{Cl_2^{\bullet-},DMB}$

The second-order rate constant for reaction of $Cl_2^{\bullet-}$ with DMB, $k_{Cl_2^{\bullet-},DMB}$, was estimated using a quantitative structure-activity relationship (QSAR) model reported by Lei et al. (2019), based upon $Cl_2^{\bullet-}$ reactions with a wide range of alkoxybenzenes (eq S2.1) (Lei et al., 2019),

$$\log\left(k_{Cl_2^{\bullet-},i}\right) = 8.25 - 0.88\sum\sigma_{o,m,p}^{+},\ R^2 = 0.95 \quad \text{(S2.1)}$$

where $k_{Cl_2^{\bullet-},i}$ represents the estimated second-order rate constant for reaction of $Cl_2^{\bullet-}$ with compound *i* (DMB in this case); the Hammett, or Brown-Okamoto, constants, σ^+, are substituent constants including a field/inductive component and a resonance component which quantitatively express the electronic effects of substituents on electrophilic substitution reactions (Hansch et al., 1991); and σ_o^+, σ_m^+ and σ_p^+ represent constants for *ortho*-, *meta*-, and *para*-substituents, respectively. As 1,4-DMB has one *para*-methoxy group (σ_p^+ = -0.78) on the benzene ring with respect to the 1-methoxy group of the unsubstituted reference compound anisole (or methoxybenzene) on which eq S2.1 is based, $k_{Cl_2^{\bullet-},DMB}$ can in turn be estimated as 8.6×10^8 $M^{-1}s^{-1}$.

Text S2.2. Calculation of $HO^{\bullet}$ scavenging efficiency of *t*-BuOH in solutions amended with *t*-BuOH

Concentrations of *t*-BuOH required to scavenge $HO^{\bullet}$ during selected $O_2^{\bullet-}$/FAC treatment experiments were determined by eq S2.2,

$$f\left(HO^{\bullet}\right) = \frac{k_{HO^{\bullet},t\text{-BuOH}}\left[t\text{-BuOH}\right]_0}{k'_{HO^{\bullet},total}} \quad \text{(S2.2)}$$

which jointly considers the reactivity of $HO^{\bullet}$ towards the predominant scavengers in solution, including $HOCl/OCl^{-}$, $HO_2^{\bullet}/O_2^{\bullet-}$, H_2O_2/HO_2^{-}, $H_2PO_4^{-}/HPO_4^{2-}/PO_4^{3-}$, and *t*-BuOH itself, where *f*($HO^{\bullet}$) is the fraction of total generated $HO^{\bullet}$ scavenged by *t*-BuOH; $k_{HO^{\bullet},t\text{-BuOH}}$ is the second-order rate constant for reaction of $HO^{\bullet}$ with *t*-BuOH (6.0×10^8 $M^{-1}s^{-1}$) (Buxton et al., 1988); and the overall, first-order scavenging rate constant for the solution composition of interest, $k'_{HO^{\bullet},total}$ (in units of s^{-1}), can be calculated according to eq S2.3 (Rodríguez and von Gunten, 2020),

$$\begin{aligned} k'_{HO^{\bullet},total} &= k_{HO^{\bullet},t\text{-BuOH}}\left[t\text{-BuOH}\right]_0 + k_{HO^{\bullet},HOCl}\left[HOCl\right]_0 + k_{HO^{\bullet},OCl^-}\left[{}^{\bullet}OCl^-\right]_0 \\ &+ k_{HO^{\bullet},H_2O_2}\left[H_2O_2\right]_0 + k_{HO^{\bullet},HO_2^-}\left[HO_2^-\right]_0 + k_{HO^{\bullet},HO_2^{\bullet}}\left[HO_2^{\bullet}\right]_0 + k_{HO^{\bullet},O_2^{\bullet-}}\left[O_2^{\bullet-}\right]_0 \\ &+ k_{HO^{\bullet},H_2PO_4^-}\left[H_2PO_4^-\right]_0 + k_{HO^{\bullet},HPO_4^{2-}}\left[HPO_4^{2-}\right]_0 + k_{HO^{\bullet},PO_4^{3-}}\left[PO_4^{3-}\right]_0 \end{aligned} \quad \text{(S2.3)}$$

Eqs S2.2-S2.3 were in turn applied with the objective of selecting a *t*-BuOH concentration that would ensure ≥90% scavenging of $HO^{\bullet}$ by *t*-BuOH, or *f*($HO^{\bullet}$) ≥ 0.90, under the investigated experimental conditions. The second-order rate constants for reactions of $HO^{\bullet}$ with HOCl, OCl^{-}, $HO_2^{\bullet}$, $O_2^{\bullet-}$, H_2O_2, HO_2^{-}, $H_2PO_4^{-}$, and HPO_4^{2-} have been reported as $k_{HO^{\bullet},HOCl}$ = 1.2×10^9 $M^{-1}s^{-1}$, $k_{HO^{\bullet},OCl^-}$ = 6.4×10^9 $M^{-1}s^{-1}$, $k_{HO^{\bullet},HO_2^{\bullet}}$ = 7.1×10^9 $M^{-1}s^{-1}$, $k_{HO^{\bullet},O_2^{\bullet-}}$ = 1.0×10^{10} $M^{-1}s^{-1}$, $k_{HO^{\bullet},H_2O_2}$ = 2.7×10^7 $M^{-1}s^{-1}$, $k_{HO^{\bullet},HO_2^-}$ = 7.5×10^9 $M^{-1}s^{-1}$, $k_{HO^{\bullet},H_2PO_4^-}$ = 2×10^4 $M^{-1}s^{-1}$, $k_{HO^{\bullet},HPO_4^{2-}}$ = 1.5×10^5 $M^{-1}s^{-1}$, and $k_{HO^{\bullet},PO_4^{3-}}$ < 1.0×10^7 $M^{-1}s^{-1}$, respectively (Black and Hayon, 1970; Bulman et al., 2019; Buxton et al., 1988; Buxton and Subhani, 1972; Christensen et al., 1989; Christensen et al., 1982; Elliot and Buxton, 1992; Maruthamuthu and Neta, 1978; Sehested et al., 1968). Under the conditions of the experiments in which *t*-BuOH was used, the concentrations of each of the preceding reactants (calculated at pH 7) were $[HOCl]_0$ = 38-190 μM, $[OCl^{-}]_0$ = 12-60 μM,

$[HO_2^{\bullet}]_0$ = 0.03-3 μM, $[O_2^{\bullet-}]_0$ = 4.97-397 μM, $[H_2O_2]_0$ = 150-700 μM, $[HO_2^-]_0$ = negligible, $[H_2PO_4^-]$ = 31 mM, $[HPO_4^{2-}]$ = 19 mM, and $[PO_4^{3-}]$ = 91 nM. Based on the maximum values of these ranges, a concentration of [*t*-BuOH] = 50 mM was selected to ensure ≥90% of $HO^{\bullet}$ scavenging under nearly all conditions. For example, this concentration of *t*-BuOH was sufficient to ensure $f(HO^{\bullet}) \geq 0.93$ over the range of $[HO_2^{\bullet}/O_2^{\bullet-}]_0$ values applied when $[FAC]_0$ = 50 μM, $f(HO^{\bullet}) \geq 0.90$ when $[FAC]_0$ = 100 μM (except at the highest $[HO_2^{\bullet}/O_2^{\bullet-}]_0$ of 400 μM, at which $f(HO^{\bullet})$ = 0.88), and $f(HO^{\bullet}) \geq 0.96$ when $[FAC]_0$ = 250 μM.

Text S2.3. Estimating contributions of $HO^{\bullet}$, $Cl^{\bullet}$, and $ClO^{\bullet}/Cl_2^{\bullet-}$ to probe compound degradation

By assuming NB only reacts with $HO^{\bullet}$, the fractional relative contributions of $HO^{\bullet}$, $Cl^{\bullet}$ and $ClO^{\bullet}/Cl_2^{\bullet-}$ to the overall degradation of BA and DMB could be calculated according to the following expressions (eqs S2.4-S2.6):

$$f_{HO^{\bullet},\text{BA or DMB}} = -k_{HO^{\bullet},\text{BA or DMB}} \times \frac{\int_0^t [HO^{\bullet}]\,dt}{\ln\left(\frac{[\text{BA or DMB}]}{[\text{BA or DMB}]_0}\right)} \quad \text{(S2.4)}$$

$$f_{Cl^{\bullet},\text{BA or DMB}} = -k_{Cl^{\bullet},\text{BA or DMB}} \times \frac{\int_0^t [Cl^{\bullet}]\,dt}{\ln\left(\frac{[\text{BA or DMB}]}{[\text{BA or DMB}]_0}\right)} \quad \text{(S2.5)}$$

$$f_{ClO^{\bullet}/Cl_2^{\bullet-},\text{DMB}} = -k_{ClO^{\bullet},\text{DMB}} \times \frac{\left(\int_0^t [ClO^{\bullet}]\,dt + 0.41\int_0^t [Cl_2^{\bullet-}]\,dt\right)}{\ln\left(\frac{[\text{DMB}]}{[\text{DMB}]_0}\right)} = -k_{ClO^{\bullet},\text{DMB}} \times \frac{\int_0^t [ClO^{\bullet}/Cl_2^{\bullet-}]\,dt}{\ln\left(\frac{[\text{DMB}]}{[\text{DMB}]_0}\right)} \quad \text{(S2.6)}$$

where the exposure terms, $\int_0^t [HO^{\bullet}]\,dt$, $\int_0^t [Cl^{\bullet}]\,dt$, and $\int_0^t [ClO^{\bullet}/Cl_2^{\bullet-}]\,dt$ are calculated as described in Section 2.2.5; values of $k_{HO^{\bullet},i}$, $k_{Cl^{\bullet},i}$ and $k_{ClO^{\bullet}/Cl_2^{\bullet-},i}$ are as noted in Section 2.2.5,

and [BA or DMB]$_0$ and [BA or DMB] represent the concentrations of BA or DMB before and after $O_2^{\bullet-}$/FAC treatment, respectively.

Text S2.4. Uncertainties in calculation of radical exposures

Estimation of radical exposures was based on the extents of organic probe compound degradation (NB, BA and DMB) and their reaction rate constants with each radical species ($HO^{\bullet}$, $Cl^{\bullet}$, $ClO^{\bullet}$ and $Cl_2^{\bullet-}$). It is important to note that the values of $\int_0^t [\text{radical}]dt$ determined here do not account for uncertainties associated with the rate constants used in their determination, due to the lack of reported error bounds for most of the associated rate constants. These radical exposures are thus most appropriately interpreted as estimates, rather than exact values of $\int_0^t [\text{radical}]dt$. Furthermore, exposures of $Cl^{\bullet}$ and $ClO^{\bullet}/Cl_2^{\bullet-}$ have greater uncertainties than $HO^{\bullet}$ exposure due to greater uncertainties in the small changes in probe concentrations from which $Cl^{\bullet}$ and $ClO^{\bullet}/Cl_2^{\bullet-}$ exposures were determined.

We performed a series of propagation of uncertainty (or error propagation) to examine the effect of uncertainties of probes' reaction rate constants on the calculation of radical exposures. Error propagation, in short, is a statistical method to investigate variables' uncertainties on the uncertainty of a function based on them. When the variables are the values of experimental measurements that have uncertainties due to measurement limitations or data standard error, the uncertainties will propagate due to the combination of variables in the function (Clifford, 1973). Estimation of uncertainties for each of the radical exposures were calculated as following expressions (eqs 2.7-2.9):

HO• exposure

$$\mathrm{HO^{\bullet}exposure} = \int_0^t \left[\mathrm{HO^{\bullet}}\right] dt = \frac{\ln\left(\frac{\left[\mathrm{NB}\right]}{\left[\mathrm{NB}\right]_0}\right)}{-k_{\mathrm{HO^{\bullet},NB}}}$$

Uncertainty of $\mathrm{HO^{\bullet}}$ exposure = $\sigma_{\mathrm{HO^{\bullet}}} = \left|\frac{1}{-k_{\mathrm{HO^{\bullet},NB}}}\right| \times \frac{\sigma_{[\mathrm{NB}]}}{\left[\mathrm{NB}\right]}$, where $\sigma_{[\mathrm{NB}]}$ is the standard deviation of NB

$$\sigma_{\mathrm{HO^{\bullet}}} = \left|\frac{1}{-k_{\mathrm{HO^{\bullet},NB}}}\right| \times \frac{\sigma_{[\mathrm{NB}]}}{\left[\mathrm{NB}\right]} = \left|\frac{1}{-3.9\times10^{9}}\right| \times \frac{\sigma_{[\mathrm{NB}]}}{\left[\mathrm{NB}\right]} = 2.56\times10^{-10} \times \frac{\sigma_{[\mathrm{NB}]}}{\left[\mathrm{NB}\right]} \quad \text{(S2.7)}$$

Cl• exposure

$$\mathrm{Cl^{\bullet}exposure} = \int_0^t \left[\mathrm{Cl^{\bullet}}\right] dt = \frac{\ln\left(\frac{\left[\mathrm{BA}\right]}{\left[\mathrm{BA}\right]_0}\right) + k_{\mathrm{HO^{\bullet},BA}} \int_0^t \left[\mathrm{HO^{\bullet}}\right] dt}{-k_{\mathrm{Cl^{\bullet},BA}}}$$

$$\sigma_{\mathrm{Cl^{\bullet}}} = \sqrt{\left\{\left|\frac{1}{-k_{\mathrm{Cl^{\bullet},BA}}}\right| \times \frac{\sigma_{[\mathrm{BA}]}}{\left[\mathrm{BA}\right]}\right\}^2 + \left\{\left|\frac{k_{\mathrm{HO^{\bullet},BA}}}{-k_{\mathrm{Cl^{\bullet},BA}}}\right| \times \left(\left|\frac{1}{-k_{\mathrm{HO^{\bullet},NB}}}\right| \times \frac{\sigma_{[\mathrm{NB}]}}{\left[\mathrm{NB}\right]}\right)\right\}^2}$$

$$= \sqrt{\left\{\frac{1}{1.8\times10^{10}} \times \frac{\sigma_{[\mathrm{BA}]}}{\left[\mathrm{BA}\right]}\right\}^2 + \left\{\frac{5.9\times10^{9}}{(1.8\times10^{10})\times(3.9\times10^{9})} \times \frac{\sigma_{[\mathrm{NB}]}}{\left[\mathrm{NB}\right]}\right\}^2}$$

$$= \sqrt{\left\{5.56\times10^{-11} \times \frac{\sigma_{[\mathrm{BA}]}}{\left[\mathrm{BA}\right]}\right\}^2 + \left\{8.40\times10^{-11} \times \frac{\sigma_{[\mathrm{NB}]}}{\left[\mathrm{NB}\right]}\right\}^2}$$

(S2.8)

Aggregate ClO•/$Cl_2^{\bullet-}$ exposure

$$\left(\int_0^t \left[\mathrm{ClO^{\bullet}}\right] dt + 0.41\int_0^t \left[\mathrm{Cl_2^{\bullet-}}\right] dt\right) = \text{Aggregate } \mathrm{ClO^{\bullet}/Cl_2^{\bullet-}} \text{ exposure, or} \int_0^t \left[\mathrm{ClO^{\bullet}/Cl_2^{\bullet-}}\right] dt =$$

$$= \frac{\ln\left(\frac{\left[\mathrm{DMB}\right]}{\left[\mathrm{DMB}\right]_0}\right) + k_{\mathrm{HO^{\bullet},DMB}}\int_0^t \left[\mathrm{HO^{\bullet}}\right] dt + k_{\mathrm{Cl^{\bullet},DMB}}\int_0^t \left[\mathrm{Cl^{\bullet}}\right] dt}{-k_{\mathrm{ClO^{\bullet},DMB}}}$$

$$\sigma_{\mathrm{ClO^{\bullet}/Cl_2^{\bullet-}}} =$$

$$\sqrt{\left\{\left|\frac{1}{-k_{\mathrm{ClO^{\bullet},DMB}}}\right| \times \frac{\sigma_{[\mathrm{DMB}]}}{[\mathrm{DMB}]}\right\}^2 + \left\{\left|\frac{k_{\mathrm{HO^{\bullet},DMB}}}{-k_{\mathrm{ClO^{\bullet},DMB}}}\right| \times \left(\left|\frac{1}{-k_{\mathrm{HO^{\bullet},NB}}}\right| \times \frac{\sigma_{[\mathrm{NB}]}}{[\mathrm{NB}]}\right)\right\}^2 + \left\{\left|\frac{k_{\mathrm{Cl^{\bullet},DMB}}}{-k_{\mathrm{ClO^{\bullet},DMB}}}\right| \times \sqrt{\left\{\left|\frac{1}{-k_{\mathrm{Cl^{\bullet},BA}}}\right| \times \frac{\sigma_{[\mathrm{BA}]}}{[\mathrm{BA}]}\right\}^2 + \left\{\left|\frac{k_{\mathrm{HO^{\bullet},BA}}}{-k_{\mathrm{Cl^{\bullet},BA}}}\right| \times \left(\left|\frac{1}{-k_{\mathrm{HO^{\bullet},NB}}}\right| \times \frac{\sigma_{[\mathrm{NB}]}}{[\mathrm{NB}]}\right)\right\}^2}\right\}^2}$$

$$= \sqrt{\left\{\frac{1}{2.1\times10^9} \times \frac{\sigma_{[\mathrm{DMB}]}}{[\mathrm{DMB}]}\right\}^2 + \left\{\frac{7.0\times10^9}{2.1\times10^9} \times \left(2.56\times10^{-10} \times \frac{\sigma_{[\mathrm{NB}]}}{[\mathrm{NB}]}\right)\right\}^2 + \left\{\frac{1.8\times10^9}{2.1\times10^9} \times \sqrt{\left\{5.56\times10^{-11} \times \frac{\sigma_{[\mathrm{BA}]}}{[\mathrm{BA}]}\right\}^2 + \left\{8.40\times10^{-11} \times \frac{\sigma_{[\mathrm{NB}]}}{[\mathrm{NB}]}\right\}^2}\right\}^2}$$

(S2.9)

where $k_{\mathrm{HO^{\bullet},\,}i}$, $k_{\mathrm{Cl^{\bullet},\,}i}$, $k_{\mathrm{ClO^{\bullet},\,}i}$, and $k_{\mathrm{Cl_2^{\bullet-},\,}i}$ represent the second-order rate constants for reactions of $\mathrm{HO^{\bullet}}$, $\mathrm{Cl^{\bullet}}$, $\mathrm{ClO^{\bullet}}$, and $\mathrm{Cl_2^{\bullet-}}$ with probe compound *i*; and $[i]_0$ and $[i]$ represent the concentrations of *i* before and after $\mathrm{O_2^{\bullet-}}$/FAC treatment, respectively.

$k_{\mathrm{HO^{\bullet},NB}}$, $k_{\mathrm{HO^{\bullet},BA}}$ and $k_{\mathrm{HO^{\bullet},DMB}}$ have been reported as 3.9×10^9 $\mathrm{M^{-1}s^{-1}}$ (Buxton et al., 1988), 5.9×10^9 $\mathrm{M^{-1}s^{-1}}$ (for the benzoate ion) (Buxton et al., 1988), and 7.0×10^9 $\mathrm{M^{-1}s^{-1}}$ (O'Neill et al., 1975), respectively. $k_{\mathrm{Cl^{\bullet},BA}}$ and $k_{\mathrm{Cl^{\bullet},DMB}}$ have each been reported as 1.8×10^{10} $\mathrm{M^{-1}s^{-1}}$ (Alfassi et al., 1989; Mártire et al., 2001), and $k_{\mathrm{ClO^{\bullet},DMB}}$ has been reported as 2.1×10^9 $\mathrm{M^{-1}s^{-1}}$ (Alfassi et al., 1988). The second-order rate constant for reaction of $\mathrm{Cl_2^{\bullet-}}$ with DMB was not found in the literature; therefore, it was estimated as described in Text S2.1, yielding a value of $k_{\mathrm{Cl_2^{\bullet-},DMB}}$ = 8.6×10^8 $\mathrm{M^{-1}s^{-1}}$. Because values of $\int_0^t \left[\mathrm{ClO^{\bullet}}\right] dt$ and $0.41\int_0^t \left[\mathrm{Cl_2^{\bullet-}}\right] dt$ could not be independently

determined, their sums $\left(\int_0^t \left[ClO^{\bullet}\right] dt + 0.41\int_0^t \left[Cl_2^{\bullet-}\right] dt\right)$ are reported together here as aggregate values abbreviated as $\int_0^t \left[ClO^{\bullet}/Cl_2^{\bullet-}\right] dt$.

Uncertainty estimation of radical exposure from $O_2^{\bullet-}$/FAC treatment data:

Initial concentrations of the three radical probes for $O_2^{\bullet-}$/FAC treatment were at 1 μM. Uncertainties of reaction rate constants were not considered here as error ranges not available from literature. Selecting single-dose data shown in Table S2.1 with $[HO_2^{\bullet}/O_2^{\bullet-}]/[FAC]_0$ = (a) 200 μM/100 μM, (b) 100 μM/50 μM, (c) 50 μM/25 μM, and (d) 20 μM/10 μM, respectively, the calculated radical exposures (based on extend of probe compound degradation) and estimated uncertainties were compared in Table S2.2.

Table S2.1. Experimental probe compound degradation after $O_2^{\bullet-}$/FAC treatment under different $[HO_2^{\bullet}/O_2^{\bullet-}]/[FAC]_0$

	$[NB]_{after\ treatment}$		$[BA]_{after\ treatment}$		$[DMB]_{after\ treatment}$	
$[HO_2^{\bullet}/O_2^{\bullet-}]/[FAC]_0$	Average (μM)	STD	Average (μM)	STD	Average (μM)	STD
200 μM/100 μM	0.367	0.019	0.218	0.006	0.098	0.009
100 μM/50 μM	0.439	0.002	0.286	0.025	0.088	0.018
50 μM/25 μM	0.564	0.003	0.398	0.006	0.304	0.008
20 μM/10 μM	0.802	0.006	0.644	0.004	0.657	0.013

Table S2.2. Calculated exposure vs. estimated uncertainty

	$HO^{\bullet}$ exposure		$Cl^{\bullet}$ exposure		$ClO^{\bullet}/Cl_2^{\bullet-}$ exposure	
$[HO_2^{\bullet}/O_2^{\bullet-}]/[FAC]_0$	Calculated exposure[a] (M×s)	Estimated uncertainty[b] (M×s)	Calculated exposure[a] (M×s)	Estimated uncertainty[b] (M×s)	Calculated exposure[a] (M×s)	Estimated uncertainty[b] (M×s)
200 μM/100 μM	2.67×10^{-10}	1.33×10^{-11}	-1.74×10^{-11}	4.61×10^{-12}	2.00×10^{-10}	6.23×10^{-11}
100 μM/50 μM	2.10×10^{-10}	1.17×10^{-12}	4.14×10^{-12}	4.88×10^{-12}	4.94×10^{-10}	9.76×10^{-11}
50 μM/25 μM	1.48×10^{-10}	1.36×10^{-12}	2.29×10^{-12}	9.50×10^{-13}	4.79×10^{-11}	1.34×10^{-11}
20 μM/10 μM	5.54×10^{-11}	1.92×10^{-12}	6.52×10^{-12}	7.17×10^{-13}	-3.43×10^{-11}	1.14×10^{-11}

[a] Calculated exposure: directly calculated based on experimental results in Table S2.1. [b] Estimated uncertainty: estimated based on experimental results in Table S2.1 and the error propagation equations expressed in eqs 2.7-2.9.

Estimated uncertainties based on results from the LOD tests:

The LODs of NB, BA, DMB were determined by repeated ten analyses of the three probe compounds at 0.05 μM for NB and DMB, and 0.1 μM for BA on the HPLC. Uncertainty propagation was then calculated according to the LOD test results with a summary shown in Table S2.3. Estimated uncertainties in Table S2.2 and S2.3 indicate that the uncertainty of $HO^{\bullet}$ exposure was at least one order of magnitude lower than its calculated exposure, meaning that $HO^{\bullet}$ exposures reported in this study are reliable. On the contrary, uncertainties for $Cl^{\bullet}$ and $ClO^{\bullet}/Cl_2^{\bullet-}$ have the same order of magnitude as their calculated exposures, indicating that RCS exposures reported in this study can only be regarded as "estimations".

Table S2.3. Uncertainties estimated based on LOD tests

Compound	[NB]		[BA]		[DMB]	
	Measured concentration (μM)	STD	Measured concentration (μM)	STD	Measured concentration (μM)	STD
Concentration (μM)	0.05	0.0051	0.1	0.0072	0.05	0.0050
LOD (= STD×3)	0.015		0.022		0.015	
LOQ (= STD×10)	0.051		0.072		0.050	
Estimated uncertainty[a] (M×s)	$HO^{\bullet}$ exposure: 2.62×10^{-11}		$Cl^{\bullet}$ exposure: 9.46×10^{-12}		$ClO^{\bullet}/Cl_2^{\bullet-}$ exposure: 9.95×10^{-11}	

[a] Estimated uncertainty: estimated based on results from the LOD tests in Table S2.3 and the error propagation equations expressed in eqs 2.7-2.9

Text S2.5. Calculation of $HO^{\bullet}$ scavenging efficiency of phosphate and borate buffers

The $OH^{\bullet}$ scavenging efficiency due to buffer species during $O_2^{\bullet-}$/FAC treatment experiments in this study can in general be determined by the following equation (eq S2.10):

$$f\left(HO^{\bullet}\right) = \frac{\sum k_{HO^{\bullet},\text{buffer species } i}\left[\text{buffer species } i\right]_0}{k'_{HO^{\bullet},\text{total}}} \quad \text{(S2.10)}$$

where $f(HO^{\bullet})$ is the fraction of total generated $HO^{\bullet}$ scavenged by the buffer species of interest; $k_{HO^{\bullet},\text{buffer species } i}$ (in units of $M^{-1}s^{-1}$) is the second-order rate constant for reaction of $HO^{\bullet}$ with specific phosphate or borate species; and the overall, first-order $HO^{\bullet}$ scavenging rate constant for the solution composition of interest, $k'_{HO^{\bullet},\text{total}}$ (in units of s^{-1}), can be calculated according to equation below (eq S2.11):

$$\begin{aligned} k'_{HO^{\bullet},\text{total}} &= k_{HO^{\bullet},HOCl}\left[HOCl\right]_0 + k_{HO^{\bullet},OCl^-}\left[OCl^-\right]_0 \\ &+ k_{HO^{\bullet},H_2O_2}\left[H_2O_2\right]_0 + k_{HO^{\bullet},HO_2^-}\left[HO_2^-\right]_0 + k_{HO^{\bullet},HO_2^{\bullet}}\left[HO_2^{\bullet}\right]_0 + k_{HO^{\bullet},O_2^{\bullet-}}\left[O_2^{\bullet-}\right]_0 \\ &+ k_{HO^{\bullet},H_3PO_4}\left[H_3PO_4\right]_0 + k_{HO^{\bullet},H_2PO_4^-}\left[H_2PO_4^-\right]_0 + k_{HO^{\bullet},HPO_4^{2-}}\left[HPO_4^{2-}\right]_0 + k_{HO^{\bullet},PO_4^{3-}}\left[PO_4^{3-}\right]_0 \text{ (in case of phosphate buffer)} \\ &\text{or} \\ &+ k_{HO^{\bullet},H_3BO_3}\left[H_3BO_3\right]_0 + k_{HO^{\bullet},B(OH)_4^-}\left[B(OH)_4^-\right]_0 \text{ (in case of borate buffer)} \end{aligned} \quad \text{(S2.11)}$$

The second-order rate constants for reactions of $OH^{\bullet}$ with borate species are reported as $k_{OH^{\bullet},H_3BO_3} < 5\times10^4\ M^{-1}s^{-1}$, and $k_{OH^{\bullet},B(OH)_4^-} < 1\times10^6\ M^{-1}s^{-1}$ (Buxton and Sellers, 1987; Janovsky, 1980). All other rate constants are as listed in Text S2.2. The calculated $HO^{\bullet}$ scavenging fractions, $f(HO^{\bullet})$, by 50 mM of total phosphate or total borate were calculated to be less than 3% within the pH range from 6 to 9 at the typical [HOCl/OCl^-], [$HO_2^{\bullet}/O_2^{\bullet-}$], and [$H_2O_2/HO_2^-$] concentrations present in $O_2^{\bullet-}$/FAC treatment experiments. Therefore, the contributions of buffers to $HO^{\bullet}$ scavenging in this study were minimal.

Table S2.4. Native water quality parameters for natural water samples[a]

Parameter	Local Reservoir	Lake Washington
pH	8.15	8.10
DOC (mgC/L)	0.4	1.9
Chloride (mg/L)	3	3
Bromide (µg/L)	25	24
Alkalinity (mg/L as $CaCO_3$)	31	38
$SUVA_{254}$ (L/mg-m)	1.4	2.4

[a] Chloride and bromide concentrations were as reported previously for the same samples (Young et al., 2020). Carbonate alkalinities were calculated from measurements of dissolved inorganic carbon (DIC) on the same Shimadzu analyzer used for DOC measurements, based on (bi)carbonate speciation at native sample pH. Specific 254 nm UV absorbance ($SUVA_{254}$) values were determined based on 254 nm UV absorbance measurements obtained at native sample pH, using a 1-cm optical path length. Adopted from (Liou and Dodd, 2021).

References for Chapter 2

Alfassi, Z.B., Huie, R.E., Mosseri, S. and Neta, P., 1988. Kinetics of one-electron oxidation by the ClO radical. *International Journal of Radiation Applications and Instrumentation. Part C. Radiation Physics and Chemistry* 32(1), 85-88. https://doi.org/10.1016/1359-0197(88)90018-5

Alfassi, Z.B., Mosseri, S. and Neta, P., 1989. Reactivities of chlorine atoms and peroxyl radicals formed in the radiolysis of dichloromethane. *The Journal of Physical Chemistry* 93(4), 1380-1385. 10.1021/j100341a040

Allen, A.O. and Bielski, B.H.J. (1980) Formation and disappearance of superoxide radicals in aqueous solutions., United States.

Allen, A.O., Hochanadel, C.J., Ghormley, J.A. and Davis, T.W., 1952. Decomposition of water and aqueous solutions under mixed fast neutron and γ-radiation. *The Journal of Physical Chemistry* 56(5), 575-586. 10.1021/j150497a007

APHA/AWWA/WEF, 2005. APHA Standard Methods for the Examination of Water and Wastewater, Washington.

Baxendale, J.H. and Wilson, J.A., 1957. The photolysis of hydrogen peroxide at high light intensities. *Transactions of the Faraday Society* 53(0), 344-356. 10.1039/TF9575300344

Behar, D. and Czapski, G., 1970. Ozonide and hydroperoxy radicals in flash photolysis of hydrogenperoxide. *Israel Journal of Chemistry* 8(4), 699-708. 10.1002/ijch.197000085

Bielski, B.H.J. and Allen, A.O., 1977. Mechanism of the disproportionation of superoxide radicals. *The Journal of Physical Chemistry* 81(11), 1048-1050. 10.1021/j100526a005

Bielski, B.H.J. and Cabelli, D.E., 1995. Active Oxygen in Chemistry. Foote, C.S., Valentine, J.S., Greenberg, A. and Liebman, J.F. (eds), pp. 66-104, Springer Netherlands, Dordrecht.

Bielski, B.H.J., Cabelli, D.E., Arudi, R.L. and Ross, A.B., 1985. Reactivity of $HO_2/O_2^{\bullet-}$ radicals in aqueous solution. *Journal of Physical and Chemical Reference Data* 14(4), 1041-1100. 10.1063/1.555739

Bielski, B.H.J. and Gebicki, J.M., 1982. Generation of superoxide radicals by photolysis of oxygenated ethanol solutions. *Journal of the American Chemical Society* 104(3), 796-798. 10.1021/ja00367a024

Black, E.D. and Hayon, E., 1970. Pulse radiolysis of phosphate anions $H_2PO_4^-$, HPO_4^{2-}, PO_4^{3-}, and $P_2O_7^{4-}$ in aqueous solutions. *The Journal of Physical Chemistry* 74(17), 3199-3203. 10.1021/j100711a007

Brigante, M., Minella, M., Mailhot, G., Maurino, V., Minero, C. and Vione, D., 2014. Formation and reactivity of the dichloride radical ($Cl_2^{\bullet-}$) in surface waters: A modelling approach. *Chemosphere* 95, 464-469. https://doi.org/10.1016/j.chemosphere.2013.09.098

Buehler, R.E., Staehelin, J. and Hoigne, J., 1984. Ozone decomposition in water studied by pulse radiolysis. 1. Perhydroxyl (HO_2)/hyperoxide ($O_2^{\bullet-}$) and $HO_3/O_3^{\bullet-}$ as intermediates. *The Journal of Physical Chemistry* 88(12), 2560-2564. 10.1021/j150656a026

Bulman, D.M., Mezyk, S.P. and Remucal, C.K., 2019. The impact of pH and irradiation wavelength on the production of reactive oxidants during chlorine photolysis. *Environmental Science & Technology* 53(8), 4450-4459. 10.1021/acs.est.8b07225

Bulman, D.M. and Remucal, C.K., 2020. Role of reactive halogen species in disinfection byproduct formation during chlorine photolysis. *Environmental Science & Technology* 54(15), 9629-9639. 10.1021/acs.est.0c02039

Buxton, G.V., Greenstock, C.L., Helman, W.P. and Ross, A.B., 1988. Critical review of rate constants for reactions of hydrated electrons, hydrogen atoms and hydroxyl radicals ($^{\bullet}OH/O^{\bullet-}$ in aqueous solution). *Journal of Physical and Chemical Reference Data* 17(2), 513-886. 10.1063/1.555805

Buxton, G.V. and Sellers, R.M., 1987. Reactivity of the hydrated electron and the hydroxyl radical with boric acid in aqueous solutions. *International Journal of Radiation Applications and Instrumentation. Part C. Radiation Physics and Chemistry* 29(2), 137-140. https://doi.org/10.1016/1359-0197(87)90048-8

Buxton, G.V. and Subhani, M.S., 1972. Radiation chemistry and photochemistry of oxychlorine ions. Part 1.—Radiolysis of aqueous solutions of hypochlorite and chlorite ions. *Journal of the Chemical Society, Faraday Transactions 1* 68(0), 947-957. 10.1039/F19726800947

Charbouillot, T., Brigante, M., Mailhot, G., Maddigapu, P.R., Minero, C. and Vione, D., 2011. Performance and selectivity of the terephthalic acid probe for OH as a function of temperature, pH and composition of atmospherically relevant aqueous media. *Journal of Photochemistry and Photobiology, A: Chemistry* 222(1), 70-76. https://doi.org/10.1016/j.jphotochem.2011.05.003

Christensen, H., Sehested, K. and Bjergbakke, E., 1989. Water chemistry of nuclear reactor systems 5, pp. 141-143, British Nuclear Energy Society, London.

Christensen, H., Sehested, K. and Corfitzen, H., 1982. Reactions of hydroxyl radicals with hydrogen peroxide at ambient and elevated temperatures. *The Journal of Physical Chemistry* 86(9), 1588-1590. 10.1021/j100206a023

Clifford, A.A., 1973. Multivariate Error Analysis: A Handbook of Error Propagation and Calculation in Many-parameter Systems, Applied Science Publishers.

Czapski, G. and Bielski, B.H.J., 1993. Absorption spectra of the $^{\bullet}OH$ and $O^{\bullet-}$ radicals in aqueous solutions. *Radiation Physics and Chemistry* 41(3), 503-505. https://doi.org/10.1016/0969-806X(93)90012-J

Elliot, A.J. and McCracken, D.R., 1989. Effect of temperature on O anion radical reactions and equilibria: a pulse radiolysis study. *Radiat. Phys. Chem., Int. J. Radiat. Appl. Instrum. Part C; (United Kingdom)*, Medium: X; Size: Pages: 69-74.

Elliot, A.J. and Buxton, G.V., 1992. Temperature dependence of the reactions OH + O and OH + HO_2 in water up to 200 °C. *Journal of the Chemical Society, Faraday Transactions* 88(17), 2465-2470. 10.1039/FT9928802465

Fang, X., Mark, G. and von Sonntag, C., 1996. OH radical formation by ultrasound in aqueous solutions Part I: the chemistry underlying the terephthalate dosimeter. *Ultrasonics Sonochemistry* 3(1), 57-63. https://doi.org/10.1016/1350-4177(95)00032-1

Fang, J., Fu, Y. and Shang, C., 2014. The roles of reactive species in micropollutant degradation in the UV/free chlorine system. *Environmental Science & Technology* 48(3), 1859-1868. 10.1021/es4036094

Flyunt, R., Leitzke, A., Mark, G., Mvula, E., Reisz, E., Schick, R. and von Sonntag, C., 2003. Determination of $^{\bullet}OH$, $O_2^{\bullet-}$, and hydroperoxide yields in ozone reactions in aqueous solution. *The Journal of Physical Chemistry B* 107(30), 7242-7253. 10.1021/jp022455b

Glaze, W.H., Kang, J.-W. and Chapin, D.H., 1987. The chemistry of water treatment processes involving ozone, hydrogen peroxide and ultraviolet radiation. *Ozone Science & Engineering* 9(4), 335-352. 10.1080/01919518708552148

Hand, V.C. and Margerum, D.W., 1983. Kinetics and mechanisms of the decomposition of dichloramine in aqueous solution. *Inorganic Chemistry* 22(10), 1449-1456. 10.1021/ic00152a007

Hansch, C., Leo, A. and Taft, R.W., 1991. A survey of Hammett substituent constants and resonance and field parameters. *Chemical Reviews* 91(2), 165-195. 10.1021/cr00002a004

Hasegawa, K. and Neta, P., 1978. Rate constants and mechanisms of reaction of chloride ($Cl_2^{\bullet-}$) radicals. *The Journal of Physical Chemistry* 82(8), 854-857. 10.1021/j100497a003

Held, A.M., Halko, D.J. and Hurst, J.K., 1978. Mechanisms of chlorine oxidation of hydrogen peroxide. *Journal of the American Chemical Society* 100, 5732-5740. https://ci.nii.ac.jp/naid/80013880552/en/

Hodgeson, J.W., Collins, J., Barth, R.E., Becker, D., Munch, D.J., Munch, J.W., Pawlecki, A.M. (1995) Method 552.2, Determination of Haloacetic acids and Dalapon in Drinking Water by Liquid-Liquid Extraction, Derivatization and Gas Chromatography with Electron Capture Detection, USEPA, Cincinnati, OH.

Hoigné, J., 1998. The Handbook of Environmental Chemistry, Springer Verlag, Heidelberg.

Holroyd, R.A. and Bielski, B.H.J., 1978. Photochemical generation of superoxide radicals in aqueous solutions. *Journal of the American Chemical Society* 100(18), 5796-5800. 10.1021/ja00486a034

Ike, I.A., Karanfil, T., Cho, J. and Hur, J., 2019a. Oxidation byproducts from the degradation of dissolved organic matter by advanced oxidation processes – A critical review. *Water Research* 164, 114929. https://doi.org/10.1016/j.watres.2019.114929

Ike, I.A., Lee, Y. and Hur, J., 2019b. Impacts of advanced oxidation processes on disinfection byproducts from dissolved organic matter upon post-chlor(am)ination: A critical review. *Chemical Engineering Journal* 375, 121929. https://doi.org/10.1016/j.cej.2019.121929

Janovsky, I., 1980. Pulse radiolysis of aqueous borate solutions containing iodide. *Radiochemical and Radioanalytical Letters* 44(2), 115-124. http://inis.iaea.org/search/search.aspx?orig_q=RN:11569199

Kläning, U.K. and Wolff, T., 1985. Laser flash photolysis of HClO, ClO^-, HBrO, and BrO^- in aqueous solution. Reactions of $Cl^{\bullet}$ and $Br^{\bullet}$ atoms. *Berichte der Bunsengesellschaft für physikalische Chemie* 89(3), 243-245. 10.1002/bbpc.19850890309

Lei, Y., Cheng, S., Luo, N., Yang, X. and An, T., 2019. Rate constants and mechanisms of the reactions of $Cl^{\bullet}$ and $Cl_2^{\bullet-}$ with trace organic contaminants. *Environmental Science & Technology* 53(19), 11170-11182. 10.1021/acs.est.9b02462

Liou, S.-Y. and Dodd, M.C., 2021. Evaluation of hydroxyl radical and reactive chlorine species generation from the superoxide/hypochlorous acid reaction as the basis for a novel advanced oxidation process. *Water Research* 200, 117142.

Lunak, S. and Sedlak, P., 1992. Photoinitiated reactions of hydrogen peroxide in the liquid phase. *Journal of Photochemistry and Photobiology, A: Chemistry* 68(1), 1-33. 10.1016/1010-6030(92)85014-l

Mártire, D.O., Rosso, J.A., Bertolotti, S., Le Roux, G.C., Braun, A.M. and Gonzalez, M.C., 2001. Kinetic study of the reactions of chlorine atoms and $Cl_2^{\bullet-}$ radical anions in aqueous solutions. II. Toluene, benzoic acid, and chlorobenzene. *The Journal of Physical Chemistry A* 105(22), 5385-5392. 10.1021/jp004630z

Maruthamuthu, P. and Neta, P., 1978. Phosphate radicals spectra, acid-base equilibria, and reactions with inorganic compounds. *The Journal of Physical Chemistry* 82(6), 710-713. http://inis.iaea.org/search/search.aspx?orig_q=RN:09401002

McDowell, M.S., Bakac, A. and Espenson, J.H., 1983. A convenient route to superoxide ion in aqueous solution. *Inorganic Chemistry* 22(5), 847-848.

Morgan, M.S., Van Trieste, P.F., Garlick, S.M., Mahon, M.J. and Smith, A.L., 1988. Ultraviolet molar absorptivities of aqueous hydrogen peroxide and hydroperoxyl ion. *Analytica Chimica Acta* 215, 325-329. https://doi.org/10.1016/S0003-2670(00)85294-0

Morris, J.C., 1966. The acid ionization constant of HOCl from 5 to 35°. *The Journal of Physical Chemistry* 70(12), 3798-3805. 10.1021/j100884a007

Nash, T., 1953. The colorimetric estimation of formaldehyde by means of the Hantzsch reaction. *The Biochemical journal* 55(3), 416-421. 10.1042/bj0550416

Neta, P. and Dorfman, L.M., 1968. Radiation Chemistry, pp. 222-230, American Chemical Society.

O'Neill, P., Steenken, S. and Schulte-Frohlinde, D., 1975. Formation of radical cations of methoxylated benzenes by reaction with hydroxyl radicals, thallium(2+), silver(2+), and peroxysulfate ($SO_4^{\bullet-}$) in aqueous solution. Optical and conductometric pulse radiolysis and in situ radiolysis electron spin resonance study. *The Journal of Physical Chemistry* 79(25), 2773-2779. 10.1021/j100592a013

Nowell, L.H. and Hoigné, J., 1992. Photolysis of aqueous chlorine at sunlight and ultraviolet wavelengths—II. Hydroxyl radical production. *Water Research* 26(5), 599-605. https://doi.org/10.1016/0043-1354(92)90233-T

O'Neill, P., Steenken, S. and Schulte-Frohlinde, D., 1975. Formation of radical cations of methoxylated benzenes by reaction with hydroxyl radicals, thallium(2+), silver(2+), and peroxysulfate ($SO_4^{\bullet-}$) in aqueous solution. Optical and conductometric pulse radiolysis and in situ radiolysis electron spin resonance study. *The Journal of Physical Chemistry* 79(25), 2773-2779. 10.1021/j100592a013

Oviedo, C. and Rodríguez, J., 2003. EDTA: the chelating agent under environmental scrutiny. *Química Nova* 26, 901-905. http://www.scielo.br/scielo.php?script=sci_arttext&pid=S0100-40422003000600020&nrm=iso

Page, S.E., Arnold, W.A. and McNeill, K., 2010. Terephthalate as a probe for photochemically generated hydroxyl radical. *Journal of environmental monitoring* 12(9), 1658-1665. 10.1039/c0em00160k

Pinkernell, U., Nowack, B., Gallard, H. and von Gunten, U., 2000. Methods for the photometric determination of reactive bromine and chlorine species with ABTS. *Water Research* 34(18), 4343-4350. https://doi.org/10.1016/S0043-1354(00)00216-5

Prasse, C., Ford, B., Nomura, D.K. and Sedlak, D.L., 2018. Unexpected transformation of dissolved phenols to toxic dicarbonyls by hydroxyl radicals and UV light. *Proceedings of the National Academy of Sciences of the United States of America* 115(10), 2311. 10.1073/pnas.1715821115

Richardson, S.D. and Plewa, M.J., 2020. To regulate or not to regulate? What to do with more toxic disinfection by-products? *Journal of Environmental Chemical Engineering* 8(4), 103939. https://doi.org/10.1016/j.jece.2020.103939

Rodríguez, E.M. and von Gunten, U., 2020. Generation of hydroxyl radical during chlorination of hydroxyphenols and natural organic matter extracts. *Water Research* 177, 115691. https://doi.org/10.1016/j.watres.2020.115691

Rosario-Ortiz, F.L., Mezyk, S.P., Doud, D.F.R. and Snyder, S.A., 2008. Quantitative correlation of absolute hydroxyl radical rate constants with non-isolated effluent organic matter bulk properties in water. *Environmental Science & Technology* 42(16), 5924-5930. 10.1021/es800349b

Ross, A., Bielski, B., Buxton, G., Cabelli, D., Helman, W., Huie, R., Grodkowski, J., Neta, P., Mulazzani, Q. and Wilkinson, F. (1998) NIST Standard Reference Database 40: NDRL/NIST Solutions Kinetics Database V. 3.0, Gaithersburg, MD.

Schreiber, I.M. and Mitch, W.A., 2005. Influence of the order of reagent addition on NDMA formation during chloramination. *Environmental Science & Technology* 39(10), 3811-3818. 10.1021/es0483286

Schuchmann, M.N. and Von Sonntag, C., 1979. Hydroxyl radical-induced oxidation of 2-methyl-2-propanol in oxygenated aqueous solution. A product and pulse radiolysis study. *The Journal of Physical Chemistry* 83(7), 780-784. 10.1021/j100470a004

Sehested, K., Rasmussen, O.L. and Fricke, H., 1968. Rate constants of OH with HO_2, $O_2^{\bullet-}$, and $H_2O_2^+$ from hydrogen peroxide formation in pulse-irradiated oxygenated water. *The Journal of Physical Chemistry* 72(2), 626-631. 10.1021/j100848a040

Shores, T.S., 2018. Applied Linear Algebra and Matrix Analysis, Springer International Publishing, New York City.

Staehelin, J. and Hoigne, J., 1982. Decomposition of ozone in water: rate of initiation by hydroxide ions and hydrogen peroxide. *Environmental Science & Technology* 16(10), 676-681. 10.1021/es00104a009

von Sonntag, C. and von Gunten, U., 2012. Chemistry of Ozone in Water and Wastewater Treatment: From Basic Principles to Applications, IWA Publishing, London.

Watts, M.J. and Linden, K.G., 2007. Chlorine photolysis and subsequent OH radical production during UV treatment of chlorinated water. *Water Research* 41(13), 2871-2878. https://doi.org/10.1016/j.watres.2007.03.032

USEPA (2016) Contaminant Information Sheets (CISs) for the Final Fourth Contaminant Candidate List (CCL 4).

USEPA (2020) National Primary Drinking Water Standards.

Watts, M.J. and Linden, K.G., 2007. Chlorine photolysis and subsequent OH radical production during UV treatment of chlorinated water. *Water Research* 41(13), 2871-2878. https://doi.org/10.1016/j.watres.2007.03.032

Westerhoff, P., Mezyk, S.P., Cooper, W.J. and Minakata, D., 2007. Electron pulse radiolysis determination of hydroxyl radical rate constants with suwannee River fulvic acid and other dissolved organic matter isolates. *Environmental Science & Technology* 41(13), 4640-4646. 10.1021/es062529n

Wu, Z., Guo, K., Fang, J., Yang, X., Xiao, H., Hou, S., Kong, X., Shang, C., Yang, X., Meng, F. and Chen, L., 2017. Factors affecting the roles of reactive species in the degradation of micropollutants by the UV/chlorine process. *Water Research* 126, 351-360. https://doi.org/10.1016/j.watres.2017.09.028

Young, T.R., Cheng, S., Li, W. and Dodd, M.C., 2020. Rapid, high-sensitivity analysis of oxyhalides by non-suppressed ion chromatography-electrospray ionization-mass spectrometry: application to ClO_4^-, ClO_3^-, ClO_2^-, and BrO_3^- quantification during sunlight/chlorine advanced oxidation. *Environmental Science: Water Research & Technology* 6(9), 2580-2596. 10.1039/D0EW00429D

Young, T.R., Li, W., Guo, A., Korshin, G.V. and Dodd, M.C., 2018. Characterization of disinfection byproduct formation and associated changes to dissolved organic matter during solar photolysis of free available chlorine. *Water Research* 146, 318-327. https://doi.org/10.1016/j.watres.2018.09.022

Yu, X.-Y., 2004. Critical evaluation of rate constants and equilibrium constants of hydrogen peroxide photolysis in acidic aqueous solutions containing chloride ions. *Journal of Physical and Chemical Reference Data* 33(3), 747-763. 10.1063/1.1695414

Chapter 3. POTENTIAL FOR PRACTICAL APPLICATION OF SUPEROXIDE/HYPOCHLOROUS ACID REACTION AS A NOVEL ADVANCED OXIDATION PROCESS AND SUPEROXIDE/HYPOCHLOROUS ACID REACTION MODELING

3.1 Introduction

Current application conditions for the $O_2^{\bullet-}$/FAC treatment were not ideal as the high pH of the $O_2^{\bullet-}$ stocks (pH 13.9) required higher dosage of sulfuric acid for acidification to circumneutral pH in order to initiate the reactions. There was estimated to be ~10 g/L of sulfate remaining in the treated water under such condition, which was way higher than the secondary MCL of sulfate proposed by the USEPA for drinking water at only 250 mg/L. In addition, use of large amount of NaOH also elevate the chemical cost. This work first focused on modification and evaluation of current treatment designs in order to minimize sulfate residual. Cost estimation was then performed based on the modified version of treatment approach, and the potential of practical application and procedure of the $O_2^{\bullet-}$/FAC process were suggested. Model simulation for the $O_2^{\bullet-}$/FAC process can be important to help provide better understanding in the reaction chemistries and identify those critical reactions that govern the radical production and scavenging. The model may also be used for prediction of contaminant removal after treatment. Therefore, a model was built in this work based on reactions involved in the $O_2^{\bullet-}$/FAC process.

3.2 Materials and Methods

3.2.1 Refined $O_2^{\bullet-}$ Stock Generation

(i) KO_2 dissolution in 0.05M NaOH (KO_2 solids added to NaOH solutions)

10 mL of 0.05 M NaOH (pH 12.7) at room temperature (22±2 °C) was placed in a 20 mL amber borosilicate glass vial, and stirred by a magnetic stirrer at high enough mixing speed to generate a visible vortex in the liquid. Desired masses of KO_2 were weighed and immediately added into the vial. This approach of adding KO_2 solids to vigorously mixed NaOH solutions

appears to more effectively decrease localized concentrations of $HO_2^{\bullet}/O_2^{\bullet-}$ during preparation of $O_2^{\bullet-}$ stock solutions compared to addition of NaOH solutions to KO_2 solids, and can in turn improve $O_2^{\bullet-}$ yields and stability. An initial KO_2 concentration of 20 mM was selected for use in preparing $O_2^{\bullet-}$ stocks for $O_2^{\bullet-}$/FAC treatment with this approach. Note that we have changed the KO_2-derived $O_2^{\bullet-}$ stock preparation to a solid-to-liquid method. This helped increase the mixing efficiency and yield higher initial $O_2^{\bullet-}$ concentration in the stocks.

(ii) UV irradiation of alkaline H_2O_2/HO_2^-

UV-derived $O_2^{\bullet-}$ stock was prepared by UV irradiation of alkaline H_2O_2 solutions at pH12.7 or pH12.5 using the same method and conditions described in Section 2.2.2. UV-derived $O_2^{\bullet-}$ stocks in 0.05 M NaOH were typically prepared to contain $[HO_2^{\bullet}/O_2^{\bullet-}]_{stock}$ = 900 μM and $[H_2O_2/HO_2^-]_{stock}$ = 11 mM at the time of dosing to receiving solutions, while those in 0.0316M NaOH were prepared to contain $[HO_2^{\bullet}/O_2^{\bullet-}]_{stock}$ = 500 μM and $[H_2O_2/HO_2^-]_{stock}$ = 5 mM. Figures 2.3 and 2.4 show respective profiles for $O_2^{\bullet-}$ generation during UV-irradiation of H_2O_2, and $O_2^{\bullet-}$ decay following removal of irradiated H_2O_2 solutions from the UV light source. The stocks were dosed to receiving solutions at dilution factors ranging from (a) 1:36 to 1:9 or (b) 1:20 to 1:5, yielding in situ $[HO_2^{\bullet}/O_2^{\bullet-}]$ ~ 25-100 and $[H_2O_2/HO_2^-]$ ~ 0.25-1.2 mM in the $O_2^{\bullet-}$/FAC-treated final solutions.

3.2.2 Modeling of $O_2^{\bullet-}$/FAC Reaction

Kinetic models of AOPs often consist of hundreds of reactions depending on the systems. The $O_2^{\bullet-}$/FAC process was simulated using the Kintecus kinetics software in this study (Ianni, James C., Kintecus , Windows Version 6.01, 2017, www.kintecus.com). It involves very complicated reaction mechanisms, some of which may cause violations of the principle of

detailed balancing. There are three ways such violations can occur: (1) reversible reaction loops where the rate constants do not attain closure, (2) illegal loops in which reactions never reach equilibrium (Wegscheider's condition), and (3) reversible steps having rate equations in the forward and reverse directions that are inconsistent with the equilibrium expressions (Lee et al., 2020; Stanbury, 2020; Stanbury and Harshman, 2019; Stanbury and Hoffman, 2019). However, the last one is usually hard to identify because the independent equilibrium constants (not calculated based on the forward and reverse rate constants) are usually not available. Therefore, this type of disagreement was ignored. A brief graphic summary of these three types of violations was provided in Figure 3.1. Stanbury et al. has developed a computer program called "DETBAL" to facilitate the identification of both the illegal loops and the violations using the programming language R (Stanbury, 2020; Stanbury and Harshman, 2019; Stanbury and Hoffman, 2019). The program can be run by simply downloading the Rmd file from the authors' Github page (https://github.com/jordanharshman/DETBAL), and opening it in the R studio software. Once the file is open, click the "Run Document" button to activate the user interface of the program, where one can input the chemical reactions and see the detailed analysis results. Detailed balancing analysis was also applied to the $O_2^{\bullet-}$/FAC kinetic model to identify reversible and illegal reaction loops using DETBAL. Lee et al. has already identified a couple of illegal loops in kinetic models for UV/chlorine (similar system as $O_2^{\bullet-}$/FAC process) established by some previous studies (Bulman et al., 2019; Lee et al., 2020; Sun et al., 2016). Those reactions with violations occurred were therefore removed from the model built in this work.

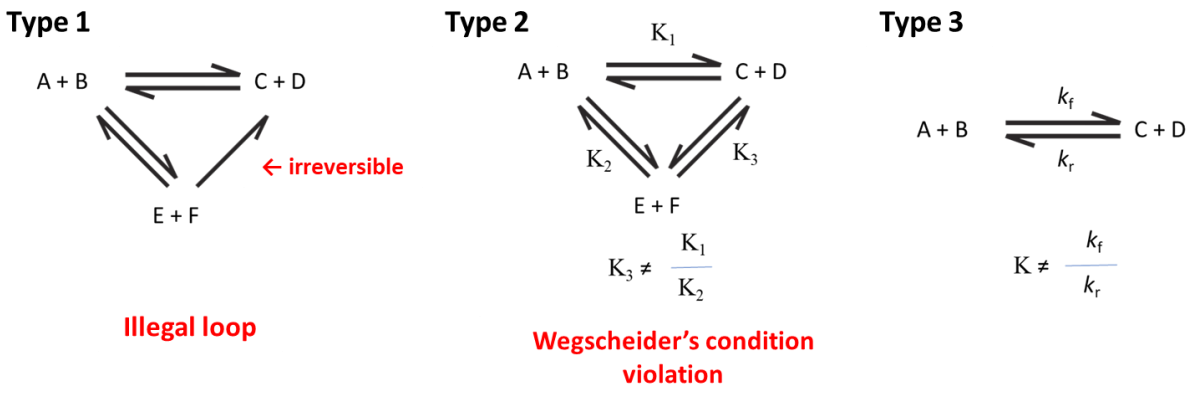

Figure 3.1. Three types of detailed balancing violations: (1) illegal loops, (2) violation of the Wegscheider's condition, and (3) disagreement of the ratio of the forward to reverse rate constants with the equilibrium constant, obtained from (Lee et al., 2020; Stanbury, 2020; Stanbury and Harshman, 2019; Stanbury and Hoffman, 2019).

3.3 Refinement of $O_2^{\bullet-}$/FAC Treatment

A potential barrier to implementation of $O_2^{\bullet-}$/FAC treatment derives from the high pH needed for $O_2^{\bullet-}$ stock solutions, and the consequent levels of acid necessary to neutralize the OH^- derived from the stock solutions upon dosing to receiving waters. Under the exploratory conditions used in many of the experiments described to this point, the use of high H_2SO_4 concentrations for NaOH neutralization would lead to levels of residual SO_4^{2-} in substantial excess of the USEPA secondary (non-enforceable) drinking water MCL of 250 mg/L as SO_4^{2-} in treated waters, potentially leading to negative aesthetic and/or gastrointestinal effects (USEPA, 2003a; b), or to enhanced risks of corrosion in materials in contact with treated waters (USEPA, 2016; Yang et al., 2014). This issue can potentially be addressed by (1) preparing $O_2^{\bullet-}$ stocks in less alkaline NaOH solutions to decrease the H_2SO_4 concentration needed for neutralization, and/or (2) increasing the concentrations of $O_2^{\bullet-}$ in the stocks to enable the use of smaller stock volumes and higher dilution factors – also resulting in decreased H_2SO_4 requirements.

A series of additional experiments was therefore undertaken in which $O_2^{\bullet-}$ stocks were prepared from KO_2 or UV irradiation of H_2O_2/HO_2^- under conditions selected to achieve elevated $[HO_2^{\bullet}/O_2^{\bullet-}]$ concentrations at lower pH, and used to degrade NB, BA, and DMB using single- and multiple-dose postmix $O_2^{\bullet-}$/FAC treatment (with H_2O_2 quenched using FAC in multiple-dosing). In so doing, it was found that for KO_2-derived $O_2^{\bullet-}$ stocks, the $O_2^{\bullet-}$ yield and stability could be significantly improved by adding KO_2 solids slowly to NaOH solutions under rapid mixing, rather than by addition of NaOH to KO_2 solids, as was the case for most of the stocks prepared in this work (see Section 2.2.2). KO_2-derived stocks were in turn prepared from 20-mM KO_2 in 0.05M NaOH (pH 12.7) – yielding concentrations of $[HO_2^{\bullet}/O_2^{\bullet-}]_{stock} \sim 2000$ μM and $[H_2O_2/HO_2^-]_{stock} \sim 6000$ μM. UV-derived $O_2^{\bullet-}$ stocks were prepared using irradiation of 20 mM $[H_2O_2/HO_2^-]_0$ in 0.05M NaOH (pH 12.7) – yielding $[HO_2^{\bullet}/O_2^{\bullet-}]_{stock} \sim 900$ μM and $[H_2O_2/HO_2^-]_{stock} \sim 11$ mM, or irradiation of 10 mM $[H_2O_2/HO_2^-]_0$ in 0.0316M NaOH (pH 12.5) – yielding $[HO_2^{\bullet}/O_2^{\bullet-}]_{stock} \sim 500$ μM and $[H_2O_2/HO_2^-]_{stock} \sim 5000$ μM (Section 2.2.2 and Figure 2.4).

The KO_2-derived stocks were dosed to receiving solutions at $[HO_2^{\bullet}/O_2^{\bullet-}]_0/[FAC]_0 = 2$, with dilution factors ranging from 1:40 to 1:10, whereas the UV-derived stocks were dosed to receiving solutions at $[HO_2^{\bullet}/O_2^{\bullet-}]_0/[FAC]_0 = 1$ due to their lower $[HO_2^{\bullet}/O_2^{\bullet-}]_{stock}$ concentrations, with dilution factors ranging from 1:40 to 1:5. As shown in Figure 3.2, these experiments yielded levels of probe degradation comparable to those obtained using $O_2^{\bullet-}$ stocks prepared from KO_2 at higher pH (Figure 2.16), with only moderately diminished effectiveness for the UV-derived stocks dosed at the lower $[HO_2^{\bullet}/O_2^{\bullet-}]_0/[FAC]_0$. At the same time, the use of the KO_2 stocks required only 2.5 mM of H_2SO_4 to neutralize OH^- – resulting in residual SO_4^{2-} concentrations of 240 mg/L (below the secondary MCL); and the use of the UV-derived stocks required only 2.8

and 3.2 mM of H_2SO_4 to neutralize OH^- – resulting in residual SO_4^{2-} concentrations of 260 mg/L and 300 mg/L, respectively (just above the secondary MCL). Continued optimization of $O_2^{\bullet-}$ stock preparation and handling at lower pH values will be needed to enable further decreases in residual H_2SO_4 dosing requirements and consequent residual SO_4^{2-} concentrations. Residual [H_2O_2/HO_2^-] levels in receiving solutions did not exceed ~600 μM or ~1200 μM when using either KO_2-derived or UV-derived stocks, respectively. At these [H_2O_2/HO_2^-] levels, the use of excess FAC to quench H_2O_2/HO_2^- in either single- or multiple-dosing approaches would be expected to contribute no more than ~50 mg/L of total residual Cl^- to treated waters (assuming equimolar [Cl^-] and [FAC] in FAC stocks and 100% conversion of FAC to Cl^- upon reaction with $HO_2^{\bullet}/O_2^{\bullet-}$ or H_2O_2/HO_2^-) – well below the secondary MCL of 250 mg/L as Cl^-.

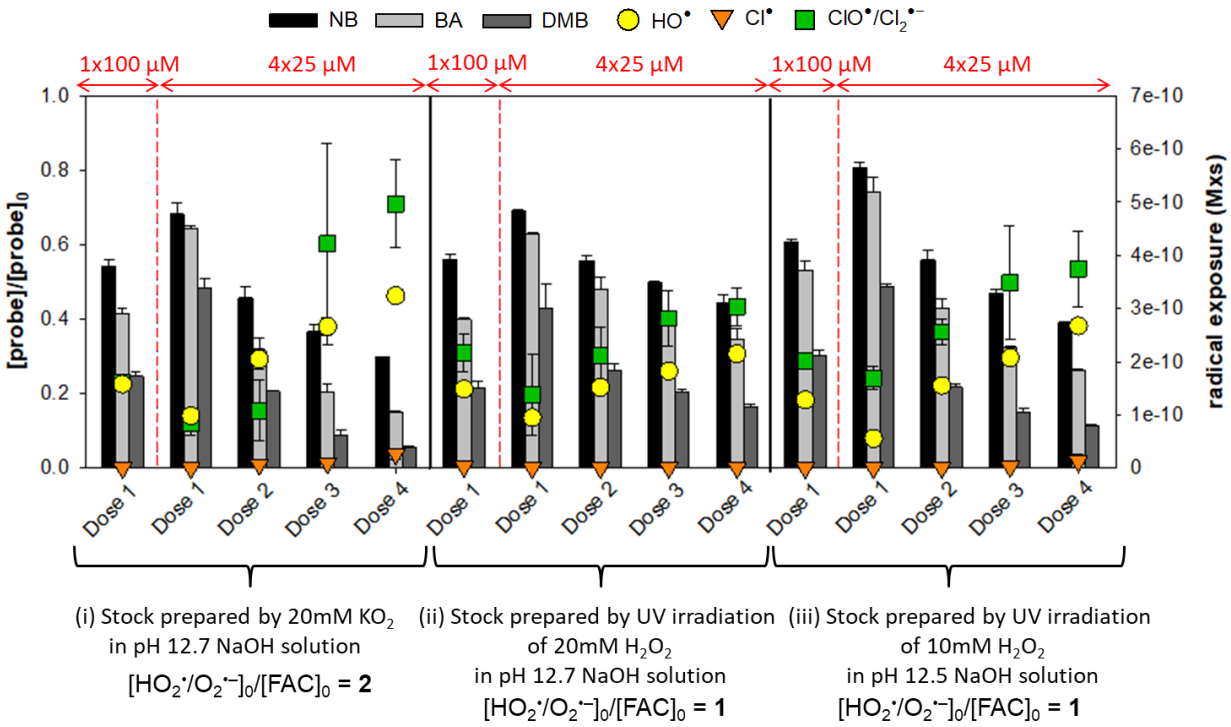

Figure 3.2. Modified $O_2^{\bullet-}$/FAC treatment approaches using $O_2^{\bullet-}$ stock solutions generated at pH<13 by KO_2 dissolution or UV irradiation of H_2O_2/HO_2^- solutions, and dosed at $[HO_2^{\bullet}/O_2^{\bullet-}]_0/[FAC]_0$ ratios of 1 or 2. Probe compound concentrations and in situ radical exposures ($\int_0^t [\text{radical}]\,dt$) resulting from multiple-dose postmix $O_2^{\bullet-}$/FAC treatment of pH 7, 5mM phosphate buffer containing $[NB, BA, DMB]_0$ = 1 µM. In multiple-dose treatment, residual $[H_2O_2/HO_2^-]$ present after each $O_2^{\bullet-}$ dose (typically 150-300 mM) was first measured by the Allen reagent method, after which sufficient FAC was added to scavenge all H_2O_2/HO_2^- and leave the desired [FAC] residual in solution for the following $O_2^{\bullet-}$ dose. $O_2^{\bullet-}$ stocks for dosing were prepared by (i) dissolution of KO_2 in 0.05M NaOH at pH 12.7, (ii) photolysis of H_2O_2/HO_2^- in 0.05M NaOH solutions at 12.7, or (iii) photolysis of H_2O_2/HO_2^- in 0.0316M NaOH solutions at 12.5 (see text for corresponding $[HO_2^{\bullet}/O_2^{\bullet-}]_{stock}$ and $[H_2O_2/HO_2^-]_{stock}$ concentrations). For (i), experiments were undertaken by dosing $[HO_2^{\bullet}/O_2^{\bullet-}]_0/[FAC]_0$ = (200 µM)/(100 µM) once (1×100 µM) or by dosing $[HO_2^{\bullet}/O_2^{\bullet-}]_0/[FAC]_0$ = (50 µM)/(25 µM) four times (4×25 µM). For (ii) and (iii), experiments were undertaken by dosing $[HO_2^{\bullet}/O_2^{\bullet-}]_0/[FAC]_0$ = (100 µM)/(100 µM) once (1×100 µM) or by dosing $[HO_2^{\bullet}/O_2^{\bullet-}]_0/[FAC]_0$ = (25 µM)/(25 µM) four times (4×25 µM). Error bars represent one standard deviation about the mean of duplicate measurements. Adopted from (Liou and Dodd, 2021).

3.4 Cost Estimation of $O_2^{\bullet-}$/FAC Treatment

The high cost of commercially-available KO_2 solids likely precludes their use as a means of preparing $O_2^{\bullet-}$ stocks in large-scale treatment applications. However, UV-derived $O_2^{\bullet-}$ stocks may present a more practical option for implementing $O_2^{\bullet-}$/FAC treatment at scale. For example, such stocks could be continuously generated on-site by using LP Hg or UV LED irradiation of alkaline H_2O_2/HO_2^- in a flow-through cell for online infusion into process waters. With this in mind, a preliminary estimate of the electrical and chemical costs for implementing such an approach was performed using data from the bench-scale experiments undertaken here with UV-derived $O_2^{\bullet-}$ stocks, with 90% degradation of BA in phosphate buffer during single-dose postmix treatment selected as a reference condition (with costs determined in units of \$ per m^3 of treated water per order of magnitude BA degradation, or $\$\cdot m^{-3}\cdot order^{-1}$) (see Text S3.2 for details). The resulting calculations yield a cost estimate of ~$\$1.0\text{-}1.1\cdot m^{-3}\cdot order^{-1}$ for $O_2^{\bullet-}$/FAC treatment (including costs for UV lamp output, H_2O_2, NaOH, H_2SO_4, and FAC) (Table 3.1 and 3.2). By comparison, the costs for O_3/H_2O_2 (including costs for O_3 generation and H_2O_2) and UV/H_2O_2 (including costs for UV lamp output and H_2O_2) to yield 90% degradation of the very similar pCBA in various natural waters were estimated as $\$0.0043\text{-}0.008\cdot m^{-3}\cdot order^{-1}$ and $\$0.075\text{-}0.192\cdot m^{-3}\cdot order^{-1}$, respectively (based on previously reported findings (Katsoyiannis et al., 2011)) (Table 3.2). It should be noted that these estimates do not account for variations in capital costs.

Table 3.1. Prices and estimated Cost/$O_{chemical}$ values for specific chemicals[a]

Chemical	$/mol[b]	mol of chemical for treatment of volume V [c]	Cost/$O_{chemical}$ ($·m^{-3}·order^{-1})	References
H_2O_2	0.031	2.2×10^{-5}	0.17	(Rosenfeldt et al., 2006)
NaOH	0.04	5.6×10^{-5}	0.56	(USEPA, 2005)
NaOCl	0.71	1×10^{-6}	0.18	(USEPA, 1999; 2005; 2006)
H_2SO_4	0.01	2.8×10^{-5}	0.070	(USEPA, 2005; 2006)

[a] Adopted from (Liou and Dodd, 2021). [b]Data are corrected for inflation of currency from their published date to Dec. 2020 using the CPI Inflation Calculator from U.S. Bureau of Labor Statistics (https://www.bls.gov/data/inflation_calculator.htm). Average prices are provided if based on more than one source. [c] V = 10 mL treated receiving solution volume

Table 3.2. Comparison of Cost/O values for $O_2^{\bullet-}$/FAC with O_3/H_2O_2 and UV/H_2O_2[a]

Chemical	Cost/O_{UV} ($·m^{-3}·order^{-1})	Cost/$O_{chemical}$ ($·m^{-3}·order^{-1})	Cost/O_{total} ($·m^{-3}·order^{-1})	References
$O_2^{\bullet-}$/FAC	0.137[b] 0.069[c]	0.98[b] 0.90[c]	1.12[b] 0.97[c]	This study
O_3/H_2O_2	n.a.	n.a.	0.0043-0.008	(Katsoyiannis et al., 2011)
UV/H_2O_2	n.a.	n.a.	0.075-0.19	(Katsoyiannis et al., 2011)

[a] Adopted from (Liou and Dodd, 2021). [b] Calculated based on $O_2^{\bullet-}$ stock generated with 4.5 min UV irradiation of 20mM alkaline H_2O_2 solution in 0.05M NaOH (pH12.7), [c] Calculated based on $O_2^{\bullet-}$ stock generated with 2.5 min UV irradiation of 20mM alkaline H_2O_2 solution in 0.05M NaOH (pH12.7)

The ≥5-fold higher cost estimate for $O_2^{\bullet-}$/FAC treatment primarily reflects costs of NaOH (~50% of the total) and to a lesser extent H_2O_2 and FAC (~31% of the total combined), followed by H_2SO_4 (~6% of the total); the costs for UV lamp output (~13% of the total) are similar to those for UV/H_2O_2 (Tables 3.1 and 3.2). Further improvements in $O_2^{\bullet-}$/FAC treatment performance and cost can likely be realized through continued refinement of approaches for $O_2^{\bullet-}$ stock preparation to improve $HO_2^{\bullet}/O_2^{\bullet-}$ yield and stability at lower pH values. For example, if $O_2^{\bullet-}$ stock solution pH could be lowered by one unit (from 12.7 to 11.7) while still maintaining equivalent $O_2^{\bullet-}$ concentrations, NaOH and H_2SO_4 requirements could in turn be lowered by 10-fold, with a corresponding reduction of $\$0.57 \cdot m^{-3} \cdot order^{-1}$ (or ~50-60%) in overall costs. Alternatively, improvements in $O_2^{\bullet-}$ stability and/or yield from UV irradiation of alkaline H_2O_2/HO_2^- solutions at pH 12.7 (e.g., through the use of higher-intensity lamps or more efficient lamp geometries) could allow the accumulation of higher $O_2^{\bullet-}$ concentrations in stocks. This could in turn enable decreases in the required volumes of $O_2^{\bullet-}$ stock solutions to implement $O_2^{\bullet-}$/FAC treatment at a given $[HO_2^{\bullet}/O_2^{\bullet-}]_0/[FAC]_0$ ratio, which would lead to lower NaOH, H_2O_2/HO_2^-, *and* H_2SO_4 requirements. For example, a 2-fold increase in peak $O_2^{\bullet-}$ concentrations achievable in stocks could lead to a commensurate 2-fold decrease in $O_2^{\bullet-}$ stock volume requirements, in turn cutting NaOH, H_2O_2/HO_2^-, and H_2SO_4 requirements in half and lowering the associated costs by $\$0.28 \cdot m^{-3} \cdot order^{-1}$, $\$0.085 \cdot m^{-3} \cdot order^{-1}$, and $\$0.035 \cdot m^{-3} \cdot order^{-1}$ respectively (for a decrease of ~35-45% in overall costs).

It is also worthwhile to note that even if $\$ \cdot m^{-3} \cdot order^{-1}$ costs for $O_2^{\bullet-}$/FAC treatment remain higher than for more conventional AOPs, its simplicity, rapid operational time-scales (and as a consequence, its low required reactor volume and footprint), potential for on-site $O_2^{\bullet-}$ generation, and widespread accessibility of FAC (also including potential for on-site generation)

and other reagents could make this process uniquely advantageous for certain applications; in particular smaller-scale decentralized and/or point-of-use (waste)water treatment.

As the first investigation exploring the possibility of directly applying $O_2^{\bullet-}$/FAC treatment for advanced oxidation, this work is principally intended to elucidate process chemistry and to provide a foundation from which to explore future applications. More definitive assessments of costs and implementation strategies will require studies dedicated to these aims and conducted at pilot- and/or full-scale. Future research on these topics is therefore highly encouraged, and will be needed to more fully evaluate the potential of the $O_2^{\bullet-}$/FAC process for applications in (waste)water treatment and reuse.

3.5 Potential Practical Implementation

The $O_2^{\bullet-}$/FAC process could be useful in smaller-scale decentralized and point-of-use water treatments by generating $O_2^{\bullet-}$ stocks with small UV lamp array. Figure 3.3 shows the potential schematic for implementation of the $O_2^{\bullet-}$/FAC process in water treatment. Note that the use of UV/H_2O_2 approach for $O_2^{\bullet-}$ stock preparation would be at smaller scale and off-line, so that the whole volume of water passing through a water treatment facility would not need to be irradiated, and thus, that a large, expensive online array of UV lamps would not be required. In another word, only relatively small volumes of stock solutions to be injected into the main flow of the water treatment plant would need to be irradiated. This requires a much smaller lamp array and associated capital costs, and have less concern regarding UV light transmission limitation as compared to a typical UV/H_2O_2 treatment process.

Alkaline H_2O_2 solution for stock generation can be prepared by the mixture of H_2O_2 with NaOH or $Ca(OH)_2$. The resulted $O_2^{\bullet-}$ stocks can than be applied in three different scenarios,

depending on the needs, including the premix dosing (blue pathway) and postmix dosing (red pathway). If the feed water already contains chlorine, then no chlorine or less amount of chlorine would be required for the postmix dosing treatment (black pathway).

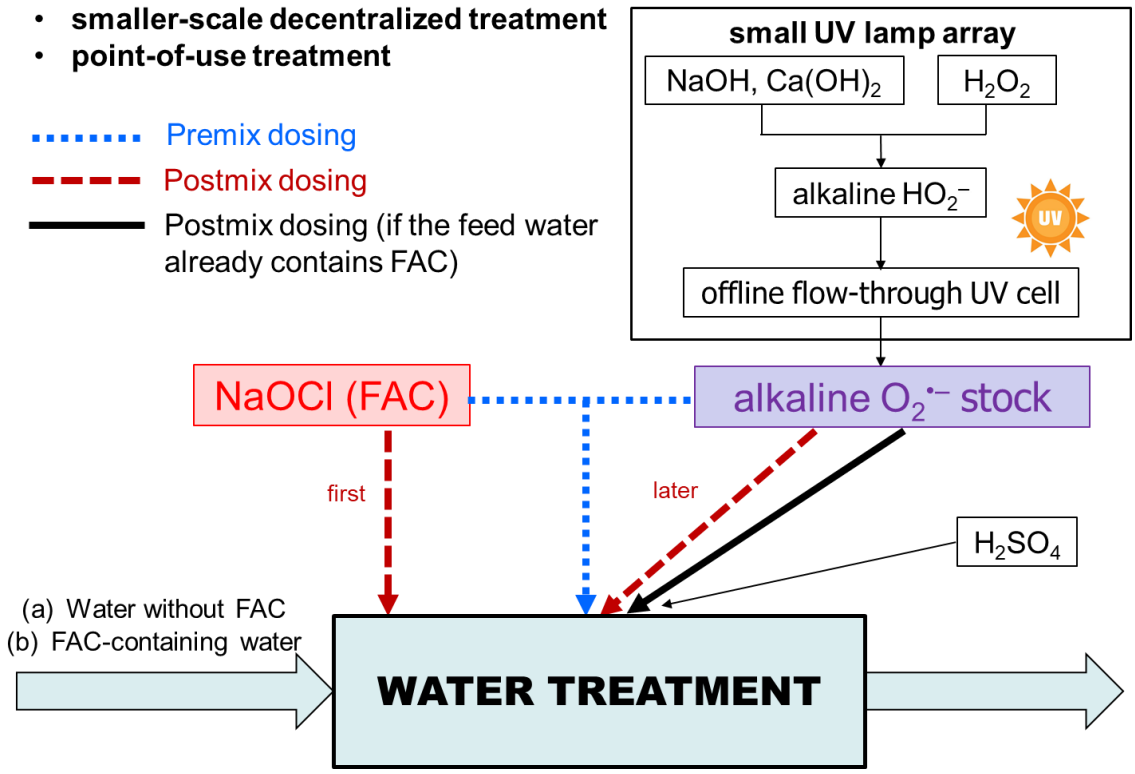

Figure 3.3. Schematic for potential implementation of the $O_2^{\bullet-}$/FAC process in water treatment

In this study, most of the experiments were conducted in batch reactors. Since batch reaction kinetics are equivalent to reaction kinetics in a PFR under ideal conditions, the batch kinetics should theoretically be applicable to a PFR with appropriate mass balance consideration. However, it should be noted that the time scale of $O_2^{\bullet-}$/FAC reactions is so fast that it could be similar to the time scale of mixing among the $O_2^{\bullet-}$ stock, the FAC solution and the acid for neutralization. Therefore, most of the reactions involved in the $O_2^{\bullet-}$/FAC process would complete at the point of mixing. Little additional reactions would proceed after that time frame.

In another word, little reactions would occur in the subsequent length of a PFR. As a result, using a PFR following a CSTR (as a flash mixer for $O_2^{\bullet-}$, FAC and acid) may not provide more benefits than directly using a CSTR. One possibility could be using multiple CSTRs in series, which can be applied for multiple-dosing treatment. Another way to address this could be using static mixers or venturi mixers inside a pipe to ensure effective mixing, and the reaction reagents can be infused at different locations of a pipeline for multiple-dosing application. Pilot-scale or larger-scale tests would be needed to fully evaluate these approaches.

3.6 Other Superoxide Production Approaches

3.6.1 KrCl* Lamp (222 nm) for $O_2^{\bullet-}$ Stock Generation

Improving $O_2^{\bullet-}$ concentration and its stability in the stocks can help reduce stocks needed for dosing during $O_2^{\bullet-}$/FAC treatment and minimize the chemical cost. One possibility could be producing $O_2^{\bullet-}$ stocks through photochemical irradiation of alkaline H_2O_2 solution but with higher-intensity lamps. It is expected to achieve higher $O_2^{\bullet-}$ yield in the stocks with more powerful UV254 lamps than the one (a 5W low-pressure Hg lamp, fluence rate = 39.5 mW/cm^2) used in the preceding experiments; however, more intensive UV254 lamp could also self-limit $O_2^{\bullet-}$ accumulation in the stock as it also facilitates $O_2^{\bullet-}$ photo-decomposition. One way to address this is switch to a wavelength which maximize H_2O_2 photolysis while minimizing $O_2^{\bullet-}$ decomposition during irradiation. Emerging far-UVC devices (emitting UVC irradiation in the wavelength range of 220 to 225 nm) like the krypton chloride (KrCl*) excimer lamp could be a good candidate for this purpose. Spectra KrCl* lamp emission and adsorption of H_2O_2 and $O_2^{\bullet-}$ are shown in Figure 3.4. At pH ≥ 13, extinction coefficients of H_2O_2/HO_2^- ($\varepsilon_{H_2O_2/HO_2^-}$) have been reported as 539.4, 277.7, 194.8 M^{-1}cm^{-1} at 220, 250 and 260 nm (Morgan et al., 1988), and

$HO_2^{\bullet}/O_2^{\bullet-}$ has extinction coefficients ($\varepsilon_{HO_2^{\bullet}/O_2^{\bullet-}}$) of 1920, 2260, and 1940 $M^{-1}cm^{-1}$, respectively (Bielski, 1978). Absorbance ratio of H_2O_2/HO_2^- over $HO_2^{\bullet}/O_2^{\bullet-}$ can then be calculated as 0.281, 0.123, 0.100 in order under these three wavelengths. Therefore, one could expect irradiation at 220 nm to more effectively photolyze H_2O_2 while causing slower $O_2^{\bullet-}$ photolysis. Interestingly, far-UVC light has been reported to have low adverse effect on skin and eyes as well as no DNA damage in animals due to its very limited penetration into biological materials (Buonanno et al., 2017; Buonanno et al., 2020; Kaidzu et al., 2021; Narita and Asano, 2018), and thus it causes less biosafety concern than those commonly applied UV254 devices.

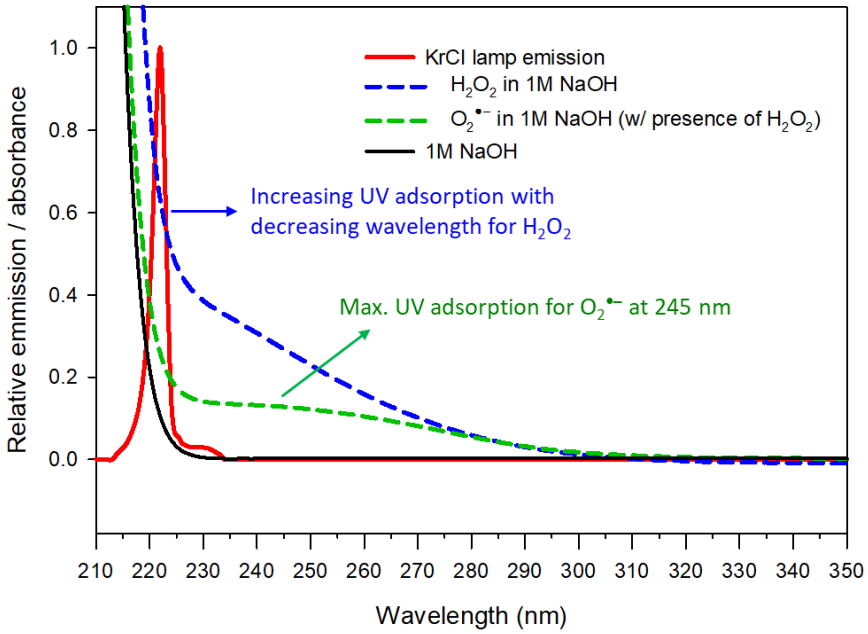

Figure 3.4. Relative emission spectrum of the KrCl* lamp and relative adsorption spectra of 1M NaOH, alkaline H_2O_2 (in 1M NaOH), and $O_2^{\bullet-}/H_2O_2$ mixture (in 1M NaOH).

A KrCl* lamp emitting 222 nm UVC equipped with a 222-nm bandpass filter was therefore used to generate $O_2^{\bullet-}$ stock from alkaline H_2O_2 solution. The configuration and setup were as shown in Figure 3.5. From the top to bottom in order are a KrCl* lamp, a piece of

cardboard with a circle cutout that matches diameter of the beneath lens, a plano convex lens (LA4464-ML, Thorlabs), a UV-resistant PTFE reactor with alkaline H_2O_2 solution and a micro magnetic stir bar, a magnetic stir plate, and a lab jack for adjusting the distance between the reactor and the light source. The convex lens can enhance the light intensity by around 15% compared to that without the lens installed. The fluence rate at the surface of the lens (the point where the reactors receive irradiation) was measured to be 5.56 mW/cm^2.

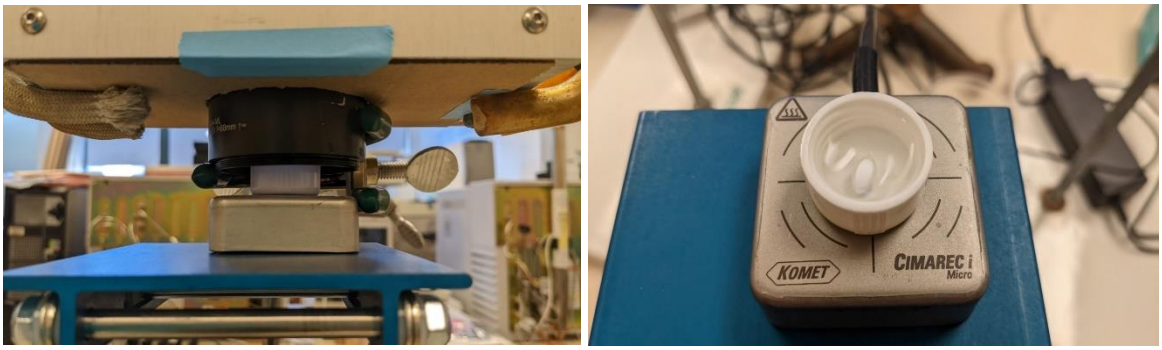

Figure 3.5. KrCl* lamp setup for generating $O_2^{\bullet-}$ stock

Irradiations were initiated by placing a reactor containing 1, 0.1 or 0.05M NaOH and H_2O_2/HO_2^- at various initial concentrations in the path of the emitted light. The reactor was place at the surface of the lens below the KrCl* lamp (222 nm, fluence rate = 5.56 mW/cm^2) for irradiations, with the contents continuously stirred by a magnetic stir bar at 200 rpm (Figure 3.5). At pre-defined times, the reactor was removed from the light and samples were collected for spectrophotometric analyses of [$HO_2^{\bullet}/O_2^{\bullet-}$] and [$H_2O_2/HO_2^-$]. As comparison, a few tests using a low-pressure Hg lamp (254 nm, fluence rate = 39.5 mW/cm^2) were conducted by placing a quartz cuvette containing alkaline H_2O_2 solutions at the surface of the Hg lamp.

Irradiation at initial concentrations of H_2O_2/HO_2^- ranging from 1-20 mM resulted in the buildup of $HO_2^{\bullet}/O_2^{\bullet-}$ over 2-5 minutes to maximal $HO_2^{\bullet}/O_2^{\bullet-}$ concentrations in 1, 0.1 and 0.05M

NaOH solutions, respectively (Figure 3.6), with higher $[H_2O_2/HO_2^-]_0$ yielding higher $[HO_2^\bullet/O_2^{\bullet-}]$ (consistent with eqs 2.4-2.9). These values are in excess of the highest $O_2^{\bullet-}$ concentrations (~400 μM) reported when using vacuum-UV photolysis of oxygenated aqueous ethanol and/or formate solutions, or UV photolysis of mixture of ketones with alcohols (Bielski and Gebicki, 1982; Holroyd and Bielski, 1978; McDowell et al., 1983). Although the LP Hg lamp was able to generate a bit higher maximal $HO_2^\bullet/O_2^{\bullet-}$ concentration of ~1.3mM from initial $[H_2O_2/HO_2^-]_0$ = 20 mM than that from the KrCl* lamp of ~1.0 mM, $HO_2^\bullet/O_2^{\bullet-}$ were less stable under the LP Hg lamp irradiation due to its higher emission intensity and higher UV_{254} absorption ratio of superoxide over H_2O_2. Interestingly, this could also explain another finding that we were able to generate nearly "pure" $O_2^{\bullet-}$ under extended irradiation when H_2O_2/HO_2^- were completely photolyzed while $O_2^{\bullet-}$ still remained in the stock. For example, 222-nm, 5.56 mW/cm^2 irradiation of a pH13.9, $[H_2O_2/HO_2^-]$ = 1 mM solution by the KrCl* lamp for 6 min generated a pure 200μM $O_2^{\bullet-}$ stock; whereas 254-nm, 39.5 mW/cm^2 irradiation of the same solution by the LP Hg lamp for 3 min produced a pure 100μM $O_2^{\bullet-}$ stock. Therefore, KrCl* lamp could potentially provide some benefits over the 254 nm lamp during $O_2^{\bullet-}$ stock generation in regard to (i) higher stability of $O_2^{\bullet-}$ in the stock, and (ii) lower operation energy required, (iii) higher yield of pure $O_2^{\bullet-}$ stock in absence of H_2O_2/HO_2^-, and (iv) less biosafety concern.

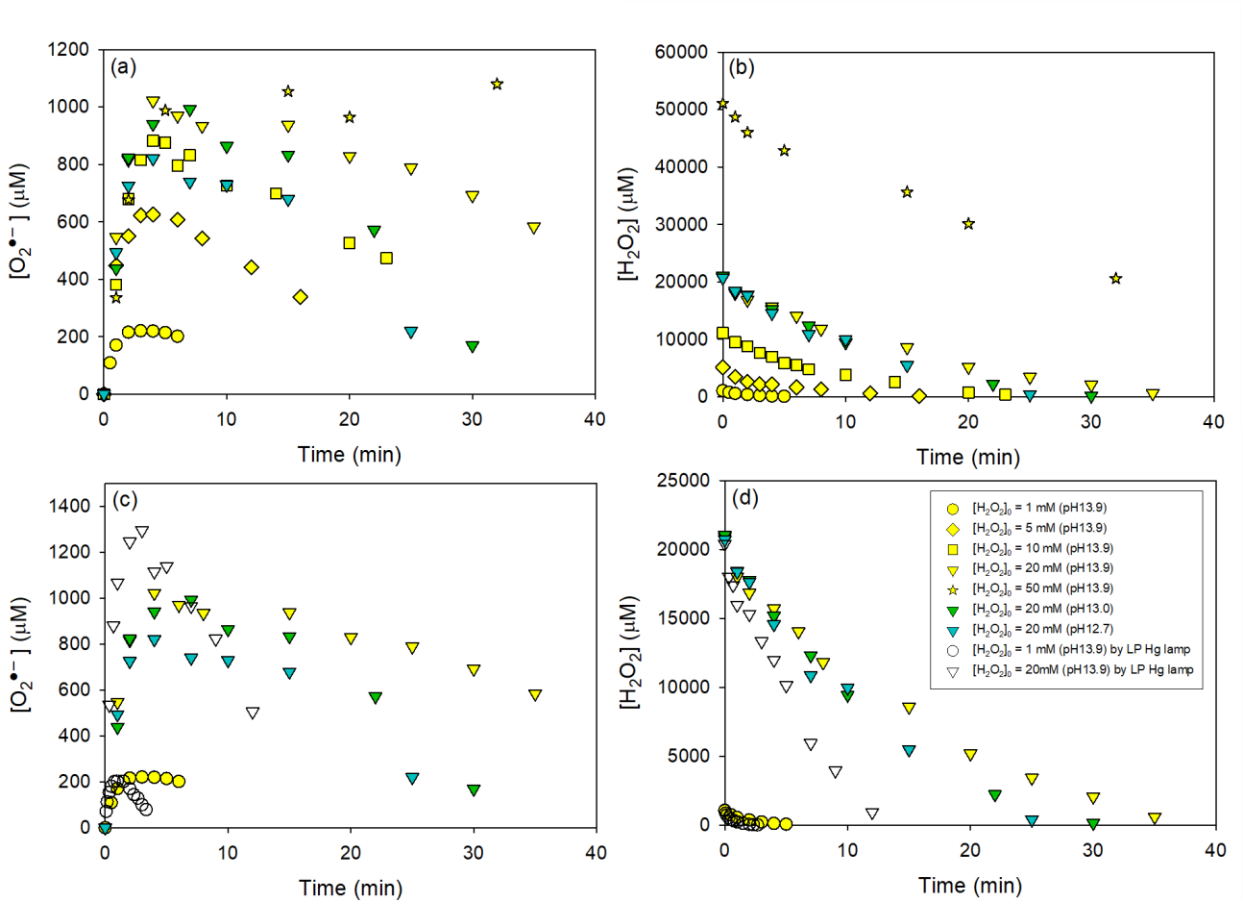

Figure 3.6. Evolution of (a) [$HO_2^{\bullet}/O_2^{\bullet-}$] and (b) [$H_2O_2/HO_2^-$] during continuous photolysis of H_2O_2/HO_2^- in 1, 0.1, or 0.05M NaOH solutions at pH 13.9, 13.0 or 12.7, using a KrCl* lamp (222 nm, fluence rate = 5.56 mW/cm^2); (c) [$HO_2^{\bullet}/O_2^{\bullet-}$] and (d) [$H_2O_2/HO_2^-$] during continuous photolysis of H_2O_2/HO_2^- by a low-pressure Hg lamp (254 nm, fluence rate = 39.5 mW/cm^2). H_2O_2/HO_2^- solutions were prepared using Milli-Q water and NaOH (≥98%, Sigma-Aldrich). Filled symbols are results by the KrCl* lamp, and unfilled symbols are results by the LP Hg lamp.

3.6.2 Electrochemical Approaches

The mechanism of the electrochemical O_2 reduction reaction (ORR) can be quite complicated and involves many intermediates, primarily depending on the natures of the electrode material, catalyst, and electrolyte. Eqs 3.1 to 3.7 below lists several typical ORR processes in alkaline aqueous solution with their corresponding thermodynamic electrode

potentials at standard conditions (Anastasijević et al., 1987; Horsman et al., 2012; Yeager, 1986; 1976).

Direct 4-electron transfer pathway:

$$O_2 + 2\ H_2O + 4\ e^- \rightarrow 4\ OH^- \qquad E_0 = 0.401\ V \qquad (3.1)$$

2-electron transfer pathway (peroxide pathway):

$$O_2 + H_2O + 2\ e^- \rightarrow HO_2^- + OH^- \qquad E_0 = -0.065\ V \qquad (3.2)$$

followed by either the further reduction reaction,

$$HO_2^- + H_2O + 2\ e^- \rightarrow 3\ OH^- \qquad E_0 = 0.867\ V \qquad (3.3)$$

or the decomposition reaction,

$$2\ HO_2^- \rightarrow 2\ OH^- + O_2 \qquad (3.4)$$

1-electron transfer pathway (superoxide pathway):

$$O_2 + e^- \rightarrow O_2^{\bullet -} \qquad E_0 = 0.286\ V \qquad (3.5)$$

followed by dismutation reaction,

$$2\ O_2^{\bullet -} + H_2O \leftrightarrow O_2 + HO_2^- + OH^- \qquad pK = -7.51 \text{ at } 20℃ \qquad (3.6)$$

or further reduction,

$$2\ O_2^{\bullet -} + HOH + e^- \rightarrow OH_2^- + OH^- \qquad (3.7)$$

ORR can be improved significantly through employing an electrolyte with low viscosity, high O_2 solubility, and weak adsorption species (Jin et al., 2010). There have been a bunch of

electrochemical methods reported to generate $O_2^{\bullet-}$ by single electron transfer to electrode-adsorbed O_2, while the majority of them need to use aprotic solvents or organic substances as the bases because $O_2^{\bullet-}$ is unstable in protic solvent like water (Maricle and Hodgson, 1965; Sawyer and Roberts Jr, 1966; Singh and Misra, 1989; Wadhawan et al., 2003). However, these may not be beneficial for $O_2^{\bullet-}$ application in water treatments as aprotic solvents and organic additives may cause additional contamination and organic substances can cause undesirable radical scavenging. Nevertheless, some studies of $O_2^{\bullet-}$ generation in protic aqueous solution have been proposed (Forman and Fridovich, 1972; Shao et al., 2006; Spendelow and Wieckowski, 2007). There is also possibility to produce $O_2^{\bullet-}$ and FAC simultaneously on each of the electrode with the cathode accepting electron to generate $O_2^{\bullet-}$, and the anode where releases electron to yield free chlorine (Czarnetzki and Janssen, 1992; Hubler et al., 2014; Kraft et al., 1999). If so, this will create great advantages of applying the $O_2^{\bullet-}$/FAC process as the two key reactants can be generated in situ at the same time.

We have tested using platinum (Pt) wires and platinum sheets as the electrodes and with different concentrations of NaOH/Na_2SO_4 mixtures containing [NaOH] = 0.01, 0.1 or 1 M, and [Na_2SO_4] = 0.1 or 0.5 M as the electrolytes. Nafion membrane was used to separate the cathode and the anode solutions. Scheme and photo of the experimental setup are shown in Figure 3.7. The reactions were operated at voltages of 1.0-1.5V. Unfortunately, none of these conditions generated noticeable level of $O_2^{\bullet-}$ based on TNM analyses and UV spectrum measurements. Some possibilities for modification or means to improve $O_2^{\bullet-}$ yield include: (1) increasing the electrode surface area contacting the electrolytes (i.e., reducing the ratio of fluid volume/electrode surface area), (2) trying O_2-saturated electrolytes, (3) testing out different compositions and types of electrolyte and electrode (e.g., glassy carbon, graphite, or other metal-

based electrodes), (4) adding chelating agent such as EDTA or phosphate-based chelators to stabilize trace metals in the electrolytes, (5) improving the mixing efficiency, (6) testing higher reaction voltage, and (7) using high-purity chemicals to prepare the electrolytes.

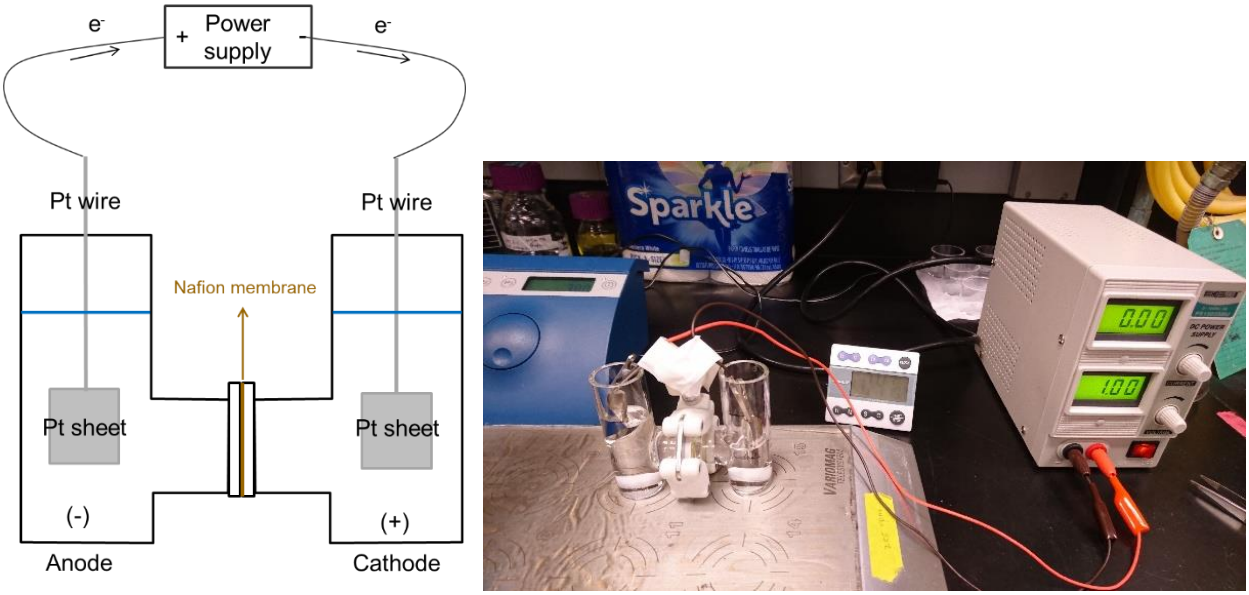

Figure 3.7. Experimental setup for electrochemical generation of $O_2^{\bullet-}$

Transition metals like Fe, Mn or Cu are likely strong $O_2^{\bullet-}$ scavengers and can rapidly consume $O_2^{\bullet-}$, or cause additional contamination. Inert metal-based or carbon-based electrodes would be preferable in terms of $O_2^{\bullet-}$ stock preparation. Ideally, we want to find electrode materials (and appropriate electrolytes) that can cause fast O_2 reduction reaction (to generate $O_2^{\bullet-}$) but slow reduction of $O_2^{\bullet-}$ to H_2O_2/HO_2^- at the cathode, so that $O_2^{\bullet-}$ can accumulate in the electrolytes. Using electrode materials that do not strongly adsorb charged species (like $O_2^{\bullet-}$) could be one way to prevent fast reduction of $O_2^{\bullet-}$ to H_2O_2/HO_2^-. Alternatively, it may also be possible to generate $O_2^{\bullet-}$ at the anode through H_2O_2 oxidation with appropriate design.

3.7 Modeling of $O_2^{\bullet-}$/FAC Treatment

3.7.1 Development of Model

The reaction mechanisms in AOPs are usually complex as the reactions between reactive species and organic contaminants generate many intermediates/products, which can further react with the reactive species, causing complicated chain reactions. Kinetic modeling is a powerful approach to gain mechanistic understanding of these systems and can help formulate strategies for improving AOP treatment efficiency. Therefore, building a simulation model for the $O_2^{\bullet-}$/FAC can be beneficial. Ultimately, the goal was to accurately estimate the removal of trace organic contaminants (TrOCs) during the $O_2^{\bullet-}$/FAC treatment and predict radical exposures as long as their reaction rate constants with $HO^{\bullet}$ and RCS are available. Details in chemicals and individual reactions used in the Kintecus model in this study can be found in the Supporting Information Table S3.1. The model was developed based on over two hundreds of reactions describing radical generation, radical scavenging, acid-base speciation, probe compound degradation, etc. Reactions with violations of detailed balancing were removed from the model. In addition, some reactions that were identified not critical to radical formation or scavenging and may complicate the calculations, were deactivated (muted) in the model. Such reactions, though still listed in Table S3.1 in the Supporting Information, were marked with symbol # in front of their reaction rate constant values. The performance of developed model were verified by comparing the model-predicted contaminant degradation (for NB, BA, and DMB) and radical exposures (for $HO^{\bullet}$, $Cl^{\bullet}$, and $ClO^{\bullet}/Cl_2^{\bullet-}$) with experimental results in Figure 3.8 below.

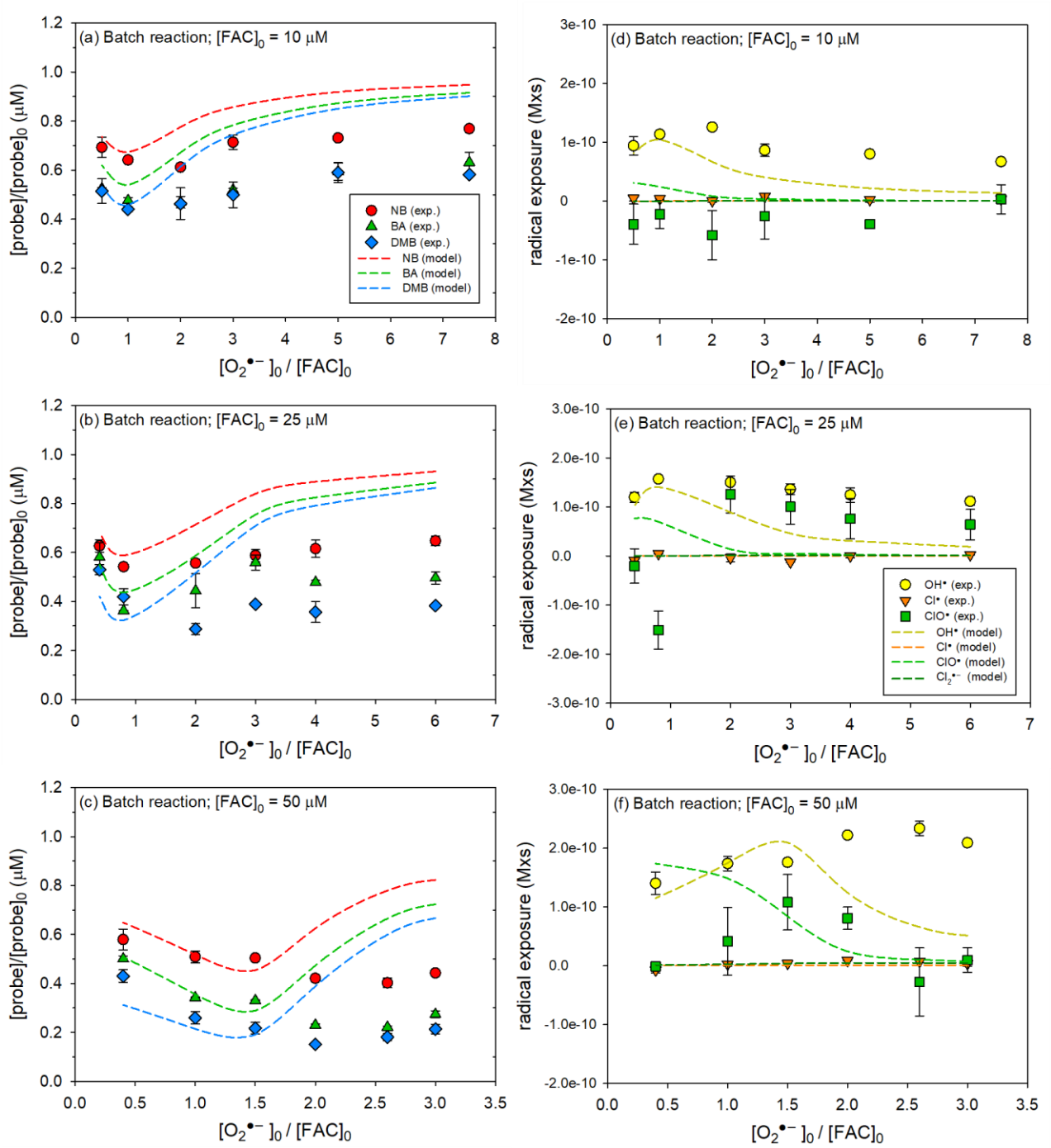

Figure 3.8. Model prediction and empirical data using batch reactions for (a)(b)(c) probe compound degradation and (d)(e)(f) radical exposures. Experiments were conducted using $O_2^{\bullet-}$ stock solutions generated at pH13.9 by KO_2 dissolution, during single-dose, post-mix $O_2^{\bullet-}$/FAC treatment of pH 7, 45mM phosphate buffer containing [NB, BA, DMB]$_0$ = 1 μM. [sulfate] derived from addition of sulfuric acid in the final solution was 0.0493 M. The empirical and Kintecus model simulation results were expressed by the symbols and dash lines, respectively.

Simulation seems to underestimate probe degradation at high $[O_2^{\bullet-}]$/[FAC] ratios above 1 to 1.5. Some potential explanations may include: (a) unrecognized reactions leading to higher than anticipated radical generation or lower than anticipated radical scavenging at high $[O_2^{\bullet-}]$/[FAC] ratios; (b) uncertainties in and/or lack of error ranges for reaction rate constants reported in literature; (c) unknown reaction rate constants for some reactions; and (d) mixing limitation during batch reactions. $O_2^{\bullet-}$ and sulfuric acid were manually added into waters for treatment, while the reaction time scale of $O_2^{\bullet-}$/FAC process (<1 sec) was much smaller than the time of mixing. Therefore, at the moment when $O_2^{\bullet-}$ stock was dosed, certain amount of $O_2^{\bullet-}$ was gone in local region due to unideal mixing through $O_2^{\bullet-}$ disproportionation or scavenging by other species in waters. Note that $O_2^{\bullet-}$ disproportionation is a second-order reaction. Unperfect mixing may lead to high concentrations of $O_2^{\bullet-}$ at a certain region and result in quick $O_2^{\bullet-}$ disappearance. As a result, the actual $[O_2^{\bullet-}]$/[FAC] during treatment may be lower than expected, which could be an explanation for higher than anticipated probe compound degradation and radicals at high $[O_2^{\bullet-}]$/[FAC] ratios.

To verify this hypothesis, the $O_2^{\bullet-}$/FAC treatments were also examined using a continuous flow reaction system that provided better mixing efficiency (Figure 3.9). Reactions were initiated by pre-mixing two solutions of (a) KO_2-derived $O_2^{\bullet-}$ stocks at varying desired $O_2^{\bullet-}$concentrations in 1M NaOH, and (b) 0.4M sulfuric acid, at the same flow rate of 5 mL/min. The (a)(b) mixture was then mixed with another two solutions each at flow rate of 10 mL/min with (c) mixture of radical probes ([NB, BA and DMB] = 3 μM) with FAC solution at varying concentrations in 75mM phosphate buffer, and (d) 0.05M sulfuric acid. These solutions were passed through 15-cm, 1/32 inch (inner diameter) PTFE reaction tubes, and polyether ether ketone (PEEK) or Tefzel™ ethylene-tetrafluoroethylene (ETFE) mixing tees (IDEX), using dual-

channel syringe pumps (Harvard Apparatus). Upon exiting the first mixing tee, the $O_2^{\bullet-}$ stock (originally in pH13.9, 1M NaOH) was partially acidified by sufficient H_2SO_4 to a pH13.0 $O_2^{\bullet-}$ stock. At the final mixing cross, where another stream of phosphate buffer solution containing FAC and radical probes was introduced, H_2SO_4 was injected by another syringe pump to completely neutralize the reaction solution and initiate $O_2^{\bullet-}$/FAC treatment at pH7. Pre-acidifying the $O_2^{\bullet-}$ stock to pH13.0 at the first mixing tee was to ensure a better control on the final reaction pH as we found it could be very tricky to obtain a pH7 final solution if a pH13.9 $O_2^{\bullet-}$ stock was directly neutralized by H_2SO_4. The final solutions were collected, and prior to the HPLC analyses of probe compounds, sufficient catalase or equal amount of FAC were added to completely quench residual H_2O_2. Experiments at different $[O_2^{\bullet-}]_0/[FAC]_0$ ratios and various absolute $[O_2^{\bullet-}]_0$ and $[FAC]_0$ were conducted, and the results were also compared with those from the Kintecus model simulation in Figure 3.10. It was observed that the "optimal" $[O_2^{\bullet-}]_0/[FAC]_0$ ratio shifted to the right in Figure 3.10 using continuous-flow reactions when compared with Figure 3.8 using batch reactions. The batch experiments were likely to underestimate reaction $[O_2^{\bullet-}]_0/[FAC]_0$ when dosing $O_2^{\bullet-}$ stock into the receiving solution containing FAC, due to higher than anticipated local $O_2^{\bullet-}$ concentration caused by unideal mixing.

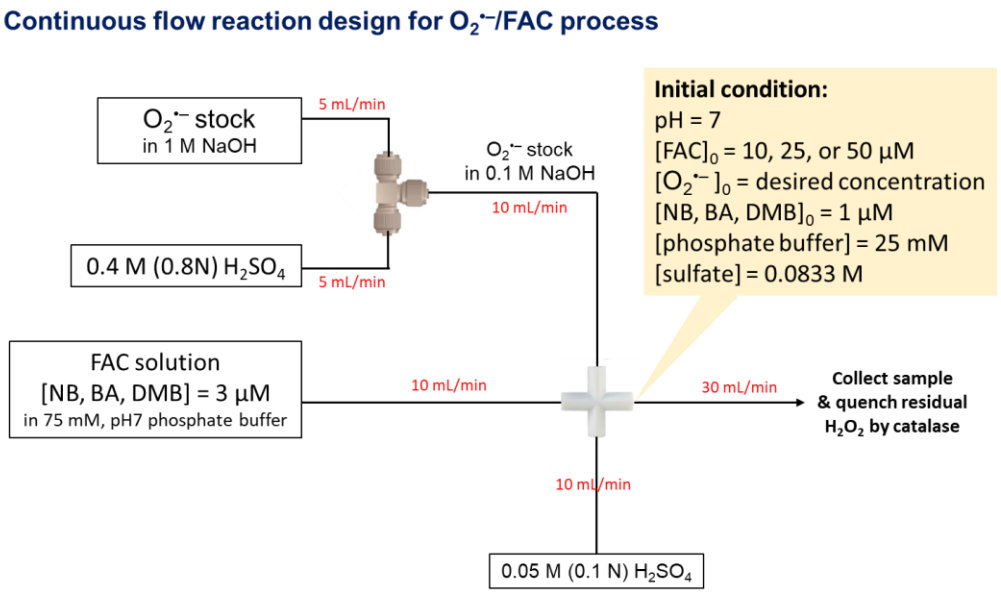

Figure 3.9. Continuous flow reaction design for $O_2^{\bullet-}$/FAC process

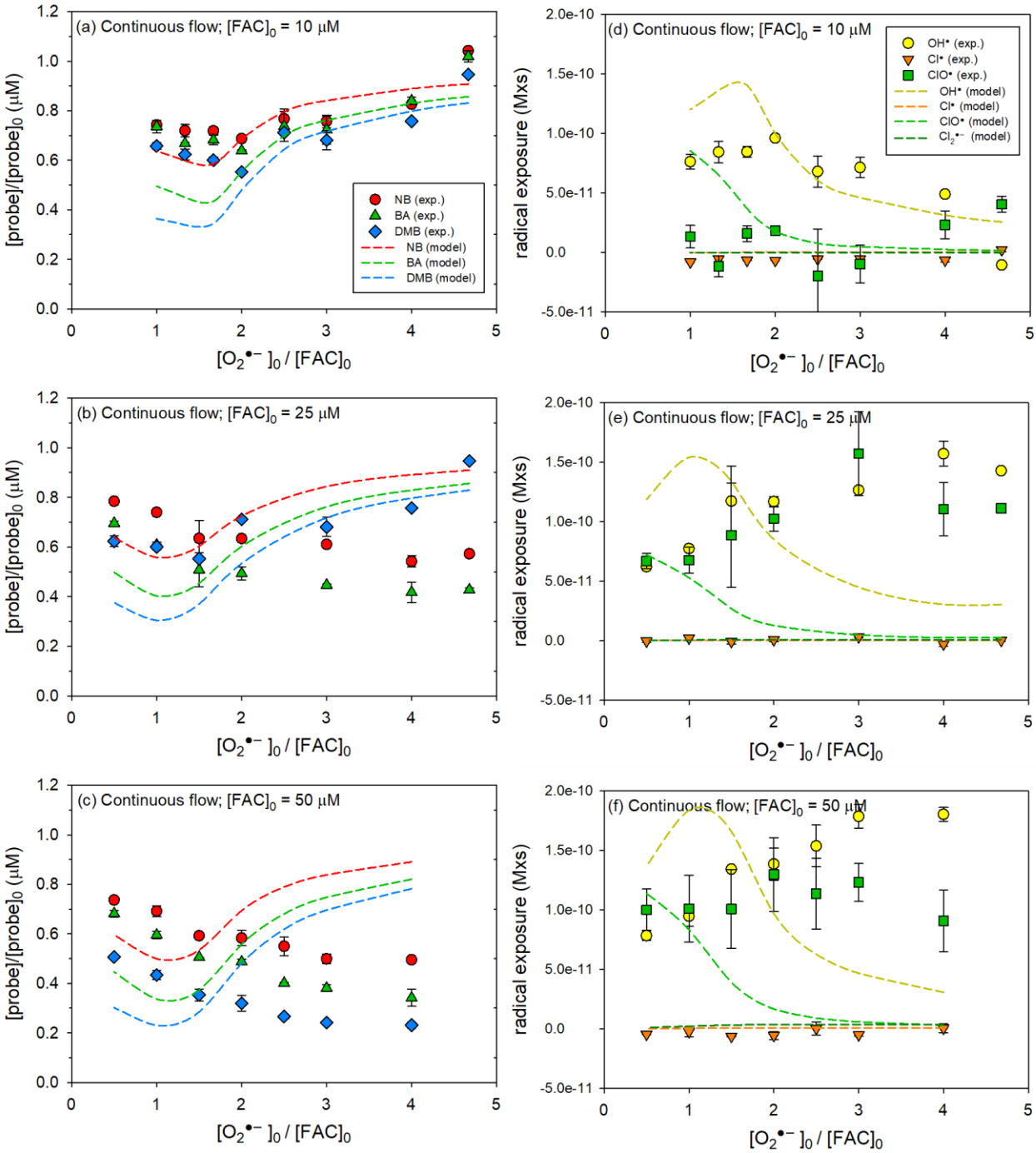

Figure 3.10. Model prediction and empirical data using continuous flow reactions for (a)(b)(c) probe compound degradation and (d)(e)(f) radical exposures. Experiments were conducted using $O_2^{\bullet-}$ stock solutions generated at pH13.9 by KO_2 dissolution, during single-dose, continuos-flow $O_2^{\bullet-}$/FAC treatment of pH 7, 25mM phosphate buffer containing [NB, BA, DMB]$_0$ = 1 μM. [sulfate] derived from addition of sulfuric acid in the final solution was 0.0833 M. The empirical and Kintecus model simulation results were expressed by the symbols and dash lines, respectively.

3.7.2 Limitation and Challenge for Modeling

(i) Numbers of reactions not available or with uncertainties

The Kintecus model was established based on over two hundreds of reactions describing radical generation, radical scavenging, acid-base speciation, probe compound degradation, etc. As discussed previously, plausible explanations for the discrepancy between the modeling and empirical results may include: (a) unrecognized reactions leading to higher than anticipated radical generation or lower than anticipated radical scavenging at high $[O_2^{\bullet-}]$/[FAC] ratios; (b) uncertainties in and/or lack of error ranges for reaction rate constants reported in literature; (c) unknown reaction rate constants for some reactions; and (d) unideal mixing. A matrix was created showing a summary of reactions input in the Kintecus model for $O_2^{\bullet-}$/FAC process (Figure 3.11). The red "No" blocks indicate no reaction in between the associated two species, the pink "On" blocks represent active reactions, and the yellow "Off" blocks represent unactive (muted) reactions in the model. A few active reactions were labled "Est", indicating the reactions are likely to occur, while the reaction rate constants were estimated since they were not available in literature. Some reactions were not activated (muted) in the Kintecus model due to the following reasons: (1) reaction is published in literature, but its chemical equation is not balanced, (2) reaction not significant in the $O_2^{\bullet-}$/FAC process, (3) duplicate reaction equation, and (4) reaction that causes illegal loop. A bunch of reactions in white "?" marks are those without known reaction rate constants. These question-marked reactions account for over half of the total reaction pairs, implying it can be very challenging to build a kinetic model properly in lack of information.

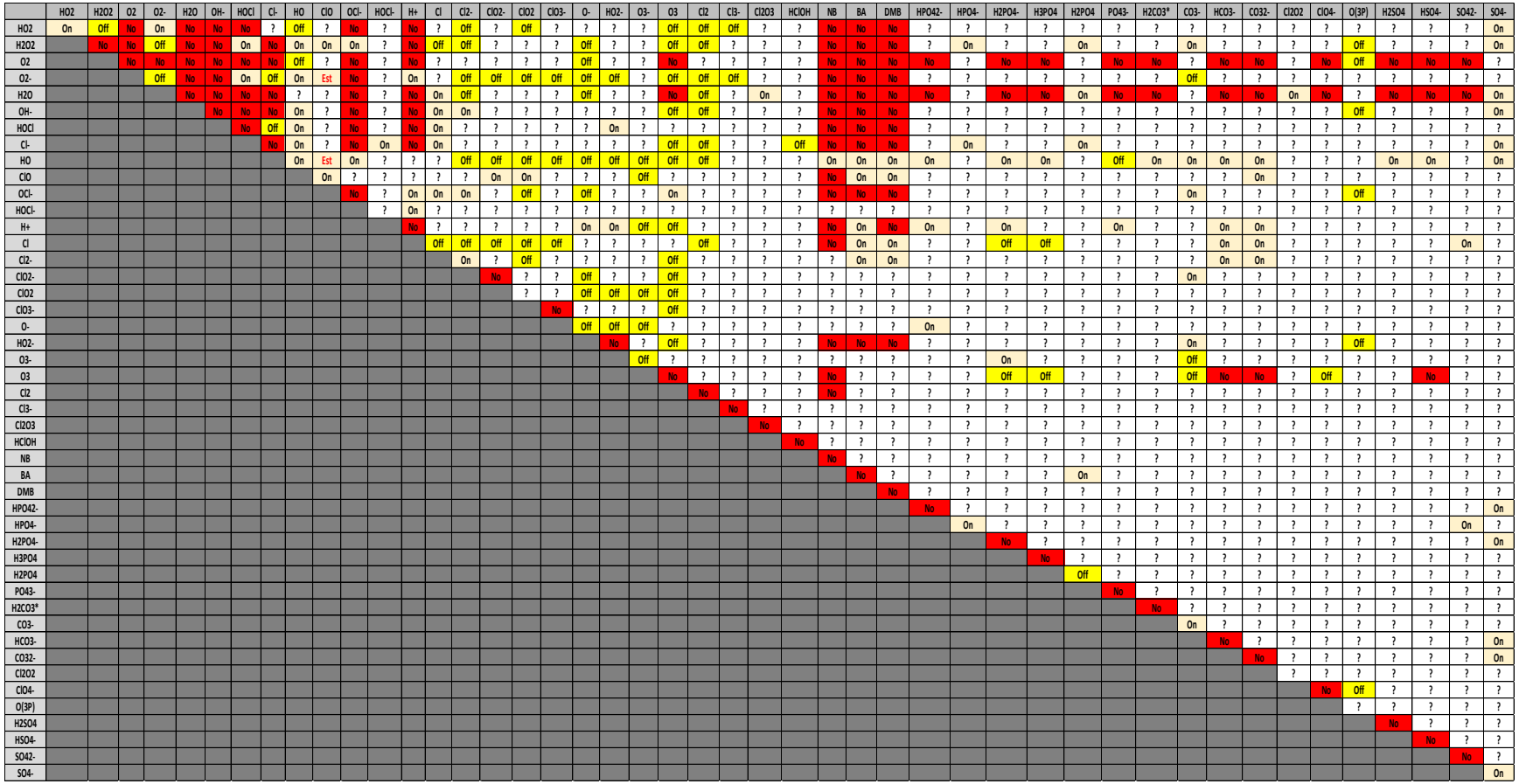

	HO2	H2O2	O2	O2-	H2O	OH-	HOCl	Cl-	HO	ClO	OCl-	HOCl-	H+	Cl	Cl2-	ClO2-	ClO2	ClO3-	O-	HO2-	O3-	O3	Cl2	Cl3-	Cl2O3	HClOH	NB	BA	DMB	HPO42-	HPO4-	H2PO4-	H3PO4	H2PO4	PO43-	H2CO3*	CO3-	HCO3-	CO32-	Cl2O2	ClO4-	O(3P)	H2SO4	HSO4-	SO42-	SO4-
HO2	On	Off	No	On	No	No	No	?	Off	?	No	?	No	?	Off	?	Off	?	?	?	?	Off	Off	Off	?	?	No	No	No	?	?	?	?	?	?	?	?	?	?	?	?	?	?	?	?	?	On
H2O2		No	No	Off	No	No	On	No	On	On	On	?	No	Off	Off	?	?	?	Off	?	?	Off	Off	?	?	?	No	No	No	?	On	?	?	On	?	?	On	?	?	?	?	Off	?	?	?	?	On
O2			No	No	No	No	No	No	Off	?	No	?	No	?	?	?	?	?	Off	?	?	No	?	?	?	?	No	No	No	No	?	No	No	?	No	No	?	No	No	?	No	Off	No	No	No	?	?
O2-				Off	No	No	On	Off	On	Est	No	?	On	?	Off	Off	Off	Off	Off	Off	?	Off	Off	Off	?	?	No	No	No	?	?	?	?	?	?	?	Off	?	?	?	?	?	?	?	?	?	?
H2O					No	No	No	No	?	?	No	?	No	On	Off	?	?	?	Off	?	?	No	Off	?	On	?	No	No	No	No	?	No	No	On	No	No	?	No	No	On	No	?	No	No	No	No	On
OH-						No	No	No	On	?	No	?	No	On	On	?	?	?	?	?	?	Off	Off	?	?	?	No	No	No	?	?	?	?	?	?	?	?	?	?	?	?	?	Off	?	?	?	On
HOCl							No	Off	On	?	No	?	No	On	?	?	?	?	?	On	?	?	?	?	?	?	No	No	No	?	?	?	?	?	?	?	?	?	?	?	?	?	?	?	?	?	?
Cl-								No	On	?	No	On	No	On	?	?	?	?	?	?	?	Off	Off	?	?	Off	No	No	No	?	On	?	?	On	?	?	?	?	?	?	?	?	?	?	?	?	On
HO									On	Est	On	?	?	?	Off	Off	Off	Off	Off	Off	Off	Off	Off	?	?	?	On	On	On	?	On	On	?	Off	On	On	On	On	?	?	?	On	On	?	On
ClO										On	?	?	?	?	?	On	On	?	?	?	Off	?	?	?	?	?	No	On	On	?	?	?	?	?	?	?	?	?	On	?	?	?	?	?	?	?
OCl-											No	?	On	On	On	?	Off	?	Off	?	?	On	?	?	?	?	No	No	No	?	?	?	?	?	?	?	On	?	?	?	?	Off	?	?	?	?
HOCl-												?	On	?	?	?	?	?	?	?	?	?	?	?	?	?	?	?	?	?	?	?	?	?	?	?	?	?	?	?	?	?	?	?	?	?
H+													No	?	?	?	?	?	On	On	Off	Off	?	?	?	?	No	On	No	On	?	On	?	?	On	?	?	On	On	?	?	?	?	?	?	?
Cl														Off	Off	Off	Off	Off	?	?	?	?	Off	?	?	?	No	On	On	?	?	Off	Off	?	?	?	?	On	On	?	?	?	?	?	On	?
Cl2-															On	?	Off	?	?	?	?	Off	?	?	?	?	?	On	On	?	?	?	?	?	?	?	?	On	On	?	?	?	?	?	?	?
ClO2-																No	?	?	Off	?	?	Off	?	?	?	?	?	?	?	?	?	?	?	?	?	?	?	On	?	?	?	?	?	?	?	?	?
ClO2																	?	?	Off	Off	Off	Off	?	?	?	?	?	?	?	?	?	?	?	?	?	?	?	?	?	?	?	?	?	?	?	?	?
ClO3-																		No	?	?	Off	?	?	?	?	?	?	?	?	?	?	?	?	?	?	?	?	?	?	?	?	?	?	?	?	?	?
O-																			Off	Off	Off	?	?	?	?	?	?	?	?	On	?	?	?	?	?	?	?	?	?	?	?	?	?	?	?	?	?
HO2-																				No	?	Off	?	?	?	?	No	No	No	?	?	?	?	?	?	?	On	?	?	?	?	Off	?	?	?	?	?
O3-																					Off	?	?	?	?	?	?	?	?	?	?	?	?	?	?	?	Off	?	?	?	?	?	?	?	?	?	?
O3																						No	?	?	?	?	No	?	?	?	Off	Off	?	?	?	Off	No	No	?	Off	?	?	No	?	?	?	?
Cl2																							No	?	?	?	No	?	?	?	?	?	?	?	?	?	?	?	?	?	?	?	?	?	?	?	?
Cl3-																								No	?	?	?	?	?	?	?	?	?	?	?	?	?	?	?	?	?	?	?	?	?	?	?
Cl2O3																									No	?	?	?	?	?	?	?	?	?	?	?	?	?	?	?	?	?	?	?	?	?	?
HClOH																										No	?	?	?	?	?	?	?	?	?	?	?	?	?	?	?	?	?	?	?	?	?
NB																											No	?	?	?	?	?	?	?	?	?	?	?	?	?	?	?	?	?	?	?	?
BA																												No	?	?	?	?	?	?	On	?	?	?	?	?	?	?	?	?	?	?	?
DMB																													No	?	?	?	?	?	?	?	?	?	?	?	?	?	?	?	?	?	?
HPO42-																														No	?	?	?	?	?	?	?	?	?	?	?	?	?	?	?	?	On
HPO4-																															On	?	?	?	?	?	?	?	?	?	?	?	?	?	?	?	?
H2PO4-																																No	?	?	?	?	?	?	?	?	?	?	?	?	?	?	On
H3PO4																																	No	?	?	?	?	?	?	?	?	?	?	?	?	?	?
H2PO4																																		Off	?	?	?	?	?	?	?	?	?	?	?	?	?
PO43-																																			No	?	?	?	?	?	?	?	?	?	?	?	?
H2CO3*																																				No	?	?	?	?	?	?	?	?	?	?	?
CO3-																																					On	?	?	?	?	?	?	?	?	?	?
HCO3-																																						No	?	?	?	?	?	?	?	?	On
CO32-																																							No	?	?	?	?	?	?	?	On
Cl2O2																																								?	?	?	?	?	?	?	?
ClO4-																																										No	Off	?	?	?	?
O(3P)																																											?	?	?	?	?
H2SO4																																												No	?	?	?
HSO4-																																													No	?	?
SO42-																																														No	?
SO4-																																															On

Figure 3.11. Matrix of reactions input in the Kintecus model for $O_2^{\bullet-}$/FAC process

(ii) Effect of chemical protonation and deprotonation on the reaction chemistries

The time scale for the $O_2^{\bullet-}$/FAC process is less than 1 sec. The reaction rate constants for the $O_2^{\bullet-}$/FAC reactions involved are 10^6~10^{10} $M^{-1}s^{-1}$. The acid-base protonation reactions usually have rate constants of 10^9~10^{10} $M^{-1}s^{-1}$ (close to diffusion limit) (Eigen, 1963; 1964; von Sonntag, 2006), and the deprotonation rate constants can be calculated from the protonation rate constants and the pKa values of each species of interest. Therefore, protonation (or sometimes deprotonation) reactions for chemical species are at similar time scale as some of the radical generation/scavenging reactions in the $O_2^{\bullet-}$/FAC system, leading to some uncertainties.

Using the current Kintecus model, we can estimate this effect by setting the protonation rate constants at values between 10^9 and 10^{10} $M^{-1}s^{-1}$ and their corresponding deprotonation rate constants for constituents including HOCl/OCl^-, HO/O^-, $HO_2^{\bullet}$/$O_2^{\bullet-}$, H_2O_2/HO_2^-, carbonate species and phosphate species. As the protonation rate constants decrease, the estimated organic probe compound degradations also slightly decrease according to the modeling results. This proves that the effects of protonation/deprotonation rates of species involved in the $O_2^{\bullet-}$/FAC process may not be ignored. As future works, further refinement of the model is needed since we are now using assumed values for those protonation/deprotonation rates (see the Table S3.1). More certain values, if available from literature, can help obtain more accurate predications. In addition, non-ideal mixing of the reactants ($O_2^{\bullet-}$, FAC, and acid) can cause pH gradients (different local pHs) throughout the reaction solutions. This can further affect the chemical protonation/deprotonation, leading to the discrepancies between the modeling and the empirical results. It would be better to perform the $O_2^{\bullet-}$/FAC treatments in a continuous flow setup with improved mixing to evaluate the importance of mixing efficiencies as suggested.

(iii) Effect of carbonate/decarbonate during $O_2^{\bullet-}$/FAC treatment (at neutral pH) and $O_2^{\bullet-}$ stock preparation (at high pH)

For $O_2^{\bullet-}$ stock with consideration of the presence of carbonate, Bielski and Richter reported a reaction rate constant of $HO_2^{\bullet}/O_2^{\bullet-}$ with $H_2CO_3/HCO_3^-/CO_3^{2-}$ to be < 0.04 $M^{-1}s^{-1}$ at pH 10.1, and Schmidt reported a rate constant of ~$1x10^6$ $M^{-1}s^{-1}$ at pH 5.5 (Bielski and Richter, 1977; Schmidt, 1972). Second-order reaction rate constant of $O_2^{\bullet-}$ with CO_3^{2-} (or total carbonate) seems to be very slow at high pH. However, the CO_3^{2-} (or total carbonate) concentration can be extremely high at higher pHs, leading to large first-order reaction rate constants. Theoretically, CO_3^{2-} (~TOTCO3, total carbonate, when pH>11) in an open system can reach ~10^2, 10^4, and 10^6 M at pH12, pH13 and pH14, respectively, by assuming the NaOH solutions we used for $O_2^{\bullet-}$ stock preparation had reached equilibrium with the atmosphere (regarded as an open system). However, solubility limits of CO_3^{2-} salts, including $NaCO_3$ and K_2CO_3, may control the upper bound of CO_3^{2-} dissolving in the $O_2^{\bullet-}$ stock. The water solubility of K_2CO_3 is ~8 M (111 g/100 g water at room temperature), and the solubility of Na_2CO_3 is ~3M (30.7 g/100 g water at room temperature) (Haynes, 2014). The KO_2 used for stock preparation was no more than 20 mM, so the maximum concentration of K_2CO_3 should be no more than 10 mM. The NaOH used for stock preparation was no more than 1 M, so the maximum concentration of Na_2CO_3 should be no more than 0.5 M. These show that K^+ and Na^+ ion concentrations in our typical $O_2^{\bullet-}$ stocks were not high enough to achieve saturation for K_2CO_3 and Na_2CO_3. In addition to the salt solubilities, we also tried to take their solubility products into account to further examine whether the presence of these K^+ and Na^+ could limit dissolved CO_3^{2-} concentration. Unfortunately, we were not able to locate solubility products (K_{sp}) for K_2CO_3 and Na_2CO_3 in the literature. Therefore, we assume that the highest possible CO_3^{2-} concentrations

(~TOTCO3 at high pHs) in the $O_2^{\bullet-}$ stocks may be the theoretical concentrations as discussed above.

Unfortunately, we were not able to calculate $O_2^{\bullet-}$/ CO_3^{2-} reaction rate constant based on the two research articles from Bielski and Schmidt as they are not providing certain values but ranges for rate constants, and that we don't know details regarding how they conducted the experiments (e.g., in open or close system, carbonate concentrations during the experiments, etc.). We can still briefly simulate the effect of carbonate on pH12~14 $O_2^{\bullet-}$ stock solutions using the Kintecus model. Bielski and Richter reported a reaction rate constant of $HO_2^{\bullet}/O_2^{\bullet-}$ with $H_2CO_3/HCO_3^{-}/CO_3^{2-}$ to be < 0.04 $M^{-1}s^{-1}$ at pH 10.1, and Schmidt reported a rate constant of ~1x10^6 $M^{-1}s^{-1}$ at pH 5.5 (Bielski and Richter, 1977; Schmidt, 1972). By assuming a highest possible CO_3^{2-} concentration of 10^2, 10^4, and 10^6 M at pH12, pH13 and pH14, respectively (see discussion above), the modeling results show significant decrease of $O_2^{\bullet-}$ stability due to carbonate regardless of assuming rate constants of 0.04 $M^{-1}s^{-1}$ or 1x10^6 $M^{-1}s^{-1}$ (with same values assumed for all reaction combinations, including $HO_2^{\bullet}+H_2CO_3$, $HO_2^{\bullet}+HCO_3^{-}$, $HO_2^{\bullet}+CO_3^{2-}$, $O_2^{\bullet-}+H_2CO_3$, $O_2^{\bullet-}+HCO_3^{-}$ and $O_2^{\bullet-}+CO_3^{2-}$ since individual reaction rate constants are not available).

It is also worthwhile to note that $HO_2^{\bullet}/O_2^{\bullet-}$ reactions with carbonate species may generate $CO_3^{\bullet-}$ radical as the product (Bielski and Richter, 1977; Schmidt, 1972). $CO_3^{\bullet-}$ may further react with $O_2^{\bullet-}$ with reaction rate constants of (4~6.5)x10^8 $M^{-1}s^{-1}$ (Behar et al., 1970; Eriksen et al., 1985). To sum up, for high-pH $O_2^{\bullet-}$ stocks, effect of carbonate and carbonate radical on $O_2^{\bullet-}$ stability may be important, while it is hard to make a conclusion or proper estimation based on information currently available.

For $O_2^{\bullet-}$/FAC treatment in the presence of carbonate species, we simulated the reaction system using the Kintecus model. First, by assuming the NaOH solutions we used for $O_2^{\bullet-}$ stock preparation have reached theoretical equilibrium with the atmosphere (open system), 1M NaOH solution (pH~14) may contain up to 10^6 M of TOTCO3 as an extreme upper bound (though again, this does not take into account solubility limits of K_2CO_3 or Na_2CO_3). At the moment when acidifying the reaction solution to pH7 by dosed with a ratio of 1:4 for $O_2^{\bullet-}$ stock to the receiving solution, the TOTCO3 in the reaction solution should still be around 10^5 M. We can expect the rate constants of CO_3^{2-} and HCO_3^- protonation (~10^{10} $M^{-1}s^{-1}$) to be much higher than $O_2^{\bullet-}$/FAC reaction (10^6~10^7 $M^{-1}s^{-1}$), so all carbonate species should be in the forms of HCO_3^- (80%) or $H_2CO_3^*$ (20%) when the $O_2^{\bullet-}$/FAC reactions take place at pH7. Through simulation by the Kintecus model (see individual reactions in the Appendix), generation of HO and RCS radicals are almost quenched in the presence of 10^5 M of TOTCO3 at pH7. However, this assumed TOTCO3 concentration may not reflect the real conditions when we performed the experiments because the NaOH solutions may not have reached equilibrium with the atmosphere as we stored them in close bottles (though with some head spaces) before using them for $O_2^{\bullet-}$ stock preparation. That is, we do not know the exact TOTCO3 derived from the $O_2^{\bullet-}$ stocks when the experiments were conducted. Nevertheless, the model simulation results still suggest that carbonate species may significantly affect the $O_2^{\bullet-}$/FAC treatment efficiency and radical production if the dosed TOTCO3 derived from the $O_2^{\bullet-}$ stock is high.

3.8 Summary and Potential Practical Implications

- Several refined versions of $O_2^{\bullet-}$/FAC treatments were conducted by (1) preparing $O_2^{\bullet-}$ stocks in less alkaline NaOH solutions to decrease the H_2SO_4 concentration needed for neutralization, and/or (2) increasing the concentrations of $O_2^{\bullet-}$ in the stocks to enable the use

of smaller stock volumes and higher dilution factors – also resulting in decreased H_2SO_4 requirements.

- Cost evaluation for the $O_2^{\bullet-}$/FAC process was performed based on current lab-scale treatment condition and setup. Although its chemical/operating costs seem to be higher than those more conventional AOPs. There is possibility to reduce the costs further by appropriate treatment method modification, using higher concentration of $O_2^{\bullet-}$ stock for dosing, or established more cost-effective approaches in generating $O_2^{\bullet-}$ stock.
- The $O_2^{\bullet-}$/FAC process has several benefits over some current commercially-applied AOPs in light of its simplicity, low required reactor volume, potential for on-site $O_2^{\bullet-}$ generation, and widespread accessibility of required chemicals. It could be a promising novel AOP in particular for smaller-scale decentralized and/or point-of-use (waste)water treatment.
- $O_2^{\bullet-}$ stock preparation was conducted using a high-output mercury lamp (254 nm) and a lower-output KrCl* lamp (222 nm) from alkaline H_2O_2/HO_2^- at different pH from 12.5 to 13.9. The former yielded higher maximal $O_2^{\bullet-}$ stock concentration but with lower stock stability, while the latter generated only a bit less maximal concentration but with higher $O_2^{\bullet-}$ stability.
- Electrochemical generation of $O_2^{\bullet-}$ stock using Pt electrodes was tested under different setups and reaction conditions; however, it still requires further method development and modification.
- The kinetics-based model required further refinement. The discrepancies between the empirical data and the modeling results may be resulted from (a) unrecognized reactions leading to higher than anticipated radical generation or lower than anticipated radical scavenging at high $[O_2^{\bullet-}]$/[FAC] ratios; (b) uncertainties in and/or lack of error ranges for

reaction rate constants reported in literature; (c) unknown reaction rate constants for some reactions; and (d) mixing limitation during batch reactions.

Supporting Information for Chapter 3

Text S3.1. Measurement of fluence rate for UV irradiation

The fluence rate at 254 nm (I, in mW/cm^2) for irradiations undertaken using the 5W, low-pressure Hg lamp was determined by atrazine actinometry (Canonica et al., 2008), under optically dilute conditions (with $\varepsilon_{254,\text{atrazine}} \times l \times C_{\text{atrazine}} \leq 0.02$). I was calculated as $I = (\frac{k_{254,\text{atrazine}}}{2.303 \times \varepsilon_{254,\text{atrazine}} \times \phi_{254,\text{atrazine}}})\text{U}_{254}$, where $\varepsilon_{254,\text{atrazine}}$ (= 3860 M^{-1}cm^{-1}) is the molar extinction coefficient of atrazine solution at 254 nm (Nick et al., 1992), l is the pathlength (= 1.0 cm) of the quartz cuvette used for irradiations, $C_{254,\text{atrazine}}$ = 5×10^{-6} M (buffered with 5mM, pH7 phosphate), $k_{254,\text{atrazine}}$ is the first-order rate constant (s^{-1}) measured for atrazine photolysis in solutions irradiated at 254 nm, U_{254} (= 4.72×10^5 J/Einstein) is the molar photon energy at 254 nm (Rahn, 1997), and $\phi_{254,\text{atrazine}}$ (= 0.046 mol/Einstein at 254 nm) is the quantum yield for atrazine photolysis at 254 nm (Hessler et al., 1993). I was determined here as 39.5 mW/cm^2.

Text S3.2. Cost estimation for the $O_2^{\bullet-}$/FAC process

Calculation of EE/O associated to UV. The cost for UV irradiation has been estimated here in terms of electrical energy per order (EE/O, kWh·m^{-3}·order^{-1}) (Bolton et al., 2001). The EE/O (kWh·m^{-3}·order^{-1}) is defined as the electrical energy necessary to decrease the concentration of a contaminant by one order of magnitude (i.e., 90 % loss) per m^3 of treated water, and can be calculated by the following equation (eq S3.1):

$$\mathrm{EE/O_{UV}} = \frac{P \times t}{V \times \log\left(\frac{C_0}{C_t}\right)} = \frac{\left(\frac{I \times A}{\eta}\right) \times t}{(nv) \times \log\left(\frac{C_0}{C_t}\right)} \quad \text{(S3.1)}$$

where P represent the electric power output of the UV device (kW); V is the total volume of the treated receiving solution (m^3); v is the volume of $O_2^{\bullet-}$ stock used here for dosing to the receiving solution (m^3), n is the dilution factor for addition of stock volume (v) to total volume (V) (or V/v); t is photolysis time (h); $log(C_0/C_t)$ is the logarithm of the ratio of the contaminant's initial concentration and its concentration at time t; A is the irradiated surface area (m^2); η is the energy efficiency of the UV lamp (dimensionless); and I is fluence rate (kW/m^2).

Assumptions for cost estimation. (i) The total volume of the treated receiving solution (V) = 10 mL = 10^{-5} m^3; (ii) $O_2^{\bullet-}$ stock was prepared by UV irradiation of $[H_2O_2/HO_2^-]_{stock,0}$ = 20 mM in 0.05M NaOH, and dosed into the receiving solution containing FAC when $[HO_2^{\bullet}/O_2^{\bullet-}]_{stock}$ = 900 μM; (iii) $O_2^{\bullet-}$ stock dosing volume (v) = 1.11 mL = 1.11×10^{-6} m^3, resulting in a dilution factor of $n = V/v$ = 9; (iv) UV irradiation time (t) to generate 900 μM of $O_2^{\bullet-}$ stock = 4.5 min = 0.075 h; (v) irradiation area (A) = 0.5 cm × 1.0 cm = 5×10^{-5} m^2; (vi) $log(C_0/C_t)$ = 0.4 for benzoic acid (BA) decreasing from 1 μM to 0.4 μM after treatment via single-dosing postmix $O_2^{\bullet-}$/FAC treatment – using the results in Figure 3.2(ii) as a reference; (vii) energy efficiency (η) of lamp is 30% (Rosenfeldt et al., 2006); (viii) the fluence rate (I) determined by atrazine actinometry is 39.5 mW/cm^2 = 0.395 kW/m^2 (see Text S3.1).

Calculation of total cost. EE/O can be calculated as 1.37 $kWh\cdot m^{-3}\cdot order^{-1}$ based on the assumptions above. For treatment per m^3 of water, the cost in $ associated with the UV lamp output needed for 1 order of magnitude of removal, $Cost/O_{UV}$, can be calculated by using the average energy cost in the U.S. (~$0.1/kWh) as $0.137 $m^{-3}\cdot order^{-1}$ (Energy Information

Administration; Sharma et al., 2013; Sun et al., 2016b). We can then define the total cost for 1-order treatment per m^3 as $Cost/O_{total}$ (in units of $\$\cdot m^{-3}\cdot order^{-1}$) using eq S3.2, with the latter four terms in eq S3.2 determined using eq S3.3,

$$\begin{aligned} Cost/O_{total} &= Cost/O_{UV} + Cost/O_{chemical} \\ &= [EE/O_{UV} \times (\text{energy cost})] + [Cost/O_{H_2O_2} + Cost/O_{NaOH} + Cost/O_{NaOCl} + Cost/O_{H_2SO_4}] \end{aligned} \quad \text{(S3.2)}$$

$$Cost/O_{chemical} = \frac{(\$/\text{mol of chemical}) \times (\text{mol of chemical for treatment of volume } V) \times (1000 \text{ L/m}^3)}{(V, \text{in L}) \times \log\left(\frac{C_0}{C_t}\right)} \quad \text{(S3.3)}$$

where the volume of the treated receiving solution is V = 10 mL as above.

The prices of H_2O_2, NaOH, NaOCl, and H_2SO_4, as well as the calculated $Cost/O_{chemical}$ for each chemical are summarized in Table 3.1. The overall $Cost/O_{total}$ can then be determined by eq S3.2 as \$1.12 $m^{-3}\cdot order^{-1}$. The preceding calculation is performed based on the experimental conditions used for generating the data in Figure 3.2. It is worth noting that an even higher level of $[HO_2^{\bullet}/O_2^{\bullet-}]_{stock}$ (= 1000 μM) could be generated in the $O_2^{\bullet-}$ stock under the same irradiation conditions after 2.5 min of irradiation (see Figure 2.3). In this case, the corresponding $Cost/O_{UV}$ and $Cost/O_{total}$ would be \$0.069 $m^{-3}\cdot order^{-1}$ and \$0.97 $m^{-3}\cdot order^{-1}$, respectively.

Comparison with other AOPs. Katsoyiannis et al. (2011) conducted a series of AOP treatments with O_3/H_2O_2 and UV/H_2O_2 for different water sources, and reported corresponding energy requirements, or EE/O (kWh/m^3) values, for 90% removal of pCBA by each treatment in the investigated water sources (Katsoyiannis et al., 2011). For O_3/H_2O_2 and UV/H_2O_2 treatments of natural waters, the resulting EE/O values ranged from 0.043-0.080 and 0.75-1.92 kWh/m^3, respectively. Corresponding $Cost/O_{total}$ values can be calculated from these EE/O values as $(4.3\text{-}8.0)\times10^{-3}$ and 0.075-0.192 $\$\cdot m^{-3}\cdot order^{-1}$. Because the second-order reaction rate constants for

reactions of $HO^{\bullet}$ with pCBA (5×10^9 $M^{-1}s^{-1}$) and BA (5.9×10^9 $M^{-1}s^{-1}$) are very close (Buxton et al., 1988; Neta and Dorfman, 1968), the Cost/O_{total} for pCBA degradation during O_3/H_2O_2 and UV/H_2O_2 treatments in the previous work can be compared with BA degradation during $O_2^{\bullet-}$/FAC treatment in the present work. Cost/O_{total} values for each AOP are summarized in Table 3.2.

Table S3.1 Individual reaction and assumption for the Kintecus model

No.	Reaction rate constant k ($M^{-1}s^{-1}$)[a]	Reaction	Reference/Comment
$O_2^{\bullet-}$ disproportionation			
1	8.30E+05	$HO_2^\bullet + HO_2^\bullet \Longrightarrow H_2O_2 + O_2$	(Bielski et al., 1985)
2	9.70E+07	$HO_2^\bullet + O_2^{\bullet-} \Longrightarrow HO_2^- + O_2$	(Bielski et al., 1985) Estimated based on second-order rate constant of 9.7×10^7 $M^{-1}s^{-1}$ for $HO_2^\bullet + O_2^{\bullet-}$, $[H_2O] = 55.6$ M
3	#3.5E-01	$O_2^{\bullet-} + O_2^{\bullet-} \Longrightarrow O_2^{2-} + O_2$	(Bielski, 1978; Bielski et al., 1985)
Reactions of ozone			
4	1.10E+02	$OCl^- + O_3 \Longrightarrow 2O_2 + Cl^-$	(Haag and Hoigne, 1983)
5	3.00E+01	$OCl^- + O_3 \Longrightarrow O_2 + ClO_2^-$	(Haag and Hoigne, 1983)
Reactions of $HO^\bullet$ and $Cl^\bullet$ with chlorine species and $ClO^\bullet$ formation			
6	1.40E+08	$HOCl + HO^\bullet \Longrightarrow ClO^\bullet + H_2O$	(Lee et al., 2020)
7	2.00E+09	$OCl^- + HO^\bullet \Longrightarrow ClO^\bullet + OH^-$	(Lee et al., 2020)
8	3.00E+09	$HOCl + Cl^\bullet \Longrightarrow ClO^\bullet + H^+ + Cl^-$	(Lee et al., 2020)
9	1.00E+10	$OCl^- + Cl^\bullet \Longrightarrow ClO^\bullet + Cl^-$	(Lee et al., 2020)
10	2.90E+08	$OCl^- + Cl_2^{\bullet-} \Longrightarrow ClO^\bullet + 2Cl^-$	(Lee et al., 2020)
11	3.60E+09	$HO^\bullet + HO^\bullet \Longrightarrow H_2O_2$	(Elliot, 1989)
12	#7.0E+09	$HO^\bullet + ClO_2^- \Longrightarrow ClO_2^\bullet + OH^-$	(Eriksen et al., 1981)
13	#4.0E+09	$HO^\bullet + ClO_2^\bullet \Longrightarrow ClO_3^- + H^+$	(Klaning et al., 1985)
14	#1.0E+06	$HO^\bullet + ClO_3^- \Longrightarrow HO\_ClO_3^-\_products$	(Buxton and Subhani, 1972)
15	#6.0E+09	$HO^\bullet + HO_2^\bullet \Longrightarrow O_2 + H_2O$	(Buxton et al., 1988)
16	1.00E+10	$HO^\bullet + O_2^{\bullet-} \Longrightarrow O_2 + OH^-$	(Christensen et al., 1989)
17	1.30E+10	$HO^\bullet + OH^- \Longrightarrow H_2O + O^{\bullet-}$	(Rabani and Zehavi, 1971)
18	#2.0E+10	$HO^\bullet + O^{\bullet-} \Longrightarrow HO_2^-$	(Rabani and Matheson, 1966)
19	#8.5E+09	$HO^\bullet + O_3^{\bullet-} \Longrightarrow HO_2^\bullet + O_2^{\bullet-}$	(Sehested et al., 1984a)
20	#1.1E+08	$HO^\bullet + O_3 \Longrightarrow HO_2^\bullet + O_2$	(Sehested et al., 1984b)
21	#1.0+09	$HO^\bullet + Cl_2^{\bullet-} \Longrightarrow HOCl + Cl^-$	(Wagner et al., 1986)
22	#1.0+09	$HO^\bullet + Cl_2 \Longrightarrow HOCl + Cl^-$	(Sun et al., 2016a)
23	1.00E+09	$HO^\bullet + ClO^\bullet \Longrightarrow ClO_2^- + H^+$	(Lee et al., 2020)
24	1.00E+10	$HO^\bullet + ClO^\bullet \Longrightarrow Cl^\bullet + HO_2^\bullet$	Assumed
25	#1.1E+05	$HO^\bullet + O_2 \Longrightarrow O_3^{\bullet-} + H^+$	(Lee et al., 2020)
Reactions of $HO^\bullet$ with Cl^-			
26	4.30E+09	$HO^\bullet + Cl^- \Longrightarrow HOCl^{\bullet-}$	(Kläning and Wolff, 1985)
27	1.80E+10	$Cl^\bullet + OH^- \Longrightarrow HOCl^{\bullet-}$	(Kläning and Wolff, 1985)
28	2.50E+05	$Cl^\bullet + H_2O \Longrightarrow HOCl^{\bullet-} + H^+$	(Buxton et al., 1988)
29	6.10E+09	$HOCl^{\bullet-} \Longrightarrow HO^\bullet + Cl^-$	(Kläning and Wolff, 1985)
30	2.30E+01	$HOCl^{\bullet-} \Longrightarrow OH^- + Cl^\bullet$	(Kläning and Wolff, 1985)
31	2.10E+10	$HOCl^{\bullet-} + H^+ \Longrightarrow Cl^\bullet + H_2O$	(Kläning and Wolff, 1985)
Reactions of $Cl^\bullet$			
32	#8.80E+07	$Cl^\bullet + Cl^\bullet \Longrightarrow Cl_2$	(Wu et al., 1980)
33	#2.10E+09	$Cl^\bullet + Cl_2^{\bullet-} \Longrightarrow Cl_2 + Cl^-$	(Yu, 2004)
34	#7.00E+09	$Cl^\bullet + ClO_2^- \Longrightarrow ClO_2^\bullet + Cl^-$	(Chuang et al., 2017)

35	#1.00E+09	$Cl^{\bullet} + ClO_2^{\bullet} \Rightarrow Cl^{\bullet}\_ClO_2^{\bullet}\_products$	(Lee et al., 2020)
36	#5.30E+08	$Cl^{\bullet} + Cl_2 \Rightarrow Cl_3^{\bullet}$	(Lee et al., 2020)
37	#2.00E+04	$Cl_2 + Cl^- \Rightarrow Cl_3^-$	(Ershov, 2004)
38	#1.10E+05	$Cl_3^- \Rightarrow Cl_2 + Cl^-$	(Ershov, 2004)
Reactions of $Cl_2^{\bullet-}$			
39	6.50E+09	$Cl^{\bullet} + Cl^- \Rightarrow Cl2^{\bullet-}$	(Buxton et al., 2000)
40	1.10E+05	$Cl2^{\bullet-} \Rightarrow Cl^{\bullet} + Cl^-$	(Buxton et al., 2000)
41	4.50E+07	$Cl2^{\bullet-} + OH^- \Rightarrow HOCl^{\bullet-} + Cl^-$	(Grigor'ev et al., 1987)
42	1.00E+04	$HOCl^{\bullet-} + Cl^- \Rightarrow OH^- + Cl2^{\bullet-}$	(Grigor'ev et al., 1987)
43	9.00E+08	$2Cl_2^{\bullet-} \Rightarrow Cl_2 + 2Cl^-$	(Yu and Barker, 2003)
44	4.10E+09	$2Cl_2^{\bullet-} \Rightarrow Cl_3^- + Cl^-$	(Ferraudi, 1993)
45	#1.4E+05	$Cl_2^{\bullet-} + H_2O_2 \Rightarrow HO_2^{\bullet} + 2Cl^- + H^+$	(Hasegawa and Neta, 1978)
46	#1.3+E03	$Cl_2^{\bullet-} + H_2O \Rightarrow HClOH^{\bullet} + Cl^-$	(McElroy, 1990)
47	#1.3+E03	$Cl_2^{\bullet-} + H_2O \Rightarrow HOCl^{\bullet-} + Cl^-$	(Bulman et al., 2019)
48	#3.0E+09	$Cl_2^{\bullet-} + HO_2^{\bullet} \Rightarrow 2Cl^- + H^+ + O_2$	(Gogolev et al., 1984)
49	#2.3E+01	$Cl_2^{\bullet-} + HO_2^{\bullet} \Rightarrow HClOH^{\bullet} + Cl^-$	(Sun et al., 2016b)
50	#2.0E+09	$Cl_2^{\bullet-} + O_2^{\bullet-} \Rightarrow O_2 + 2Cl^-$	(Zhestkova and Pikaev, 1974)
51	#1.0E+09	$Cl_2^{\bullet-} + ClO_2^{\bullet} \Rightarrow Cl_2^{\bullet-}\_ClO_2^{\bullet}\_products$	(Mialocq et al., 1973)
Reactions of chlorine species with H_2O_2 and peroxyl radicals ($HO_2^{\bullet}$ and $O_2^{\bullet-}$)			
52	1.10E+04	$HOCl + H_2O_2 \Rightarrow O_2 + H_2O + Cl^- + H^+$	(Grebel et al., 2010)
53	7.50E+06	$HOCl + O_2^{\bullet-} \Rightarrow HO^{\bullet} + O_2 + Cl^-$	(Long and Bielski, 1980)
54	7.50E+06	$HOCl + O_2^{\bullet-} \Rightarrow Cl^{\bullet} + O_2 + OH^-$	(Long and Bielski, 1980)
55	4.40E+07	$HOCl + HO_2^- \Rightarrow O_2 + H_2O + Cl^-$	(Held et al., 1978)
56	#7.5E+06	$HOCl + HO_2^{\bullet} \Rightarrow Cl^{\bullet} + OH^- + O_2$	(Grebel et al., 2010)
57	1.70E+05	$OCl^- + H_2O_2 \Rightarrow O_2 + H_2O + Cl^-$	(Grebel et al., 2010)
58	#2.0E+08	$OCl^- + O_2^{\bullet-} + H_2O \Rightarrow Cl^{\bullet} + O_2 + 2OH^-$	(Matthew and Anastasio, 2006), estimated
59	#2.8E+10	$H_2O_2 + Cl^{\bullet} \Rightarrow H^+ + Cl^- + HO_2^{\bullet}$	(Nadtochenko and Kiwi, 1998)
60	#1.3E+04	$H_2O_2 + Cl_2 \Rightarrow 2H^+ + 2Cl^- + O_2$	(Matthew and Anastasio, 2006), estimated
Reactions of other chlorine species			
61	#2.1E-02	$HOCl + Cl^- + H^+ \Rightarrow Cl_2 + H_2O$	(Lee et al., 2020)
62	#1.5E+04	$HOCl + Cl^- \Rightarrow Cl_2OH^-$	(Lee et al., 2020)
63	#5.5E+09	$Cl_2OH^- \Rightarrow HOCl + Cl^-$	(Lee et al., 2020)
64	#2.2E+01	$Cl_2 + H_2O \Rightarrow HOCl + Cl^- + H^+$	(Lee et al., 2020)
65	#1.0E+09	$Cl_2 + OH^- \Rightarrow HOCl + Cl^-$	(Lee et al., 2020)
66	#5.0E+09	$HClOH^{\bullet} + Cl^- \Rightarrow Cl_2^{\bullet-} + H_2O$	(McElroy, 1990)
67	#1.0E+08	$HClOH^{\bullet} \Rightarrow HOCl^{\bullet-} + H^+$	(McElroy, 1990)
68	#1.0E+02	$HClOH^{\bullet} \Rightarrow Cl^{\bullet} + H_2O$	(McElroy, 1990)
69	#6.7E+09	$ClO_2^{\bullet} \Rightarrow O_2 + Cl^{\bullet}$	(Lee et al., 2020)
70	#9.1E-01	$ClO_2^{\bullet} + OCl^- \Rightarrow ClO^{\bullet} + ClO_2^-$	(Wang and Margerum, 2002)
71	#1.0E+06	$ClO_2^{\bullet} + HO_2^{\bullet} \Rightarrow ClO_2^{\bullet}\_HO_2^{\bullet}\_products$	(Lee et al., 2020)
72	#3.0E+09	$ClO_2^{\bullet} + O_2^{\bullet-} \Rightarrow ClO_2^- + O_2$	(Huie and Neta, 1986)
73	#1.3E+05	$ClO_2^{\bullet} + HO_2^- \Rightarrow ClO_2^- + HO_2^{\bullet}$	(Hoigné and Bader, 1994)
74	#4.0E+01	$ClO_2^- + O_2^{\bullet-} \Rightarrow ClO_2^-\_O_2^{\bullet-}\_products$	(Lee et al., 2020)
75	#1.0E+06	$ClO_3^- + Cl^{\bullet} \Rightarrow ClO_3^-\_Cl^{\bullet}\_products$	(Lee et al., 2020)
76	#3.0E-03	$ClO_3^- + O_2^{\bullet-} \Rightarrow ClO_3^-\_O_2^{\bullet-}\_products$	(Lee et al., 2020)

Reactions of $ClO^{\bullet}$			
77	2.50E+09	$2ClO^{\bullet} \Longrightarrow Cl_2O_2$	(Kläning and Wolff, 1985)
78	1.00E+04	$Cl_2O_2 + H_2O \Longrightarrow OCl^- + ClO_2^- + 2H^+$	(Mialocq et al., 1973)
79	5.20E+03	$Cl_2O_2 + H_2O \Longrightarrow Cl^- + O_2 + OCl^- + 2H^+$	(Buxton and Subhani, 1972)
80	9.40E+08	$ClO_2^- + ClO^{\bullet} \Longrightarrow ClO_2^{\bullet} + OCl^-$	(Alfassi et al., 1988)
81	7.40E+09	$ClO_2^{\bullet} + ClO^{\bullet} \Longrightarrow Cl_2O_3$	(Quiroga and Perissinotti, 2005)
82	1.00E+04	$Cl_2O_3 + H_2O \Longrightarrow ClO_3^- + OCl^- + 2H^+$	(Quiroga and Perissinotti, 2005)
83	4.50E+07	$ClO^{\bullet} + ClO^{\bullet} + H_2O \Longrightarrow ClO_2^- + OCl^- + 2H^+$	(Kläning and Wolff, 1985), estimated based on second-order rate constant of 2.5×10^9 $M^{-1}s^{-1}$ for $ClO^{\bullet} + ClO^{\bullet}$, $[H_2O] = 55.6$ M
84	1.00E+09	$ClO^{\bullet} + O_2^{\bullet-} \Longrightarrow OCl^- + O_2$	Estimated based on $ClO^{\bullet} + O_3^{\bullet-}$
85	2.70E+07	$ClO^{\bullet} + H_2O_2 \Longrightarrow ClO^{\bullet}\_H_2O_2\_products$	Estimated based on H_2O_2+$HO^{\bullet}$
Reactions of H_2O_2 and $O_2^{\bullet-}$			
86	2.70E+07	$H_2O_2 + HO^{\bullet} \Longrightarrow H_2O + HO_2^{\bullet}$	(Christensen et al., 1982)
87	#7.5E+09	$HO_2^- + HO^{\bullet} \Longrightarrow H_2O + O_2^{\bullet-}$	(Christensen et al., 1982)
88	#5.0E+09	$HO_2^- + HO^{\bullet} \Longrightarrow HO_2^{\bullet} + OH^-$	(Buxton, 1969)
89	#3.0E+00	$H_2O_2 + HO_2^{\bullet} \Longrightarrow O_2 + HO^{\bullet} + H_2O$	(Lee et al., 2020)
90	#1.3E-01	$H_2O_2 + O_2^{\bullet-} \Longrightarrow O_2 + HO^{\bullet} + OH^-$	(Judith and Bielski, 1979)
91	#2.0E+00	$HO_2^- + O_2^{\bullet-} \Longrightarrow O_2 + H_2O_2$	(Marklund, 1976)
92	#5.0E+08	$H_2O_2 + O^{\bullet-} \Longrightarrow O_2^{\bullet-} + H_2O$	(Buxton et al., 1988)
93	#4.0E+08	$HO_2^- + O^{\bullet-} \Longrightarrow O_2^{\bullet-} + OH^-$	(Buxton et al., 1988)
94	#1.4E+02	$O_2^{\bullet-} + Cl^- \Longrightarrow O_2^{\bullet-}\_Cl^-\_products$	(Lee et al., 2020)
95	#3.8E+09	$O_2^{\bullet-} + Cl_3^- \Longrightarrow Cl_2^{\bullet-} + Cl^- + O_2$	(Matthew and Anastasio, 2006), estimated
96	#1.0E+09	$O_2^{\bullet-} + Cl_2 \Longrightarrow Cl_2^{\bullet-} + O_2$	(Matthew and Anastasio, 2006), estimated
97	#1.0E+09	$HO_2^{\bullet} + Cl_3^- \Longrightarrow Cl_2^{\bullet-} + HCl + O_2$	(Lee et al., 2020)
98	#1.0E+09	$HO_2^{\bullet} + Cl_2 \Longrightarrow Cl_2^{\bullet-} + O_2 + H^+$	(Lee et al., 2020)
Reactions of other ROS			
99	#6.0E+08	$O^{\bullet-} + O_2^{\bullet-} \Longrightarrow 2OH^- + O_2$	(Buxton et al., 1988)
100	#3.6E+09	$O^{\bullet-} + O_2^{\bullet} \Longrightarrow O_3^{\bullet-}$	(Buxton et al., 1988)
101	#2.6E+03	$O_3^{\bullet-} \Longrightarrow O^{\bullet-} + O_2$	(Elliot and McCracken, 1989)
102	#5.0E+08	$O^{\bullet-} + O_3^{\bullet-} \Longrightarrow O_4^{2-}$	(Gall and Dorfman, 1969)
103	#7.0E+08	$O^{\bullet-} + O_3^{\bullet-} \Longrightarrow 2O_2^{\bullet-}$	(Sehested et al., 1982)
104	#2.3E+08	$O^{\bullet-} + OCl^- \Longrightarrow ClO^{\bullet} + OH^-$	(Buxton and Subhani, 1972)
105	#9.3E+07	$O^{\bullet-} + H_2O \Longrightarrow HO^{\bullet} + OH^-$	(Buxton, 1970)
106	#2.0E+08	$O^{\bullet-} + ClO_2^- \Longrightarrow OH^- + ClO_2^{\bullet}$	(Eriksen et al., 1981)
107	#8.4E+09	$O^{\bullet-} + O^{\bullet-} \Longrightarrow O_2^{2-}$	(Adams et al., 1966)
108	#2.7E+09	$O^{\bullet-} + ClO_2^{\bullet} \Longrightarrow ClO_3^-$	(Klaning et al., 1985)
109	#1.0E+09	$O_3^{\bullet-} + ClO^{\bullet} \Longrightarrow OCl^- + O_3$	(Kläning et al., 1984)
110	#9.0E+08	$O_3^{\bullet-} + O_3^{\bullet-} \Longrightarrow O_3^{\bullet-}\_products$	(Subhani, 1978)
111	#9.0E+10	$O_3^{\bullet-} + H^+ \Longrightarrow HO^{\bullet} + O_2$	(Sehested et al., 1984a)
112	#5.2E+10	$O_3^{\bullet-} + H^+ \Longrightarrow HO_3^{\bullet}$	(Lee et al., 2020)
113	#1.8E+05	$O_3^{\bullet-} + ClO_2^{\bullet} \Longrightarrow O_2 + ClO_3^-$	(Klaning et al., 1985)
114	#1.8E+05	$O_3^{\bullet-} + ClO_2^{\bullet} \Longrightarrow O_3 + ClO_2^-$	(Klaning et al., 1985)
115	#7.0E+01	$O_3 + OH^- \Longrightarrow HO_2^- + O_2$	(Staehelin and Hoigne, 1982)
116	#4.0E-03	$O_3 + H^+ \Longrightarrow O_3\_H^+\_products$	(Lee et al., 2020)

117	#2.8E+06	$O_3 + HO_2^- \Longrightarrow HO^\bullet + O_2 + O_2^{\bullet-}$	(Staehelin and Hoigne, 1982)
118	#5.5E+06	$O_3 + HO_2^- \Longrightarrow O_3^{\bullet-} + HO_2^\bullet$	(Lee et al., 2020)
119	#1.6E+09	$O_3 + HO_2^\bullet \Longrightarrow H^+ + O_2 + O_3^{\bullet-}$	(Lee et al., 2020)
120	#1.6E+09	$O_3 + O_2^{\bullet-} \Longrightarrow O_3^{\bullet-} + O_2$	(Buehler et al., 1984)
121	#1.6E-03	$O_3 + Cl^- \Longrightarrow O_2 + OCl^-$	(Lee et al., 2020)
122	#2.7E-02	$O_3 + H_2O_2 \Longrightarrow O_2 + HO^\bullet + HO_2^\bullet$	(Lee et al., 2020)
123	#9.0E+07	$O_3 + Cl_2^{\bullet-} \Longrightarrow O_3\_Cl_2^{\bullet-}\_products$	(Lee et al., 2020)
124	#1.0E-03	$O_3 + ClO_3^- \Longrightarrow O_3\_ClO_3^-\_products$	(Lee et al., 2020)
125	#2.0E-04	$O_3 + ClO_4^- \Longrightarrow O_3\_ClO_4^-\_products$	(Lee et al., 2020)
126	#4.0E+06	$O_3 + ClO_2^- \Longrightarrow O_3^{\bullet-} + ClO_2^\bullet$	(Klaning et al., 1985)
127	#1.4E+03	$O_3 + ClO_2^\bullet \Longrightarrow O_2 + ClO_3^\bullet$	(Hoigné and Bader, 1994)
128	#4.5E-06	$O_3 \Longrightarrow O_2 + O(^3P)$	(Lee et al., 2020)
129	#4.0E+09	$O_2 + O(^3P) \Longrightarrow O_3$	(Lee et al., 2020)
130	#9.4E+09	$O(^3P) + OCl^- \Longrightarrow ClO_2^-$	(Lee et al., 2020)
131	#1.6E+09	$O(^3P) + H_2O_2 \Longrightarrow HO^\bullet + HO_2^\bullet$	(Lee et al., 2020)
132	#5.3E+09	$O(^3P) + HO_2^- \Longrightarrow HO^\bullet + O_2^{\bullet-}$	(Lee et al., 2020)
133	#6.0E+05	$O(^3P) + ClO_4^- \Longrightarrow O(^3P)\_ClO_4^-\_products$	(Lee et al., 2020)
134	#4.2E+08	$O(^3P) + OH^- \Longrightarrow HO_2^-$	(Lee et al., 2020)
135	#1.1E+05	$HO_3^\bullet \Longrightarrow HO^\bullet + O_2$	(Buehler et al., 1984)
Reactions of reactive species with probe compounds			
136	3.80E+09	$NB + HO^\bullet \Longrightarrow NB\_HO^\bullet\_products$	(Lee et al., 2020)
137	5.90E+09	$BA + HO^\bullet \Longrightarrow BA\_HO^\bullet\_products$	(Buxton et al., 1988)
138	1.80E+10	$BA + Cl^\bullet \Longrightarrow BA\_Cl^\bullet\_products$	(Mártire et al., 2001)
139	5.00E+05	$BA + ClO^\bullet \Longrightarrow BA\_ClO^\bullet\_products$	(Lee et al., 2020), estimated
140	2.00E+06	$BA + Cl_2^{\bullet-} \Longrightarrow BA\_Cl_2^{\bullet-}\_products$	(Hasegawa and Neta, 1978)
141	7.00E+09	$DMB + HO^\bullet \Longrightarrow DMB\_HO^\bullet\_products$	(O'Neill et al., 1975)
142	1.80E+10	$DMB + Cl^\bullet \Longrightarrow DMB\_Cl^\bullet\_products$	(Alfassi et al., 1989)
143	2.10E+09	$DMB + ClO^\bullet \Longrightarrow DMB\_ClO^\bullet\_products$	(Alfassi et al., 1988)
144	2.40E+09	$DMB + Cl_2^{\bullet-} \Longrightarrow DMB\_Cl_2^{\bullet-}\_products$	(Lei et al., 2019), estimated
Reactions of $HO^\bullet$ and $Cl^\bullet$ with t-BuOH			
145	6.00E+08	$t\text{-}BuOH + HO^\bullet \Longrightarrow H_2O + {}^\bullet CH_2C(CH_3)_2OH$	(Buxton et al., 1988)
146	5.00E+08	$t\text{-}BuOH + O^{\bullet-} \Longrightarrow OH^- + {}^\bullet CH_2C(CH_3)_2OH$	(Bobrowski and Zagórski, 1977)
147	1.50E+09	$t\text{-}BuOH + Cl^\bullet \Longrightarrow H^+ + Cl^- + {}^\bullet CH_2C(CH_3)_2OH$	(Gilbert et al., 1988)
148	7.00E+08	$t\text{-}BuOH + Cl^\bullet \Longrightarrow H^+ + Cl^- + (CH_3)_3CO^\bullet$	(Gilbert et al., 1988)
149	1.40E+09	${}^\bullet CH_2C(CH_3)_2OH + O_2 \Longrightarrow {}^\bullet OOCH_2C(CH_3)_2OH$	(Reisz et al., 2003)
150	8.00E+07	${}^\bullet OOCH_2C(CH_3)_2OH + {}^\bullet OOCH_2C(CH_3)_2OH \Longrightarrow O_2 + HOC(CH_3)_2CH_2OH + HOC(CH_3)_2CHO$	(Reisz et al., 2003)
151	1.20E+08	${}^\bullet OOCH_2C(CH_3)_2OH + {}^\bullet OOCH_2C(CH_3)_2OH \Longrightarrow H_2O_2 + 2HOC(CH_3)_2CHO$	(Reisz et al., 2003)

152	1.00E+08	$^{\bullet}OOCH_2C(CH_3)_2OH$ + $^{\bullet}OOCH_2C(CH_3)_2OH$ ==> O_2 + 2formaldehyde + $2C(CH_3)_2OH$	(Reisz et al., 2003)
153	1.00E+08	$^{\bullet}OOCH2C(CH_3)_2OH$ + $^{\bullet}OOCH_2C(CH3)_2OH$ ==> O_2 + $HO(CH_3)_2CCH_2OOCH_2C(CH_3)_2OH$	(Reisz et al., 2003)
154	2.00E+09	$^{\bullet}C(CH_3)_2OH + O_2$ ==> $^{\bullet}OOC(CH_3)_2OH$	(Reisz et al., 2003)
155	6.00E+02	$^{\bullet}OOC(CH_3)_2OH$ ==> $(CH_3)_2CO + HO_2^{\bullet}$	(Reisz et al., 2003)
156	7.00E+02	t-BuOH + $Cl_2^{\bullet-}$ ==> t-BuOH_$Cl_2^{\bullet-}$_products	(Hasegawa and Neta, 1978)
157	1.30E+07	t-BuOH + $ClO^{\bullet}$ ==> t-BuOH_$ClO^{\bullet}$_products	(Wu et al., 2017)
158	1.00E-03	t-BuOH + O_3 ==> t-BuOH_O_3_products	(Yao and Haag, 1991)
Equilibrium reactions			
FAC equilibrium			
159	3.16E+03	HOCl ==> OCl^- + H^+	K=3.16E-8, pK_a = 7.5 (Morris, 1966)
160	1.00E+11	OCl^- + H^+ ==> HOCl	Assumed
HO equilibrium			
161	1.26E-01	$HO^{\bullet}$ ==> $O^{\bullet-}$ + H^+	K=1.26E-12, pK_a = 11.9 (Rabani and Matheson, 1964)
162	1.00E+11	$O^{\bullet-}$ + H^+ ==> $HO^{\bullet}$	Assumed
O2- radical			
163	1.58E+06	$HO_2^{\bullet}$ ==> $O_2^{\bullet-}$ + H+	K=1.58E-5, pK_a=4.8 (Bielski et al., 1985)
164	1.00E+11	$O_2^{\bullet-}$ + H^+ ==> $HO_2^{\bullet}$	Assumed
H2O2 equilibrium			
165	2.51E-01	H_2O_2 ==> HO_2^- + H^+	K=2.5E-12, pK_a=11.6 - CRC Handbook (95th) (Haynes, 2014)
166	1.00E+11	HO_2^- + H^+ ==> H_2O_2	Assumed
BA			
167	6.31E+06	BA^+ ==> BA + H^+	pK_a=4.2
168	1.00E+11	BA + H^+ ==> BA^+	Assumed
Carbonate equilibrium			
169	4.47E+04	$H_2CO_3^*$ ==> HCO_3^- + H^+	pK_a = 6.35 - CRC Handbook (95th) (Haynes, 2014)
170	1.00E+11	HCO_3^- + H^+ ==> $H_2CO_3^*$	Assumed
171	4.68E+00	HCO_3^- ==> CO_3^{2-} + H^+	pK_a = 10.33 - CRC Handbook (95th) (Haynes, 2014)
172	1.00E+11	CO_3^{2-} + H^+ ==> HCO_3^-	Assumed
Phosphate equilibrium			
173	6.92E+08	H_3PO_4 ==> $H_2PO_4^-$ + H^+	pK_a=2.16 - CRC Handbook (95th) (Haynes, 2014)
174	1.00E+11	$H_2PO_4^-$ + H^+ ==> H_3PO_4	Assumed
175	6.17E+03	$H_2PO_4^-$ ==> HPO_4^{2-} + H+	pK_a=7.21 - CRC Handbook (95th) (Haynes, 2014)
176	1.00E+11	HPO_4^{2-} + H^+ ==> $H_2PO_4^-$	Assumed
177	4.79E-02	HPO_4^{2-} ==> PO_4^{3-} + H^+	pK_a=12.32 - CRC Handbook (95th) (Haynes, 2014)
178	1.00E+11	PO_4^{3-} + H^+ ==> HPO_4^{2-}	Assumed
Other equilibrium reactions			
179	#1.20E+10	$HO^{\bullet}$ + OH^- ==> $O^{\bullet-}$ + H_2O	Duplicate reaction, muted (Buxton et al., 1988)

180	#9.30E+07	$O^{\bullet-} + H_2O$ ==> $HO^{\bullet} + OH^-$	Duplicate reaction, muted (Buxton, 1970)
Reactions with phosphate buffer			
181	#1.00E+07	$HO^{\bullet} + PO_4^{3-}$ ==> $HO^{\bullet}_PO_4^{3-}$_products	(Black and Hayon, 1970)
182	1.50E+05	$HO^{\bullet} + HPO_4^{2-}$ ==> $HPO_4^{\bullet-} + OH^-$	(Maruthamuthu and Neta, 1978)
183	2.00E+04	$HO^{\bullet} + H_2PO_4^-$ ==> $HPO_4^{\bullet-} + H_2O$	(Maruthamuthu and Neta, 1978)
184	4.20E+04	$HO^{\bullet} + H_3PO_4$ ==> $H_2PO_4^{\bullet} + H_2O$	(Jiang et al., 1992)
185	2.70E+07	$H_2O_2 + HPO_4^{\bullet-}$ ==> $H_2PO_4^- + 2H^+ + O_2^{\bullet-}$	(Nakashima and Hayon, 1970)
186	5.50E+07	$H_2O_2 + H_2PO_4^{\bullet}$ ==> $H_2PO_4^- + 2H^+ + O_2^{\bullet-}$	(Nakashima and Hayon, 1970)
187	3.50E+06	$O^{\bullet-} + HPO_4^{2-}$ ==> $O^{\bullet-}_HPO_4^{2-}$_products	(Grabner et al., 1973)
188	9.10E+07	$O_3^{\bullet-} + H_2PO_4^-$ ==> $HPO_4^{2-} + HO_3^{\bullet}$	(Buehler et al., 1984)
189	1.20E+05	$H_2O + H_2PO_4^{\bullet}$ ==> $H_3PO_4 + HO^{\bullet}$	(Jiang et al., 1992)
190	2.20E+06	$Cl^- + H_2PO_4^{\bullet}$ ==> $H_2PO_4^- + Cl^{\bullet}$	(Maruthamuthu and Neta, 1978)
191	1.90E+09	$Cl^- + H_2PO_4^{\bullet} + H^+$ ==> $H_3PO_4 + Cl^{\bullet}$	(Jiang et al., 1992)
192	1.00E+04	$Cl^- + HPO_4^{\bullet-}$ ==> $Cl^-_HPO_4^{\bullet-}$_products	(Maruthamuthu and Neta, 1978)
193	1.50E+08	$HPO_4^{\bullet-} + HPO_4^{\bullet-}$ ==> $P_2O_8^{4-} + 2H^+$	(Grabner et al., 1973)
194	2.40E+08	$BA + H_2PO_4^{\bullet}$ ==> $BA^{\bullet+} + H_2PO_4^-$	(Maruthamuthu and Neta, 1978)
195	#49000	$H_2PO_4^- + Cl^{\bullet}$ ==> $Cl^- + H_2PO_4^{\bullet}$	(Lee et al., 2020)
196	#340000	$H_3PO_4 + Cl^{\bullet}$ ==> $H_2PO_4^{\bullet} + Cl^- + H^+$	(Lee et al., 2020)
197	#0.0002	$O_3 + H_2PO_4^-$ ==> $O_3_H_2PO_4^-$_products	(Lee et al., 2020)
198	#0.02	$O_3 + H_3PO_4$ ==> $O_3_H_3PO_4$_products	(Lee et al., 2020)
199	#1.00E+9	$H_2PO_4^{\bullet} + H_2PO_4^{\bullet}$ ==> $H_2P_2O_8^{2-} + 2H^+$	(Grabner et al., 1973)
Reactions with carbonate			
200	1.00E+06	$HO^{\bullet} + H_2CO_3^*$ ==> $CO_3^{\bullet-} + H_2O + H^+$	(Keene et al., 1965)
201	8.50E+06	$HO^{\bullet} + HCO_3^-$ ==> $CO_3^{\bullet-} + H_2O$	(Buxton et al., 1988)
202	3.90E+08	$HO^{\bullet} + CO_3^{2-}$ ==> $CO3^{\bullet-} + OH^-$	(Buxton et al., 1988)
203	4.30E+05	$H_2O_2 + CO_3^{\bullet-}$ ==> $HCO_3^- + HO_2^{\bullet}$	(Draganić et al., 1991)
204	3.00E+07	$HO_2^- + CO_3^{\bullet-}$ ==> $HCO_3^- + O_2^{\bullet-}$	(Draganić et al., 1991)
205	3.00E+09	$HO^{\bullet} + CO_3^{\bullet-}$ ==> $HO^{\bullet}_CO_3^{\bullet-}$_products	(Holcman et al., 1987)
206	2.00E+07	$CO_3^{\bullet-} + CO_3^{\bullet-}$ ==> $CO_3^{\bullet-}$_products	(Czapski et al., 1994)
207	2.20E+08	$Cl^{\bullet} + HCO_3^-$ ==> $H^+ + Cl^- + CO_3^{\bullet-}$	(Mertens and von Sonntag, 1995)
208	5.00E+08	$Cl^{\bullet} + CO_3^{2-}$ ==> $Cl^- + CO_3^{\bullet-}$	(Mertens and von Sonntag, 1995)
209	5.70E+05	$CO_3^{\bullet-} + OCl^-$ ==> $ClO^{\bullet} + CO_3^{2-}$	(Huie et al., 1991b)
210	6.00E+02	$ClO^{\bullet} + CO_3^{2-}$ ==> $CO_3^{\bullet-} + OCl^-$	(Huie et al., 1991b)
211	8.00E+07	$Cl_2^{\bullet-} + HCO_3^-$ ==> $2Cl^- + H^+ + CO_3^{\bullet-}$	(Matthew and Anastasio, 2006), estimated
212	1.60E+08	$Cl_2^{\bullet-} + CO_3^{2-}$ ==> $2Cl^- + CO_3^{\bullet-}$	(Matthew and Anastasio, 2006), estimated
213	3.40E+07	$ClO_2^- + CO_3^{\bullet-}$ ==> $ClO_2^{\bullet} + CO_3^{2-}$	(Huie et al., 1991a)
214	#6.00E+07	$O_3^{\bullet-} + CO_3^{\bullet-}$ ==> $CO_3^{2-} + O_3$	(Holcman et al., 1982)
215	#6.50E+08	$O_2^{\bullet-} + CO_3^{\bullet-}$ ==> $CO_3^{2-} + O_2$	(Eriksen et al., 1985)
216	#1.00E+05	$O_3 + CO_3^{\bullet-}$ ==> $O_3_CO_3^{\bullet-}$_products	(Sehested et al., 1983)
Reactions with sulfate			
217	2.50E+08	$Cl^{\bullet} + SO_4^{2-}$ ==> $Cl^- + SO_4^{\bullet-}$	(Huie et al., 1991b)
218	1.00E+04	$HPO_4^{\bullet-} + SO_4^{2-}$ ==> $HPO_4^{\bullet-}_SO_4^{2-}$_products	(Maruthamuthu and Neta, 1978)

219	8.03E+05	$HPO_4^{\bullet-} + HO^{\bullet} ==> H_2O + SO_4^{\bullet-}$	(Ross et al., 1998); average value
220	1.40E+07	$H_2SO_4 + HO^{\bullet} ==> H_2O + H^+ + SO_4^{\bullet-}$	(Jiang et al., 1992)
221	3.07E+02	$SO_4^{\bullet-} + H_2O ==> HO^{\bullet} + SO_4^{2-} + H^+$	(Ross et al., 1998); average value
222	1.20E+07	$SO_4^{\bullet-} + H_2O_2 ==> HO_2^{\bullet} + HSO_4^-$	(Wine et al., 1989)
223	1.20E+07	$SO_4^{\bullet-} + H_2O_2 ==> HO_2^{\bullet} + SO_4^{2-} + H^+$	(Maruthamuthu and Neta, 1978)
224	5.95E+06	$SO_4^{\bullet-} + HCO_3^- ==> CO_3^{\bullet-} + SO_4^{2-} + H^+$	(Ross et al., 1998); average value
225	4.10E+06	$SO_4^{\bullet-} + CO_3^{2-} ==> CO_3^{\bullet-} + SO_4^{2-}$	(Padmaja et al., 1993)
226	1.00E+10	$SO_4^{\bullet-} + HO^{\bullet} ==> HSO_5^-$	(Klaning et al., 1991)
227	3.50E+09	$SO_4^{\bullet-} + HO_2^{\bullet} ==> O_2 + HSO_4^-$	(Jiang et al., 1992)
228	3.31E+08	$SO_4^{\bullet-} + Cl^- ==> Cl^{\bullet} + SO_4^{2-}$	(Ross et al., 1998); average value
229	5.62E+07	$SO_4^{\bullet-} + OH^- ==> HO^{\bullet} + SO_4^{2-}$	(Ross et al., 1998); average value
230	7.00E+04	$SO_4^{\bullet-} + H_2PO_4^- ==>$ $SO_4^{\bullet-}_H_2PO_4^-$_products	(Maruthamuthu and Neta, 1978)
231	1.20E+06	$SO_4^{\bullet-} + HPO_4^{2-} ==> HPO_4^{\bullet-} + SO_4^{2-}$	(Maruthamuthu and Neta, 1978)
232	6.04E+08	$SO_4^{\bullet-} + SO_4^{\bullet-} ==> S_2O_8^{2-}$	(Ross et al., 1998); average value

[a] Reactions with raction rate constant marked with symbol # were not actived (muted) in the Kintecus model due to the following reasons: (1) reaction is published in literature, but its chemical equation is not balanced, (2) reaction not significant in the $O_2^{\bullet-}$/FAC process, (3) duplicate reaction equation, and (4) reaction that causes illegal loop

References for Chapter 3

Adams, G., Boag, J. and Michael, B., 1966. Transient species produced in irradiated water and aqueous solutions containing oxygen. *Proceedings of the Royal Society of London. Series A. Mathematical and Physical Sciences* 289(1418), 321-341.

Alfassi, Z.B., Huie, R.E., Mosseri, S. and Neta, P., 1988. Kinetics of one-electron oxidation by the ClO radical. *International Journal of Radiation Applications and Instrumentation. Part C. Radiation Physics and Chemistry* 32(1), 85-88. https://doi.org/10.1016/1359-0197(88)90018-5

Alfassi, Z.B., Mosseri, S. and Neta, P., 1989. Reactivities of chlorine atoms and peroxyl radicals formed in the radiolysis of dichloromethane. *The Journal of Physical Chemistry* 93(4), 1380-1385. 10.1021/j100341a040

Anastasijević, N.A., Vesović, V. and Adžić, R.R., 1987. Determination of the kinetic parameters of the oxygen reduction reaction using the rotating ring-disk electrode: Part I. Theory. *Journal of electroanalytical chemistry and interfacial electrochemistry* 229(1-2), 305-316.

Behar, D., Czapski, G. and Duchovny, I., 1970. Carbonate radical in flash photolysis and pulse radiolysis of aqueous carbonate solutions. *The Journal of Physical Chemistry* 74(10), 2206-2210.

Bielski, B.H. and Richter, H.W., 1977. A study of the superoxide radical chemistry by stopped-flow radiolysis and radiation induced oxygen consumption. *Journal of the American Chemical Society* 99(9), 3019-3023.

Bielski, B.H.J., 1978. Reevaluation of the spectral and kinetic properties of HO_2 and $O_2^{\bullet-}$ free radicals. *Photochemistry and Photobiology* 28(4-5), 645-649. 10.1111/j.1751-1097.1978.tb06986.x

Bielski, B.H.J. and Gebicki, J.M., 1982. Generation of superoxide radicals by photolysis of oxygenated ethanol solutions. *Journal of the American Chemical Society* 104(3), 796-798. 10.1021/ja00367a024

Bielski, B.H.J., Cabelli, D.E., Arudi, R.L. and Ross, A.B., 1985. Reactivity of $HO_2/O_2^{\bullet-}$ radicals in aqueous solution. *Journal of Physical and Chemical Reference Data* 14(4), 1041-1100. 10.1063/1.555739

Black, E.D. and Hayon, E., 1970. Pulse radiolysis of phosphate anions H2PO4-, HPO42-, PO43-, and P2O74- in aqueous solutions. *The Journal of Physical Chemistry* 74(17), 3199-3203. 10.1021/j100711a007

Bobrowski, K. and Zagórski, Z., 1977. Kinetics of transient oxygen compounds formation measured from Čerenkov emission in pulse radiolysis. *Radiation Effects* 33(1), 39-42.

Bolton, J., Bircher, K., Tumas, W. and Tolman, C., 2001. Figures-of-merit for the technical development and application of advanced oxidation technologies for both electric- and solar-driven systems – (IUPAC Technical Report). *Pure and Applied Chemistry* 73, 627-637. 10.1351/pac200173040627

Buehler, R.E., Staehelin, J. and Hoigne, J., 1984. Ozone decomposition in water studied by pulse radiolysis. 1. Perhydroxyl (HO_2)/hyperoxide ($O_2^{\bullet-}$) and $HO_3/O_3^{\bullet-}$ as intermediates. *The Journal of Physical Chemistry* 88(12), 2560-2564. 10.1021/j150656a026

Bulman, D.M., Mezyk, S.P. and Remucal, C.K., 2019. The impact of pH and irradiation wavelength on the production of reactive oxidants during chlorine photolysis. *Environmental Science & Technology* 53(8), 4450-4459. 10.1021/acs.est.8b07225

Buonanno, M., Ponnaiya, B., Welch, D., Stanislauskas, M., Randers-Pehrson, G., Smilenov, L., Lowy, F.D., Owens, D.M. and Brenner, D.J., 2017. Germicidal Efficacy and Mammalian Skin Safety of 222-nm UV Light. *Radiation Research* 187(4), 493-501. 10.1667/rr0010cc.1

Buonanno, M., Welch, D., Shuryak, I. and Brenner, D.J., 2020. Far-UVC light (222 nm) efficiently and safely inactivates airborne human coronaviruses. *Scientific Reports* 10(1), 10285. 10.1038/s41598-020-67211-2

Buxton, G., 1969. Pulse radiolysis of aqueous solutions. Some rates of reaction of OH and O–and pH dependence of the Yield of O–3. *Transactions of the Faraday Society* 65, 2150-2158.

Buxton, G.V., 1970. Pulse radiolysis of aqueous solutions. Rate of reaction of OH with OH–. *Transactions of the Faraday Society* 66, 1656-1660.

Buxton, G.V., Bydder, M., Arthur Salmon, G. and Williams, J.E., 2000. The reactivity of chlorine atoms in aqueous solution. Part III. The reactions of $Cl^{\bullet}$ with solutes. *Physical Chemistry Chemical Physics* 2(2), 237-245. 10.1039/A907133D

Buxton, G.V., Greenstock, C.L., Helman, W.P. and Ross, A.B., 1988. Critical review of rate constants for reactions of hydrated electrons, hydrogen atoms and hydroxyl radicals ($^{\bullet}OH/O^{\bullet-}$ in aqueous solution). *Journal of Physical and Chemical Reference Data* 17(2), 513-886. 10.1063/1.555805

Buxton, G.V. and Subhani, M.S., 1972. Radiation chemistry and photochemistry of oxychlorine ions. Part 1.—Radiolysis of aqueous solutions of hypochlorite and chlorite ions. *Journal of the Chemical Society, Faraday Transactions 1* 68(0), 947-957. 10.1039/F19726800947

Canonica, S., Meunier, L. and von Gunten, U., 2008. Phototransformation of selected pharmaceuticals during UV treatment of drinking water. *Water Research* 42(1), 121-128. https://doi.org/10.1016/j.watres.2007.07.026

Christensen, H., Sehested, K. and Bjergbakke, E., 1989. Water chemistry of nuclear reactor systems 5, pp. 141-143, British Nuclear Energy Society, London.

Christensen, H., Sehested, K. and Corfitzen, H., 1982. Reactions of hydroxyl radicals with hydrogen peroxide at ambient and elevated temperatures. *The Journal of Physical Chemistry* 86(9), 1588-1590. 10.1021/j100206a023

Chuang, Y.-H., Chen, S., Chinn, C.J. and Mitch, W.A., 2017. Comparing the UV/monochloramine and UV/free chlorine advanced oxidation processes (AOPs) to the UV/hydrogen peroxide AOP under scenarios relevant to potable reuse. *Environmental Science & Technology* 51(23), 13859-13868. 10.1021/acs.est.7b03570

Czapski, G., Holcman, J. and Bielski, B.H., 1994. Reactivity of nitric oxide with simple short-lived radicals in aqueous solutions. *Journal of the American Chemical Society* 116(25), 11465-11469.

Czarnetzki, L. and Janssen, L., 1992. Formation of hypochlorite, chlorate and oxygen during NaCl electrolysis from alkaline solutions at an RuO 2/TiO 2 anode. *Journal of Applied Electrochemistry* 22(4), 315-324.

Draganić, Z.D., Negron-Mendoza, A., Sehested, K., Vujošević, S.I., Navarro-Gonzales, R., Albarran-Sanchez, M. and Draganić, I.G., 1991. Radiolysis of aqueous solutions of ammonium bicarbonate over a large dose range. *International Journal of Radiation Applications and Instrumentation. Part C. Radiation Physics and Chemistry* 38(3), 317-321.

Elliot, A.J., 1989. A pulse radiolysis study of the temperature dependence of reactions involving H, OH and e-aq in aqueous solutions. *International Journal of Radiation Applications and Instrumentation. Part C. Radiation Physics and Chemistry* 34(5), 753-758.

Elliot, A.J. and McCracken, D.R., 1989. Effect of temperature on O anion radical reactions and equilibria: a pulse radiolysis study. *Radiat. Phys. Chem., Int. J. Radiat. Appl. Instrum. Part C; (United Kingdom)*, Medium: X; Size: Pages: 69-74.

Eigen, M., 1963. Protonenübertragung, Säure-Base-Katalyse und enzymatische Hydrolyse. Teil I: Elementarvorgänge. *Angewandte Chemie* 75(12), 489-508.

Eigen, M., 1964. Rate constants of protolytic reactions in aqueous solution. *Progress in reaction kinetics* 2, 287-318.

Energy Information Administration "2019 Utility Bundled Retail Sales- Industrial" (https://www.eia.gov/electricity/sales_revenue_price/pdf/table8.pdf).

Eriksen, T., Lind, J. and Merenyi, G., 1985. On the acid-base equilibrium of the carbonate radical. *Radiation Physics and Chemistry (1977)* 26(2), 197-199.

Eriksen, T.E., Lind, J. and Merényi, G., 1981. Generation of chlorine dioxide from ClO–2 by pulse radiolysis. *Journal of the Chemical Society, Faraday Transactions 1: Physical Chemistry in Condensed Phases* 77(9), 2115-2123.

Ershov, B.G., 2004. Kinetics, mechanism and intermediates of some radiation-induced reactions in aqueous solutions. *Russian chemical reviews* 73(1), 101-113.

Ferraudi, G., 1993. Magnetic field effects on the rates of Cl2-and Br2-reactions: the dependence of the rates of radical disporportionation and oxidation of Mn (II) complexes on field intensity. *Journal of physical chemistry (1952)* 97(11), 2793-2797.

Forman, H. and Fridovich, I., 1972. Electrolytic univalent reduction of oxygen in aqueous solution demonstrated with superoxide dismutase. *Science* 175(4019), 339-339.

Gall, B.L. and Dorfman, L.M., 1969. Pulse radiolysis studies. XV. Reactivity of the oxide radical ion and of the ozonide ion in aqueous solution. *Journal of the American Chemical Society* 91(9), 2199-2204.

Gilbert, B.C., Stell, J.K., Peet, W.J. and Radford, K.J., 1988. Generation and reactions of the chlorine atom in aqueous solution. *Journal of the Chemical Society, Faraday Transactions 1: Physical Chemistry in Condensed Phases* 84(10), 3319-3330.

Gogolev, A., Makarov, I. and Pikaev, A., 1984. Pulsed radiolysis of concentrated hydrochloric acid. *High Energy Chemistry* 18(6), 390-395.

Grabner, G., Getoff, N. and Schwörer, F., 1973. Pulsradiolyse von H3PO4, H2PO4-, HPO42− und P2O74− in wässriger lösung—II. Spektren und kinetik der Zwischenprodukte. *International Journal for Radiation Physics and Chemistry* 5(5), 405-417. https://doi.org/10.1016/0020-7055(73)90003-X

Grebel, J.E., Pignatello, J.J. and Mitch, W.A., 2010. Effect of halide ions and carbonates on organic contaminant degradation by hydroxyl radical-based advanced oxidation processes in saline waters. *Environmental science & technology* 44(17), 6822-6828.

Grigor'ev, A.E., Makarov, I.E. and Pikaev, A.K., 1987. Formation of Cl2- in the bulk of solution during radiolysis of concentrated aqueous solutions of chlorides. *Khimiya Vysokikh Ehnergij* 21(2), 123-126. http://inis.iaea.org/search/search.aspx?orig_q=RN:18088764

Haynes, W.M. (2014) CRC Handbook of Chemistry and Physics, 95th Edition, CRC Press, Hoboken.

Haag, W.R. and Hoigne, J., 1983. Ozonation of water containing chlorine or chloramines. Reaction products and kinetics. *Water Research* 17(10), 1397-1402.

Hasegawa, K. and Neta, P., 1978. Rate constants and mechanisms of reaction of chloride ($Cl_2^{\bullet-}$) radicals. *The Journal of Physical Chemistry* 82(8), 854-857. 10.1021/j100497a003

Haynes, W.M. (2014) CRC Handbook of Chemistry and Physics, 95th Edition, CRC Press, Hoboken.

Held, A.M., Halko, D.J. and Hurst, J.K., 1978. Mechanisms of chlorine oxidation of hydrogen peroxide. *Journal of the American Chemical Society* 100, 5732-5740. https://ci.nii.ac.jp/naid/80013880552/en/

Hessler, D.P., Gorenflo, V. and Frimmel, F.H., 1993. Degradation of aqueous atrazine and metazachlor solutions by UV and UV/H_2O_2 — Influence of pH and herbicide concentration. *Acta hydrochimica et hydrobiologica* 21(4), 209-214. https://doi.org/10.1002/aheh.19930210404

Hoigné, J. and Bader, H., 1994. Kinetics of reactions of chlorine dioxide (OClO) in water—I. Rate constants for inorganic and organic compounds. *Water Research* 28(1), 45-55.

Holcman, J., Bjergbakke, E. and Sehested, K. (1987) The importance of radical-radical reactions in pulse radiolysis of aqueous carbonate/bicarbonate, pp. 149-153, Akadémiai Kiadó.

Holcman, J., Sehested, K., Bjergbakke, E. and Hart, E.J., 1982. Formation of ozone in the reaction between the ozonide radical ion, O3-, and the carbonate radical ion, CO3-, in aqueous alkaline solutions. *The Journal of Physical Chemistry* 86(11), 2069-2072. 10.1021/j100208a032

Holroyd, R.A. and Bielski, B.H.J., 1978. Photochemical generation of superoxide radicals in aqueous solutions. *Journal of the American Chemical Society* 100(18), 5796-5800. 10.1021/ja00486a034

Horsman, P., Conway, B.E. and Yeager, E., 2012. Comprehensive Treatise of Electrochemistry: Volume 7 Kinetics and Mechanisms of Electrode Processes, Springer Science & Business Media.

Hubler, D., Baygents, J.C., Chaplin, B. and Farrell, J., 2014. Understanding chlorite and chlorate formation associated with hypochlorite generation at boron doped diamond film anodes. *Journal of The Electrochemical Society* 161(12), E182.

Huie, R., Shoute, L. and Neta, P., 1991a. Temperature dependence of the rate constants for reactions of the carbonate radical with organic and inorganic reductants. *International journal of chemical kinetics* 23(6), 541-552.

Huie, R.E., Clifton, C.L. and Neta, P., 1991b. Electron transfer reaction rates and equilibria of the carbonate and sulfate radical anions. *International Journal of Radiation Applications and Instrumentation. Part C. Radiation Physics and Chemistry* 38(5), 477-481.

Huie, R.E. and Neta, P., 1986. Kinetics of one-electron transfer reactions involving chlorine dioxide and nitrogen dioxide. *The Journal of Physical Chemistry* 90(6), 1193-1198.

Jin, W., Du, H., Zheng, S., Xu, H. and Zhang, Y., 2010. Comparison of the oxygen reduction reaction between NaOH and KOH solutions on a Pt electrode: the electrolyte-dependent effect. *The Journal of Physical Chemistry B* 114(19), 6542-6548.

Jiang, P.-Y., Katsumura, Y., Domae, M., Ishikawa, K., Nagaishi, R., Ishigure, K. and Yoshida, Y., 1992. Pulse radiolysis study of concentrated phosphoric acid solutions. *Journal of the Chemical Society, Faraday Transactions* 88(22), 3319-3322.

Judith, W. and Bielski, B., 1979. Kinetics of the interaction of HO2 and O2-radicals with hydrogen peroxide. *J. Am. Chem. Soc* 101, 58-62.

Kaidzu, S., Sugihara, K., Sasaki, M., Nishiaki, A., Ohashi, H., Igarashi, T. and Tanito, M., 2021. Re-Evaluation of Rat Corneal Damage by Short-Wavelength UV Revealed Extremely Less Hazardous Property of Far-UV-C†. *Photochemistry and Photobiology* 97(3), 505-516. https://doi.org/10.1111/php.13419

Katsoyiannis, I.A., Canonica, S. and von Gunten, U., 2011. Efficiency and energy requirements for the transformation of organic micropollutants by ozone, O_3/H_2O_2 and UV/H_2O_2. *Water Research* 45(13), 3811-3822. https://doi.org/10.1016/j.watres.2011.04.038

Keene, J., Raef, Y. and Swallow, A. (1965) Pulse radiolysis studies of carboxyl and related radicals, p. 99, Academic Press: London, New York.

Klaning, U., Sehested, K. and Holcman, J., 1985. Standard Gibbs energy of formation of the hydroxyl radical in aqueous solution. Rate constants for the reaction chlorite (ClO2-)+ ozone. dblarw. ozone (1-)+ chlorine dioxide. *The Journal of Physical Chemistry* 89(5), 760-763.

Klaning, U.K., Sehested, K. and Appelman, E.H., 1991. Laser flash photolysis and pulse radiolysis of aqueous solutions of the fluoroxysulfate ion, SO4F. *Inorganic Chemistry* 30(18), 3582-3584.

Kläning, U.K., Sehested, K. and Wolff, T., 1984. Ozone formation in laser flash photolysis of oxoacids and oxoanions of chlorine and bromine. *Journal of the Chemical Society, Faraday Transactions 1: Physical Chemistry in Condensed Phases* 80(11), 2969-2979.

Kläning, U.K. and Wolff, T., 1985. Laser flash photolysis of HClO, ClO^-, HBrO, and BrO^- in aqueous solution. Reactions of $Cl^\bullet$ and $Br^\bullet$ atoms. *Berichte der Bunsengesellschaft für physikalische Chemie* 89(3), 243-245. 10.1002/bbpc.19850890309

Kraft, A., Stadelmann, M., Blaschke, M., Kreysig, D., Sandt, B., Schröder, F. and Rennau, J., 1999. Electrochemical water disinfection Part I: Hypochlorite production from very dilute chloride solutions. *Journal of Applied Electrochemistry* 29(7), 859-866.

Lee, W., Lee, Y., Allard, S., Ra, J., Han, S. and Lee, Y., 2020. Mechanistic and kinetic understanding of the UV254 photolysis of chlorine and bromine species in water and formation of oxyhalides. *Environmental Science & Technology* 54(18), 11546-11555. 10.1021/acs.est.0c02698

Lei, Y., Cheng, S., Luo, N., Yang, X. and An, T., 2019. Rate constants and mechanisms of the reactions of $Cl^{\bullet}$ and $Cl_2^{\bullet-}$ with trace organic contaminants. *Environmental Science & Technology* 53(19), 11170-11182. 10.1021/acs.est.9b02462

Liou, S.-Y. and Dodd, M.C., 2021. Evaluation of hydroxyl radical and reactive chlorine species generation from the superoxide/hypochlorous acid reaction as the basis for a novel advanced oxidation process. *Water Research* 200, 117142.

Long, C.A. and Bielski, B.H.J., 1980. Rate of reaction of superoxide radical with chloride-containing species. *The Journal of Physical Chemistry* 84(5), 555-557. 10.1021/j100442a023

Marklund, S., 1976. Spectrophotometric study of spontaneous disproportionation of superoxide anion radical and sensitive direct assay for superoxide dismutase. *Journal of Biological Chemistry* 251(23), 7504-7507.

Maricle, D. and Hodgson, W., 1965. Reducion of oxygen to superoxide anion in aprotic solvents. *Analytical Chemistry* 37(12), 1562-1565.

Mártire, D.O., Rosso, J.A., Bertolotti, S., Le Roux, G.C., Braun, A.M. and Gonzalez, M.C., 2001. Kinetic study of the reactions of chlorine atoms and $Cl_2^{\bullet-}$ radical anions in aqueous solutions. II. Toluene, benzoic acid, and chlorobenzene. *The Journal of Physical Chemistry A* 105(22), 5385-5392. 10.1021/jp004630z

Maruthamuthu, P. and Neta, P., 1978. Phosphate radicals spectra, acid-base equilibria, and reactions with inorganic compounds. *The Journal of Physical Chemistry* 82(6), 710-713. http://inis.iaea.org/search/search.aspx?orig_q=RN:09401002

Matthew, B. and Anastasio, C., 2006. A chemical probe technique for the determination of reactive halogen species in aqueous solution: Part 1–bromide solutions. *Atmospheric Chemistry and Physics* 6(9), 2423-2437.

McDowell, M.S., Bakac, A. and Espenson, J.H., 1983. A convenient route to superoxide ion in aqueous solution. *Inorganic Chemistry* 22(5), 847-848.

McElroy, W.J., 1990. A laser photolysis study of the reaction of sulfate (1-) with chloride and the subsequent decay of chlorine (1-) in aqueous solution. *Journal of Physical Chemistry* 94(6), 2435-2441.

Mertens, R. and von Sonntag, C., 1995. Photolysis (λ= 354 nm of tetrachloroethene in aqueous solutions. *Journal of Photochemistry and Photobiology A: Chemistry* 85(1-2), 1-9.

Mialocq, J.-C., Barat, F., Gilles, L., Hickel, B. and Lesigne, B., 1973. Flash photolysis of chlorine dioxide in aqueous solution. *The Journal of Physical Chemistry* 77(6), 742-749.

Morgan, M.S., Van Trieste, P.F., Garlick, S.M., Mahon, M.J. and Smith, A.L., 1988. Ultraviolet molar absorptivities of aqueous hydrogen peroxide and hydroperoxyl ion. *Analytica Chimica Acta* 215, 325-329. https://doi.org/10.1016/S0003-2670(00)85294-0

Morris, J.C., 1966. The acid ionization constant of HOCl from 5 to 35°. *The Journal of Physical Chemistry* 70(12), 3798-3805. 10.1021/j100884a007

Narita, K. and Asano, K., 2018. Chronic irradiation with 222-nm UVC light induces neither DNA damage nor epidermal lesions in mouse skin, even at high doses. 13(7), e0201259. 10.1371/journal.pone.0201259

Nadtochenko, V. and Kiwi, J., 1998. Primary photochemical reactions in the photo-fenton system with ferric chloride. 1. A case study of xylidine oxidation as a model compound. *Environmental Science & Technology* 32(21), 3273-3281. 10.1021/es970962e

Nakashima, M. and Hayon, E., 1970. Rates of reaction of inorganic phosphate radicals in solution. *The Journal of Physical Chemistry* 74(17), 3290-3291.

Neta, P. and Dorfman, L.M., 1968. Radiation Chemistry, pp. 222-230, American Chemical Society.

Nick, K., Schöler, H., Mark, G., Söylemez, T., Akhlaq, M., Schuchmann, H. and Von Sonntag, C., 1992. Degradation of some triazine herbicides by UV radiation such as used in the UV disinfection of drinking water. *Journal of Water Supply: Research and Technology - AQUA* 41(2), 82-87.

O'Neill, P., Steenken, S. and Schulte-Frohlinde, D., 1975. Formation of radical cations of methoxylated benzenes by reaction with hydroxyl radicals, thallium(2+), silver(2+), and peroxysulfate ($SO_4^{\bullet-}$) in aqueous solution. Optical and conductometric pulse radiolysis and in situ radiolysis electron spin resonance study. *The Journal of Physical Chemistry* 79(25), 2773-2779. 10.1021/j100592a013

Padmaja, S., Neta, P. and Huie, R., 1993. Rate constants for some reactions of inorganic radicals with inorganic ions. Temperature and solvent dependence. *International journal of chemical kinetics* 25(6), 445-455.

Quiroga, S.L. and Perissinotti, L.J., 2005. Reduced mechanism for the 366 nm chlorine dioxide photodecomposition in N2-saturated aqueous solutions. *Journal of Photochemistry and Photobiology A: Chemistry* 171(1), 59-67.

Rabani, J. and Matheson, M., 1966. The pulse radiolysis of aqueous solutions of potassium ferrocyanide. *The Journal of Physical Chemistry* 70(3), 761-769.

Rabani, J. and Matheson, M.S., 1964. Pulse radiolytic determination of p K for hydroxyl ionic dissociation in water. *Journal of the American Chemical Society* 86(15), 3175-3176.

Rabani, J. and Zehavi, D., 1971. Pulse radiolytic investigation of Oaq-radical ions. *The Journal of Physical Chemistry* 75(11), 1738-1744.

Rahn, R.O., 1997. Potassium Iodide as a Chemical Actinometer for 254 nm Radiation: Use of Iodate as an Electron Scavenger. *Photochemistry and Photobiology* 66(4), 450-455. https://doi.org/10.1111/j.1751-1097.1997.tb03172.x

Reisz, E., Schmidt, W., Schuchmann, H.-P. and von Sonntag, C., 2003. Photolysis of ozone in aqueous solutions in the presence of tertiary butanol. *Environmental science & technology* 37(9), 1941-1948.

Rosenfeldt, E.J., Linden, K.G., Canonica, S. and von Gunten, U., 2006. Comparison of the efficiency of OH radical formation during ozonation and the advanced oxidation processes O_3/H_2O_2 and UV/H_2O_2. *Water Research* 40(20), 3695-3704. https://doi.org/10.1016/j.watres.2006.09.008

Ross, A., Bielski, B., Buxton, G., Cabelli, D., Helman, W., Huie, R., Grodkowski, J., Neta, P., Mulazzani, Q. and Wilkinson, F. (1998) NIST Standard Reference Database 40: NDRL/NIST Solutions Kinetics Database V. 3.0, Gaithersburg, MD.

Sawyer, D.T. and Roberts Jr, J.L., 1966. Electrochemistry of oxygen and superoxide ion in dimethylsulfoxide at platinum, gold and mercury electrodes. *Journal of Electroanalytical Chemistry (1959)* 12(2), 90-101.

Schmidt, K., 1972. Electrical conductivity techniques for studying the kinetics of radiation-induced chemical reactions in aqueous solutions. *International Journal for Radiation Physics and Chemistry* 4(4), 439-468.

Sehested, K., Holcman, J., Bjergbakke, E. and Hart, E.J., 1984a. Formation of ozone in the reaction of hydroxyl with O3-and the decay of the ozonide ion radical at pH 10-13. *The Journal of Physical Chemistry* 88(2), 269-273.

Sehested, K., Holcman, J., Bjergbakke, E. and Hart, E.J., 1984b. A pulse radiolytic study of the reaction hydroxyl+ ozone in aqueous medium. *The Journal of Physical Chemistry* 88(18), 4144-4147.

Sehested, K., Holcman, J., Bjergbakke, E. and Hart, E.J., 1982. Ultraviolet spectrum and decay of the ozonide ion radical, O3-, in strong alkaline solution. *The Journal of Physical Chemistry* 86(11), 2066-2069.

Sehested, K., Holcman, J. and Hart, E.J., 1983. Rate constants and products of the reactions of e-aq, dioxide(1-) (O2-) and proton with ozone in aqueous solutions. *The Journal of Physical Chemistry* 87(11), 1951-1954. 10.1021/j100234a024

Shao, M.-h., Liu, P. and Adzic, R.R., 2006. Superoxide anion is the intermediate in the oxygen reduction reaction on platinum electrodes. *Journal of the American Chemical Society* 128(23), 7408-7409.

Singh, M. and Misra, R.A., 1989. Electrogenerated superoxide initiated oxidation with oxygen: a convenient method for the conversion of secondary alcohols to ketones. *Synthesis (Stuttgart)* (5), 403-404.

Sharma, J.R., Najafi, M. and Qasim, S.R., 2013. Preliminary cost estimation models for construction, operation, and maintenance of water treatment plants. *Journal of Infrastructure Systems* 19(4), 451-464. doi:10.1061/(ASCE)IS.1943-555X.0000155

von Sonntag, C., 2006. Free-radical-induced DNA damage and its repair, Springer.

Spendelow, J.S. and Wieckowski, A., 2007. Electrocatalysis of oxygen reduction and small alcohol oxidation in alkaline media. *Physical Chemistry Chemical Physics* 9(21), 2654-2675.

Staehelin, J. and Hoigne, J., 1982. Decomposition of ozone in water: rate of initiation by hydroxide ions and hydrogen peroxide. *Environmental Science & Technology* 16(10), 676-681. 10.1021/es00104a009

Stanbury, D.M., 2020. Mechanisms of advanced oxidation processes, the principle of detailed balancing, and specifics of the UV/chloramine process. *Environmental Science & Technology* 54(7), 4658-4663.

Stanbury, D.M. and Harshman, J., 2019. Large-scale models of radiation chemistry and the principle of detailed balancing. *The Journal of Physical Chemistry A* 123(47), 10240-10245.

Stanbury, D.M. and Hoffman, D., 2019. Systematic Application of the Principle of Detailed Balancing to Complex Homogeneous Chemical Reaction Mechanisms. *The Journal of Physical Chemistry A* 123(26), 5436-5445.

Subhani, M.S.K., Z., 1978. Flash photolysis decomposition of sulphate and sulphite anions in aqueous solution.

Sun, P., Lee, W.-N., Zhang, R. and Huang, C.-H., 2016. Degradation of DEET and caffeine under UV/chlorine and simulated sunlight/chlorine conditions. *Environmental Science & Technology* 50(24), 13265-13273. 10.1021/acs.est.6b02287

Sun, P., Tyree, C. and Huang, C.-H., 2016b. Inactivation of Escherichia coli, bacteriophage MS2, and Bacillus Spores under UV/H_2O_2 and UV/peroxydisulfate advanced disinfection conditions. *Environmental Science & Technology* 50(8), 4448-4458. 10.1021/acs.est.5b06097

USEPA (1999) Alternative Disinfectants and Oxidants Guidance Manual.

USEPA (2003a) Contaminant Candidate List Regulatory Determination Support Document for Sulfate, Washington, DC.

USEPA (2003b) Drinking Water Advisory: Consumer Acceptability Advice and Health Effects Analysis on Sulfate, Washington, DC.

USEPA (2016) Optimal Corrosion Control Treatment Evaluation Technical Recommendations for Primacy Agencies and Public Water Systems, Washington, DC.

USEPA (2005) Technologies and Costs Document for the Final Long Term 2 Enhanced Surface Water Treatment Rule and Final Stage 2 Disinfectants and Disinfection Byproducts Rule.

USEPA (2006) Technology and Cost Document for the Final Ground Water Rule.

Wadhawan, J.D., Welford, P.J., McPeak, H.B., Hahn, C.E. and Compton, R.G., 2003. The simultaneous voltammetric determination and detection of oxygen and carbon dioxide: A study of the kinetics of the reaction between superoxide and carbon dioxide in non-aqueous media using membrane-free gold disc microelectrodes. *Sensors and Actuators B: Chemical* 88(1), 40-52.

Wagner, I., Karthäuser, J. and Strehlow, H., 1986. On the decay of the dichloride anion Cl2- in aqueous solution. *Berichte der Bunsengesellschaft für physikalische Chemie* 90(10), 861-867.

Wang, L. and Margerum, D.W., 2002. Hypohalite ion catalysis of the disproportionation of chlorine dioxide. *Inorganic Chemistry* 41(23), 6099-6105. 10.1021/ic020440m

Wine, P., Tang, Y., Thorn, R., Wells, J. and Davis, D., 1989. Kinetics of aqueous phase reactions of the SO4− radical with potential importance in cloud chemistry. *Journal of Geophysical Research: Atmospheres* 94(D1), 1085-1094.

Wu, D., Wong, D. and Di Bartolo, B., 1980. Evolution of Cl− 2 in aqueous NaCl solutions. *Journal of Photochemistry* 14(4), 303-310.

Wu, Z., Guo, K., Fang, J., Yang, X., Xiao, H., Hou, S., Kong, X., Shang, C., Yang, X., Meng, F. and Chen, L., 2017. Factors affecting the roles of reactive species in the degradation of micropollutants by the UV/chlorine process. *Water Research* 126, 351-360. https://doi.org/10.1016/j.watres.2017.09.028

Yang, F., Shi, B., Bai, Y., Sun, H., Lytle, D.A. and Wang, D., 2014. Effect of sulfate on the transformation of corrosion scale composition and bacterial community in cast iron water distribution pipes. *Water Research* 59, 46-57. https://doi.org/10.1016/j.watres.2014.04.003

Yao, C.D. and Haag, W.R., 1991. Rate constants for direct reactions of ozone with several drinking water contaminants. *Water research* 25(7), 761-773.

Yeager, E., 1986. Dioxygen electrocatalysis: mechanisms in relation to catalyst structure. *J. Mol. Catal.;(Switzerland)* 38(1/2).

Yeager, E., 1976. Electrocatalysis on non-metallic surfaces. *NBS Special Publication* 455, 203.

Yu, X.-Y., 2004. Critical evaluation of rate constants and equilibrium constants of hydrogen peroxide photolysis in acidic aqueous solutions containing chloride ions. *Journal of Physical and Chemical Reference Data* 33(3), 747-763. 10.1063/1.1695414

Yu, X.-Y. and Barker, J.R., 2003. Hydrogen peroxide photolysis in acidic aqueous solutions containing chloride ions. I. Chemical mechanism. *The Journal of Physical Chemistry A* 107(9), 1313-1324.

Zhestkova, T. and Pikaev, A., 1974. Destruction rate of Cl 2− anion-radicals during pulse radiolysis of concentrated aqueous lithium chloride solutions. *Bulletin of the Academy of Sciences of the USSR, Division of chemical science* 23(4), 877-878.

Chapter 4. GENERATION OF REACTIVE SPECIES AND OXIDANT DESTRUCTION FROM REACTIONS OF METAL(LOID) OXIDES WITH HYDROGEN PEROXIDE AND FREE AVAILABLE CHLORINE

4.1 Introduction

Many studies have reported decomposition of H_2O_2 via reactions with metal or metalloid oxides (MeOx) are often accompanied by ROS generation, such as hydroxyl radical ($HO^{\bullet}$), superoxide radical ($O_2^{\bullet-}$), and singlet oxygen ($^1O_2$) (Bedilo et al., 2005; Hiroki and LaVerne, 2005; Nosaka and Nosaka, 2016; Sobańska et al., 2017; Wang et al., 2017). On the basis of these findings, it was hypothesized that other common oxidants such as free available chlorine (FAC) may also have potential in producing ROS and RCS during reactions with MeOx. Fe-based and Cu-based species and materials have been widely studied for water treatment purpose in terms of Fenton and Fenton-like reactions as catalysts in the presence of H_2O_2 (Ghiselli et al., 2004; Nichela et al., 2013; Nieto-Juarez et al., 2010; Pereira et al., 2012; Rusevova et al., 2012). Such reactions usually require to be operated at low pH and have potential of releasing Fe and Cu and increasing risk of transition metal contamination. Therefore, this study intended to select some other MeOx minerals that have yet been well studied and to investigate their reactions with H_2O_2 and FAC.

H_2O_2 and FAC reactions with various non-ferrous and non-cuprous MeOx, including amorphous zirconium oxide (a-ZrO_2), monoclinic zirconium oxide (m-ZrO_2), cerium oxide (CeO_2), titanium oxide (TiO_2), aluminum oxide (Al_2O_3) and silicon oxide (SiO_2), were systematically examined in this work. These minerals were selected due to their relatively low biotoxicity and less health and water quality concerns as compared to minerals such as CuO and ZnO (Heinlaan et al., 2008; Karlsson et al., 2022; Puzyn et al., 2011). Two zirconium species, a-ZrO_2 and m-ZrO_2 were selected in particular in light of their potentials for used in water treatment as sorbents or membrane materials (Bouzerara et al., 2012; He et al., 2019; Kwaśny et

al., 2018; Luo et al., 2016; Padungthon et al., 2015; Padungthon et al., 2014; Sobańska et al., 2017).

4.2 Materials and Methods

4.2.1 Chemicals

m-ZrO_2, TiO_2 and SiO_2 were purchased from Sigma Aldrich. CeO_2 was obtained from Beantown Chemical Corporation, and Al_2O_3 was from Alfa Aesar. Synthetic method for a-ZrO_2 were described in Section 4.2.2 below. Other chemicals, including furfuryl alcohol (FFA), methanol (MeOH), isopropanol (iPrOH), *tert*-butanol (*t*-BuOH), tetranitromethane (TNM), free available chlorine (4.00-4.99% w/w), acetone, and formaldehyde were from Sigma-Aldrich. Hydrogen peroxide (30%), ammonium hydroxide (28-30%), nitro blue tetrazolium (NBT), and *o*-phenylenediamine (OPD) were obtained from Fisher Scientific. Zirconium dichloride oxide octahydrate ($ZrOCl_2 \cdot 8H_2O$) used for a-ZrO_2 synthesis was purchased from Alfa Aesar and 2,4-dinitrophenylhydrazine (70%) was from the Spectrum Chemical.

4.2.2 Characterization of MeOx

(i) Specific surface area and pore volume measurement for MeOx particles (BET analyzer)

Detailed MeOx properties including particle size, specific surface area, point of zero charge (PZC), and pore volume are summarized in Table 4.1. Surface area were measured by N_2 adsorption at 77K based on the Brunauer-Emmett-Teller (BET) technique using a BET Surface Area and Porosity Analyzer (Micromeritics, USA) in the relative pressure (P/P_0) ranging from 0.01 to 0.1. Pore volume measurement was performed simultaneously according to the Barrett-Joyner-Halenda (BJH) method, which uses the modified Kelvin equation to relate the amount of

adsorbate adsorption/desorption from the pores of the material to the size of the pores. As shown in Table 4.1 for the two zirconia, a-ZrO_2 appears to have much larger surface area and pore volume than m-ZrO_2. This is consistent with other studies suggesting that amorphous zirconia usually has much higher specific surface area and pore volume than its crystallized counterparts (e.g., m-ZrO_2 and t-ZrO_2) (Cui et al., 2012; Ma et al., 2005).

Table 4.1. MeOx particle characteristics

MeOx	Manufacturer	Labeled particle size by manufacturer	Measured particle size	Surface area (m^2/g)[a]	Pore volume (cm^3/g)[a]	Point of zero charge (PZC)[b]
a-ZrO_2	self-synthesized	Not available (self-synthesized)	d50: 8 µm	292	0.230	5.8 (Blesa et al., 1985)
m-ZrO_2	Sigma-Aldrich	<5 µm; 0.6 µm (certificate of analysis)	d50: 2.5 µm	7.58	0.019	6.1 (Megias-Alguacil et al., 2000)
CeO_2	Beantown Chemical	5 µm (average)	d50: 11 µm	13.5	0.054	6~7.5 (Kosmulski, 2016)
TiO2	Sigma-Aldrich	<5 µm	d50: 8 µm	4.41	0.007	4.8 (Morris et al., 1999)
Al_2O_3	Alfa Aesar	2.5 µm	d50: 2 µm	174	0.547	8.2~9.5 (Del Nero et al., 2010; Moreau et al., 2013)
SiO_2	Sigma-Aldrich	0.5-10 µm (~80% between 1-5 µm)	d50: 0.4 µm	9.25	0.071	< 3 if any (Janusz et al., 2003; Kosmulski, 2016)

[a] Specific surface area and pore volume were measured by a Micromeritics BET analyzer. [b] Values of PZC were obtained for the same product from the same manufacturer, except for CeO_2; PZC value of a-ZrO_2 was obtained from literature using similar synthetic method.

(ii) Scanning electron microscope (SEM) imaging for MeOx particles

Scanning electron microscope (SEM) samples for MeOx were made by sticking MeOx particles onto SEM sample mounts. Prior to imaging, samples were sputtered with gold for 5 min, and placed into a Phenom ProX Desktop Scanning Electron Microscope (Depprich et al., 2008; Dercz et al., 2008; Ke et al., 2007). The electron beam mode was then turned on, and the brightness, contrast and focus were adjusted until clear images were seen (Figure 4.1).

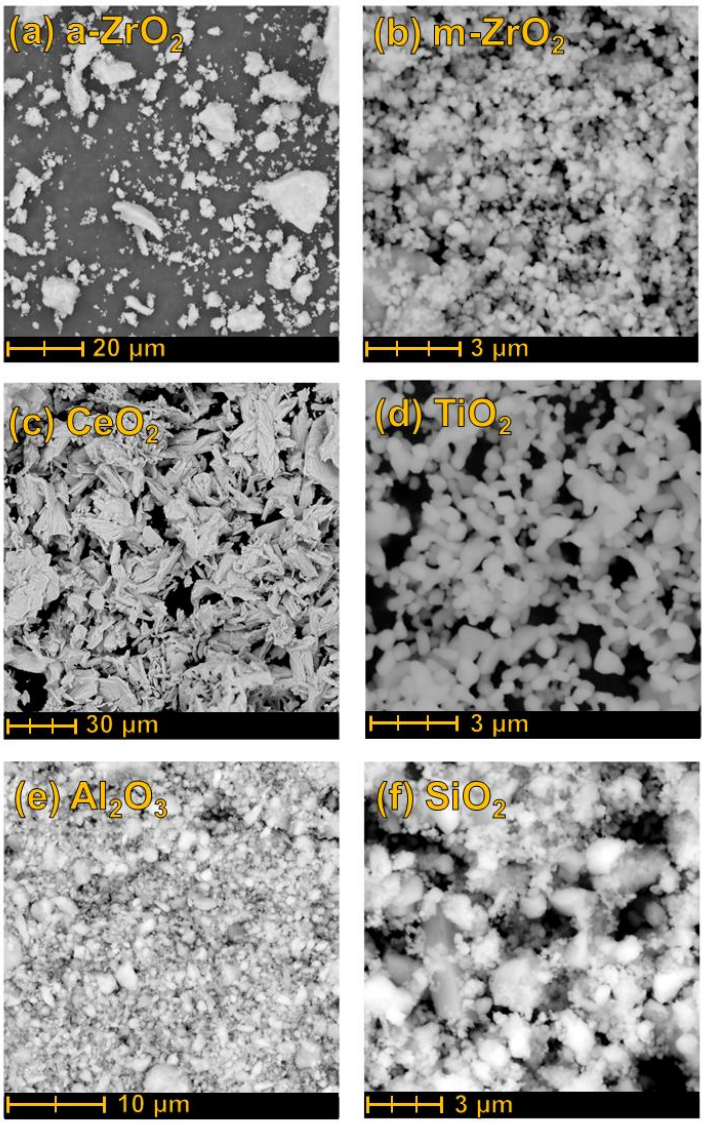

Figure 4.1. SEM images of MeOx minerals used in this study

(iii) Particle size measurement for MeOx particles

A Horiba particle size analyzer (LA-950V2) was used to measure the particle size distribution of each MeOx minerals. Reflective indices inputted during particle size analyses were obtained as average values from a carefully reviewed paper by Shannon et al. (Shannon et al., 2002). The indices are 2.2560 for a-ZrO_2 and m-ZrO_2, 2.335 for CeO_2, 2.4633 for TiO_2, 1.7592 for Al_2O_3, and 1.5347 for SiO_2. Results of relative particle size distribution and cumulative particle size distribution for MeOx are shown in Figure 4.2 and 4.3, respectively.

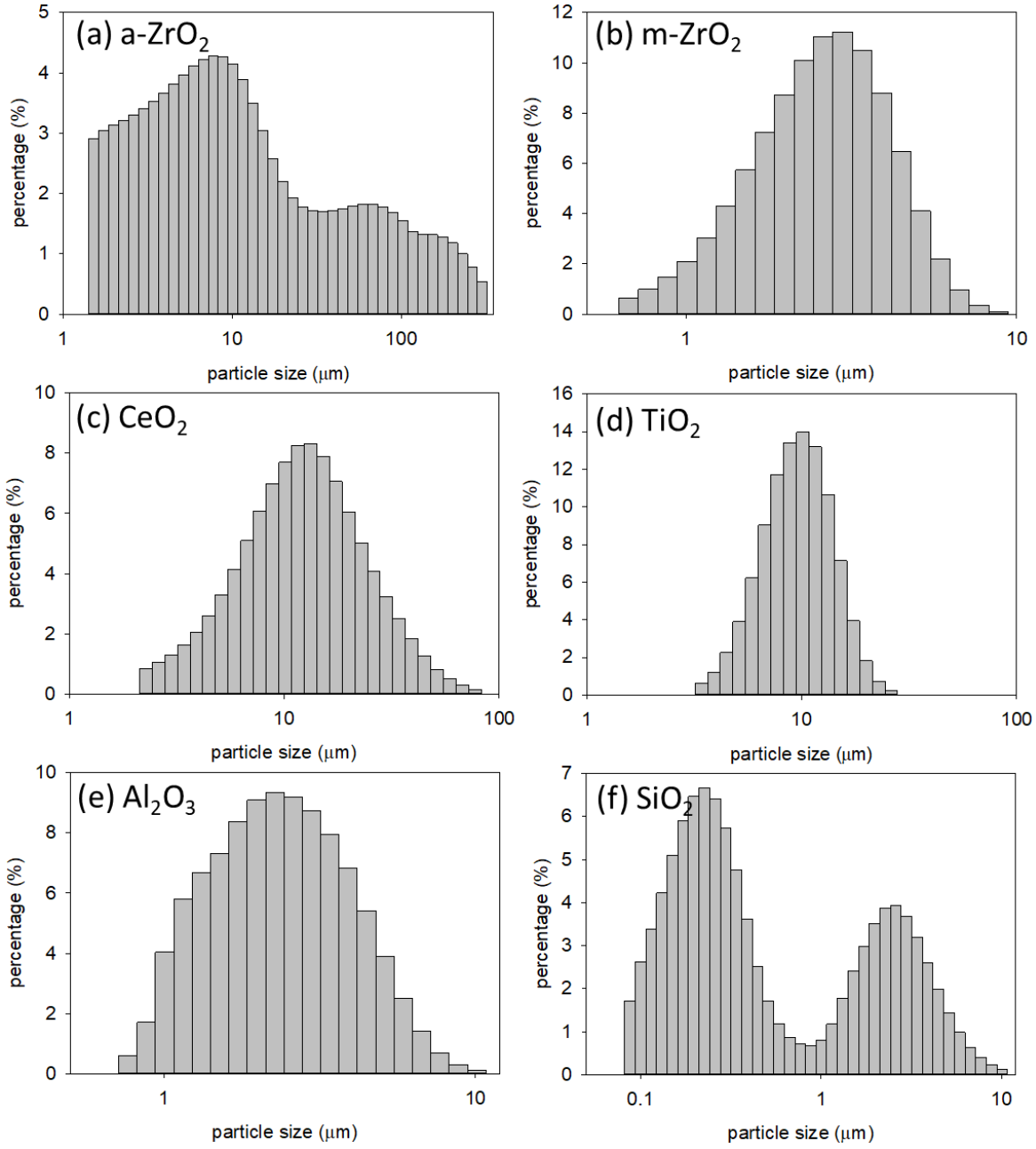

Figure 4.2. Relative particle size measurements for MeOx

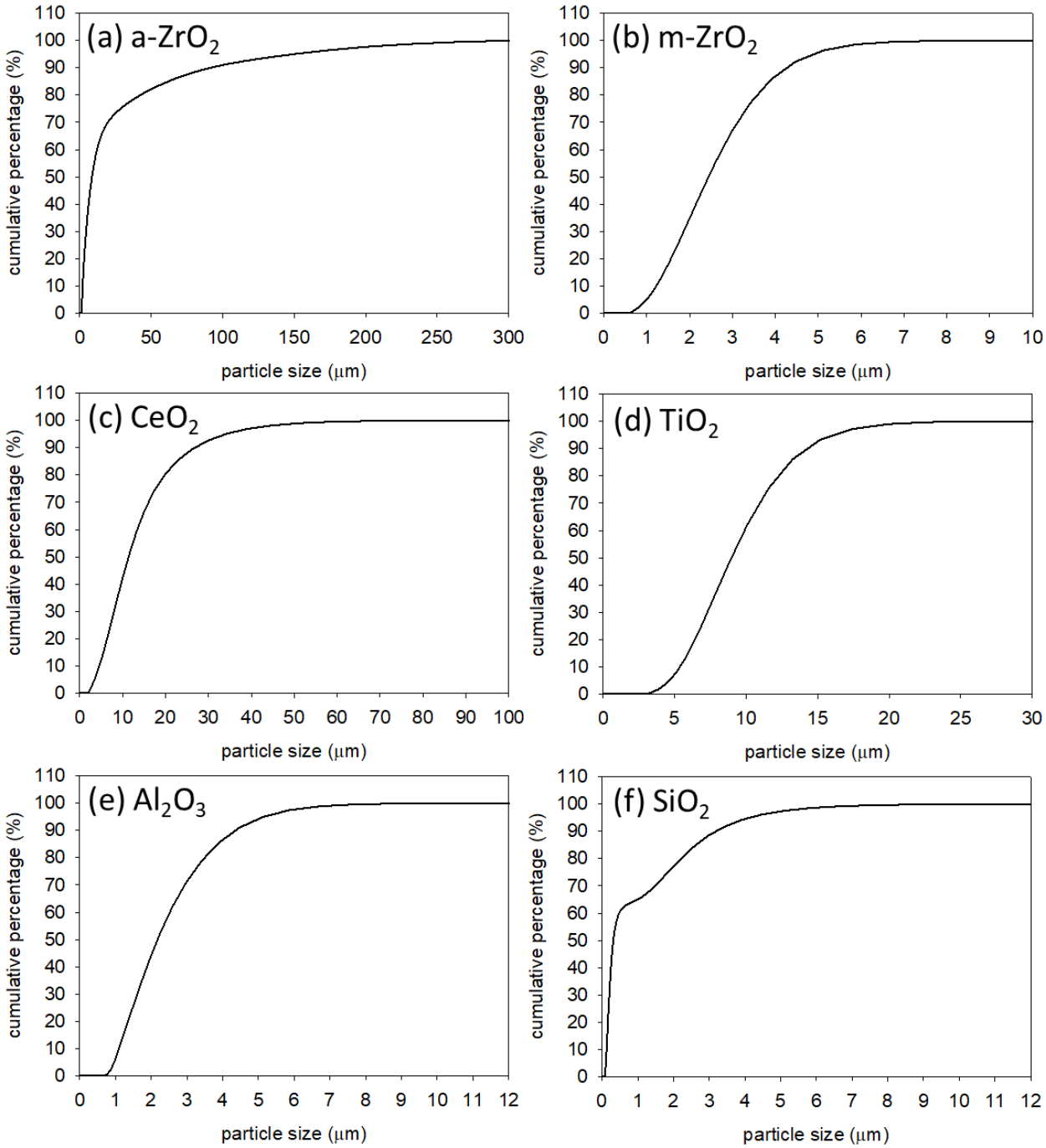

Figure 4.3. Cumulative distribution of particle size for MeOx

4.2.3 Synthesis and Purification of a-ZrO_2

a-ZrO_2 was synthesized from a solution of zirconium oxydichloride co-precipitation with ammonia (Cui et al., 2012; Sobańska et al., 2017). Fist, $ZrOCl_2$•$8H_2O$ was dissolved in Milli-Q water at a concentration of 0.2 mol/L. Aqueous ammonia (28-30%) was then slowly dropped into the former solution with rigious stirring until the solution pH reach ~10. The precipitate a-ZrO_2 gel was transferred into centrifuge tubes and centrifuged at 5,000 rpm for 5 min. The supernatant with concentrate ammonia was discarded, and then the precipicate was washed by fresh Milli-Q ultrapure water repeatedly for 10 times in order to remove most ammonia and residual chloride. During the washing steps, the a-ZrO_2 solid to water volume ratio was maintained at 1:4. The presence of Cl^- can be detected by dropping 0.1 M $AgNO_3$ solution into the upper clear solution separated by centrifugation during the washing steps. When no white AgCl precipitation was observed, the absence of Cl^- was determined. Residual ammonia in the 10 cycles-washed solution was measured to be only ~10 μM, determined by the phenol-hypochlorite method (Berthelot reagent) (Harwood and Kühn, 1970; Ngo et al., 1982). The a-ZrO_2 precipitate was then dried at 100 °C for 8-12 h, and then grinded into fine powder. Drying at 100 °C can help facilitate the drying process and remove residual ammonia completely; meanwhile, does not modify its amorphous structure when drying under this temperature (Stichert and Schüth, 1998). Residual ammonia was not detected in both water- and 0.1M potassium chloride-amended suspensions of the 100°C-dried a-ZrO_2 powder, confirming that ammonia has been completely removed after the drying process. KCl solution was used here for ion exchange of possible residual of NH_4^+ that could adsorb on the a-ZrO_2 surface.

4.2.4 MeOx/H_2O_2 and MeOx/FAC Treatment Procedures

Reaction pH, if not specified, were not adjusted or controlled through addition of buffer species since commonly used buffers like phosphate and borate were found to have high adsorption tendency toward MeOx minerals and could occupy the surface sites, hindering their reactions with H_2O_2 or FAC. Organic buffers should be avoid as they can scavenge reactive species/radicals being generated during the reactions. Carbonate buffer may also have potential of scavenging, and off-gassing of CO_2 can make it challenging to control the reaction pH. Although carbonate was not applied to most experiments in this work, it was used as a buffer for several microbial inactivation experiments discussed in Chapter 5 as we have later confirmed that using low carbonate concentration ($\leq$ 5 mM) would not significantly affect H_2O_2 or FAC decomposition and reactive species/radical exposures. For certain situations when pH adjustment were required, NaOH and H_2SO_4 were used.

(i) Single-dosing experiments

Batch reactions were conducted by dosing H_2O_2 (1, 10 or 100mM) or FAC (0.1 or 1mM) into 0.001-0.1 g/mL suspensions of MeOx solids. MeOx were first placed in 20-mL amber vials, followed by solutions containing probe compounds or radical scavengers, and finally H_2O_2 or FAC were added to initiate reactions with rapid mixing at 500 rpm. At desired reaction time, MeOx suspensions were taken out by polypropylene syringes and pushed through 0.2 μm, polyethersulfone (PES) filters to remove MeOx solids. The filtrates were later used for aqueous oxidant concentration and pH measurements, and part of the solutions were quenched by sufficient catalase (in the case of H_2O_2) or thiosulfate (in the case of FAC) for FFA and acetone analyses on the HPLC. Samples used for formaldehyde measurement were not quenched to avoid

interference of quenching reagents on the colorimetric measurements. It was confirmed that the presence of H_2O_2 and FAC does not affect the Hantzsch reaction.

(ii) Multiple-dosing experiments

Several experiments were conducted by multiple dosing of H_2O_2 (10 or 100 mM) or FAC (0.1 or 1 mM) into 0.1 g/mL MeOx suspensions. Batch reactions were operated as described previously with MeOx first placed in 20-mL amber vials, followed by solutions containing probe compounds or radical scavengers, and finally H_2O_2 or FAC were added to initiate reactions with rapid mixing at 500 rpm. At designed time, MeOx suspensions were transferred to centrifuge tubes for centrifugation at 10,000 rpm for 5 min, and then the supernatants were collected, filtered through 0.2 μm PES membrane filters prior to oxidant concentration and pH measurements. The rest MeOx precipitates were reused for the next round of treatment. At each dosing step, H_2O_2 or FAC following additions of fresh probes or 100mM radical scavengers (MeOH, iPrOH or t-BuOH) were repeatedly added.

(iii) MeOx-precoated membrane filtration

One hundred milligram of MeOx were first blended with Milli-Q ultrapure water, and then the suspensions were passed through syringe filter cartridges installed with 13mm, 0.2 μM PES membrane (Sterlitech, USA) for MeOx layer coating driven by a syringe pump. Figure 4.4 shows experimental setup for the precoat filtration experiments. For the MeOx/H_2O_2 system, solutions containing $[FFA]_0$ = 1 μM and $[H_2O_2]_0$ = 1 mM were pushed through a MeOx-precoated filter cartridge for treatment at flow rates of 0.167 or 0.0167 mL/min (Figure 4.4a). As for the MeOx/FAC system, [FFA] = 2 μM and [FAC] = 200 μM were initially loaded into two separate syringes, and then pushed simultaneously through a MeOx-precoated filter each at flow

rates of 0.083 or 0.0083 mL/min (Figure 4.4b). The cartridges should be placed vertically as shown in the figures to make sure the liquid can flow evenly through the MeOx coatings. The overall flow rates were therefore the sum from the two injection channels (i.e., 0.167 or 0.0167 mL/min), and with initial reaction concentrations of $[FFA]_0$ = 1 μM and $[FAC]_0$ = 100 μM. FFA and FAC cannot be premixed beforehand as the MeOx/H_2O_2 experiment since FAC was found to slowly degrade FFA. Note that after locking the membranes onto the filter cartridges, the actual treatment contact diameter was 10 mm with area calculated as 78.54 mm^2. When operating at overall flow rates of 0.167 and 0.0167 mL/min, the fluxes were 127 and 12.7 L/m^2-h, respectively. These covered the operating fluxes of membrane filtration in water treatment, which are typically around 10 to 100 L/m^2-h (Ersahin et al., 2012; Yang et al., 2019). Catalase and thiosulfate were used to quench residual H_2O_2 and FAC, respectively, prior to FFA analyses on the HPLC. Sufficient quenching reagents were pre-added in HPLC vials, and then the vials were placed under the filter cartridges for filtrate collection. Meanwhile, parallel reactions were conducted to collect filtrates for oxidant concentration and pH measurements without quenching oxidants.

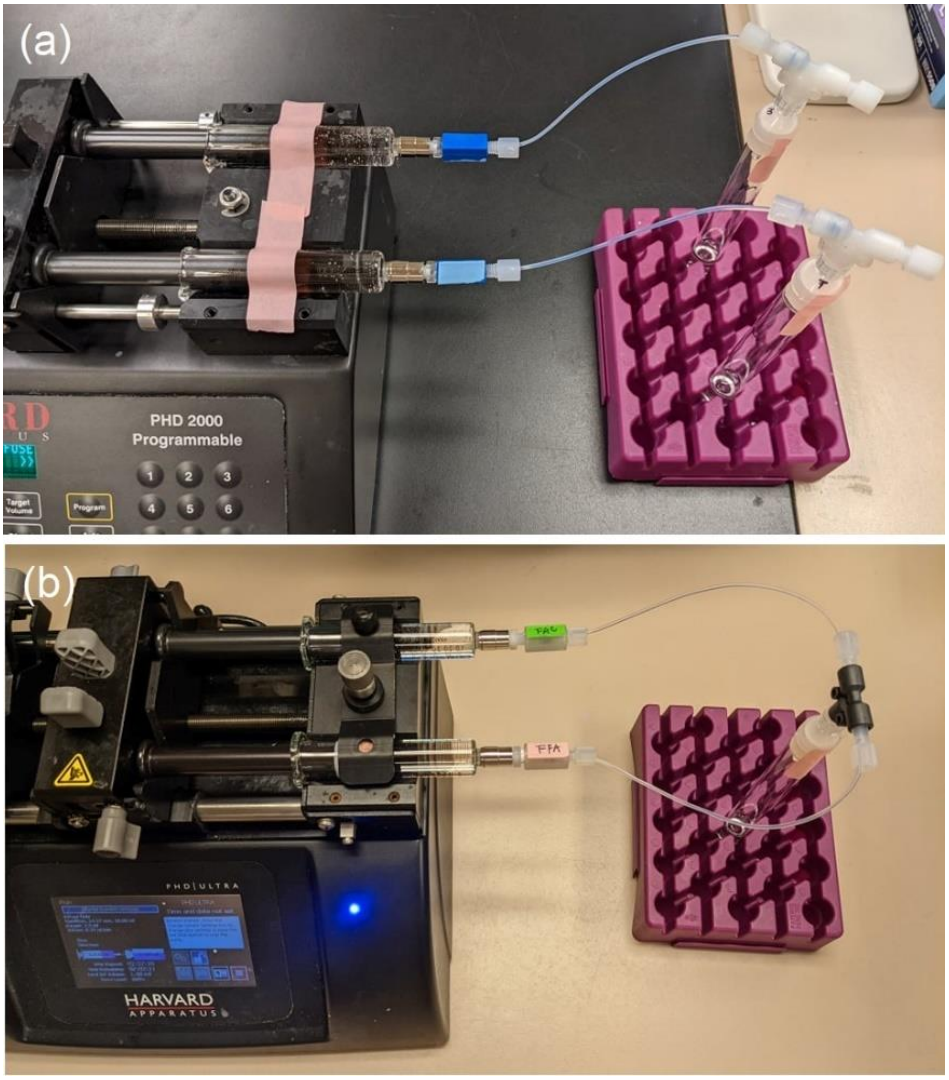

Figure 4.4. Precoat filtration experiment setup for (a) MeOx/H_2O_2 and (b) MeOx/FAC.

4.2.5 Analytical Methods

o-phenylenediamine (OPD) was applied as a non-selective reactive species/radical probe. It has been reported to react with $HO^{\bullet}$ to form an orange product 2,3-diaminophenazine (DAPN), which has absorbance band at around 440 nm (Fang et al., 2009; Sobańska et al., 2017). Formation of DAPN was semi-quantified by measuring the changes of absorbance at 440 nm by a UV-Vis spectrophotometer before and after treatment (Sobańska et al., 2017). Experiments were conducted by adding solutions containing 1mM OPD into MeOx solids, followed by dosing H_2O_2 to initiate the reactions. OPD measurements were only undertaken for MeOx/H_2O_2 systems as OPD was found directly react with FAC (Ma et al., 2017).

Furfuryl alcohol (FFA) was used as a $^1O_2$ probe. Experiments were conducted by adding solutions containing 5μM FFA into MeOx solids, followed by dosing H_2O_2 or FAC to initiate the reactions. Residual FFA was measured by a high performance liquid chromatography (HPLC) equipped with a diode-array UV/Vis detector and a Supelco Ascentis C18 column (150 × 2.1 mm, 3 μm). The mobile phases were composed of 80% 50mM phosphoric acid and 20% acetonitrile at a flow rate of 0.2mL/min. Prior to HPLC analyses, H_2O_2 and FAC were quenched by catalase enzyme and sodium thiosulfate, respectively.

Methanol (MeOH), isopropanol (iPrOH) and *tert*-butanol (*t*BuOH) were used as radical/reactive species scavengers, which yield formaldehyde (in cases of MeOH and *t*-BuOH) and acetone (in case of iPrOH) upon reaction with $HO^{\bullet}$ and certain other oxidants, such as $^1O_2$, $Cl^{\bullet}$, $ClO^{\bullet}$, and $Cl_2^{\bullet-}$ (Ross et al., 1998) (see details in Table S4.1). MeOH and *t*-BuOH reacting with $HO^{\bullet}$ can generate formaldehyde as the primary product with yield of ≥ 93% and 25-30%, respectively (Asmus et al., 1973; Flyunt et al., 2003; Wang et al., 1996). Reactions of iPrOH

with $HO^{\bullet}$ can form acetone as a primary intermediate with maximal yield of 78% (Kawaguchi, 1993; Wu et al., 2008). Acetone formation was measured by the DNPH-derivatization method (Soman et al., 2008). In brief, the DNPH reagent was prepared by dissolving 143mg 70% DNPH solid (contains 30% water) in 100mL acetonitrile (~7200 μM DNPH). To a HPLC vial, 0.5 mL of sample (or acetone standard solutions), 10 μL of 5N phosphoric acid, and 100 μL of 2,4-DNPH solution were added in order. The mixture was fully mixed and reacted for at least 30 min and then 0.5 mL of acetonitrile was added for dilution. The acetone-DNPH derivative was detected at 360 nm by a HPLC using the same column and UV/Vis detector described above. The mobile phases were composed of 40% water and 60% acetonitrile at a flow rate of 0.2 mL/min.

$O_2^{\bullet-}$ generation in the MeOx/H_2O_2 systems were measured using tetranitromethane (TNM) as the indicator. TNM can react with $O_2^{\bullet-}$ at a rate constant of 2×10^9 $M^{-1}s^{-1}$ to form nitroform, which has an extinction coefficient of 15,000 $M^{-1}cm^{-1}$ at 350 nm (Henglein et al., 1959; Rao and Hayon, 1975). The experiments were undertaken by either (i) dosing solutions containing 1mM TNM and H_2O_2 (1, 10 or 100 mM) into MeOx solids for reactions with rapid mixing at 500 rpm (hereafter referred to as *pre-add dosing*), or (ii) dosing H_2O_2 solutions into MeOx solids first, followed by 1mM TNM addition at designed reaction time (hereafter referred to as *post-add dosing*). The samples were then filtered through 0.2 μm PES membrane for nitroform measurement on a spectrophotometer (UV-2700, Shimadzu, Japan). TNM measurements were only undertaken for MeOx/H_2O_2 systems as nitroform was found directly react with FAC.

Another way to identify presence of $O_2^{\bullet-}$ was by using nitro blue tetrazolium (NBT) as a indicator. Bielski et al. (1980) reported the reaction rate constant for NBT with $O_2^{\bullet-}$ to be $5.88x10^4$ $M^{-1}s^{-1}$. The purple blue product, monoformazan, has maximum absorbance at 530 nm with extinction coefficients 25,400 $M^{-1}cm^{-1}$ at pH 9.5-11.0, and 12,800 $M^{-1}cm^{-1}$ at pH 5.7-6.7 (Bielski et al., 1980). 2 mM of NBT was (i) pre-amended with H_2O_2 and then dosed into MeOx for reaction (*pre-add dosing*), or (ii) dosed into the MeO_2+H_2O_2 mixture at specific reaction time of 15 min or 120 min (*post-add dosing*) to investigate $O_2^{\bullet-}$ retained on the MeOx surfaces after aqueous H_2O_2 has been partially or completely consumed. Samples were separated into two parts with one for vacuum filtration (to observe MeOx solid color change), and the other for syringe filtration (to detect aqueous phase monformazan formation). The filtrates were later buffered to pH6.0 by a phosphate buffer so as to quantify aqueous monformazan using the determinate ε = 12,800 $M^{-1}cm^{-1}$.

Ortho-phosphate was measured by the ascorbic acid approach as described in the Standard Method 4500-P E (APHA/AWWA/WEF, 2005). Ammonium molybdate and antimony potassium tartrate can react in acid medium with orthophosphate to form a heteropoly acid—phosphomolybdic acid—that is reduced to intensely colored molybdenum blue by ascorbic acid. After mixing the combined reagent with samples, measurements were taken after at least 10 min but no more than 30 min at 880 nm using a UV/vis spectrophotometer (UV2700, Shimadzu, Japan). The solution should turn into blue in the presence of orthophosphate. To achieve lower detection limit, it is recommended to use a infrared cuvette with longer path length. The LOD was found to be around 0.5 μM when using a cuvette with 4-cm path length.

The measurements of formaldehyde, H_2O_2 and FAC were as described previously in Section 2.2.4. In brief, formaldehyde was detected by the Hantzsch reagent. Concentrations of

H_2O_2 and FAC were determined by the Allen reagent and the DPD colorimetric method, respectively, using a UV/vis spectrophotometer (UV2700, Shimadzu, Japan).

4.3 Results and Discussion

4.3.1 Identification of Reactive Oxygen Species Formation

(i) OPD measurement

Figure 4.5 shows DAPN formation via OPD reactions with reactive species/radicals during the MeOx/H_2O_2 treatment. OPD analyses were not performed for the MeOx/FAC systems as OPD was reported to react with FAC (Ma et al., 2017). Control tests conducted in the absence of MeOx or H_2O_2 indicate no DAPN formation. Some experiments exhibited decreases of absorbance at later reaction stages, which may be due to further decomposition of DAPN reacting with ROS generated in the suspensions. Sobańska et al. reported that crystalline ZrO_2 shows less activity during the reactions with H_2O_2, accounting for only 30% of that obtained for a-ZrO_2 when treated 1.3 mg/mL zirconia with 300mM H_2O_2 (reaction pH not indicated in the article) (Sobańska et al., 2017). In contrast, our results exhibited that m-ZrO_2 was more reactive than a-ZrO_2 during treatment of 1-100mM H_2O_2 with 0.1g/mL of zirconia at pH between 5-7 (Figure 4.5). However, Sobańska et al. also suggested a-ZrO_2 could achieve highest reactivity in generating reactive radical species at pH 3.0-3.5. Figure 4.6 shows OPD experiments for the two zirconia with reaction pH adjusted to 3 by sulfuric acid. a-ZrO_2 activity was found greatly enhanced and became more reactive than m-ZrO_2 under pH 3 in terms of DAPN formation, which is consistent with Sobańska's observation. This implied reaction pH can play important roles in reactive/radical species production during MeOx/H_2O_2 reactions. It also needs to be clarified that Sobańska et al. considered OPD as a $HO^{\bullet}$ indicator; however, it is non-selective and

can actually react with other ROS such as $^1O_2$ (Ross et al., 1998). It may be possible that the color changes due to DAPN formation observed by the authors were attributed to other reactive species in addition to $HO^{\bullet}$ (Sobańska et al., 2017).

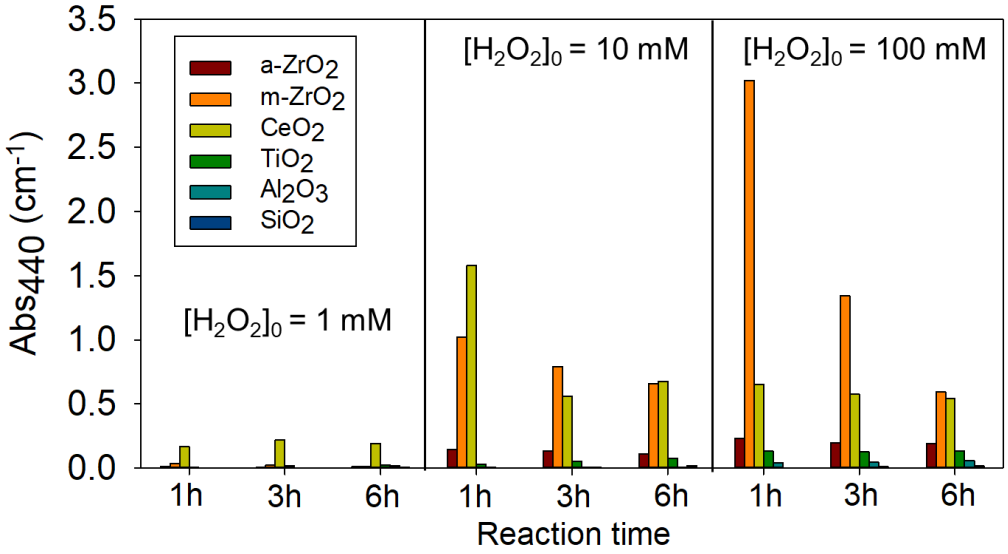

Figure 4.5. DAPN formation during MeOx/H_2O_2 treatment. Experiments were conducted by dosing solutions containing $[OPD]_0$ = 1 mM and $[H_2O_2]_0$ = 1, 10, or 100 mM into MeOx solids to a MeOx/liquid concentration of 0.1 g/mL. The reaction pHs (between pH 5-7) were not adjusted throughout the reactions.

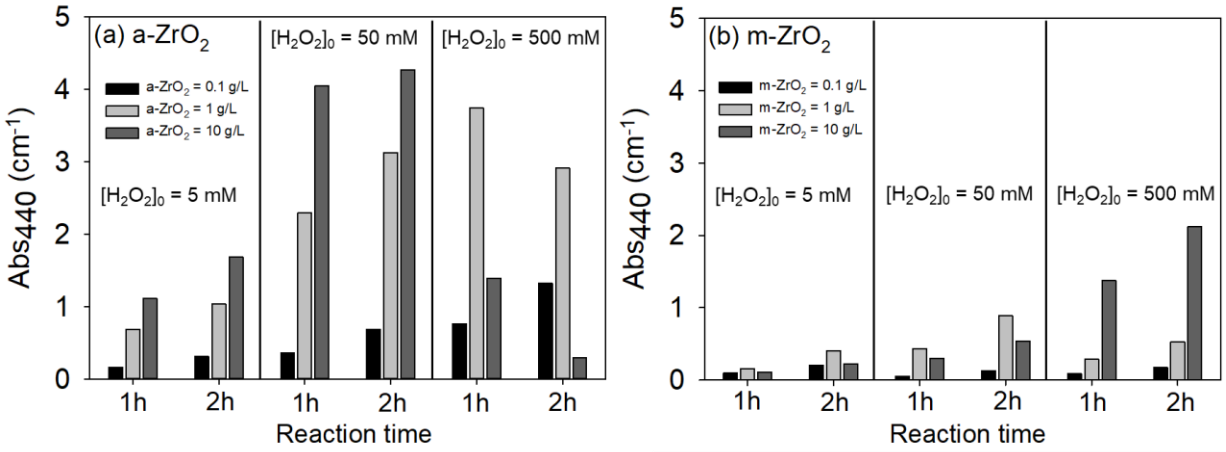

Figure 4.6. DAPN formation during treatment of (a) a-ZrO_2/H_2O_2 and (b) m-ZrO_2/H_2O_2. Experiments were conducted by dosing solutions containing $[OPD]_0$ = 1 mM and $[H_2O_2]_0$ = 5, 50, or 500 mM into MeOx solids to a MeOx/liquid concentration of 0.1, 1,or 10 g/L. The reaction pHs were adjusted to pH 3 by sulfuric acid.

(ii) Formation of $^1O_2$

$^1O_2$ has a unique reactivity which makes it highly useful for a wide range of chemical and industrial applications and plays significant roles in many biological processes (Dąbrowski, 2017; Ogilby, 2010; Pibiri et al., 2018). There have been a number of studies suggesting $^1O_2$ utilization in water treatment, including removal of phenolic compounds and antibiotics, and for microbial disinfection (Al-Nu'airat et al., 2019; Gerdes et al., 1997; Nowakowska and Kępczyński, 1998; Rule Wigginton et al., 2010; Tian et al., 2017; Villén et al., 2006).

$^1O_2$ formation was detected by mixing MeOx (0.1 g/mL) with solutions containing H_2O_2 (10 or 100 mM) or FAC (0.1 or 1 mM) in the presence of FFA as a $^1O_2$ probe. Note that chloride ion (Cl^-) usually present in commercial NaOCl stock at equal molar, which was confirmed in this study by measuring Cl^- concentration in the chlorine stock. Ion chromatography analyses show that the stock contained [FAC]:[Cl^-] ratio of 1:1.03. Corresponding chlorine speciation, including Cl_2, HOCl, OCl^- and Cl_2O, as well as their molarities at varying pH were plotted in Figure S4.1. HOCl can self-react to form Cl_2O, and Cl_2 can be generated through reaction of Cl^- with HOCl (eqs 4.1 to 4.3), with Cl_2O often presenting at a negligible level. It was observed FFA can directly react with Cl_2 derived from the NaOCl stock solution (Figure 4.7). Figure S4.2 shows the apparent first-order reaction rate constant for FFA reaction with Cl_2, with measured apparent reaction rate constants fitted by a three parameters exponential model using the SigmaPlot software. Residual FFA associated to direct reaction with Cl_2 can then be calculated based on the model fitting equation (expressed as ▼ symbols in Figure 4.8, 4.9 and S4.3). Importantly note that these Cl_2-mediated residual FFA concentrations were estimated assuming constant [FAC] = 0.1 or 1 mM throughout the entire period of reactions. However, during MeOx/FAC reactions, FAC keep being decomposed by MeOx over time. Actual time-dependent

"residual" FFA attributed to Cl_2 oxidation alone should be higher than those estimated values (▼) displayed in the figures. Other oxidants, including H_2O_2, HOCl and OCl^- were found not react with FFA (Figure 4.7).

$$HOCl \leftrightarrow H^+ + OCl^- \qquad pK_a = 7.5 \text{ (Morris, 1966)} \qquad (4.1)$$

$$HOCl + OCl^- + H^+ \leftrightarrow Cl_2 + H_2O \qquad \log K = 3.36 \text{ (Sivey et al., 2010)} \qquad (4.2)$$

$$2HOCl \leftrightarrow Cl_2O + H_2O \qquad \log K = -2.06 \text{ (Sivey et al., 2010)} \qquad (4.3)$$

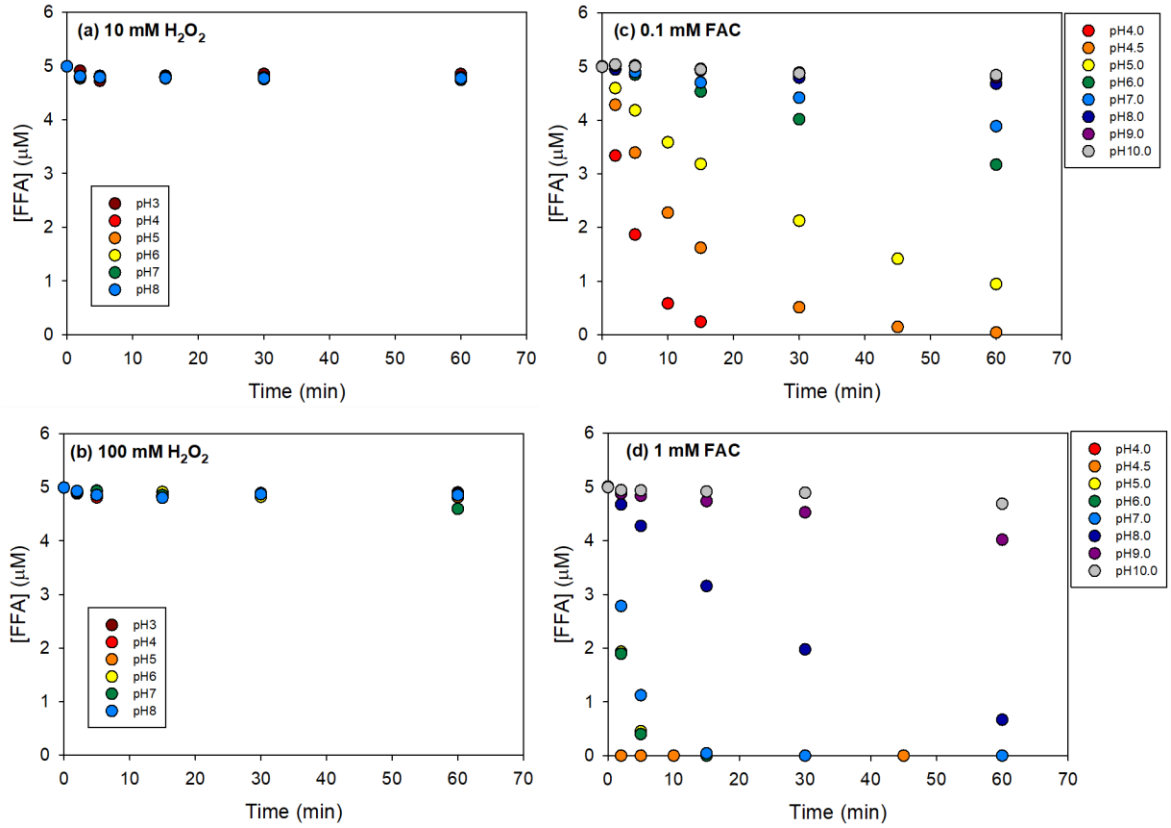

Figure 4.7. Direct reaction of FFA with H_2O_2 and FAC (i.e., Cl_2/HOCl/OCl^-) at varying pH; (a) 10 mM H_2O_2, (b) 100 mM H_2O_2, (c) 0.1 mM FAC, and (d) 1 mM FAC.

FFA degradation was found to be enhanced as increasing MeOx mass loading and oxidant concentration (data not shown). Figure 4.8, 4.9 and S4.3 demonstrate FFA degradation, oxidant decomposition and pH monitoring during MeOx/oxidant treatment with higher oxidant dosage ($[H_2O_2]_0$ = 100 mM and $[FAC]_0$ = 1mM; see Figure 4.8 and S4.3) and lower oxidant dosage ($[H_2O_2]_0$ = 10 mM and $[FAC]_0$ = 0.1mM; see Figure 4.9). Results of H_2O_2 reactions with TiO_2, Al_2O_3 and SiO_2, and FAC reaction with a-ZrO_2 were not shown as these conditions did not yield significant FFA degradation, though it was noteworthy that a-ZrO_2 was found decomposing H_2O_2 and FAC very rapidly (FAC results not shown). For instance, a-ZrO_2 removed 100mM H_2O_2 and 1mM FAC within 10 min (Figure 4.8). CeO_2 was the secondly most effective mineral in decomposing H_2O_2 and FAC while causing more significant FFA degradation than a-ZrO_2. Interestingly, TiO_2 however not reactive in the H_2O_2 system, can yield noticeable FFA degradation while only consuming a little FAC. This implies that the reactions involved in the two oxidant systems with TiO_2 (likely also other MeOx) were following different mechanisms. Al_2O_3 and SiO_2 were less effective compared to the other minerals.

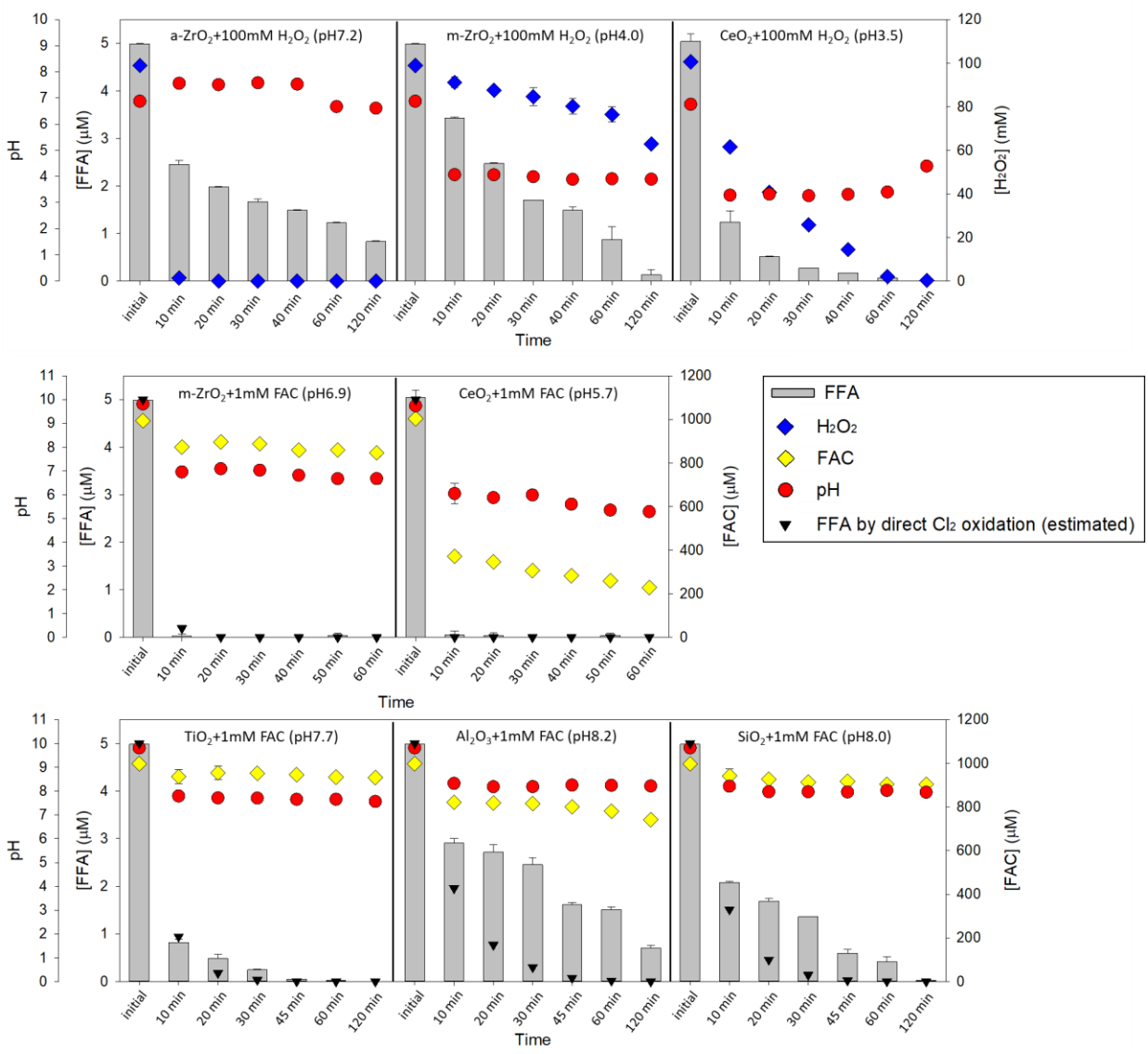

Figure 4.8. FFA degradation, oxidant decomposition and pH monitoring with MeOx/oxidant treatment at higher dose of oxidants. Experiments were conducted by dosing solutions containing $[FFA]_0$ = 1 μM and $[H_2O_2]_0$ = 100 mM or $[FAC]_0$ = 1 mM into MeOx solids to a MeOx/liquid concentration of 0.1 g/mL. The reaction pHs were not adjusted throughout the reactions. pH values displayed at time zero are pH readings of the pure water prior to MeOx addition (MeOx-free). Error bars represent one standard deviation about the mean of duplicate measurements.

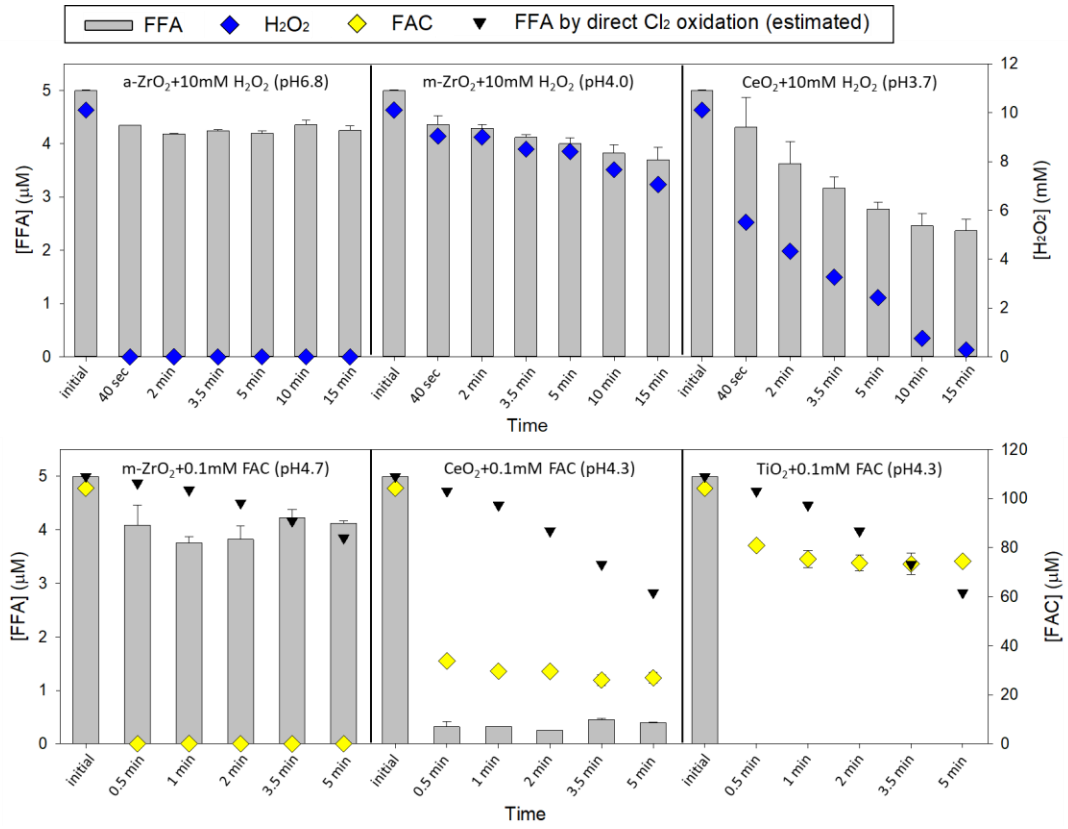

Figure 4.9. FFA degradation and oxidant decomposition with MeOx/oxidant treatment at lower dose of oxidants. Experiments were conducted by dosing solutions containing $[FFA]_0$ = 1 μM and $[H_2O_2]_0$ = 10 mM or $[FAC]_0$ = 0.1 mM into MeOx solids to a MeOx/liquid concentration of 0.1 g/mL. The reaction pHs were not adjusted throughout the reactions. Error bars represent one standard deviation about the mean of duplicate measurements.

(iii) Formation of HO•

Formation of HO• was monitored using alcohols (MeOH, iPrOH and *t*-BuOH) as radical scavengers. MeOH and *t*-BuOH reacting with HO• can generate formaldehyde as the primary product with yield of ≥93% and 25-30%, respectively (Asmus et al., 1973; Flyunt et al., 2003; Wang et al., 1996). Reactions of iPrOH with HO• can form acetone as a primary intermediate with maximal yield of 78% (Kawaguchi, 1993; Wu et al., 2008).

Formation of formaldehyde (Figure 4.10) and acetone (Figure 4.11) were measured in the presence of excess MeOH and iPrOH as radical scavengers at 100mM. Note that only conditions in which formaldehyde and acetone were significantly generated were exhibited in the following figures. Formaldehyde (≥100 μM) and acetone (≥30 μM) were observed over 6 hours of reaction in systems of m-ZrO_2+H_2O_2, m-ZrO_2+FAC, CeO_2+FAC and TiO_2+FAC containing MeOH and iPrOH, respectively. Control experiments show formaldehyde and acetone were not detected in the absence of H_2O_2, FAC, or MeOx. However, lower levels of formaldehyde formation (≤ 5 μM) were observed when using *t*-BuOH as a scavenger, indicating that other weaker reactive species may be responsible for formaldehyde and acetone formation in the presence of MeOH and iPrOH because they are less selective to $HO^{\bullet}$ (i.e., MeOH and iPrOH can also react with other ROS or RCS to generate formaldehyde and acetone; *t*-BuOH is more selective to $HO^{\bullet}$). Some other reactive species being produced in addition to $^1O_2$ and $HO^{\bullet}$ could be $O_2^{\bullet-}$, and/or $Cl^{\bullet}$, $ClO^{\bullet}$ and $Cl_2^{\bullet-}$ in the presence of FAC. Table S4.1 listed the reaction mechanisms of these alcohol scavengers with each ROS and RCS, as well as reactions leading to formaldehyde and acetone formation. More discussions regarding *t*-BuOH as $HO^{\bullet}$ scavenger are provided in Section 4.3.1(v). One interesting observation worth notice here is that formaldehyde formation rate in the TiO_2+FAC system increased significantly over time, which was in the opposite trend compared to the other reaction systems. It could be due to TiO_2 surface structure modification by FAC or some currently unknown mechanisms that facilitate reactive species generation at the later stage of reaction.

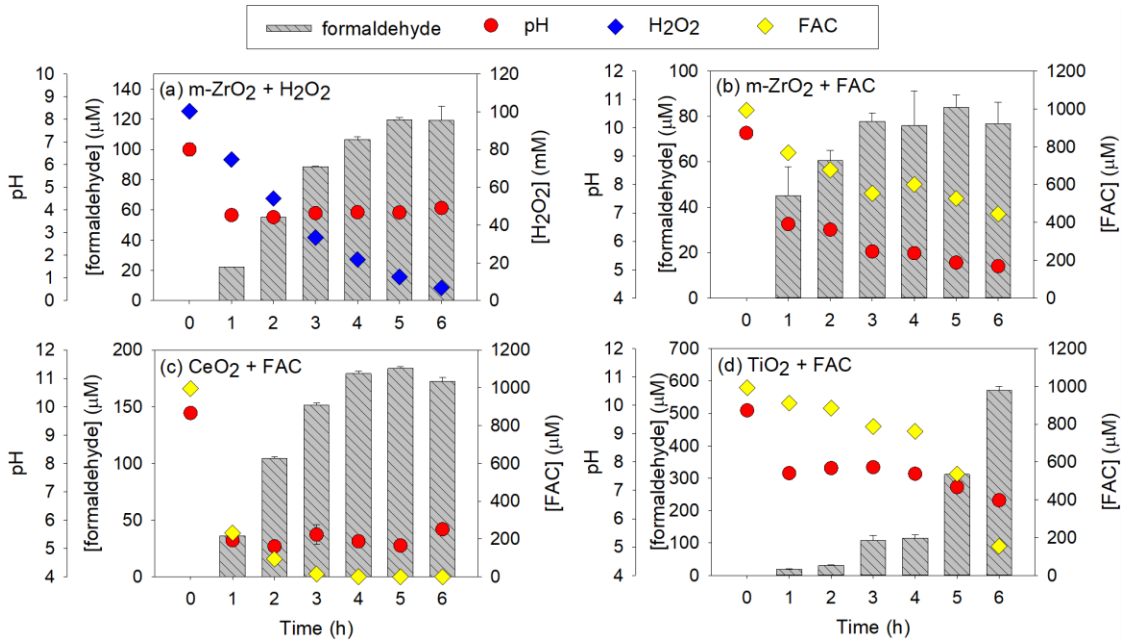

Figure 4.10. Formaldehyde formation, oxidant decomposition and pH monitoring with MeOx/oxidant treatment. Experiments were conducted by dosing solutions containing $[MeOH]_0$ = 100 mM and $[H_2O_2]_0$ = 100 mM or $[FAC]_0$ = 1 mM into MeOx solids to a MeOx/liquid concentration of 0.1 g/mL. The reaction pHs were not adjusted throughout the reactions. pH values displayed at time zero are pH readings of the pure water prior to MeOx addition (MeOx-free). Error bars represent one standard deviation about the mean of duplicate measurements.

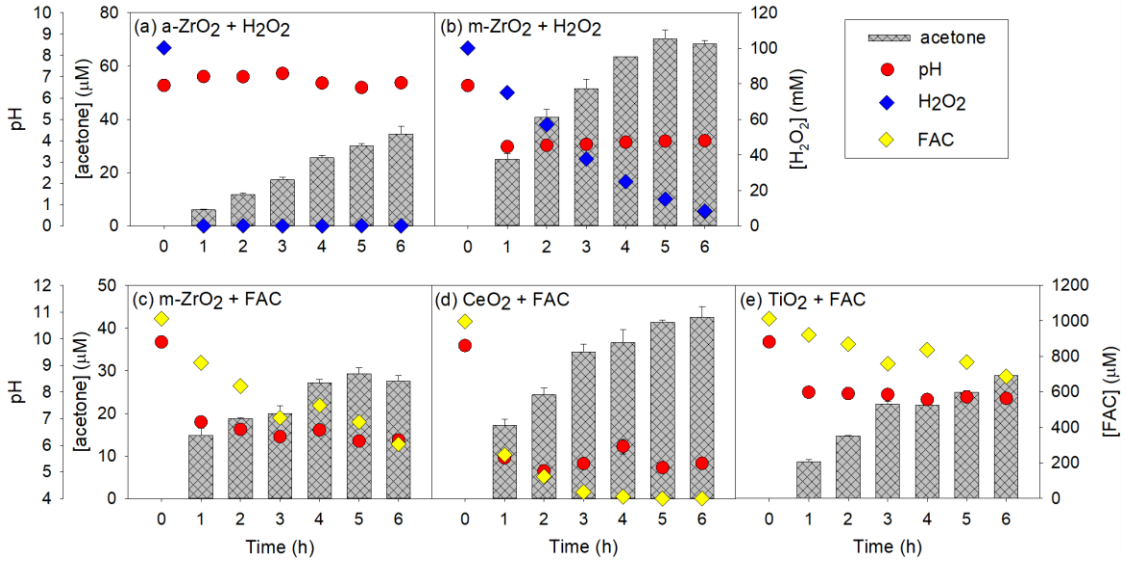

Figure 4.11. Acetone formation, oxidant decomposition and pH monitoring with MeOx/oxidant treatment. Experiments were conducted by dosing solutions containing $[iPrOH]_0$ = 100 mM and $[H_2O_2]_0$ = 100 mM or $[FAC]_0$ = 1 mM into MeOx solids to a MeOx/liquid concentration of 0.1 g/mL. The reaction pHs were not adjusted throughout the reactions. pH values displayed at time zero are pH readings of the pure water prior to MeOx addition (MeOx-free). Error bars represent one standard deviation about the mean of duplicate measurements.

(iv) Formation of $O_2^{\bullet-}$

TNM measurements for $O_2^{\bullet-}$ were conducted for reaction conditions a-ZrO_2+H_2O_2, m-ZrO_2+H_2O_2 and CeO_2+H_2O_2. MeOx/FAC systems were not tested here since FAC was found to react with nitroform, and currently we are not able to find a selective $O_2^{\bullet-}$ indicator as an alternative. Among the three MeOx, significant formation of nitroform was observed in the m-ZrO_2+H_2O_2 system at pH ~4 without additional pH adjustment (Figure 4.12a). Note that y-axes here were expressed as Δ[350 nm] instead of [nitroform] as nitroform can only be semi-quantified due to the fact that TNM reacts slowly with $HO_2^{\bullet}$ radicals under acidic conditions. Minor nitroform formation was observed in a-ZrO2+H_2O_2 and CeO_2+H_2O_2 systems (Figure 4.12a), while its formation in a-ZrO2+H_2O_2 was enhanced when reacting at pH3 (Figure 4.12b) as compared to neutral pH. This was consistent with Sobańska's observation that a-ZrO_2 exhibited higher tendency in generating reactive/radical species at acidic condition (Sobańska et al., 2017). Formation of nitroform increase with higher dose of H_2O_2 (Figure 4.12b).

Figure 4.13 compared the TNM analyses for *pre-add dosing* and *post-add dosing* of H_2O_2 to the a-ZrO2+H_2O_2 system, with the later case that TNM was added after aqueous H_2O_2 has been completely decomposed (15 min after reacting with 100mM H_2O_2). The results show that nitroform can still be generated after aqueous H_2O_2 was consumed, implying accumulation of $HO_2^{\bullet}/O_2^{\bullet-}$ on a-ZrO_2 surfaces. To investigate the stability of surface-adsorbed $HO_2^{\bullet}/O_2^{\bullet-}$ on a-ZrO_2, a series of *post-add dosing* experiments were conducted with TNM dosed at 15, 30, 60 and 120 min, respectively (Figure 4.14). The results show that surface-adsorbed $HO_2^{\bullet}/O_2^{\bullet-}$ were moderately stable with 50% loss after 2 hours.

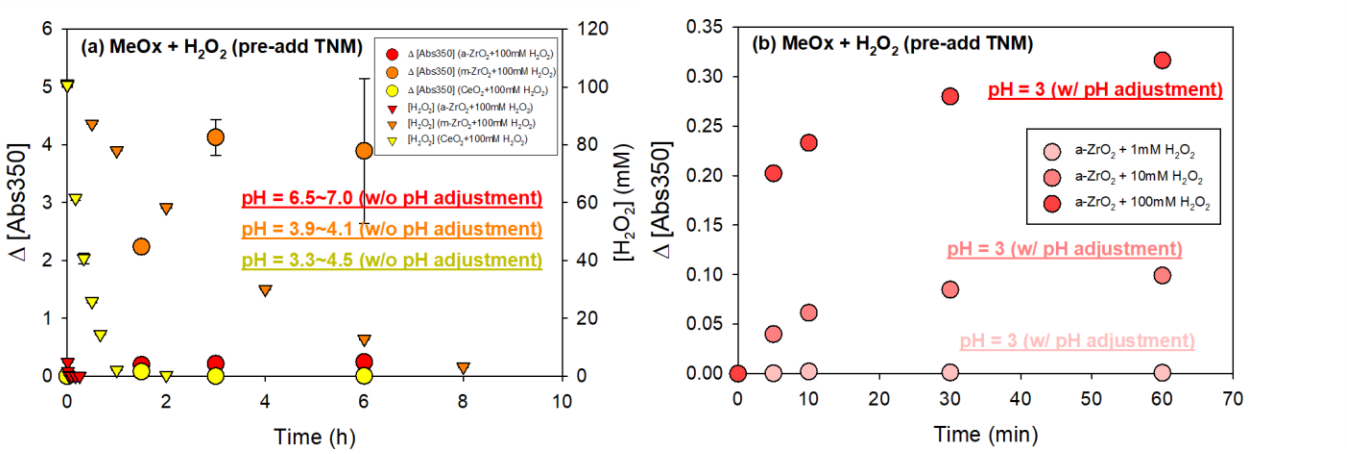

Figure 4.12. Aqueous $O_2^{\bullet-}$ analyses and H_2O_2 measurement of the MeOx+H_2O_2 system using TNM; (a) a-ZrO_2, m-ZrO_2 and CeO_2 without pH adjustment by treatment of 100mM H_2O_2; (b) a-ZrO_2 with pH adjustment to 3.0 by treatment with 1, 10, and 100mM H_2O_2. Experiments were conducted by dosing solutions containing $[TNM]_0$ = 1 mM and $[H_2O_2]_0$ = 100 mM into MeOx solids to a MeOx/liquid concentration of 0.1 g/mL (*pre-add dosing*).

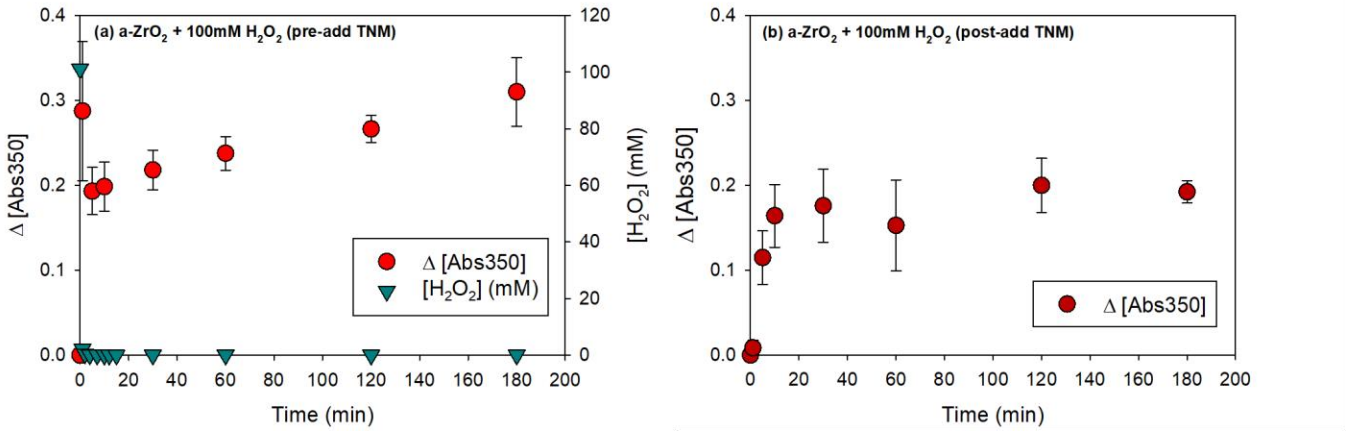

Figure 4.13. Aqueous $O_2^{\bullet-}$ analyses and H_2O_2 measurement of the a-ZrO_2+H_2O_2 system using TNM; (a) a-ZrO_2 with pH adjustment to 3.0 by treatment of 100mM H_2O_2. Experiments were conducted by dosing solutions containing $[TNM]_0$ = 1 mM and $[H_2O_2]_0$ = 100 mM into MeOx solids to a MeOx/liquid concentration of 0.1 g/mL (*pre-add dosing*); (b) a-ZrO_2 with pH adjustment to 3.0 by treatment with 100mM H_2O_2. Experiments were conducted by dosing $[TNM]_0$ = 1 mM into aqueous H_2O_2-free suspension after 15 min reaction with initial dose of $[H_2O_2]_0$ = 100 mM and MeOx solids of 0.1 g/mL (*post-add dosing*), followed by nitroform monitoring for up to 180 min.

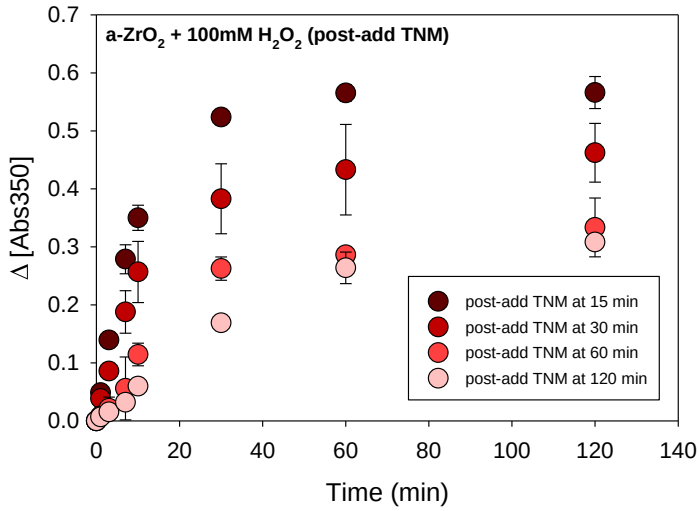

Figure 4.14. Aqueous $O_2^{\bullet-}$ analyses and H_2O_2 measurement of the a-ZrO_2+H_2O_2 system using TNM with pH adjustment to 3.0 by treatment of 100mM H_2O_2. Experiments were conducted by dosing $[TNM]_0$ = 1 mM into aqueous H_2O_2-free suspension after 15, 30, 60 or 120 min reaction with initial dose of $[H_2O_2]_0$ = 100 mM and MeOx solids of 0.1 g/mL (*post-add dosing*), followed by nitroform monitoring for up to 120 min. Note that different batches of a-ZrO_2 were used for experiments in Figure 4.13 and 4.14, so their activities in generating $O_2^{\bullet-}$ can be a bit different. Error bars represent one standard deviation about the mean of duplicate measurements.

When using NBT as a $O_2^{\bullet-}$ indicator, aqueous formazan was not observed in a-ZrO_2+H_2O_2 system at pH3, while solid phase-associated (sorbed) formazan was observed in a-ZrO_2+H_2O_2 system at pH3 with mineral surface turning into purple (Figure 4.15). In the m-ZrO_2+H_2O_2 system, formazan was not observed both in the aqueous phase and the solid phase on m-ZrO_2 surface. In a-ZrO_2+H_2O_2 system, TNM and NBT results imply that there could be both aqueous- and solid-phase superoxide formation at acidic to neutral condition. However, TNM and NBT cannot capture all superoxide ($HO_2^{\bullet}/O_2^{\bullet-}$) (i.e., not quantitatively) due to (i) of superoxide speciation and (ii) low scavenging reaction rate of NBT toward $O_2^{\bullet-}$ ($k = 6\text{x}10^4$ $M^{-1}s^{-1}$) compared to TNM with $O_2^{\bullet-}$ ($k = 2\text{x}10^9$ $M^{-1}s^{-1}$) (Bielski et al., 1980; Bielski and Schwarz, 1968). Note that superoxide has pK_a at 4.8, so $HO_2^{\bullet}$ was more dominant than $O_2^{\bullet-}$ at acidic condition. $HO_2^{\bullet}$ reacts very slowly with TNM with $k < 2\text{x}10^4$ $M^{-1}s^{-1}$, and does not react with NBT (Bielski et al., 1980; Bielski and Schwarz, 1968; Greenwald, 2018; Rabani et al., 1965;

Watts and Teel, 2019). Summarizing these observations, it was suggested that superoxide in the m-ZrO_2+H_2O_2 system may primarily be in aqueous phase as no color changes were seen on m-ZrO_2 surface with NBT present. The much smaller reaction rate constant of NBT with superoxide versus TNM can explain why aqueous formazan was not observed in a-ZrO_2+H_2O_2 and m-ZrO_2+H_2O_2 when using NBT, while nitroform formation was detected when using TNM. These observations generally agree with the reaction mechanisms proposed by Sobańska et al. who indicated (i) formation of surfaced-bounded $O_2^{\bullet-}$ during a-ZrO_2+H_2O_2 reaction, confirmed by electron paramagnetic resonance spectroscopy (EPR); (ii) crystalline m-ZrO_2 has weaker activity in ROS production on mineral surface than a-ZrO_2; and (iii) absence of $O_2^{\bullet-}$ in the liquid phase during a-ZrO_2+H_2O_2 reaction, confirmed by NBT analyses (Sobańska et al., 2017). Control experiments for the a-ZrO_2 only, m-ZrO_2 only, CeO_2 only and H_2O_2 only conditions between pH 3~7 did not show any clear evidences indicating $O_2^{\bullet-}$ generation by using both TNM and NBT as $O_2^{\bullet-}$ indicators.

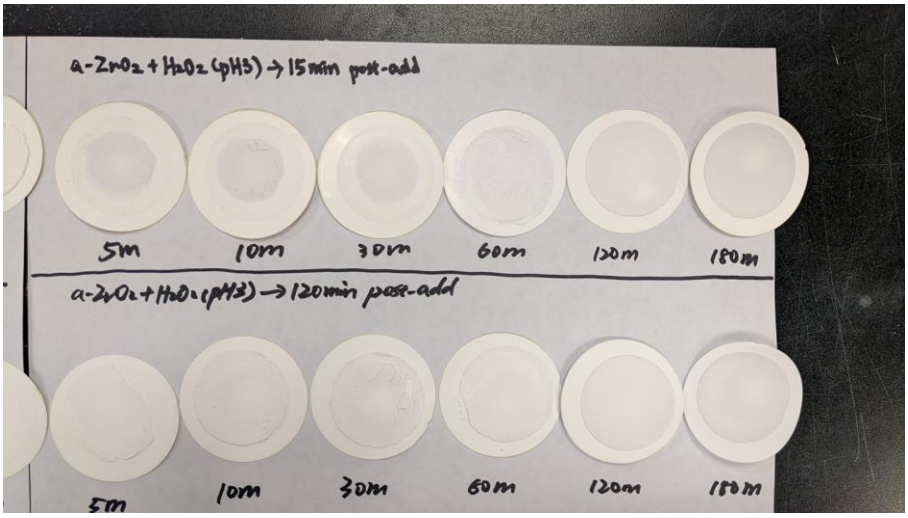

Figure 4.15. Formazan formation due to surface-adsorbed $O_2^{\bullet-}$ on a-ZrO_2 surface with pH adjustment to 3.0 by treatment of 100mM H_2O_2. Experiments were conducted by dosing $[NBT]_0$ = 2 mM into MeOx/H_2O_2 suspension after 15 or 120 min reaction with initial dose of $[H_2O_2]_0$ = 100 mM and MeOx solids of 0.1 g/mL (*post-add dosing*), followed by color change observation for up to 180 min. MeOx suspensions were filtrated out by 0.2μm PES membrane for color observation.

(v) Other qualification approaches

Due to the intrinsic lifetime of $^1O_2$, its probability of deactivation before reaction with the probe is strongly dependent on the solvent (Schmidt and Afshari, 1992; Wilkinson et al., 1995). In addition to H_2O, in which FFA reacts with $^1O_2$ at a rate constant of 1.2×10^8 $M^{-1}s^{-1}$ (Scully Jr and Hoigné, 1987), FFA degradation was also tested in D_2O which was suggested significantly increase the lifetime of $^1O_2$ and hence its chance of reacting with FFA. The reported half-life of $^1O_2$ was around 4 μS in H_2O (Jensen et al., 2010; Schmidt and Afshari, 1992; Wilkinson et al., 1995), whereas longer lifetimes were found in D_2O, ranging from 40 to 69 μS with stabilities increased by 10- to 17-fold (Aubry et al., 1995; Jensen et al., 2010; Lee and Rodgers, 1987; Matheson and Massoudi, 1980; Schmidt and Afshari, 1992; Wilkinson et al., 1995). Figure 4.16 and 4.17 summarize FFA degradation in pure H_2O and D_2O during a-ZrO_2, m-ZrO_2 and CeO_2 reactions with H_2O_2 (Figure 4.16) and m-ZrO_2, CeO_2, TiO_2, Al_2O_3 and SiO_2 reactions with FAC (Figure 4.17). Distinct kinetics can be observed during MeOx/H_2O_2 reactions, indicating formation of $^1O_2$. In contrast, no clear evidence of $^1O_2$ formation was found during MeOx/FAC reactions.

Similar sets of experiment were conducted in 100mM *t*-BuOH and natural water sample (containing DOC = 2.32 mgC/L) collected locally from the Lake Washington, Seattle. Detailed water quality measurements can be found in Table S4.2. In general, presence of *t*-BuOH appeared to have little to slight inhibition on FFA degradation, implying that $HO^{\bullet}$ generation was minor. This observation was consistent with previous discussion in Section 4.3.1(iii) that only minor formaldehyde formed when using *t*-BuOH as a selective $HO^{\bullet}$ scavenger. Experiments conducted in natural waters suggested little to slight inhibition (e.g., CeO_2+H_2O_2) on FFA degradation in the case of H_2O_2, and little to moderate enhancement on FFA degradation in the

case of FAC (e.g., CeO_2+FAC and TiO_2+FAC). The former could be resulted from scavenging of reactive species by NOM, and the later could be due to side reaction with NOM (as precursor) with chlorine, forming additional reactive species that enhance FFA decomposition. The results also suggested that effective treatment could still be achieved in typical natural waters during MeOx/H_2O_2 and MeOx/FAC processes.

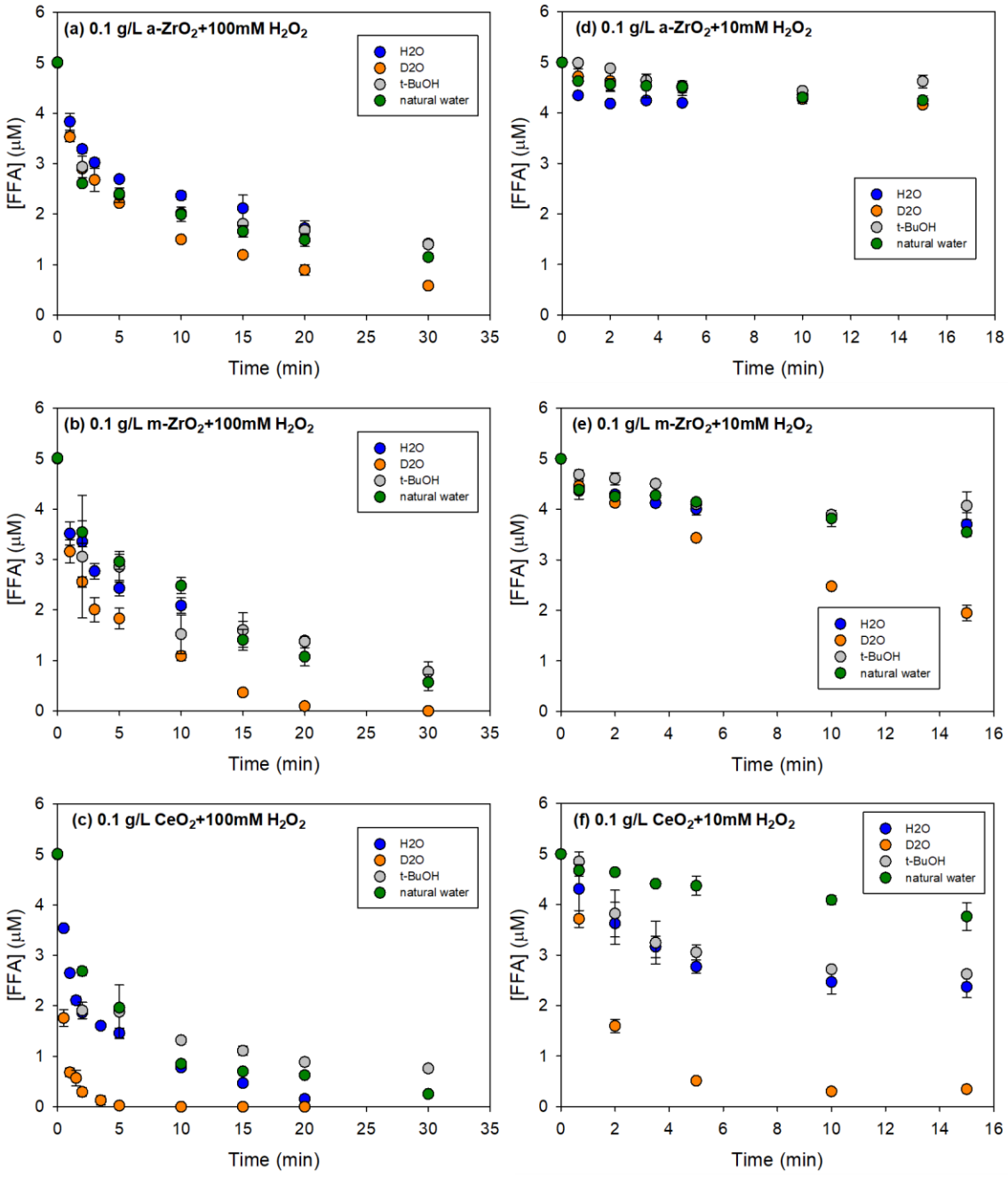

Figure 4.16. FFA degradation by MeOx/H_2O_2 in different matrix, including pure H_2O, pure D_2O, 100mM t-BuOH and natural water (Lake Washington, Seattle, WA) by treatment with (a) a-ZrO_2+100mM H_2O_2, (b) m-ZrO_2+100mM H_2O_2, (c) CeO_2+100mM H_2O_2, and (d) a-ZrO_2+10mM H_2O_2, (e) m-ZrO_2+10mM H_2O_2, (f) CeO_2+10mM H_2O_2. Error bars represent one standard deviation about the mean of duplicate measurements.

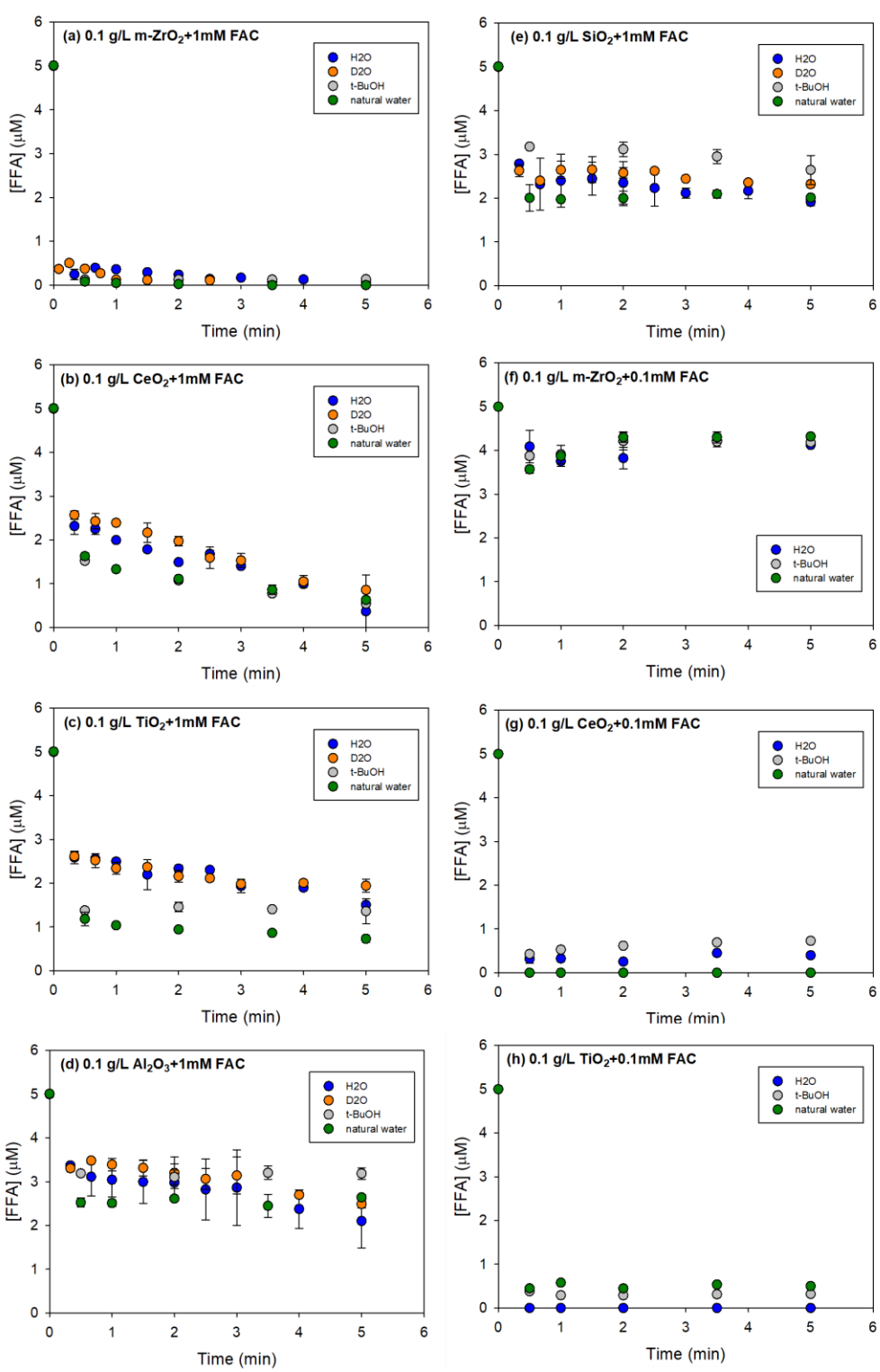

Figure 4.17. FFA degradation by MeOx/FAC in different matrix, including pure H_2O, pure D_2O, 100mM t-BuOH and natural water (Lake Washington, Seattle, WA) by treatment with (a) m-ZrO_2+1mM FAC, (b) CeO_2+1mM FAC, (c) TiO_2+1mM FAC, (d) Al_2O_3+1mM FAC, (e) SiO_2+1mM FAC, (f) m-ZrO_2+0.1mM FAC, (g) CeO_2+0.1mM FAC, (h) TiO_2+0.1mM FAC. Error bars represent one standard deviation about the mean of duplicate measurements.

Table 4.2 summarize the ability of each MeOx in decomposing H_2O_2 or FAC, and in the generation of ROS and RCS in the MeOx/H_2O_2 or MeOx/FAC reaction systems according to experimental observations discussed in Section 4.3.1.

Table 4.2. Reactivity summary of MeOx/H_2O_2 and MeOx/FAC reactions in oxidant decomposition and generation of ROS and RCS

MeOx	a-ZrO_2	m-ZrO_2	CeO_2	TiO_2	Al_2O_3	SiO_2
MeOx/H_2O_2						
H_2O_2 decomposition	very fast	moderate	fast	slow	slow	slow
$^1O_2$	moderate	significant	significant	minor	minor	minor
HO$^\bullet$	minor	minor	minor	minor	N/A	N/A
$HO_2^\bullet/O_2^{\bullet-}$	significant	significant	minor	N/A	N/A	N/A
MeOx/FAC						
FAC decomposition	very fast	moderate	fast	slow	slow	slow
$^1O_2$	minor	minor	minor	minor	minor	minor
HO$^\bullet$	minor	minor	minor	minor	minor	minor
$HO_2^\bullet/O_2^{\bullet-}$	N/A	N/A	N/A	N/A	N/A	N/A
RCS	moderate	moderate	significant	significant	moderate	moderate

N/A: Data not available due to (a) conditions not tested due to insignificant reactions, or (b) selective probes not available

4.3.2 H_2O_2 and Phosphate Adsorption on MeOx

Anions like phosphate and borate were found to have strong adsorption on MeOx minerals, a-ZrO_2 in particular due to its high specific surface area (Table 4.1). Adsorption of $[phosphate]_0$ = 10 mM on 0.005 g/mL of a-ZrO_2, m-ZrO_2 and CeO_2 at pH7 was investigated with results shown in Figure 4.18a. Corresponding adsorption experiments under the same reaction condition but with surface area normalized are displayed in Figure 4.18b. Results demonstrate

that a-ZrO_2 can strongly adsorb phosphate by ~50% at equilibrium in light of its high surface area (292 m^2/g) as compared to m-ZrO_2 (7.58 m^2/g) and CeO_2 (13.5 m^2/g). Around the same phosphate adsorption could be achieved when total surface area were normalized. Phosphate adsorption capacity of a-ZrO_2 at equilibrium was found consistent with the value reported in literature (Su et al., 2013).

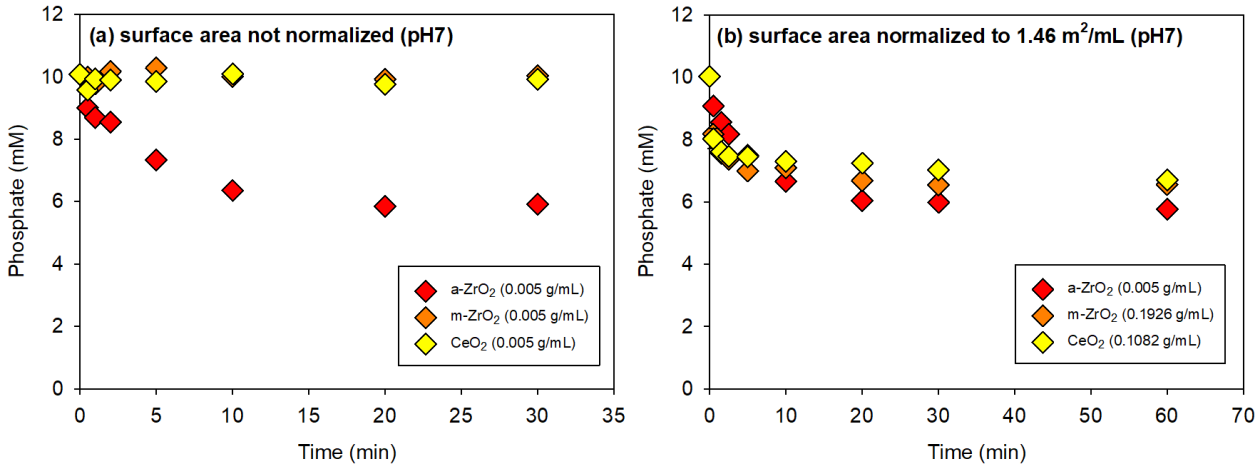

Figure 4.18. Phosphate adsorption on a-ZrO_2, m-ZrO_2 and CeO_2 at pH7 with (a) surface area not normalized, and (b) surface area normalized to 1.46 m^2/mL.

Figure 4.19 shows 10mM H_2O_2 removal from aqueous phase in the presence of 0.05, 0.005 and 0.001 g/mL a-ZrO_2 when (i) without phosphate dosing, and (ii) with pre-amended 50mM or 250mM phosphate. Phosphate was found to inhibit H_2O_2 removal by competing the surface adsorption sites. Considering the competitive adsorption of phosphate on MeOx, it can potentially used as desorbing agent for replacing surface-bounded H_2O_2. At this point, it was unclear whether the rapid removal of H_2O_2 from aqueous phase (especially a-ZrO2; see Figure 4.8 and 4.9) was resulted from adsorption or H_2O_2 chemical decomposition. Mass loadings of 0.05, 0.005 and 0.001 g/mL a-ZrO_2 were reacted with 10mM H_2O_2 at pH3 or pH7, followed by

addition of 50mM, pH7 phosphate at (i) the end of complete aqueous-H_2O_2 removal, or at (ii) when partial removal has achieved (Figure 4.20). Both scenarios show minor H_2O_2 desorption from a-ZrO_2 surfaces, which implied that rapid H_2O_2 adsorption on a-ZrO_2 should followed by instant H_2O_2 decomposition; as a result, minor sorbed-H_2O_2 were exchanged by phosphate.

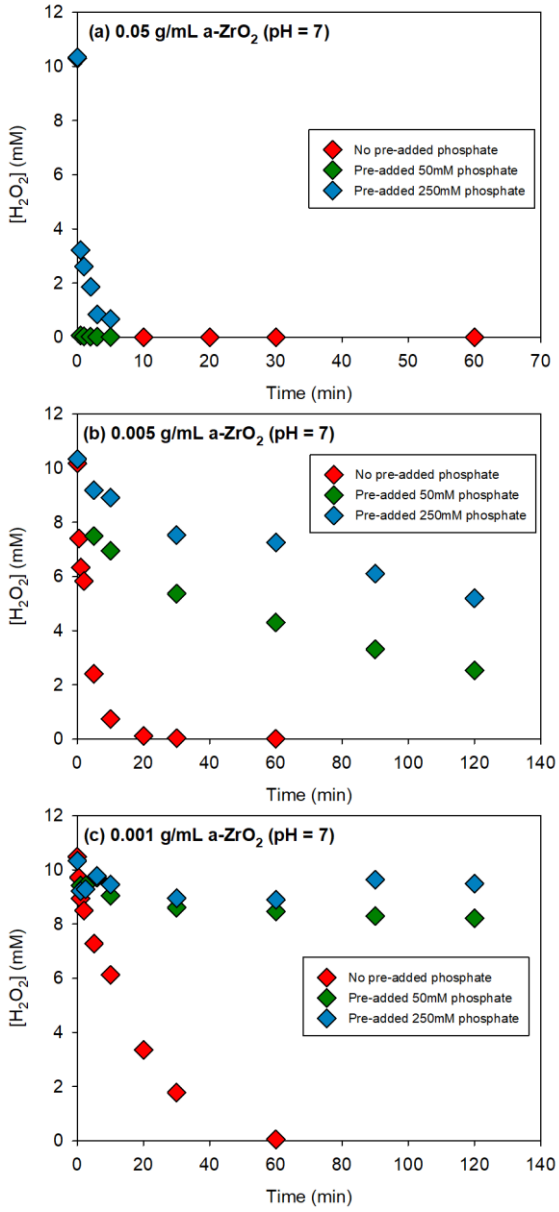

Figure 4.19. H_2O_2 decomposition by a-ZrO_2 at pH7 with mass loading of (a) 0.05, (b) 0.005, (c) 0.001 g/mL and $[H_2O_2]_0$ = 10 mM without phosphate, or in the presence of pre-amended 50mM or 250 mM phosphate.

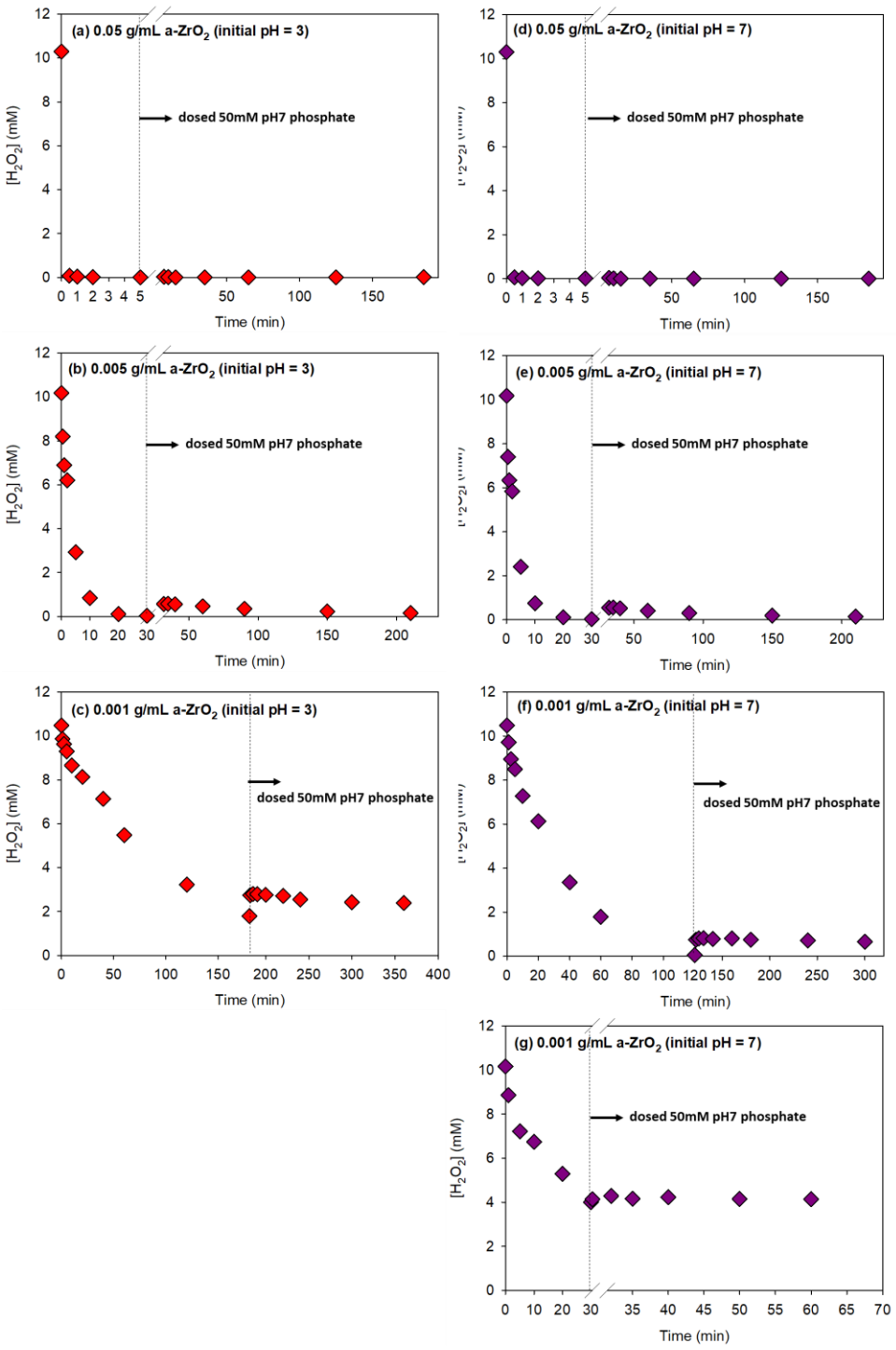

Figure 4.20. H_2O_2 desorption by a-ZrO_2 with mass loading of (a) 0.05, (b) 0.005, and (c) 0.001 g/mL and $[H_2O_2]_0$ = 10 mM at reaction pH=3, extracted by pH7, 50mM phosphate buffer. Corresponding experiments were conducted with mass loading of (d) 0.05, (e) 0.005, and (f)(g) 0.001 g/mL and $[H_2O_2]_0$ = 10 mM at reaction pH=7, extracted by pH7, 50mM phosphate buffer. The last two experiments were identical but with phosphate dosed at (f) the end of reaction, and (g) the midway of reaction.

4.3.3 Multiple-dose MeOx/Oxidant Treatment

Dosing of solutions containing FAC and FFA or MeOH were repeatedly performed to examine the capacities of MeOx in continuously generating reactive species and decomposing oxidants. Figure 4.21 demonstrate results for FFA degradation treated at higher oxidant dosage of [H_2O_2] = 100 mM or [FAC] = 1 mM, and Figure 4.22 exhibit data at lower oxidant dosage of [H_2O_2] = 10 mM or [FAC] = 0.1 mM (more realistic oxidant concentrations in terms of water treatment). Multiple treatments of H_2O_2 with TiO_2, Al_2O_3 and SiO_2 were not discussed here as they did not yield noticeable H_2O_2 decomposition, FFA degradation and formaldehyde formation. On the contrary, a-ZrO_2, m-ZrO_2 and CeO_2 can effectively decompose H_2O_2 and degrade FFA. Activities for MeOx in FAC decomposition and FFA decomposition remained constant or only slightly decreased after each dosing treatment except for CeO_2+FAC, which activity significant decreased after repeated treatment. In general, activities of the majority of MeOx were sustained in repeated use, as re-dosing of H_2O_2 or FAC yielded comparable effectiveness (some with minor decrease in performance) on FFA degradation over at least five treatment cycles. As for formaldehyde formation (Figure 4.23), m-ZrO_2+H_2O_2, CeO_2+FAC and TiO_2+FAC activities decreased significantly after multiple dosing, while the other tested conditions remains similar performance, including a-ZrO_2+H_2O_2, CeO_2+H_2O_2, a-ZrO_2+FAC, m-ZrO_2+FAC, Al_2O_3+FAC, and SiO_2+FAC.

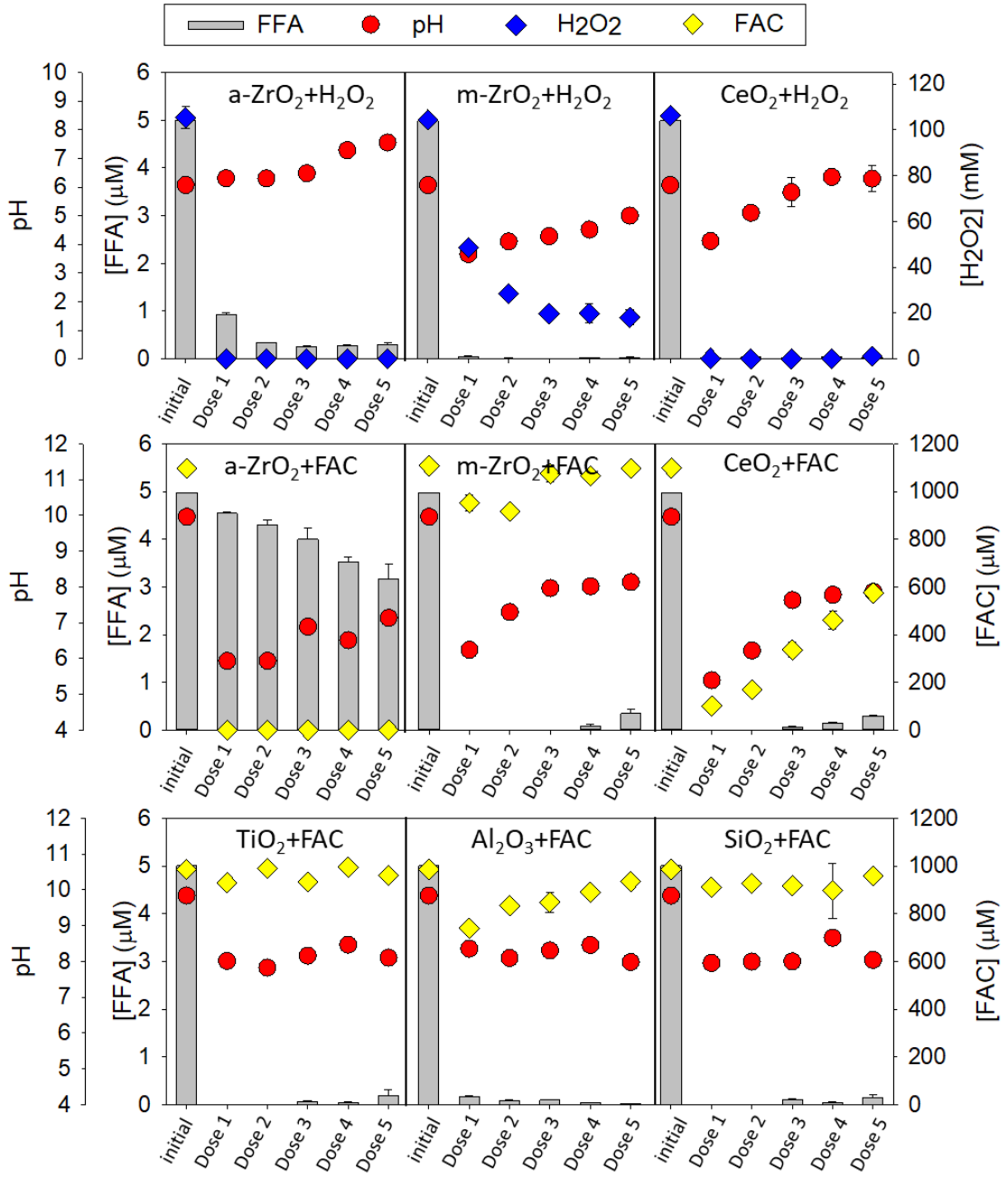

Figure 4.21. Multiple-dosing of MeOx/oxidant treatment with FFA as the probe at higher oxidant dose. Experiments were conducted by repeatedly dosing solutions containing $[FFA]_0$ = 1 μM and $[H_2O_2]_0$ = 100 mM or $[FAC]_0$ = 1 mM into MeOx solids to a MeOx/liquid concentration of 0.1 g/mL. Each dose allowed 2 hours of reaction. The reaction pHs were not adjusted throughout the reactions. pH values displayed at "initial" are pH readings of the pure water prior to MeOx addition (MeOx-free). Error bars represent one standard deviation about the mean of duplicate measurements.

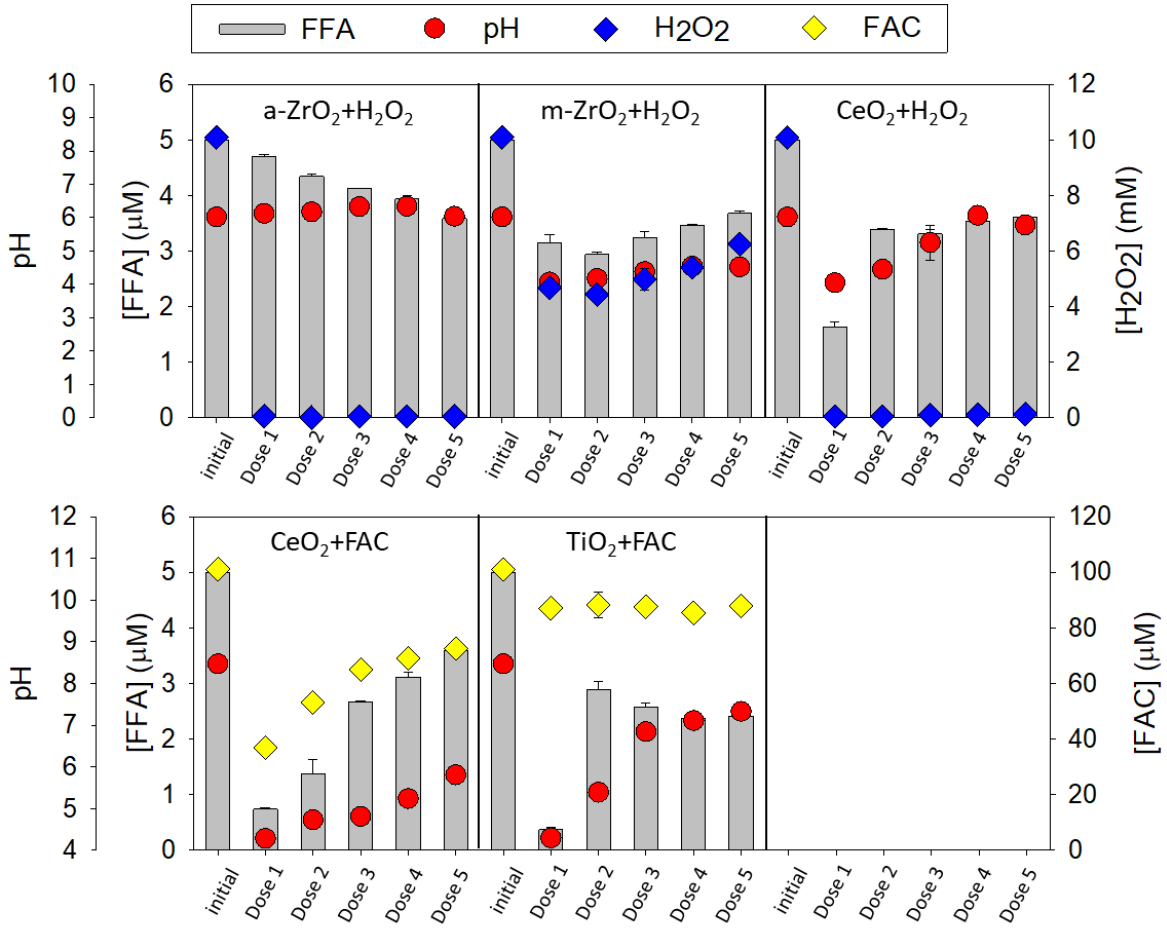

Figure 4.22. Multiple-dosing of MeOx/oxidant treatment with FFA as the probe at lower oxidant dose. Experiments were conducted by repeatedly dosing solutions containing $[FFA]_0$ = 1 μM and $[H_2O_2]_0$ = 10 mM or $[FAC]_0$ = 1 mM into MeOx solids to a MeOx/liquid concentration of 0.1 g/mL. Each dose allowed 30 min reaction in the case of MeOx/H_2O_2, and 5 min reaction in the case of MeOx/FAC. The reaction pHs were not adjusted throughout the reactions. pH values displayed at "initial" are pH readings of the pure water prior to MeOx addition (MeOx-free). Error bars represent one standard deviation about the mean of duplicate measurements.

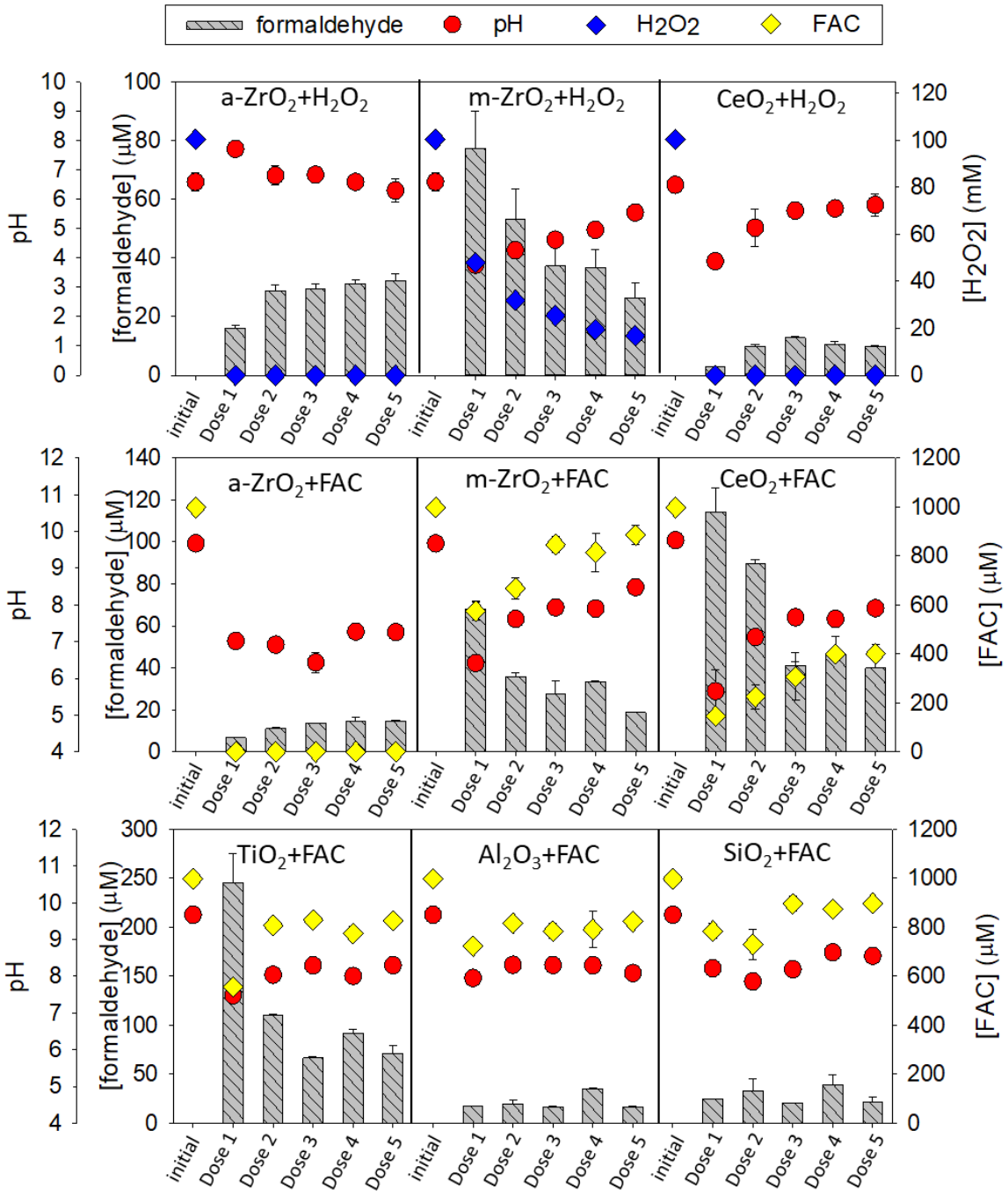

Figure 4.23. Multiple-dosing of MeOx/oxidant treatment with MeOH as radical scavenger. Experiments were conducted by repeatedly dosing solutions containing $[MeOH]_0$ = 100 mM and $[H_2O_2]_0$ = 100 mM or $[FAC]_0$ = 1 mM into MeOx solids to a MeOx/liquid concentration of 0.1 g/mL. Each dose allowed 2 hours of reaction. The reaction pHs were not adjusted throughout the reactions. pH values displayed at "initial" are pH readings of the pure water prior to MeOx addition (MeOx-free). Error bars represent one standard deviation about the mean of duplicate measurements.

4.3.4 H_2O_2 and FAC Decomposition

As discussion and figures demonstrated in previous sections, a-ZrO_2 and CeO_2 appear to be the most efficient MeOx on decomposing both H_2O_2 and FAC, followed by m-ZrO_2, TiO_2, Al_2O_3 and SiO_2. This observation agrees well with Hiroki and LaVerne (2005) where they found H_2O_2 decomposition rates follow the order of ZrO_2 > CeO_2 > TiO_2 > Al_2O_3 > SiO_2 (Hiroki and LaVerne, 2005). Amorphous zirconia a-ZrO_2, despite relatively less active in reactive species production than m-ZrO_2 and CeO_2, could be a good alternative for residual or excess oxidant removal in water treatment without causing too much undesirable radical reactions that may potentially increase DBP formation. a-ZrO_2 can maintain high oxidant decomposition reactivity after up to five treatment cycles in the multiple-dosing experiments (Figure 4.21-4.23), probably due to its high specific surface area (292 m^2/g) than the other MeOx (see Table 4.1).

4.3.5 Reaction Mechanisms

(i) Hydration and hydroxylation of MeOx surfaces

Lousada et al. proposed the steps of H_2O_2 decomposition on transition metal oxide surfaces via: (1) adsorption of H_2O molecules on MeOx surfaces (hydration and hydroxylation), (2) reaction with H_2O_2 via initial adsorption of H_2O_2 with desorption of H_2O, (3) formation of products of the decomposition of H_2O_2 and their adsorption to the surfaces. Therefore, hydration/hydroxylation of MeOx favors H_2O_2 adsorption and its subsequent decomposition (Lousada et al., 2012). MeOx surfaces usually expose oxide (O^{2-}) ions, which are strong bases and cannot exist unchanged in aqueous solution. The first step in surface hydration involves the formation of surface hydroxyl groups (dissociative adsorption) followed by molecular adsorption. The entire surface of O^{2-} ions of MeOx exposed to water molecules may undergo

this neutralizing reaction to form OH groups, which accompanies release of protons to solution (Fierro, 2006). This can explain the decreases of pH when suspending MeOx in aqueous solutions as observed in Figure 4.24, in particular for m-ZrO_2, CeO_2 and TiO_2. Thetford et al. suggested that TiO_2 hydroxylated surface can interchange between hydroxyl form (Me—OH) and water form (Me—H_2O) on a short time scale. The calculated adsorption energy for water molecule referenced to the partially hydroxylated surface left by its removal is −44 kJ mol^{-1}. The calculated adsorption energy for H_2O_2 is −68 kJ mol^{-1}, so that it is energetically favorable for hydrogen peroxide to displace water when the surface is hydroxylated (Thetford et al., 2011). Literature reported hydroxyl site density of metal oxides generally follows the order of ZrO_2 ~ CeO_2 > TiO_2 ~ Al_2O_3 > SiO_2 (Chen et al., 2012; Kijenski et al., 1977; McCafferty and Wightman, 1998; Ogata et al., 2010; Tamura et al., 2001). This is consistent with the order of H_2O_2 decomposition rate observed in this study and in literature (Hiroki and LaVerne, 2005).

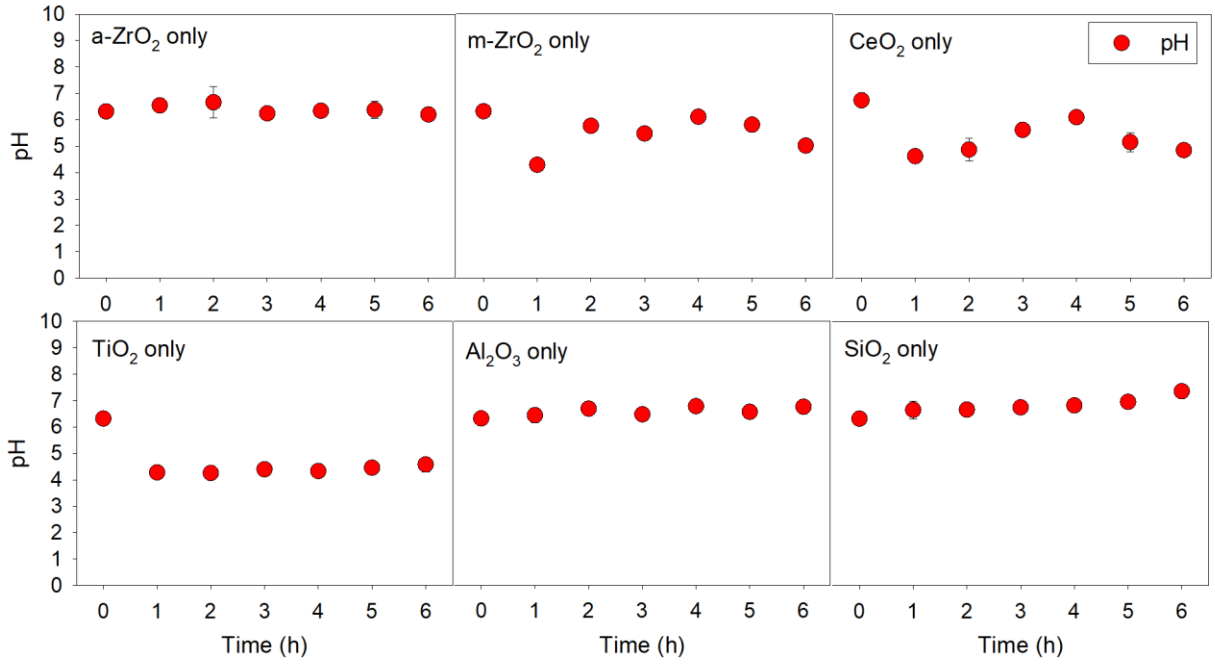

Figure 4.24. pH monitoring of suspending 0.1g/mL MeOx in pure water. pH values displayed at time zero were pH readings of the pure water prior to MeOx addition (MeOx-free).

(ii) Point of zero charge of MeOx

At pH values above PZC, the hydrated surface becomes negatively charged, while for pH values below the PZC, the hydrated surface becomes positively charged (eq 4.4). If the pH > PZC, then the terminating hydroxyl groups at the surface deprotonate as the expression below. When the net surface charge is negative, the surface can attract cationic species. Conversely, if the pH < PZC, the hydroxyl groups protonate and the surface can attract anionic species.

$$Me—OH_2^+ \text{ (pH<PZC)} \leftrightarrow Me—OH \text{ (pH= PZC)} \leftrightarrow Me—O^- \text{ (pH> PZC) (Parks and Bruyn, 1962)} \quad (4.4)$$

Table 4.3 summarizes the estimated MeOx surface charges under experimental conditions with different typical dose of H_2O_2 and FAC on account of their PZC values. Experiments with MeOx reacting with H_2O_2 demonstrate that pH had no effect on MeOx reactivities within the pH range tested in this study, probably because H_2O_2 is typically in its neutral form (pK_a = 11.6 (Black and Hayon, 1970)). In cases of MeOx/FAC, slight slow down of FAC decomposition was observed when reacting at higher pH, likely due to charge repulsion of the negative mineral surfaces and OCl^- (pK_a = 7.5 (Morris, 1966)).

Table 4.3. MeOx surface charge based on PZC for different dose of H_2O_2 and FAC

MeOx	Manufacturer	Point of zero charge (PZC)[a]	Typical reaction pH (surface charge)[b]			
			10 mM H_2O_2 (charge)	100 mM H_2O_2 (charge)	0.1 mM FAC (charge)	1 mM FAC (charge)
a-ZrO_2	self-synthesized	5.8 (Blesa et al., 1985)	7.5 (−)	7.0 (−)	6.5 (−)	6.5 (−)
m-ZrO_2	Sigma-Aldrich	6.1 (Megias-Alguacil et al., 2000)	4.5 (+)	4.0 (+)	5.8 (0)	6.0 (0)
CeO_2	Beantown Chemical	6~7.5 (Kosmulski, 2016)	4.0 (+)	3.5 (+)	4.7 (+)	5.8 (+)~(0)
TiO2	Sigma-Aldrich	4.8 (Morris et al., 1999)	4.0 (+)	3.8 (+)	5.0 (0)~(−)	7.7 (−)
Al_2O_3	Alfa Aesar	8.2~9.5 (Del Nero et al., 2010; Moreau et al., 2013)	7.5 (+)	7.5 (+)	7.5 (+)	8.2 (+)~(0)
SiO_2	Sigma-Aldrich	<3 if any (Janusz et al., 2003; Kosmulski, 2016)	6.7 (−)	6.7 (−)	6.5 (−)	8.0 (−)

[a] Values of PZC were obtained for the same product from the same manufacturer, except for CeO_2; PZC value of a-ZrO_2 was obtained from literature using similar synthetic method. [b] Estimated surface charges expressed as positive (+), neutral (0), or negative (−)

(iii) Proposed reaction mechanisms

Reported catalytic reactions ($MeOx/H_2O_2$ system):

$$H_2O_2 + MeOx \rightarrow 2OH^{\bullet} + MeOx \quad (4.5)$$

$$H_2O_2 + OH^{\bullet} \rightarrow H_2O + HO_2^{\bullet} \quad (4.6)$$

$$2HO_2^{\bullet} \rightarrow H_2O_2 + O_2 \quad (4.7)$$

$$2H_2O_2 \rightarrow 2H_2O + O_2 \text{ (net reaction) (Hiroki and LaVerne, 2005)} \quad (4.8)$$

$$\equiv Zr^{+}—HO_2^{-}{}_{(surf)} + H_2O_{2(aq)} \rightarrow OH^{\bullet}{}_{(aq)} + \equiv Zr^{+}—O_2^{\bullet-}{}_{(surf)} + H_2O \text{ (Sobańska et al., 2017)} \quad (4.9)$$

$$MeOx + 2H_2O_2 \rightarrow {}^1O_2 + 2H_2O + MeOx \quad \text{(Aubry, 1985; Aubry and Nardello, 1997)} \quad (4.10)$$

Proposed catalytic reactions (MeOx/FAC system):

$$HOCl + MeOx \rightarrow OH^{\bullet} + Cl^{\bullet} + MeOx \quad (4.11)$$

$$Cl^{\bullet} + H_2O \rightarrow\rightarrow OH^{\bullet} + Cl^{-} + H^{+} \quad (4.12)$$

$$HOCl + OH^{\bullet} \rightarrow OH^{-} + ClO^{\bullet} + H^{+} \quad (4.13)$$

$$2ClO^{\bullet} + H_2O \rightarrow\rightarrow ClO^{-} + ClO_2^{-} + 2H^{+} \quad (4.14)$$

$$2HOCl \rightarrow Cl^{-} + ClO_2^{-} + 2H^{+} \text{ (net reaction)} \quad (4.15)$$

$$HO^{\bullet} + HO^{\bullet} \rightarrow H_2O_2 \leftrightarrow HO_2^{-} + H^{+} \quad \text{(Elliot, 1989)} \quad (4.16)$$

$$HOCl + HO_2^{-} \rightarrow {}^1O_2 + H_2O + Cl^{-} \quad \text{(Held et al., 1978)} \quad (4.17)$$

Other possible reactions with H_2O_2 or FAC:

(a) Me-catalyzed reaction; There is no net redox reactions on Me (Candeias et al., 1994; Lister, 1956; Liu et al., 2012; Whiteman et al., 1997).

(b) Me reduced/H_2O_2 or FAC oxidized; FAC may potentially be oxidized to RCS (e.g. $Cl^{\bullet}$, $ClO^{\bullet}$ and $Cl_2^{\bullet-}$).

(c) Me oxidized/H_2O_2 or FAC reduced; Trace amount of Me in lower oxidation states may co-exist on MeO_2, which may be oxidized by H_2O_2 or FAC (Koch and Manzhos, 2017; Ma et al., 2015; Sinitsyn and Gracheva, 2020).

4.4 Application of Metal Oxide/Oxidant Treatment on Precoat Filtration

MeOx-precoat filtration could be a practical approach to apply the MeOx/oxidant reactions in water treatment. This work examined the treatment efficiency during the MeOx/oxidant processes using FFA as a representative of trace organic contaminant. It was expected that MeOx precoat membranes can yield ROS and RCS in the presence of H_2O_2 and FAC, leading to organic contaminant degradation while operating at typical fluxes for membrane filtration ranging from around 10 to 100 L/m^2-h (Ersahin et al., 2012; Yang et al., 2019). 0.1 g of MeOx solids were precoated on PES membrane and operated at total flow rates of 0.167 and 0.0167 mL/min, corresponding to fluxes of 12.7 and 127 L/m^2-h, respectively for a-ZrO_2+H_2O_2, m-ZrO_2+H_2O_2, CeO_2+H_2O_2 with $[H_2O_2]_0$ = 1 mM, and m-ZrO_2+FAC, CeO_2+FAC, TiO_2+FAC, with $[FAC]_0$ = 0.1 mM. Results in Figure 4.25 indicate higher treatment can be achieved under lower flux, while longer reaction time was be required. Decomposition of FFA in order was m-ZrO_2 > CeO_2 > a-ZrO_2 in the case of MeOx/H_2O_2, and TiO_2 > CeO_2 > m-ZrO_2 in the case of MeOx/FAC.

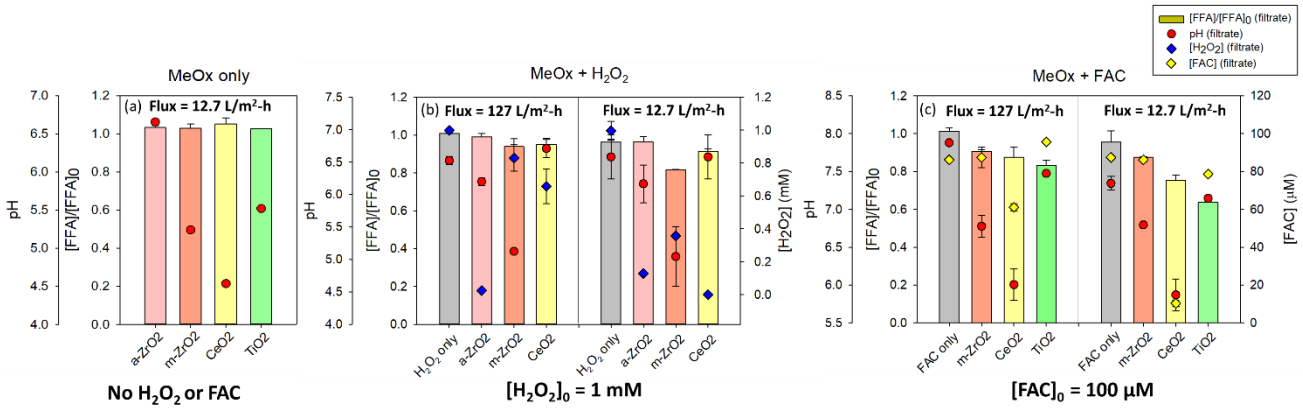

Figure 4.25. MeOx-precoat membrane filtration treatment of FFA. Experiments were operated by passing solutions containing [FFA] = 5 µM, [H_2O_2] = 1 mM, or [FAC] = 100 µM at total flux of 12.7 or 127 L/m^2-h for (a) MeOx-only controls, (b) MeOx/H_2O_2, and (c) MeOx/FAC. The reaction pHs were not adjusted throughout the reactions. Error bars represent one standard deviation about the mean of duplicate measurements.

4.5 Metal Release Tests

Micro-scaled MeOx generally are, though not necessarily, less toxic than their nano-scaled counterparts (Heinlaan et al., 2008; Jiang et al., 2009; Simon-Deckers et al., 2009). Although MeOx particles used for studies were labeled at µm scale, they may still contain some trace nanoparticles. Besides, oxidation of MeOx particles by H_2O_2 and FAC could also lead to dissolved form of metals, and some of which may reform back to nanoscale oxides afterwards. A series of ICP-MS analyses (PerkinElmer Nexion 2000B) were conducted to examine the release of free metals and nano-scale MeOx during reactions of MeO_2/H_2O_2 and MeOx/FAC (Figure 4.26). Note that ICP-MS samples were filtered through 0.2 µm PES membrane, contribution of free metal and nano-MeOx was not distinguished. The results show that a-ZrO_2, m-ZrO_2, CeO_2 and TiO_2 reacting with H_2O_2 (1 and 100 mM) or FAC (0.1 and 1mM) yielded free and/or nano-scale metals no more than ~10 µg/L, except TiO_2+1mM FAC reacting under long reaction time of 6 hours (~90 µg/L). It is worthy to note that by simply suspending CeO_2 in water, we observed high background Ce concentrations associated directly from the CeO_2. Interestingly,

upon reactions with H_2O_2 and FAC, free and/or nano Ce significantly decreased. This may be due to redox reactions that changed Ce speciation, leading to its aggregation or forming larger particles which were rejected by the 0.2 µm membrane.

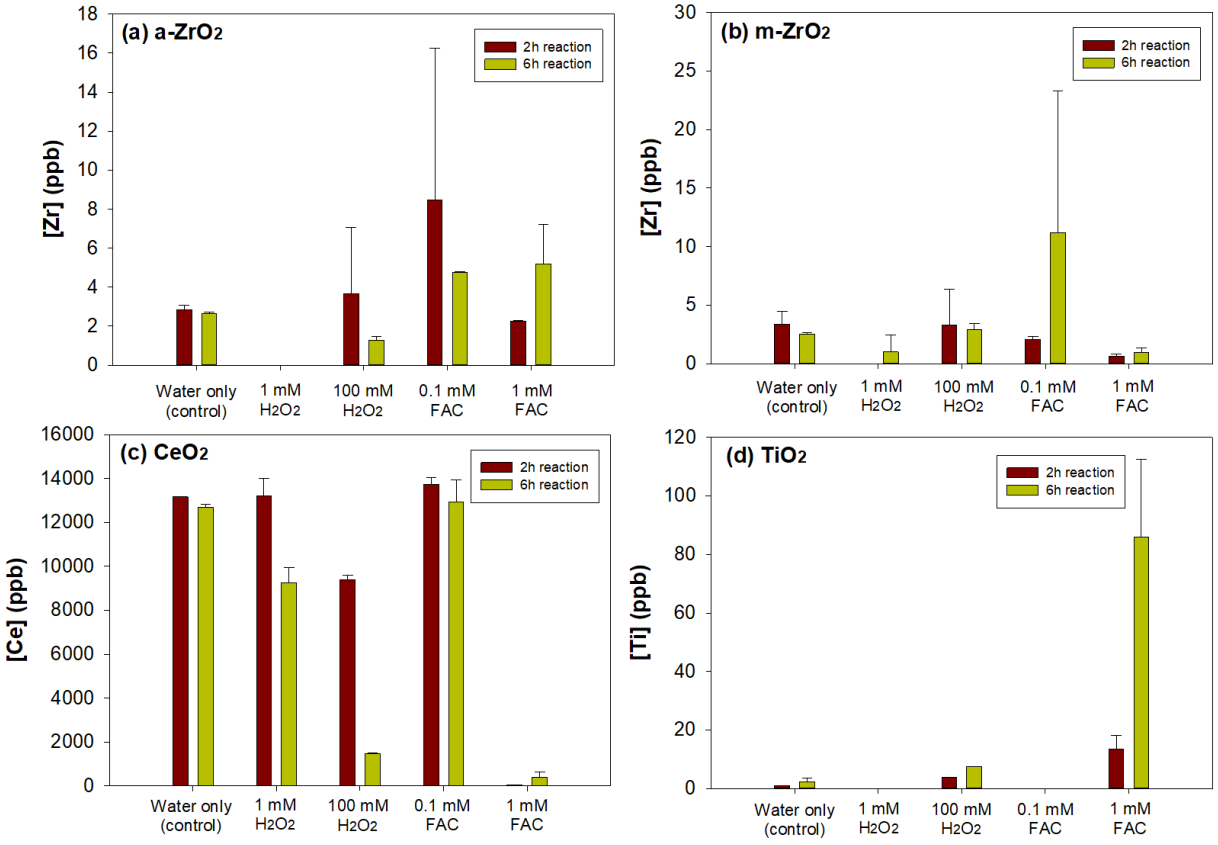

Figure 4.26. ICP-MS analyses for release of metal and/or nano-scale MeOx from reactions of MeO_2/H_2O_2 and MeOx/FAC; (a) a-ZrO_2, (b) m-ZrO_2, (c) CeO_2, and (d) TiO_2.

4.6 Summary and Potential Practical Implications

- FFA showed significant losses in the presence of H_2O_2 with a-ZrO_2, m-ZrO_2 and CeO_2, implying $^1O_2$ generation. This was further confirmed by conducting kinetic studies using D_2O as reaction matrix, which can extend the lifetime of $^1O_2$, resulting in faster FFA degradation as compared to experiments conducted in H_2O. In MeOx/FAC systems,

though significant FFA losses were also observed, did not exhibit such discrepancy between tests performed in D_2O and H_2O, suggesting that FFA decomposition in MeOx/FAC may be resulted from other reactive oxidants (likely RCS) while with partial loss associated with direct reaction with Cl_2.

- Formaldehyde (≥100 μM) and acetone (≥30 μM) were observed over 6h of reaction in systems of m-ZrO_2+H_2O_2, m-ZrO_2+FAC, CeO_2+FAC and TiO_2+FAC containing MeOH and iPrOH, respectively with $[H_2O_2]_0$ = 100 mM and [FAC] = 1 mM. However, lower levels of formaldehyde formation (≤ 5 μM) were observed when using *t*-BuOH as a scavenger, indicating that other weaker oxidizing species may be responsible for their formation as the former two alcohols are less selective to $HO^{\bullet}$. Kinetic studies conducted in 100mM *t*-BuOH as matrix also confirmed limited formation of $HO^{\bullet}$.
- Use of TNM and NBT, selective indicators for $O_2^{\bullet-}$, confirmed $O_2^{\bullet-}$ production in the MeOx/H_2O_2 system. Results suggested the presence of both aqueous and surface-bounded superoxide formation on a-ZrO_2 in the presence of H_2O_2, and superoxide in the m-ZrO_2+H_2O_2 system may primarily exist in aqueous phase.
- Activities of MeOx systems are sustained in repeated use in FFA degradation and formaldehyde formation over at least five treatment cycles. The reactions prevailing in these systems appear to involve formation of $^1O_2$, $O_2^{\bullet-}$ and limited $HO^{\bullet}$ as well as other yet unconfirmed reactive species, potentially including RCS such as $Cl^{\bullet}$, $ClO^{\bullet}$, $Cl_2^{\bullet-}$ (free or surface-bounded).
- Release of free and nano-scale metals during MeOx/H_2O_2 and MeOx/FAC treatment was found to be limited with no more than ~10 μg/L release throughout most of the conditions tested.

- Generation of more selective oxidants ($^1O_2$, $ClO^{\bullet}$) than less selective/stronger oxidants ($HO^{\bullet}$, $Cl^{\bullet}$) implies the MeOx/H_2O_2 and MeOx/FAC reactions appear less useful as AOPs, but could be quite effective as targeted oxidation processes.
- MeOx could provide benefits as (i) adsorbents (e.g., a-ZrO_2 is highly effective for adsorption of phosphate and MS2), or (ii) oxidant quenchers; a-ZrO_2 and CeO_2 in particular were found rapidly decomposing H_2O_2 and FAC (for excess H_2O_2 removal after conventional AOPs, and excess FAC removal before use or discharge). Some potential practical implementations could be MeOx-precoat membrane filtration or packed bed/column.

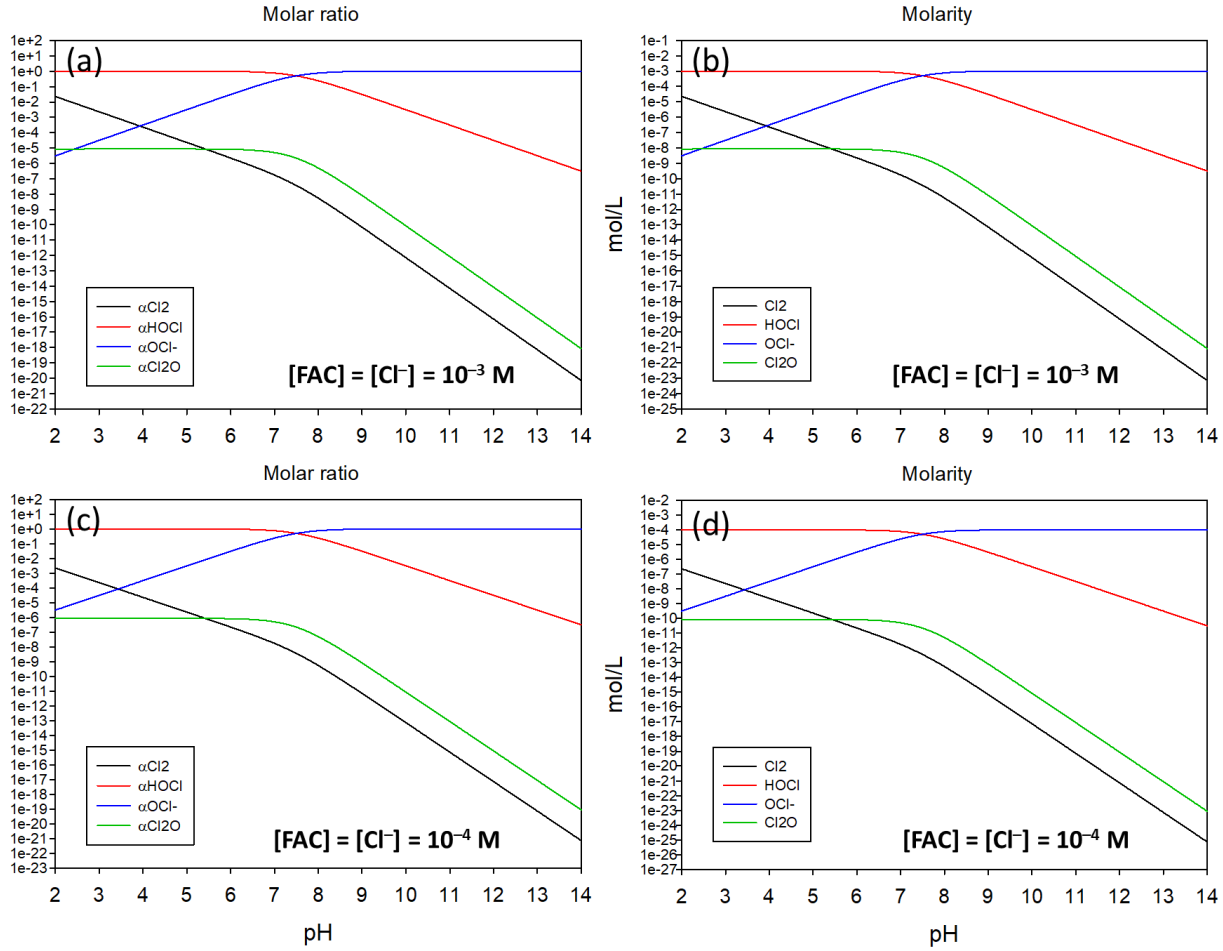

Figure S4.1. Chorine speciation at varying pH versus (a) molar ratio with [FAC] = 1 mM, (b) molarity with [FAC] = 1 mM, (c) molar ratio with [FAC] = 0.1 mM, and (d) molarity with [FAC] = 0.1 mM. Chlorine speciation was calculated assuming equal molar of Cl^- presenting in the NaOCl stock.

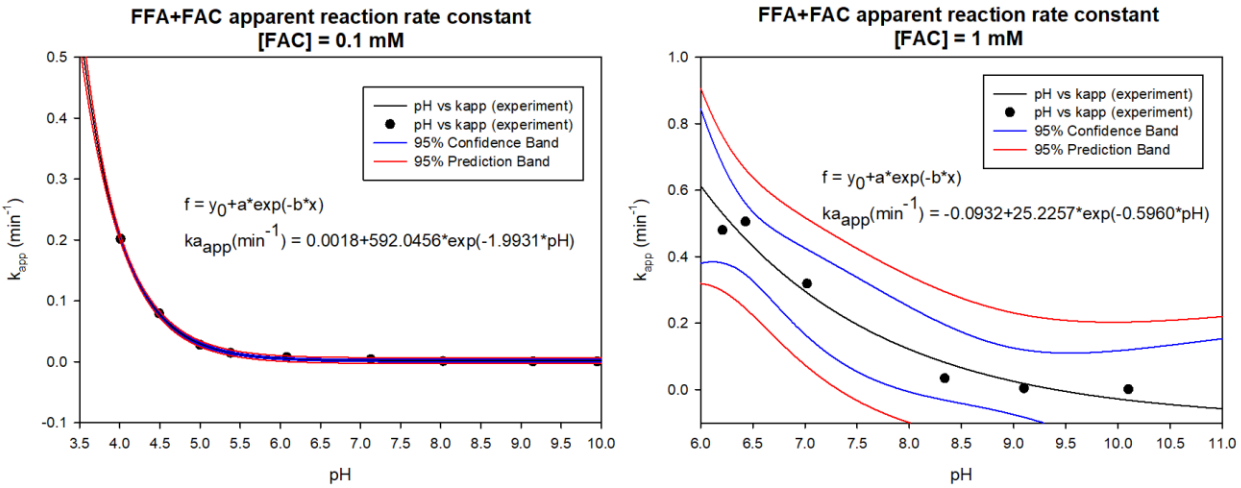

Figure S4.2. Fitting of apparent reaction rate constants for FFA+FAC reaction at varying pH. Experiments were conducted by reacting $[FFA]_0$ = 5 μM with $[FAC]_0$ = 0.1 or 1 mM. The reaction pHs were maintained by 10mM acetic acid (pH4~5), 10mM phosphate (pH6~8), or 10mM borate (pH9~10). Measured apparent reaction rate constants were fitted by a three parameters exponential model using SigmaPlot.

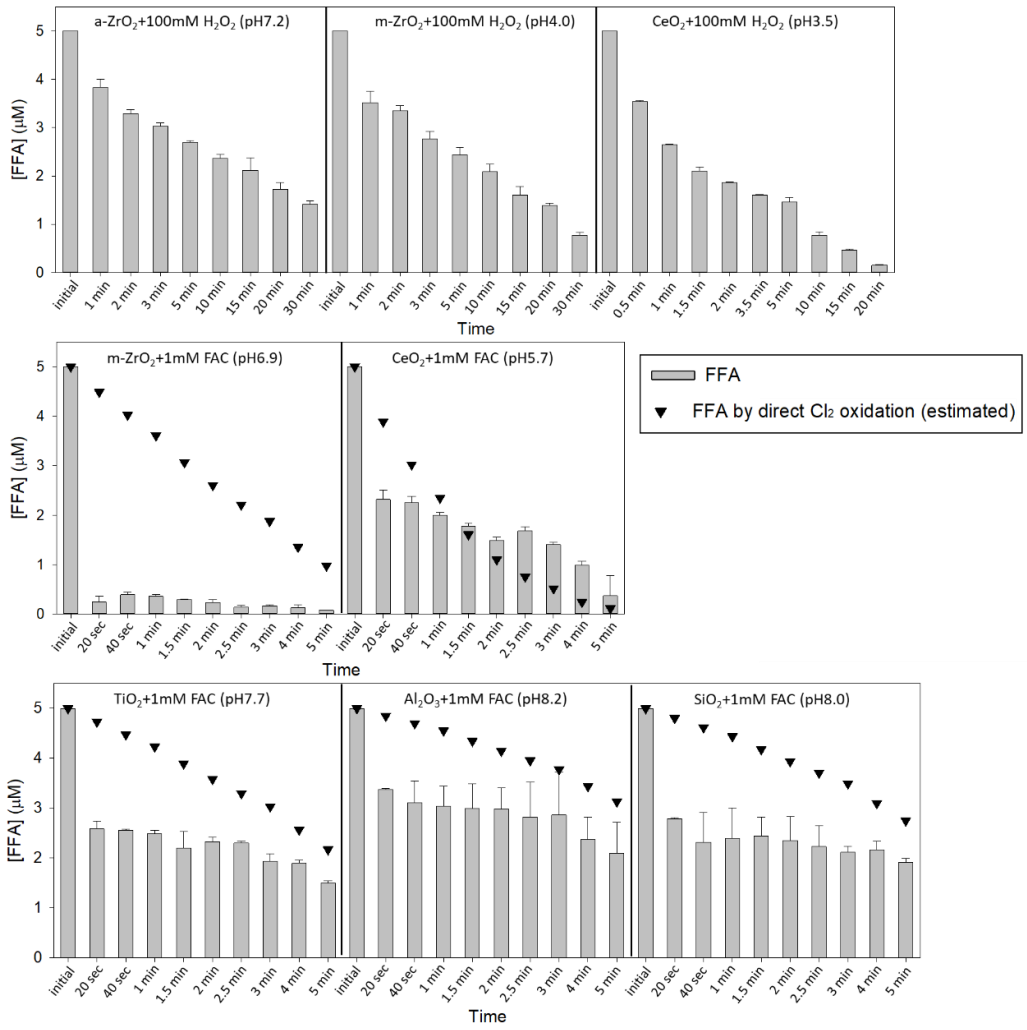

Figure S4.3. FFA degradation with MeOx/oxidant treatment. Experiments were conducted by dosing solutions containing $[FFA]_0$ = 1 μM and $[H_2O_2]_0$ = 100 mM or $[FAC]_0$ = 1 mM into MeOx solids to a MeOx/liquid concentration of 0.1 g/mL. The reaction pHs were not adjusted throughout the reactions. Error bars represent one standard deviation about the mean of duplicate measurements.

Table S4.1. Alcohols reactions with ROS and RCS, and formation of formaldehyde and acetone

Radicals/ Reactive species	Reaction	*k* ($M^{-1}s^{-1}$)	References
Methanol (MeOH)			
$HO^{\bullet}$	MeOH + $HO^{\bullet}$ ==> H_2O + $^{\bullet}CH_2OH$	$(0.78\text{-}1.2)\times10^9$	(Ross et al., 1998)
$^1O_2$	$^1O_2$ + MeOH ==> products	3×10^3	(Young and Brewer, 1976)
$Cl^{\bullet}$	MeOH + $Cl^{\bullet}$ ==> products	$\sim1.3\times10^8$	(Horvath, 1989)
	MeOH + $Cl^{\bullet}$ ==> products	$(2.7\text{-}5.7)\times10^9$	(Ross et al., 1998)
$O^{\bullet-}$	MeOH + $O^{\bullet-}$ ==> H2O + $^{\bullet}CH_2O^-$	5.8×10^8 - 8.6×10^8	(Ross et al., 1998)
$Cl_2^{\bullet-}$	MeOH + $O^{\bullet-}$ ==> HCl + $^{\bullet}CH_2OH$ + Cl^-	4×10^3	(Fel'dman et al., 1986)
	MeOH + $Cl_2^{\bullet-}$ ==> products	3.5×10^3	(Hasegawa and Neta, 1978)
e_{aq}-	e_{aq}- + MeOH ==> CH_3O^- + $H^{\bullet}$	$<1\times10^4$	(Anbar and Hart, 1964)
	$^{\bullet}CH_2OH$ + $^{\bullet}CH_2OH$ ==> $(CH_2OH)_2$	1.7×10^9	(Wang et al., 1996)
	$^{\bullet}CH_2OH$ + $^{\bullet}CH_2OH$ ==> CH_2O + CH_3OH		(Wang et al., 1996)
	$^{\bullet}CH_2OH$ + $CH_2O^{\bullet-}$ + H_2O ==> $(CH_2OH)_2$ + OH^-	1.2×10^9	(Wang et al., 1996)
	$^{\bullet}CH_2OH$ + $CH_2O^{\bullet-}$ + H_2O ==> $CH_3O{-}CH_2OH$ + OH^-		(Wang et al., 1996)
	$^{\bullet}$CH2OH + $CH_2O^{\bullet-}$ + H_2O ==> CH_2O + CH_3OH + OH^-		(Wang et al., 1996)
	$CH_2O^{\bullet-}$ + $CH_2O^{\bullet-}$ + $2H_2O$ ==> $(CH_2OH)_2$ + $2OH^-$	5×10^8	(Wang et al., 1996)
	$CH_2O^{\bullet-}$ + $CH_2O^{\bullet-}$ + $2H_2O$ ==> $CH_3O{-}CH_2OH$ + $2OH^-$		(Wang et al., 1996)
	$CH_2O^{\bullet-}$ + $CH_2O^{\bullet-}$ + $2H_2O$ ==> CH_2O + CH_3OH + $2OH^-$		(Wang et al., 1996)
Isopropanol (iPrOH or 2-PrOH)[a]			
$HO^{\bullet}$	2-PrOH + $HO^{\bullet}$ ==> H_2O + $(CH_3)_2COH$	$(1.6\text{-}2.3)\times10^9$	(Ross et al., 1998)
$^1O_2$	$^1O_2$ + 2-PrOH ==> products	1.7×10^3	(Young and Brewer, 1976)
$Cl^{\bullet}$	2-PrOH + $Cl^{\bullet}$ ==> HCl + $(CH_3)_2COH$	6×10^9	(Mertens and von Sonntag, 1995)
	2-PrOH + $Cl^{\bullet}$ ==> products	$\sim4\times10^8$	(Horvath, 1989)
	2-PrOH + $Cl^{\bullet}$ ==> products	3.7×10^9	Sumiyoshi et al. (1987)
$O^{\bullet-}$	2-PrOH + $O^{\bullet-}$ ==> $^{\bullet}CH_2CHO{-}CH_3$ + H_2O + $(CH_3)_2CO^-$	$(1.2\text{-}1.5)\times10^9$	(Ross et al., 1998)
$Cl_2^{\bullet-}$	2-PrOH + $Cl_2^{\bullet-}$ ==> $(CH_3)_2COH$ + Cl^- + Cl^- + H^+	$(1.2\text{-}1.9)\times10^5$	(Ross et al., 1998)
tert-Butanol (t-BuOH)			
$HO^{\bullet}$	*t*-BuOH + $HO^{\bullet}$	$(4.2\text{-}7.6)\times10^8$	(Ross et al., 1998)

	==> H_2O + $^{\bullet}CH_2C(CH_3)_2OH$		
$^1O_2$	1O2 + *t*-BuOH ==> products	1.8×10^3	(Young and Brewer, 1976)
$Cl^{\bullet}$	*t*-BuOH + $Cl^{\bullet}$ ==> HCl + $^{\bullet}CH_2C(CH_3)_2OH$	$(0.3\text{-}1.5)\times10^9$	(Ross et al., 1998)
	t-BuOH + $Cl^{\bullet}$ ==> HCl + $(CH_3)_3CO^{\bullet}$	$\sim7\times10^8$	(Gilbert et al., 1988)
	t-BuOH + $Cl^{\bullet}$ ==> products	3.2×10^9	Sumiyoshi et al. (1987)
$O^{\bullet-}$	*t*-BuOH + $O^{\bullet-}$ ==> products	$(3.2\text{-}5)\times10^8$	(Ross et al., 1998)
$Cl_2^{\bullet-}$	*t*-BuOH + $Cl_2^{\bullet-}$ ==> products	$\sim7\times10^2$	(Hasegawa and Neta, 1978)
e_{aq}-	e_{aq}- + *t*-BuOH ==> products	$<4\times10^5$	(Koehler et al., 1985)
$ClO^{\bullet}$	*t*-BuOH + $ClO^{\bullet}$ ==> products	1.3×10^7	(Wu et al., 2017)
	$^{\bullet}CH_2C(CH_3)_2OH$ + O_2 ==> $^{\bullet}OOCH_2C(CH_3)_2OH$	1.4×10^9	(Reisz et al., 2003)
	$^{\bullet}OOCH_2C(CH_3)_2OH$ + $^{\bullet}OOCH_2C(CH_3)_2OH$ ==> O_2 + $HOC(CH_3)_2CH_2OH$ + $HOC(CH_3)_2CHO$	8×10^7	(Reisz et al., 2003)
	$^{\bullet}OOCH_2C(CH_3)_2OH$ + $^{\bullet}OOCH_2C(CH_3)_2OH$ ==> H_2O_2 + 2HOC(CH3)2CHO	1.2×10^8	(Reisz et al., 2003)
	$^{\bullet}OOCH_2C(CH_3)_2OH$ + $^{\bullet}OOCH_2C(CH_3)_2OH$ ==> O_2 + $2CH_2O$ + $2^{\bullet}C(CH_3)_2OH$	1×10^8	(Reisz et al., 2003)
	$^{\bullet}OOCH_2C(CH_3)_2OH$ + $^{\bullet}OOCH_2C(CH_3)_2OH$ ==> O2 + $HO(CH_3)_2CCH_2OOCH_2C(CH_3)_2OH$	1×10^8	(Reisz et al., 2003)
	$^{\bullet}C(CH_3)_2OH$ + O_2 ==> $^{\bullet}OOC(CH_3)_2OH$	2×10^9	(Reisz et al., 2003)
	$^{\bullet}OOC(CH_3)_2OH$ ==> $(CH_3)_2CO$ + $HO_2^{\bullet}$	6×10^2	(Reisz et al., 2003)

[a] $(CH_3)_2COH$ is the enol isomer of acetone $(CH_3)_2C=O$ (keto/enol tautomerism)

Table S4.2 Water quality analyses for Lake Washington natural water sample

Sampling date	Water sample	pH	Alkalinity (mg/L as $CaCO_3$)	DOC (mg/L)	Cl^- (mg/L)	Br^- (mg/L)	Phosphate (mg/L)
07/27/2022	Lake Washington-Magnuson Park	8.03	34.7 ± 0.2	2.32 ± 0.03	4.5	<0.1	<0.05

References for Chapter 4

Al-Nu'airat, J., Dlugogorski, B.Z., Gao, X., Zeinali, N., Skut, J., Westmoreland, P.R., Oluwoye, I. and Altarawneh, M., 2019. Reaction of phenol with singlet oxygen. *Physical Chemistry Chemical Physics* 21(1), 171-183.

Anbar, M. and Hart, E.J., 1964. The reactivity of aromatic compounds toward hydrated electrons. *Journal of the American Chemical Society* 86(24), 5633-5637.

APHA/AWWA/WEF, 2005. APHA Standard Methods for the Examination of Water and Wastewater, Washington.

Asmus, K.D., Moeckel, H. and Henglein, A., 1973. Pulse radiolytic study of the site of hydroxyl radical attack on aliphatic alcohols in aqueous solution. *The Journal of Physical Chemistry* 77(10), 1218-1221. 10.1021/j100629a007

Aubry, J., 1985. Search for singlet oxygen in the decomposition of hydrogen peroxide by mineral compounds in aqueous solutions. *Journal of the American Chemical Society* 107(21), 5844-5849.

Aubry, J.-M., Mandard-Cazin, B., Rougee, M. and Bensasson, R.V., 1995. Kinetic studies of singlet oxygen [4+ 2]-cycloadditions with cyclic 1, 3-dienes in 28 solvents. *Journal of the American Chemical Society* 117(36), 9159-9164.

Aubry, J. and Nardello, V., 1997. Studies in Surface Science and Catalysis, pp. 883-892, Elsevier.

Bedilo, A.F., Plotnikov, M.A., Mezentseva, N.V., Volodin, A.M., Zhidomirov, G.M., Rybkin, I.M. and Klabunde, K.J., 2005. Superoxide radical anions on the surface of zirconia and sulfated zirconia: formation mechanisms, properties and structure. *Physical Chemistry Chemical Physics* 7(16), 3059-3069. 10.1039/B504262C

Bielski, B.H., Shiue, G.G. and Bajuk, S., 1980. Reduction of nitro blue tetrazolium by CO2-and O2-radicals. *The Journal of Physical Chemistry* 84(8), 830-833.

Bielski, B.H.J. and Schwarz, H.A., 1968. Absorption spectra and kinetics of hydrogen sesquioxide and the perhydroxyl radical. *The Journal of Physical Chemistry* 72(11), 3836-3841. 10.1021/j100857a024

Black, E.D. and Hayon, E., 1970. Pulse radiolysis of phosphate anions $H_2PO_4^-$, HPO_4^{2-}, PO_4^{3-}, and $P_2O_7^{4-}$ in aqueous solutions. *The Journal of Physical Chemistry* 74(17), 3199-3203. 10.1021/j100711a007

Blesa, M.A., Maroto, A.J.G., Passaggio, S.I., Figliolia, N.E. and Rigotti, G., 1985. Hydrous zirconium dioxide: interfacial properties, the formation of monodisperse spherical particles, and its crystallization at high temperatures. *Journal of Materials Science* 20(12), 4601-4609. 10.1007/BF00559350

Bouzerara, F., Harabi, A., Ghouil, B., Medjemem, N., Boudaira, B. and Condom, S., 2012. Elaboration and properties of zirconia microfiltration membranes. *Procedia Engineering* 33, 278-284.

Candeias, L.P., Stratford, M.R. and Wardman, P., 1994. Formation of hydroxyl radicals on reaction of hypochlorous acid with ferrocyanide, a model iron (II) complex. *Free radical research* 20(4), 241-249.

Chen, D., Cao, l., Hanley, T. and Caruso, R., 2012. Facile Synthesis of Monodisperse Mesoporous Zirconium Titanium Oxide Microspheres with Varying Compositions and High Surface Areas for

Heavy Metal Ion Sequestration. *Advanced Functional Materials* 22, 1966-1971. 10.1002/adfm.201102878

Cui, H., Li, Q., Gao, S. and Shang, J.K., 2012. Strong adsorption of arsenic species by amorphous zirconium oxide nanoparticles. *Journal of Industrial and Engineering Chemistry* 18(4), 1418-1427. https://doi.org/10.1016/j.jiec.2012.01.045

Dąbrowski, J.M., 2017. Advances in inorganic chemistry, pp. 343-394, Elsevier.

Del Nero, M., Galindo, C., Barillon, R., Halter, E. and Madé, B., 2010. Surface reactivity of α-Al2O3 and mechanisms of phosphate sorption: In situ ATR-FTIR spectroscopy and ζ potential studies. *Journal of Colloid and Interface Science* 342(2), 437-444.

Depprich, R., Zipprich, H., Ommerborn, M., Mahn, E., Lammers, L., Handschel, J., Naujoks, C., Wiesmann, H.-P., Kübler, N.R. and Meyer, U., 2008. Osseointegration of zirconia implants: an SEM observation of the bone-implant interface. *Head & Face Medicine* 4(1), 1-7.

Dercz, G., Prusik, K. and Pajak, L., 2008. X-ray and SEM studies on zirconia powders. *Journal of Achievements in Materials and Manufacturing Engineering* 31(2), 408-414.

Elliot, A.J., 1989. A pulse radiolysis study of the temperature dependence of reactions involving H, OH and e-aq in aqueous solutions. *International Journal of Radiation Applications and Instrumentation. Part C. Radiation Physics and Chemistry* 34(5), 753-758.

Ersahin, M.E., Ozgun, H., Dereli, R.K., Ozturk, I., Roest, K. and van Lier, J.B., 2012. A review on dynamic membrane filtration: materials, applications and future perspectives. *Bioresource technology* 122, 196-206.

Fang, Y.F., Deng, A.P. and Huang, Y.P., 2009. Determination of hydroxyl radical in Fenton system. *Chinese Chemical Letters* 20(10), 1235-1240.

Fel'dman, V., Belevskii, V., Bugaenko, L., Moralev, V. and Popov, V., 1986. Early ionic processes in the radiolysis of liquid methanol. *High Energy Chemistry* 20(2), 102-107.

Fierro, J.L.G., 2006. Metal Oxides: Chemistry & Applications, CRC Press, Taylor & Francis Group, Boca Raton, FL.

Flyunt, R., Leitzke, A., Mark, G., Mvula, E., Reisz, E., Schick, R. and von Sonntag, C., 2003. Determination of $^{\bullet}OH$, $O_2^{\bullet-}$, and hydroperoxide yields in ozone reactions in aqueous solution. *The Journal of Physical Chemistry B* 107(30), 7242-7253. 10.1021/jp022455b

Gerdes, R., Wöhrle, D., Spiller, W., Schneider, G., Schnurpfeil, G. and Schulz-Ekloff, G., 1997. Photo-oxidation of phenol and monochlorophenols in oxygen-saturated aqueous solutions by different photosensitizers. *Journal of Photochemistry and Photobiology A: Chemistry* 111(1), 65-74. https://doi.org/10.1016/S1010-6030(97)00209-8

Ghiselli, G., Jardim, W.F., Litter, M.I. and Mansilla, H.D., 2004. Destruction of EDTA using Fenton and photo-Fenton-like reactions under UV-A irradiation. *Journal of Photochemistry and Photobiology A: Chemistry* 167(1), 59-67.

Gilbert, B.C., Stell, J.K., Peet, W.J. and Radford, K.J., 1988. Generation and reactions of the chlorine atom in aqueous solution. *Journal of the Chemical Society, Faraday Transactions 1: Physical Chemistry in Condensed Phases* 84(10), 3319-3330.

Greenwald, R.A., 2018. Handbook methods for oxygen radical research, CRC press.

Harwood, J. and Kühn, A., 1970. A colorimetric method for ammonia in natural waters. *Water Research* 4(12), 805-811.

Hasegawa, K. and Neta, P., 1978. Rate constants and mechanisms of reaction of chloride ($Cl_2^{\bullet-}$) radicals. *The Journal of Physical Chemistry* 82(8), 854-857. 10.1021/j100497a003

He, Z., Lyu, Z., Gu, Q., Zhang, L. and Wang, J., 2019. Ceramic-based membranes for water and wastewater treatment. *Colloids and Surfaces A: Physicochemical and Engineering Aspects* 578, 123513.

Heinlaan, M., Ivask, A., Blinova, I., Dubourguier, H.-C. and Kahru, A., 2008. Toxicity of nanosized and bulk ZnO, CuO and TiO2 to bacteria Vibrio fischeri and crustaceans Daphnia magna and Thamnocephalus platyurus. *Chemosphere* 71(7), 1308-1316. https://doi.org/10.1016/j.chemosphere.2007.11.047

Held, A.M., Halko, D.J. and Hurst, J.K., 1978. Mechanisms of chlorine oxidation of hydrogen peroxide. *Journal of the American Chemical Society* 100, 5732-5740. https://ci.nii.ac.jp/naid/80013880552/en/

Henglein, A., Langhoff, J. and Schmidt, G., 1959. Tetranitromethane as a radical scavenger in radiation chemical studies. *The Journal of Physical Chemistry* 63(6), 980-980.

Hiroki, A. and LaVerne, J.A., 2005. Decomposition of hydrogen peroxide at water−ceramic oxide interfaces. *The Journal of Physical Chemistry B* 109(8), 3364-3370. 10.1021/jp046405d

Horvath, O., 1989. Geminate-pair scavenging mechanism in photochemical reactions of chlorocuprate (II) complexes in acetonitrile solutions containing alcohols. *Journal of Photochemistry and Photobiology A: Chemistry* 48(2-3), 243-248.

Janusz, W., Patkowski, J. and Chibowski, S., 2003. Competitive adsorption of Ca2+ and Zn (II) ions at monodispersed SiO2/electrolyte solution interface. *Journal of colloid and interface science* 266(2), 259-268.

Janusz, W., Patkowski, J. and Chibowski, S., 2003. Competitive adsorption of Ca2+ and Zn (II) ions at monodispersed SiO2/electrolyte solution interface. *Journal of colloid and interface science* 266(2), 259-268.

Jensen, R.L., Arnbjerg, J. and Ogilby, P.R., 2010. Temperature Effects on the Solvent-Dependent Deactivation of Singlet Oxygen. *Journal of the American Chemical Society* 132(23), 8098-8105. 10.1021/ja101753n

Jiang, W., Mashayekhi, H. and Xing, B., 2009. Bacterial toxicity comparison between nano- and micro-scaled oxide particles. *Environmental Pollution* 157(5), 1619-1625. https://doi.org/10.1016/j.envpol.2008.12.025

Kawaguchi, H., 1993. Photo-oxidation of 2-propanol in aqueous solution in the presence of hydrogen peroxide. *Chemosphere* 27(4), 577-584.

Karlsson, H.L., Toprak, M.S. and Fadeel, B., 2022. Handbook on the Toxicology of Metals, pp. 87-126, Elsevier.

Ke, X.B., Zhu, H.Y., Gao, X.P., Liu, J.W. and Zheng, Z.F., 2007. High-Performance Ceramic Membranes with a Separation Layer of Metal Oxide Nanofibers. *Advanced Materials* 19(6), 785-790. https://doi.org/10.1002/adma.200601984

Kijenski, J., Hombek, R. and Malinowski, S., 1977. Determination of hydroxyl groups and water adsorbed on the surface of heterogeneous catalysts by titration with alkali metal naphthenide solutions. *Journal of Catalysis* 50(1), 186-189. https://doi.org/10.1016/0021-9517(77)90023-9

Koch, D. and Manzhos, S., 2017. On the charge state of titanium in titanium dioxide. *The journal of physical chemistry letters* 8(7), 1593-1598.

Koehler, G., Solar, S., Getoff, N., Holzwarth, A. and Schaffner, K., 1985. Relationship between the quantum yields of electron photoejection and fluorescence of aromatic carboxylate anions in aqueous solution. *Journal of photochemistry* 28(3), 383-391.

Kosmulski, M., 2016. Isoelectric points and points of zero charge of metal (hydr)oxides: 50years after Parks' review. *Advances in Colloid and Interface Science* 238, 1-61. https://doi.org/10.1016/j.cis.2016.10.005

Kwaśny, J.A., Kryłów, M. and Balcerzak, W., 2018. Oily wastewater treatment using a zirconia ceramic membrane: a literature review. *Archives of Environmental Protection* 44(3), 3-10.

Lee, P.C. and Rodgers, M.A., 1987. Laser flash photokinetic studies of rose bengal sensitized photodynamic interactions of nucleotides and DNA. *Photochemistry and photobiology* 45(1), 79-86.

Lister, M., 1956. Decomposition of sodium hypochlorite: The catalyzed reaction. *Canadian Journal of Chemistry* 34(4), 479-488.

Liu, C., Von Gunten, U. and Croué, J.-P., 2012. Enhanced bromate formation during chlorination of bromide-containing waters in the presence of CuO: catalytic disproportionation of hypobromous acid. *Environmental science & technology* 46(20), 11054-11061.

Lousada, C.M., Johansson, A.J., Brinck, T. and Jonsson, M., 2012. Mechanism of H2O2 decomposition on transition metal oxide surfaces. *The Journal of Physical Chemistry C* 116(17), 9533-9543. 10.1021/jp300255h

Luo, J., Luo, X., Hu, C., Crittenden, J.C. and Qu, J., 2016. Zirconia (ZrO2) embedded in carbon nanowires via electrospinning for efficient arsenic removal from water combined with DFT studies. *ACS applied materials & interfaces* 8(29), 18912-18921.

Ma, Z.-Y., Yang, C., Wei, W., Li, W.-H. and Sun, Y.-H., 2005. Surface properties and CO adsorption on zirconia polymorphs. *Journal of Molecular Catalysis A: Chemical* 227(1), 119-124. https://doi.org/10.1016/j.molcata.2004.10.017

Ma, L., Sun, S., Wang, Y., Jiang, K., Zhu, J., Li, J. and Lin, H., 2017. A graphene quantum dot-based fluorescent nanoprobe for hypochlorite detection in water and in living cells. *Microchimica Acta* 184(10), 3833-3840.

Ma, W., Herbert, F.W., Senanayake, S.D. and Yildiz, B., 2015. Non-equilibrium oxidation states of zirconium during early stages of metal oxidation. *Applied Physics Letters* 106(10), 101603.

Matheson, I. and Massoudi, R., 1980. Photophysical and photosensitized generation of singlet molecular oxygen (1. DELTA. g) in micellar solutions at elevated pressures. Measurement of singlet molecular oxygen solvent to micelle transfer rates via both molecular diffusion and energy transfer. *Journal of the American Chemical Society* 102(6), 1942-1948.

McCafferty, E. and Wightman, J.P., 1998. Determination of the concentration of surface hydroxyl groups on metal oxide films by a quantitative XPS method. *Surface and Interface Analysis* 26(8), 549-564. https://doi.org/10.1002/(SICI)1096-9918(199807)26:8<549::AID-SIA396>3.0.CO;2-Q

Megias-Alguacil, D., Duran, J. and Delgado, A., 2000. Yield stress of concentrated zirconia suspensions: correlation with particle interactions. *Journal of colloid and interface science* 231(1), 74-83.

Mertens, R. and von Sonntag, C., 1995. Photolysis (λ= 354 nm of tetrachloroethene in aqueous solutions. *Journal of Photochemistry and Photobiology A: Chemistry* 85(1-2), 1-9.

Moreau, P., Colette-Maatouk, S., Gareil, P. and Reiller, P.E., 2013. Modelling of the adsorption of phenolic acids onto α, γ–alumina particles. *Colloids and Surfaces A: Physicochemical and Engineering Aspects* 435, 97-108.

Morris, G.E., Skinner, W.A., Self, P.G. and Smart, R.S.C., 1999. Surface chemistry and rheological behaviour of titania pigment suspensions. *Colloids and Surfaces A: Physicochemical and Engineering Aspects* 155(1), 27-41.

Morris, J.C., 1966. The acid ionization constant of HOCl from 5 to 35°. *The Journal of Physical Chemistry* 70(12), 3798-3805. 10.1021/j100884a007

Nosaka, Y. and Nosaka, A., 2016. Understanding hydroxyl radical (•OH) generation processes in photocatalysis. *ACS Energy Letters* 1(2), 356-359. 10.1021/acsenergylett.6b00174

Nowakowska, M. and Kępczyński, M., 1998. Polymeric photosensitizers 2. Photosensitized oxidation of phenol in aqueous solution. *Journal of Photochemistry and Photobiology A: Chemistry* 116(3), 251-256. https://doi.org/10.1016/S1010-6030(98)00305-0

Ngo, T., Phan, A., Yam, C. and Lenhoff, H., 1982. Interference in determination of ammonia with the hypochlorite-alkaline phenol method of Berthelot. *Analytical Chemistry* 54(1), 46-49.

Nichela, D.A., Berkovic, A.M., Costante, M.R., Juliarena, M.P. and Einschlag, F.S.G., 2013. Nitrobenzene degradation in Fenton-like systems using Cu (II) as catalyst. Comparison between Cu (II)-and Fe (III)-based systems. *Chemical engineering journal* 228, 1148-1157.

Nieto-Juarez, J.I., Pierzchła, K., Sienkiewicz, A. and Kohn, T., 2010. Inactivation of MS2 coliphage in Fenton and Fenton-like systems: role of transition metals, hydrogen peroxide and sunlight. *Environmental Science & Technology* 44(9), 3351-3356. 10.1021/es903739f

Ogata, F., Takahashi, K., Tominaga, H., Yabutani, H. and Kawasaki, N., 2010. Adsorption of Phosphate by Cerium Hydroxide. *e-Journal of Surface Science and Nanotechnology* 8, 258-260. 10.1380/ejssnt.2010.258

Ogilby, P.R., 2010. Singlet oxygen: there is indeed something new under the sun. *Chemical Society Reviews* 39(8), 3181-3209.

Padungthon, S., German, M., Wiriyathamcharoen, S. and SenGupta, A.K., 2015. Polymeric anion exchanger supported hydrated Zr (IV) oxide nanoparticles: a reusable hybrid sorbent for selective trace arsenic removal. *Reactive and Functional Polymers* 93, 84-94.

Padungthon, S., Li, J., German, M. and SenGupta, A.K., 2014. Hybrid anion exchanger with dispersed zirconium oxide nanoparticles: a durable and reusable fluoride-selective sorbent. *Environmental Engineering Science* 31(7), 360-372.

Parks, G.A. and Bruyn, P.D., 1962. The zero point of charge of oxides. *The Journal of Physical Chemistry* 66(6), 967-973.

Pereira, M., Oliveira, L. and Murad, E., 2012. Iron oxide catalysts: Fenton and Fentonlike reactions–a review. *Clay minerals* 47(3), 285-302.

Pibiri, I., Buscemi, S., Palumbo Piccionello, A. and Pace, A., 2018. Photochemically produced singlet oxygen: applications and perspectives. *ChemPhotoChem* 2(7), 535-547.

Puzyn, T., Rasulev, B., Gajewicz, A., Hu, X., Dasari, T.P., Michalkova, A., Hwang, H.-M.,

Rabani, J., Mulac, W.A. and Matheson, M.S., 1965. The Pulse Radiolysis of Aqueous Tetranitromethane.1 I. Rate Constants and the Extinction Coefficient of eaq-. II. Oxygenated Solutions. *The Journal of Physical Chemistry* 69(1), 53-70. 10.1021/j100885a011

Rao, P. and Hayon, E., 1975. Redox potentials of free radicals. IV. Superoxide and hydroperoxy radicals. O2-and. HO2. *The Journal of Physical Chemistry* 79(4), 397-402.

Reisz, E., Schmidt, W., Schuchmann, H.-P. and von Sonntag, C., 2003. Photolysis of ozone in aqueous solutions in the presence of tertiary butanol. *Environmental science & technology* 37(9), 1941-1948.

Ross, A., Bielski, B., Buxton, G., Cabelli, D., Helman, W., Huie, R., Grodkowski, J., Neta, P., Mulazzani, Q. and Wilkinson, F. (1998) NIST Standard Reference Database 40: NDRL/NIST Solutions Kinetics Database V. 3.0, Gaithersburg, MD.

Rule Wigginton, K., Menin, L., Montoya, J.P. and Kohn, T., 2010. Oxidation of virus proteins during UV254 and singlet oxygen mediated inactivation. *Environmental science & technology* 44(14), 5437-5443.

Rusevova, K., Kopinke, F.-D. and Georgi, A., 2012. Nano-sized magnetic iron oxides as catalysts for heterogeneous Fenton-like reactions—Influence of Fe (II)/Fe (III) ratio on catalytic performance. *Journal of hazardous materials* 241, 433-440.

Schmidt, R. and Afshari, E., 1992. Collisional deactivation of O2 (1Δg) by solvent molecules. Comparative experiments with 16O2 and 18O2. *Berichte der Bunsengesellschaft für physikalische Chemie* 96(6), 788-794.

Scully Jr, F.E. and Hoigné, J., 1987. Rate constants for reactions of singlet oxygen with phenols and other compounds in water. *Chemosphere* 16(4), 681-694.

Shannon, R.D., Shannon, R.C., Medenbach, O. and Fischer, R.X., 2002. Refractive Index and Dispersion of Fluorides and Oxides. *Journal of Physical and Chemical Reference Data* 31(4), 931-970. 10.1063/1.1497384

Stichert, W. and Schüth, F., 1998. Influence of crystallite size on the properties of zirconia. *Chemistry of Materials* 10(7), 2020-2026. 10.1021/cm980705o

Simon-Deckers, A., Loo, S., Mayne-L'hermite, M., Herlin-Boime, N., Menguy, N., Reynaud, C., Gouget, B. and Carrière, M., 2009. Size-, Composition- and Shape-Dependent Toxicological Impact of Metal Oxide Nanoparticles and Carbon Nanotubes toward Bacteria. *Environmental Science & Technology* 43(21), 8423-8429. 10.1021/es9016975

Sinitsyn, A.V. and Gracheva, M.E., 2020. Atomistic model of a ceria nanoparticle with Ce3+ and Ce4+ atoms. *Nanotechnology* 31(31), 315708.

Sivey, J.D., McCullough, C.E. and Roberts, A.L., 2010. Chlorine Monoxide (Cl2O) and Molecular Chlorine (Cl2) as Active Chlorinating Agents in Reaction of Dimethenamid with Aqueous Free Chlorine. *Environmental Science & Technology* 44(9), 3357-3362. 10.1021/es9038903

Sobańska, K., Pietrzyk, P. and Sojka, Z., 2017. Generation of reactive oxygen species via electroprotic interaction of H2O2 with ZrO2 gel: ionic sponge effect and pH-switchable peroxidase-and catalase-like activity. *ACS Catalysis* 7(4), 2935-2947.

Soman, A., Qiu, Y. and Chan Li, Q., 2008. HPLC-UV Method Development and Validation for the Determination of Low Level Formaldehyde in a Drug Substance. *Journal of Chromatographic Science* 46(6), 461-465. 10.1093/chromsci/46.6.461

Su, Y., Cui, H., Li, Q., Gao, S. and Shang, J.K., 2013. Strong adsorption of phosphate by amorphous zirconium oxide nanoparticles. *Water research* 47(14), 5018-5026.

Tamura, H., Mita, K., Tanaka, A. and Ito, M., 2001. Mechanism of Hydroxylation of Metal Oxide Surfaces. *Journal of Colloid and Interface Science* 243(1), 202-207. https://doi.org/10.1006/jcis.2001.7864

Thetford, A., Hutchings, G.J., Taylor, S.H. and Willock, D.J., 2011. The decomposition of H2O2 over the components of Au/TiO2 catalysts. *Proceedings of the Royal Society A: Mathematical, Physical and Engineering Sciences* 467(2131), 1885-1899. doi:10.1098/rspa.2010.0561

Tian, X., Gao, P., Nie, Y., Yang, C., Zhou, Z., Li, Y. and Wang, Y., 2017. A novel singlet oxygen involved peroxymonosulfate activation mechanism for degradation of ofloxacin and phenol in water. *Chemical Communications* 53(49), 6589-6592.

Toropov, A., Leszczynska, D. and Leszczynski, J., 2011. Using nano-QSAR to predict the cytotoxicity of metal oxide nanoparticles. *Nature nanotechnology* 6(3), 175-178.

Villén, L., Manjón, F., García-Fresnadillo, D. and Orellana, G., 2006. Solar water disinfection by photocatalytic singlet oxygen production in heterogeneous medium. *Applied Catalysis B: Environmental* 69(1), 1-9. https://doi.org/10.1016/j.apcatb.2006.05.015

Wang, W.-F., Schuchmann, M.N., Bachler, V., Schuchmann, H.-P. and von Sonntag, C., 1996. Termination of• CH2OH/CH2O•- radicals in aqueous solution. *The Journal of Physical Chemistry* 100(39), 15843-15847.

Wang, D., Zhao, L., Ma, H., Zhang, H. and Guo, L.-H., 2017. Quantitative analysis of reactive oxygen species photogenerated on metal oxide nanoparticles and their bacteria toxicity: The role of superoxide radicals. *Environmental Science & Technology* 51(17), 10137-10145. 10.1021/acs.est.7b00473

Watts, R.J. and Teel, A.L., 2019. Hydroxyl radical and non-hydroxyl radical pathways for trichloroethylene and perchloroethylene degradation in catalyzed H2O2 propagation systems. *Water research* 159, 46-54.

Whiteman, M., Jenner, A. and Halliwell, B., 1997. Hypochlorous acid-induced base modifications in isolated calf thymus DNA. *Chemical research in toxicology* 10(11), 1240-1246.

Wilkinson, F., Helman, W.P. and Ross, A.B., 1995. Rate constants for the decay and reactions of the lowest electronically excited singlet state of molecular oxygen in solution. An expanded and revised compilation. *Journal of Physical and Chemical Reference Data* 24(2), 663-677.

Wu, Z., Guo, K., Fang, J., Yang, X., Xiao, H., Hou, S., Kong, X., Shang, C., Yang, X., Meng, F. and Chen, L., 2017. Factors affecting the roles of reactive species in the degradation of micropollutants by the UV/chlorine process. *Water Research* 126, 351-360. https://doi.org/10.1016/j.watres.2017.09.028

Wu, J., Yang, J., Muruganandham, M. and Wu, C., 2008. The oxidation study of 2-propanol using ozone-based advanced oxidation processes. *Separation and Purification Technology* 62(1), 39-46.

Yang, Z., Zhou, Y., Feng, Z., Rui, X., Zhang, T. and Zhang, Z., 2019. A review on reverse osmosis and nanofiltration membranes for water purification. *Polymers* 11(8), 1252.

Young, R.H. and Brewer, D.R., 1976. Singlet Oxygen, Reactions with Organic Compounds and Polymers. Ranby, B.R., J.F. (ed), pp. 36 - 47, John Wiley & Sons, New York, NY.

Chapter 5. MICROORGANISM INACTIVATION BY MEOX/H2O2 AND MEOX/FAC TREATMENTS

5.1 Introduction

Human enteric viruses are present in wastewater as well as in natural waters impacted by raw or insufficiently treated sewage (Bosch, 1998). These viruses can cause various waterborne diseases, hence their presence in waters used for drinking or recreational purposes presents a risk to public health. Conventional disinfection practices are not always sufficient to completely disinfect viruses (Keswick et al., 1985; Thurston-Enriquez et al., 2003). Therefore, more effective oxidation practices are needed to ensure microbial water safety. MS2 bacteriophage is a nonenveloped RNA virus with an icosahedral capsid measuring 22–29 nm in diameter (Blanch et al., 2002; Golmohammadi et al., 1993). Bacteriophages have been proposed as viral indicators, in particular coliphage MS2, which is similar in size and shape to human enteric viruses, and with structure similar to that of many pathogenic enteric viruses. Therefore, MS2 phage is widely used as a model to estimate viral survival in water (Dawson et al., 2005; Grabow, 2001; Microbiology, 1991; Sobsey et al., 1995) or to quantify virus elimination by membrane filtration processes (Herath et al., 1999; Hu et al., 2003; Jacangelo et al., 1995). Spores of *Bacillus subtilis*, a FAC-resistant form of bacteria, have been successfully established for the evaluation of UV plants for water disinfection and have also been found to be a valuable surrogate for testing the inactivation of *Giardia lamblia* cysts and *Cryptosporidium parvum* oocysts (Facile et al., 2000; Sommer and Cabaj, 1993).

Given the facts that $^1O_2$ appears to be a major ROS produced in $MeOx/H_2O_2$ reactions and that $^1O_2$ is effective in inactivating MS2 bacteriophage (Kohn et al., 2007; Kohn and Nelson, 2007). MS2 virus and *B. subtilis* spores were used as model microorganism to test out the treatment efficiency of the $MeOx/H_2O_2$ systems. MeOx/FAC systems were not tested due to

rapid direct chlorination inactivation of MS2 by chlorine (Casteel et al., 2008; Lim et al., 2010; Shin and Sobsey, 2008).

5.2 Materials and Methods

5.2.1 Chemicals and Medium Preparation

All chemical reagents were purchased from Fisher or Sigma-Aldrich, and were of molecular biology grade purity, or reagent grade purity if the former was not available. The working stocks of chemical reagents (except for disinfectants and redox reactive reagents) used in bacteria culturing and inactivation experiments were sterilized either through autoclaving or 0.2 μm membrane filtration if not amenable to autoclaving. All stock solutions of general reagents were prepared in Milli-Q ultrapure water with resistivity ≥ 18.2 MΩ•cm. FAC stock solutions were prepared by diluting a commercial aqueous NaOCl stock (available chlorine, 4.00-4.99% w/w, Sigma-Aldrich) in Milli-Q water, and standardized spectrophotometrically at 292 nm (ε_{OCl^-} = 362 $M^{-1}cm^{-1}$) (Furman and Margerum, 1998). H_2O_2 stock solutions were prepared by diluting a commercial aqueous H_2O_2 stock (31.7% w/w, Fisher) in Milli-Q water, and standardized spectrophotometrically at 240 nm ($\varepsilon_{H2O2/HO2^-}$ = 38 $M^{-1}cm^{-1}$) (Morgan et al., 1988). Broths, agar and other culturing media were all purchased from BD Difco™.

5.2.2 Microorganism Preparation and Viability Assay

(i) Bacillus subtilis spores stock preparation

Vegetative cell growth. Freeze-dried *Bacillus subtilis* spore cells (2A13) were purchased from the Bacillus Genetic Stock Center (BGSC, Ohio, USA), which is identical to the

ATCC6633 strain. Stocks of *B. subtilis* were prepared under sterile conditions using aseptic techniques performed in a Biosafety Level 2 hood (BSL-2). Freeze-dried spores absorbed onto three filter disks was revived by placing the filter disk on a nutrient agar plate with drops of nutrient broth. After overnight incubation at 37°C, one colony of revived vegetative *B. subtilis* was inoculated into several 50mL sterile centrifuge tubes with each containing 30 mL nutrient broth to propagate the vegetative cells. For the case of reviving *B. subtilis* directly from spores stock, dipped sterile wire loop into spore stock, and streak plated on nutrient agar plates, allowed overnight incubation at 37 °C, and then one colony of revived vegetative *B. subtilis* was inoculated into several 50mL sterile centrifuge tubes with each containing 30 mL nutrient broth. The centrifuge tubes were loosely capped to maintain aerobic conditions (ample headspace), and incubated at 37 °C at 150 shakes/min in a benchtop shaking incubator. Incubation continued for approximately 15~20 hours if using nutrient broth, or until the solution reached peak optical density (OD) at 600 nm, and growth is on the cusp of stationary phase but still in exponential phase.

Sporulation. After achieving this degree of vegetative cell growth, the cells were concentrated by centrifuging at 3,500 G for 10 min at 4°C. Poured off the supernatant, and resuspended the pellet with ~10 mL of sterile water. These steps were repeated again. Poured off supernatant and resuspend by adding 0.2 mL of sterile water into each 50mL centrifuge tube containing the vegetative cells. Concentrated vegetative cells in each tube were then transferred to one 10-cm diameter AK#2 sporulating agar plate for sporulation, spread the cell solution using a cell spreader. Allowed for plates to dry before inverting, and then incubate the plates at 37°C for 5-7 days.

***Spore harvesting*.** Following incubation, take the AK#2 agar plates out from the incubator and allow them to acclimated to room temperature. Added 3-5 mL of sterile water or 1x phosphate-buffered saline (PBS) to each plate and allow several minutes to loosen the spores. Using a cell scraper and a pipette, scrape spores from agar and transfer spores in remaining liquid to a sterile 15mL centrifuge tube capable of withstanding centrifugation at least 10,000 G. Be careful not to scrape too hard to lift off agar.

Spore purification and wet heat purification. Spore purification involved the repetition of many centrifugation steps. First, the spores suspension were centrifuged at 10,000 G for 10 min. Pour off supernatant, and resuspend pellet in 10 mL sterile water. These steps were repeated for two more times. Add 2mL sterile water to each of the 15mL centrifuge tubes containing the cells, vortex, and then transfer the suspensions into microcentrifuge tubes which can tolerate higher centrifugation speeds for up to 20,000 G. Next, spores were centrifuged at 20,000 G for 20 minutes in microcentrifuge tubes, discarding the supernatant, pipetting out the remaining vegetative cells, and re-suspending pellet in water. This step was repeated numerous times until the pellet possessed two layers: a thin lightly colored layer (vegetative cells) resting on a thicker darker colored layer (spore cells). Modify the speed of centrifugation as desired and depending on the ease with which the upper layer of the pellet sloughs off. Eventually, the upper layer with vegetative cells was totally removed, leaving uniform darkly colored pellet of spores. Turned on a water bath with thermometer submerged to high heat 1.5 hours before heat purifying. Be sure water level is sufficiently high. Divided desired total quantity of spores needed for experiment into smaller volumes (i.e., 1-1.5 mL in microcentrifuge tubes). This is to ensure that there is uniform heating for purification. When thermometer reads 80°C place microcentrifuge tubes

with spores into floating devices. After 20 min, remove the spores and they should be purified. Allowed spore stock to cool and stored it in a 4°C refrigerator.

(ii) Bacillus subtilis spore viability test

Samples containing the *B. subtilis* spore after treatment experiments were cultured on BBL™ Nutrient Agar (BD) (Forsyth et al., 2013). The spore viability will be quantified using spot-titer method described by Beck et al. as this method is less time and material intensive and yields statistically equivalent results as traditional spread plating method (Beck et al., 2009). A serial of 10-fold dilutions will be prepared from the spore samples using sterile Milli-Q water or phosphate buffer saline (PBS). Eight replicate 10 µL droplets of three dilutions were dispensed onto a 10-cm nutrient agar petri dishes (i.e., maximum of 24 spots can fit in one 10-cm petri dish). The droplets were left to dry on the agar, and then the plates were inverted and incubated at 37 °C for ~15 hours. The colonies were counted immediately before they overlap.

This approach has been found to yield results statistically equivalent to those obtained by traditional spread plating. Additional advantages of the spot-titer method over spread plating include: (i) time-savings since it is quicker to dispense droplets than to spread over a plate and it is quicker to count colonies in distinct spots than colonies spanning the surface area of an entire plate; and (ii) cost- and resource-savings since an entire serial dilution series including replicates requires only one plate. Thus, analyses of large experiments were performed more quickly, more affordably, and with greater replicability than would have been possible with traditional spread plating methods (Figure 5.1).

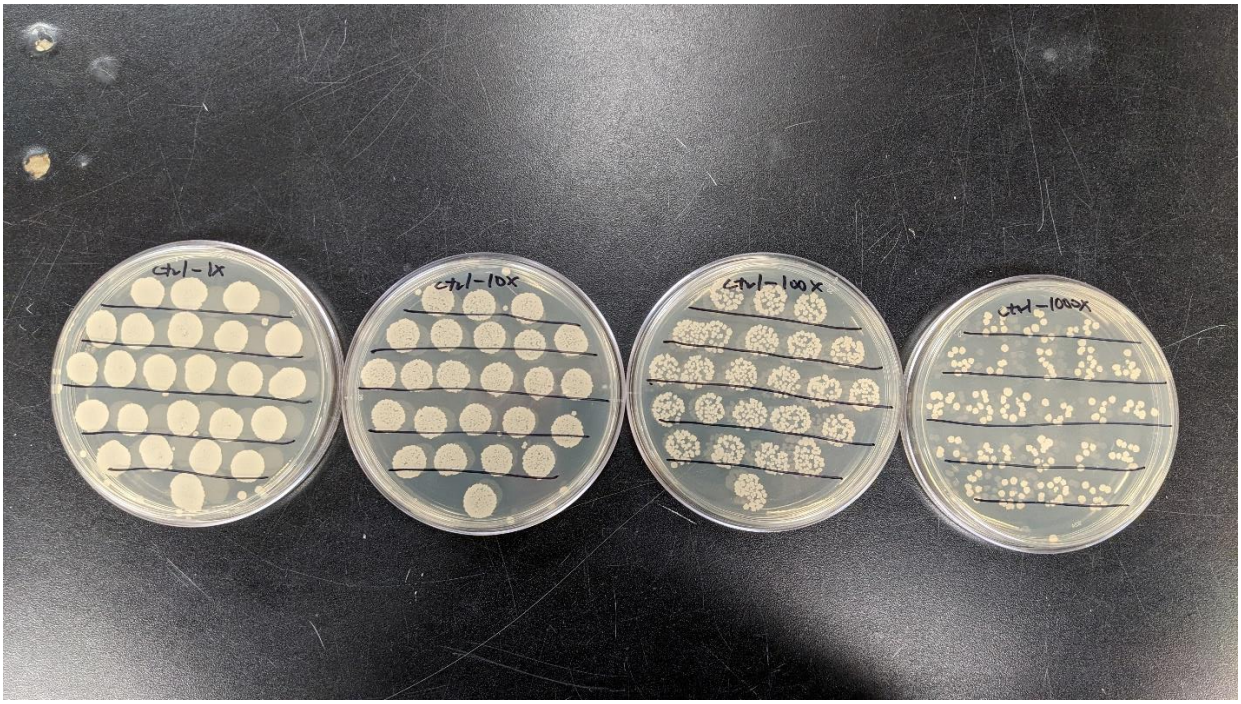

Figure 5.1. Example of spot-titering of *B. subtilis* spores on nutrient agar plates with different dilutions

(iii) MS2 bacteriophage stock preparation and purification

Culturing of MS2 and its E. coli host were performed as previous studies and the instructions on ATCC websites with appropriate modifications (Beck et al., 2009; Cho et al., 2005; Panec and Katz, 2006) (https://www.atcc.org/products/15597-b1 and https://www.atcc.org/products/15597).

E. coli host preparation and storage. Opened vial containing freeze-dried E. coli cells (ATCC15597) according to enclosed instructions. Using a single tube of #271 broth (5 to 6 mL), withdraw approximately 0.5 to 1.0 mL with a 1.0 mL pipette. Rehydrate the entire pellet. Note that this strain will grow on any standard medium (e.g. LB broth, nutrient broth). The #271 medium described above is the recommended medium for phage propagation. Aseptically transfer this aliquot back into the broth tube and mix well. Use several drops of the suspension to

inoculate a #271 (or other broths) agar slant and/or agar plate. Incubate the agar tubes or plates at 37°C for 24 hours. For short-term storage inoculate an Escherichia coli host culture onto tryptone agar slants with a sterile inoculating loop by spreading the inoculum evenly over entire slant surface. Incubate the culture overnight at 36.5 ± 2°C. Store at 4°C for up to 2 weeks. (For long-term storage inoculate a 5- to 10-mL tube of tryptone broth with host culture. Incubate overnight at 36.5 ± 2°C. Add glycerol solution to make each stock contain 15% glycerol. Dispense into 1-mL portions in 2-mL cryovials and store at -70°C, or lower.)

MS2 phage stock preparation. Before opening the vial with freeze-dried MS2 phage (ATCC15597-B1), prepare an actively growing culture of the E. coli host strain. The host should be 16-18 hours old. Pick one *E. coli* host colony from the isolation plate and homogenize in 5 mL of the appropriate broth. Incubate at 37°C while shaking (160-180 rpm) until the growth reaches OD_{600} of 0.1~0.4. Add approximately 1.0 mL of the recommended broth to a freeze-dried bacteriophage vial (or 0.5 mL to a liquid cryovial). Infect each 3 mL culture with 100 µL of the bacteriophage. Shake at 160-180 rpm in 37°C overnight. After 16-18 hours, centrifuge phage culture at 4000 ×g for 10 minutes. Filter the lysate with a 0.2 µm or 0.45 µm PES sterile filter. The filtrate can be stored at 4°C. Prior to performing a spot titer, warm bottom agar plates at 37°C. Melt the soft agar (0.5% agar added to the recommended medium #271) and maintain at 43°C to 45°C until ready to use. It is best to allow the melted agar to remain at this temperature for about an hour to ensure that it has cooled to 43°C to 45°C. Add 50 to 100 µL of the host culture from step 2 to each 9 mL (approximately) of soft agar from step 5 above. Immediately overlay the surface of each plate with 3 mL mixture. Allow the overlay to harden for 10 to 20 minutes. The phage lysate can be serial diluted using microcentrifuge tubes by PBS solution in triplicate (if desired; one can also use 96 well plates for serial dilution). Spot 5 µL of each

dilution on the plates with *E. coli* host. Up to 24 spots can fit on a 100 mm petri dish. After 6 to 8 hours of incubation at 37 °C, lysis should be visible. At the higher dilutions, individual plaques should be countable. To calculate pfu/mL, use the following formula: PFU/mL = average plaque count / [(dilution factor) ($5x10^{-3}$ mL)]. Spotting the phage on plates makes visualizing the lysis easier.

MS2 phage purification. MS2 virus was propagated in *E. coli* and subsequently purified and concentrated in different steps (Pecson et al., 2009). The unpurified MS2 virus stock was inoculated into 100 mL of ATCC#271 tryptone containing log-phase E. coli at roughly ~10^7 CFU/mL at a multiplicity of infection of 0.1 (MOI = ratio of virus PFU/mL over *E. coli* CFU/mL). Note that *E. coli* culture with OD_{600} of 1 has about 8×10^8 CFU/mL. If the *E. coli* culture overgrow a bit, you can dilute it by #271 tryptone broth to target cell concentration. After inoculation with MS2, the E.coli solution was incubated at 37 °C with shaking at 160-180 rpm for 5 hours. Following the incubation, 0.5 mL of chloroform was added into this 100 mL of E.coli-MS2 suspension to complete the lysis of all bacteria. Distributed this 100mL suspension into five 50-mL centrifuge tubes with each tube containing 20 mL, centrifuged at 4000 ×g for 15 min to separate the bacterial debris from the virus. Transferred the supernatant containing virus to 5 other new 50-mL centrifuge tubes. To each 20 mL of MS2-containing supernatant, added equal amount of sterile 20% polyethylene glycol (PEG 6000), which made the final 40mL solution contain ~10% PEG. To each 40 mL of MS2-PEG mixture, added 4.4 mL of sterile 5M NaCl, which made the final solution contain ~0.5M NaCl. Stored the MS2-PEG-NaCl mixtures overnight at 4°C. The MS2-PEG-NaCl mixtures were centrifuged at 7,000 xg for 45 min. Note that PEG has higher density than water, so the upper layer should be aqueous phase and the bottom layer should be PEG after centrifugation. Removed the supernatant, and the MS2-

containing pellet in each tube was resuspended by adding 4 mL of 1x PBS buffer. To each tube, added equal amount of 4 mL chloroform, and then centrifuged the mixture at 10,000 ×g for 30 min. After centrifugation, you will see three layers, with aqueous top layer, middle layer of PEG and bottom layer of chloroform. (density: PEG = 1.13 g/cm^3 and chloroform = 1.48 g/cm^3). Collected the top aqueous layer. The remaining aqueous phase was centrifuged for 10 min at 3,000 xg to separate it from the organic phase, transferred aqueous phase to a new tube, and sparged with zero compressed air for 30 min to volatilize any remaining chloroform. Finally, the solution was concentrated in an Amicon Ultra centrifugal filter device (100,000 Da nominal molecular weight limit, 100kDa pore size roughly equals to 4 nm; MS2 phage has size of 30 nm), washed three times with PBS in the same filters, collect the liquid with MS2 retained on the filter membranes, which could be in very small amount. Dilute the above tiny amount of MS2 stock to 2mL by PBS, and then passed it through a 0.1 μm-pore-size PES syringe filter. The dilution is to avoid the syringe filter adsorb all MS2 stock. The final MS2 stock was stored at a 4°C refrigerator.

MS2 phage stock purity tests. Organic substances (e.g. media, chloroform and PEG) applied during MS2 culturing and purification may remain in the MS2 stock. To ensure the removal efficiency of these organic substances by the Amicon Ultra 100kDa centrifugal filter device, TOC analyses were performed for the purified MS2 stocks and the filtrates. The result shows that the centrifugal filters were able to remove ~99% of dissolved organic carbon attributed to these additives. Only around 20 mg/L of DOC was measured in the MS2 stock (2.55×10^{11} PFU/mL), which could majorly be contributed by the virus itself. However, it was not clear whether trace organic remains in the purified MS2 stock were low enough to exclude their scavenging to reactive/radical species which could be generated during MeOx/H_2O_2 and

MeOx/FAC treatments. To investigate this, the purified MS2 stock was diluted to 1.0×10^6 and 1.0×10^8 PFU/mL, respectively, and treated with UV/H_2O_2 as $HO^{\bullet}$ source using nitrobenzene as a $HO^{\bullet}$ probe. The result in Figure S5.1 indicated that radical scavenging by the MS2 stock itself was negligible at the virus concentration levels used for inactivation experiments in this study.

(iv) MS2 bacteriophage viability test

MS-2 phages were quantified by the double-layer agar method using the mutant strain of *E. coli* C3000 (ATCC 15597) as the host (Cho et al., 2005; Sjogren and Sierka, 1994). For viability assessments, samples after inactivation treatment were serially diluted using PBS buffer. Inoculated single colony of E.coli (15597) into 30 mL of #271 tryptone broth, and incubated at 37 °C with shaking at 160-180 rpm. Incubated E.coli culture until OD600 reached 0.1~0.4. Melted #271 top agar in water bath or using microwave. Microwave was found to be much more efficient in melting top agar (takes only 60~80 sec). Transfer 3mL of top agar into multiple sterile 15-mL centrifuge tubes, and placed them into pre-heated digital heatblock maintaining at 60°C. Although some other literature suggested 45-50 °C. We found that agar could easily solidify under those lower temperatures. 60°C can make the agar remain as liquid, while not killing E. coli to a significant degree. To each 3 mL of top agar, dosed with 100 µL of E. coli host (OD600 at 0.1~0.4), vortexed and immediately poured over bottom agar plates. Rotated the agar plate to make sure the E.coli-containing top agar was evenly distributed. Waited for 10~20 min to let the top agar solidify. Spot-tittered 5 µL of MS2-containing samples (w/ different dilutions) onto the plates containing top agar with E. coli host. Each 10cm-diameter plate can fit 24 spots at most. Eight spots were titrated for one replicate of virus sample, and three replicates in the same concentration on a single agar plate (total 24 spots on a plate). Let the sample dry in the biosafety cabinet (BSC), inverted the plates and incubate them at a 37°C

incubator for 6~8 hours. Single virus plaques may be difficult to identify if incubated for longer time. Plaque forming unit for MS-2 phage will be counted after incubation (Figure 5.2). Selection of statistically meaningful plate counts was carried out according to Standard Methods (APHA/AWWA/WEF, 2005).

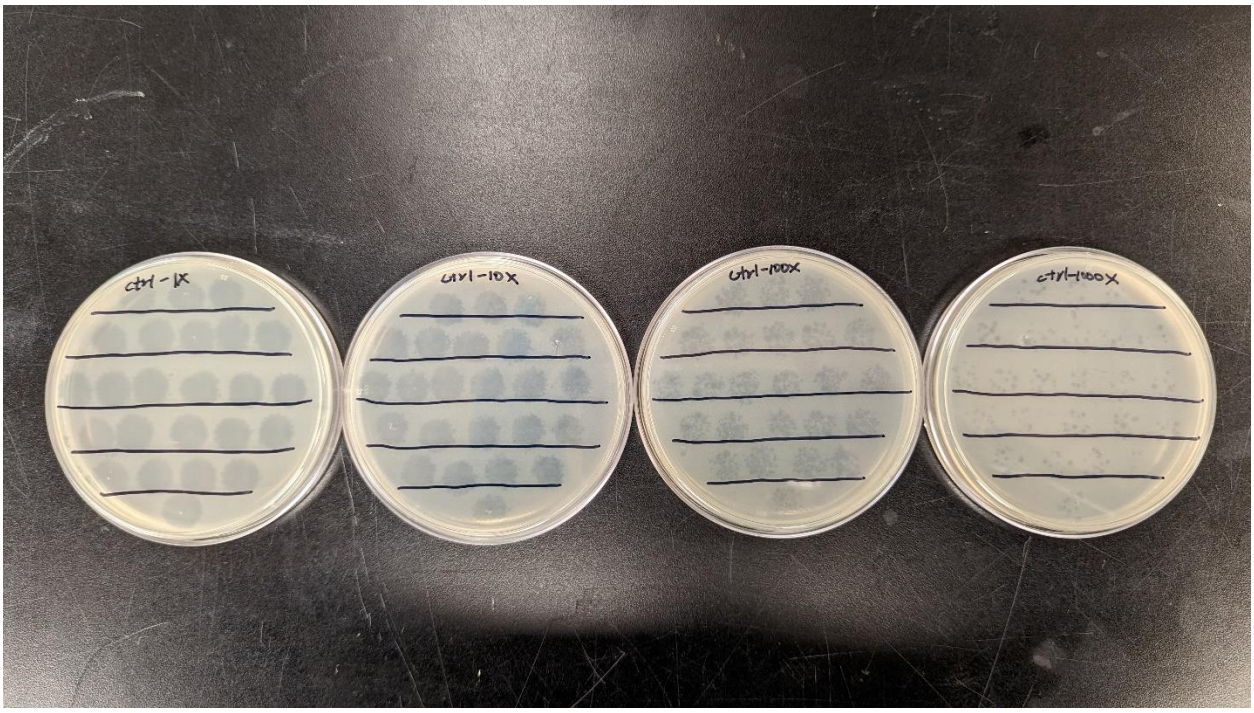

Figure 5.2. Example of spot-titering of MS2 phage on ATCC#271 tryptone agar plates with varying dilutions

5.2.3 MeOx/H_2O_2 and MeOx/FAC Treatment for *Bacillus subtilis* Spores

MeOx/FAC inactivation were conducted by single-dosing treatment by dosing ~1×10^6 CFU/mL *B. subtilis* spores and 1mM FAC into 0.1 g/mL suspension of MeOx solids. MeOx minerals were first placed in autoclaved reactors in addition to 5mM bicarbonate. The MeOx/carbonate suspensions were adjusted to pH7 using sulfuric acid, followed by magnetic stirring at 300 rpm for at least 1 hour to allow all substances reach equilibrium. After sufficient time, *B. subtilis* spores were dosed, and 1mM FAC were added immediately after to the

suspensions to initiate the reactions. Throughout the experiments, the reactors were tightly closed to prevent CO_2 off-gassing except when taking samples. MeOx/H_2O_2 inactivation were conducted in similar way, while buffers and pH adjustment were not applied because spores were found very resistant to pH changes and that pH did not appear to affect direct H_2O_2 inactivation of spores, as confirmed by the control experiments.

At designed reaction time, small aliquots of reaction suspension were taken into microcentrifuge tubes containing sufficient sodium thiosulfate for H_2O_2 or FAC quenching. The quenched-suspensions were used directly for spot-titering with adequate dilutions. Centrifugation to separate MeOx and spores would not be recommended as spores have similar density as the minerals. Meanwhile, small aliquots of reaction suspension were directly filtrated by 0.2 μm, polyethersulfone (PES) filters to remove MeOx solids without oxidant quenching. The filtrates were later used for H_2O_2, FAC and pH measurements. Control experiments with H_2O_2-only, FAC-only and MeOx-only treatments were also conducted for comparison.

5.2.4 MeOx/H_2O_2 Treatment for MS2 Bacteriophage

Experiments were conducted by single-dosing treatment by dosing ~1×10^6 PFU/mL MS2 and 10mM H_2O_2 into 0.1 g/mL suspension of MeOx solids. MeOx minerals were first placed in autoclaved reactors in addition to 5mM bicarbonate, 20 μM EDTA. The MeOx/carbonate/EDTA suspensions were adjusted to pH7 using sulfuric acid, followed by magnetic stirring at 300 rpm for at least 1 hour to allow all substances reach equilibrium. After sufficient time, MS2 phages were dosed, and 10mM H_2O_2 were added immediately after to the suspensions to initiate the reactions. Throughout the experiments, the reactors were tightly closed to prevent carbonate off-gassing except when taking samples. EDTA was required to prevent interference from reactive

species generated through trace transition metals (impurities) with H_2O_2. Without addition of EDTA, 10mM H_2O_2 was found to cause complete MS2 inactivation within 5 min. At designed reaction time, small aliquots of reaction suspension were taken into microcentrifuge tubes containing sufficient sodium thiosulfate for H_2O_2 quenching. The tubes were centrifuged at 10,000 ×g for 5 min, and the supernatants were collected. Meanwhile, small aliquots of reaction suspension were directly filtrated by 0.2 μm PES filters to remove MeOx solids without oxidant quenching. The filtrates were later used for H_2O_2 and pH measurements. Control experiments with H_2O_2-only and MeOx-only treatments were also conducted for comparison.

5.3 Results and Discussion

5.3.1 Inactivation of *B. subtilis* Spores

Control experiments of H_2O_2-only and MeOx-only suggested that there was no direct inactivation caused by H_2O_2 alone, and negligible inactivation and adsorption by the three MeOx tested, including a-ZrO_2, m-ZrO_2, and CeO_2 (Figure 5.3a and b). However, 0.1g/mL MeOx reacting with 10mM H_2O_2 did not cause spores inactivation as well. Note that MeOx/H_2O_2 inactivation were conducted in absence of buffer solution and without pH adjustment since spores were found highly resistant to pH changes. It has been confirmed that $^1O_2$, a relatively weak oxidant, was the major reactive species generated during MeOx/H_2O_2 reactions, which may not be sufficient to inactivate tenacious spores.

On the other hand, 1mM FAC can cause rapid spores inactivation with treatment efficiency enhanced with decreasing pH. HOCl species is usually believed to contribute much more than OCl^- to inactivation of microorganisms, hence acidic condition shows effective kill of microorganisms by shifting the equilibrium from OCl^- to HOCl (pK_a = 7.54) (Figure 5.3c and d)

(Barrette et al., 1989; McDonnell and Russell, 1999). Upon pH7 treatment with CT ~ 70 mg/L•min, 1mM FAC lead to 0.9-log of inactivation, and 1.4-log for both in the presence of CeO_2 and TiO_2. The slightly faster loss of spores may be resulted from RCS generated during CeO_2+FAC and TiO_2+FAC reactions. Spores possess coat proteins with FAC-reactive functional groups (like amino and sulfhydryl groups) and the coat's low-permeability required higher FAC exposure before it can permeate to damage the spore's inner membrane. This can render spore inactivation and hence loss of spore viability during disinfection usually would appear a "lag phase" (Figure 5.3d).

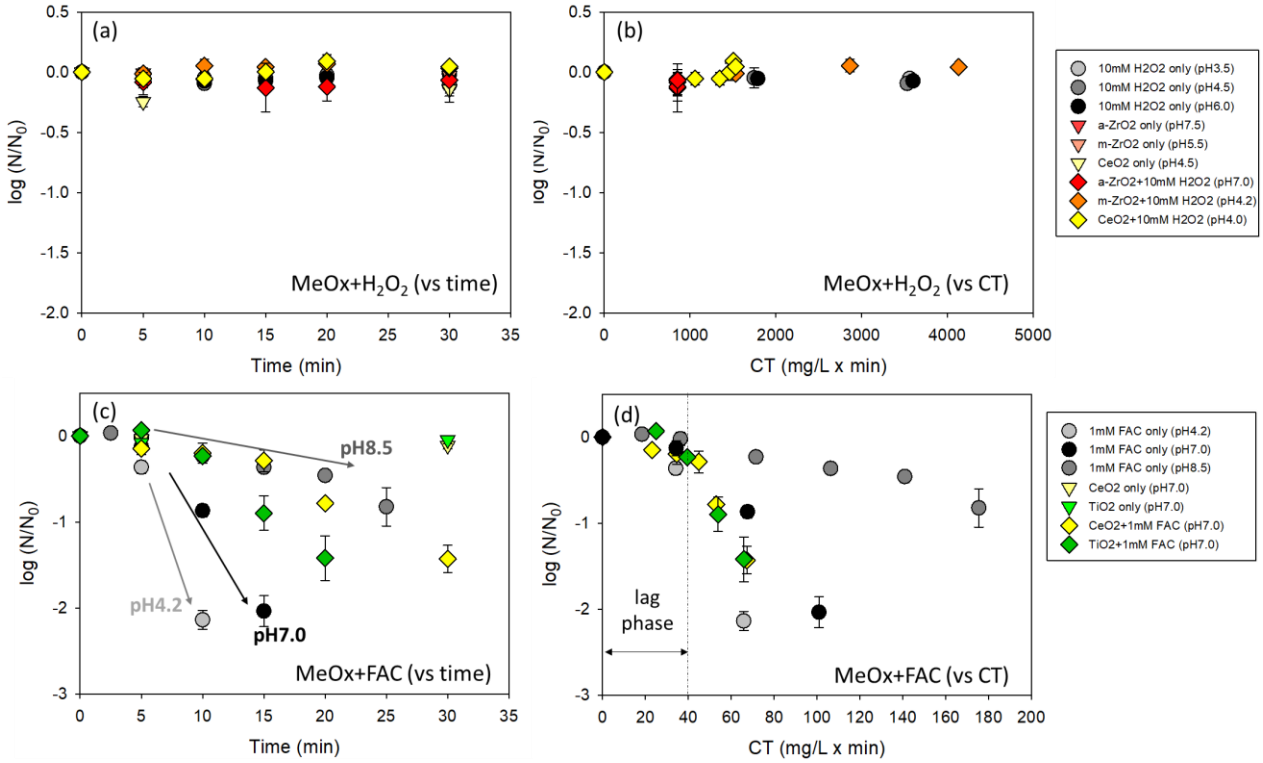

Figure 5.3. Treatment of *B. subtilis* spores from MeOx/H_2O_2 and MeOx/FAC. Data were plotted as log inactivation versus (a)(c) reaction time or (b)(d) cumulative CT valve. Error bars represent one standard deviation about the mean of triplicate measurements.

Loss of viability of a microorganism during disinfection treatment often follows second-order kinetics, according to eq 5.1,

$$\frac{dN}{dt} = -k[\text{Disinfectant}]N \tag{5.1}$$

where N is the number concentration (in units of viable units/volume) of the microorganism, [Disinfectant] is the disinfectant concentration, and k is the second-order rate, and the overall reaction is first-order in [Disinfectant] and first-order in N. By integrating the above equation, one derives the general expression for the Chick-Watson model (eq 5.2),

$$\log\left(\frac{N_t}{N_0}\right) = -k\int_0^t [\text{Disinfectant}]\text{dt} \tag{5.2}$$

where N_0 is the initial number concentration of the microorganism at time 0, and N_t is the number concentration of the microorganism after a period of t. The term, $\int_0^t [\text{Disinfectant}]\text{dt}$, is often referred to as CT, where C represents [Disinfectant] and T stands for reaction time. In the case for disinfectant-resistant microorganisms like spores, loss of viability would characterized by a lag phase followed by a post-lag phase exhibiting first-order loss of viability when $\log(N/N_0)$ is plotted versus CT, as shown in eq 5.3 below

$$\log\left(\frac{N_t}{N_0}\right) = \begin{cases} 0, \text{ if } CT \le CT_{\text{lag}} \\ \\ -k(CT - CT_{\text{lag}}), \text{ if } CT > CT_{lag} \end{cases} \tag{5.3}$$

Data in Figure 5.3 were fitted in the post-lag phase by linear regression to have the slope of inactivation rate constant k and a y-intercept of $\log(N/N_0)$. One can find that CT_{lag} will have a value of $\log(N/N_0)/k$. Inactivation rate constants k and CT_{lag} values during MeOx/H_2O_2 and

treatment for *B. subtilis* spores are summarized in Table 5.1. Treatment by FAC in the presence of CeO_2 and TiO_2 exhibited higher inactivation rate compared to the FAC-only control experiment at the same pH7, and they also shorten the lag phase CT_{lag}.

Table 5.1. Inactivation rate constants k and CT_{lag} values during MeOx/H_2O_2 and MeOx/FAC treatments against *B. subtilis* spores and MS2 phages

Condition	k ($mg/L^{-1}min^{-1}$)	y-intercept	R-square (N=data point)	Estimated CT_{lag} (mg/L×min)
B. subtilis spores				
1mM FAC-only (pH4.2)	0.0282	3.2672	1.0000[a] (N=2)	116
1mM FAC-only (pH7.0)	0.0176	1.5033	1.0000[a] (N=2)	85
1mM FAC-only (pH8.5)	0.0105	1.0261	1.0000[a] (N=2)	98
CeO_2+1mM FAC (pH7.0)	0.0503	1.9350	0.9937 (N=3)	38
TiO_2+1mM FAC (pH7.0)	0.0373	1.6942	0.9614 (N=3)	45
MS2 phages				
m-ZrO_2+10mM H_2O_2 (pH7.0)	1.09×10^{-4}	n.a.	0.9817 (N=7)	n.a.
CeO_2+10mM H_2O_2 (pH7.0)	3.54×10^{-3}	n.a.	0.9996 (N=5)	n.a.

[a] Only two data points available for regression for linear inactivation after lag phase

5.3.2 Inactivation of MS2 Bacteriophages

Preliminary tests with 0.1g/mL a-ZrO_2 show that it can strongly adsorb MS2 phages, causing around 3.5-log of MS2 removal in 5 min (data not shown). Addition of pH7, 50mM phosphate has proved to desorb MS2 from a-ZrO_2 surfaces with recovery rate around 75%. However, given that a-ZrO_2 does not seem to yield significant $^1O_2$ during reactions with H_2O_2 (Figure 4.16), m-ZrO_2 and CeO_2 were tested for MS2 inactivation (Figure 5.4). Direct reaction

with 10mM H_2O_2 was found negligible (H_2O_2-only condition). MeOx-only control experiments showed that both minerals could adsorb MS2, resulting in around one log of MS2 removal from the aqueous phase. 10mM H_2O_2 in the presence of 0.1g/mL CeO_2 caused 4.5-log of total loss of MS2 after 30 min of reaction (1-log loss by adsorption, and 3.5-log by chemical disinfection). m-ZrO_2+H_2O_2 caused rapid MS2 loss during early reaction with a total 2.5-log loss (1-log loss by adsorption, and 1.5-log by chemical disinfection), followed by slow inactivation at later time with total 3-log loss at 60 min of reaction (additional 0.5-log loss by chemical disinfection). Figure 5.4b plotted against *CT* values suggested that CeO_2 was much more effective in treating MS2 than m-ZrO_2 upon reactions with H_2O_2. These are consistent with the observation in the D_2O experiments that CeO_2+H_2O_2 can induce higher yield of $^1O_2$ (Figure 4.16).

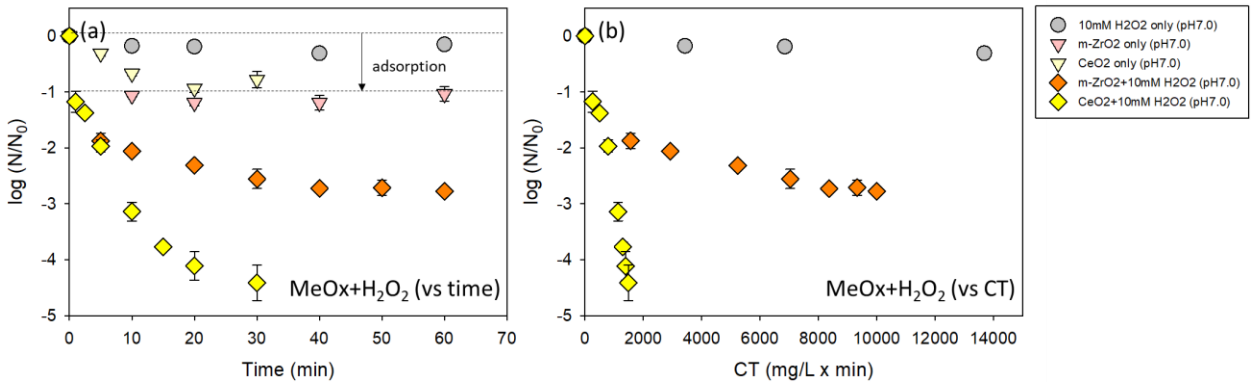

Figure 5.4. Treatment of MS2 phages from MeOx/H_2O_2. Data were plotted as log inactivation versus (a) reaction time or (b) cumulative CT valve. Error bars represent one standard deviation about the mean of triplicate measurements for MeOx+H_2O_2, and of duplicate measurements for H_2O_2-only and MeOx-only experiments.

Adsorption of MS2 on m-ZrO_2 and CeO_2 both reached equilibrium at 10 min of reaction. Inactivation rate constants *k* from disinfection by MeOx/H_2O_2 treatment were calculated based on data points after adsorption reaches equilibrium using eq 5.2 since MS2 does not show a lag phage during disinfection (Table 5.1).

5.4 Summary and Potential Practical Implications

- Results demonstrated that MeOx/H_2O_2 systems with m-ZrO_2 and CeO_2 were capable of effectively removing viruses most likely by $^1O_2$ by 4.5-log and 3-log of losses in total. One the other hand, they caused little inactivation for tenacious microorganisms like spores. The MeOx/FAC systems with CeO_2 and TiO_2 was found slightly facilitate disinfection of spores in addition to direct chlorination.
- Four tested MeOx (a-ZrO_2, m-ZrO_2, CeO_2 and TiO_2) in this study do not adsorb spores while can adsorb MS2 viruses from minor to large extend – a-ZrO_2 in particular likely due to its surface characteristics and high specific surface area.
- Despite the fact that a-ZrO_2 yielded less reactive species than other MeOx, its can be utilized in (waste)water treatment and laboratory use as a great adsorbent to remove water-borne pathogens like viruses and potentially some other microorganisms. CeO_2 was found to be the one most effective in treating MS2 via both chemical oxidation (primary) and adsorption (secondary). However, CeO_2 may result in higher potential of DBP formation if used in water treatment as it can produce more reactive/radical oxidants in the presence of H_2O_2 and FAC. m-ZrO_2 was found to function in between a-ZrO_2 and CeO_2.
- Further studies should be focused on more systematic investigation for microorganism adsorption on these MeOx minerals. Other common water pathogens (i.e., *E. coli*) are also worthwhile to be included for assessing the MeOx/H_2O_2 and MeOx/FAC treatment. In addition, the study can later be extended to modeling of microorganism inactivation, so one can use it to predict microorganism inactivation under various treatment conditions.

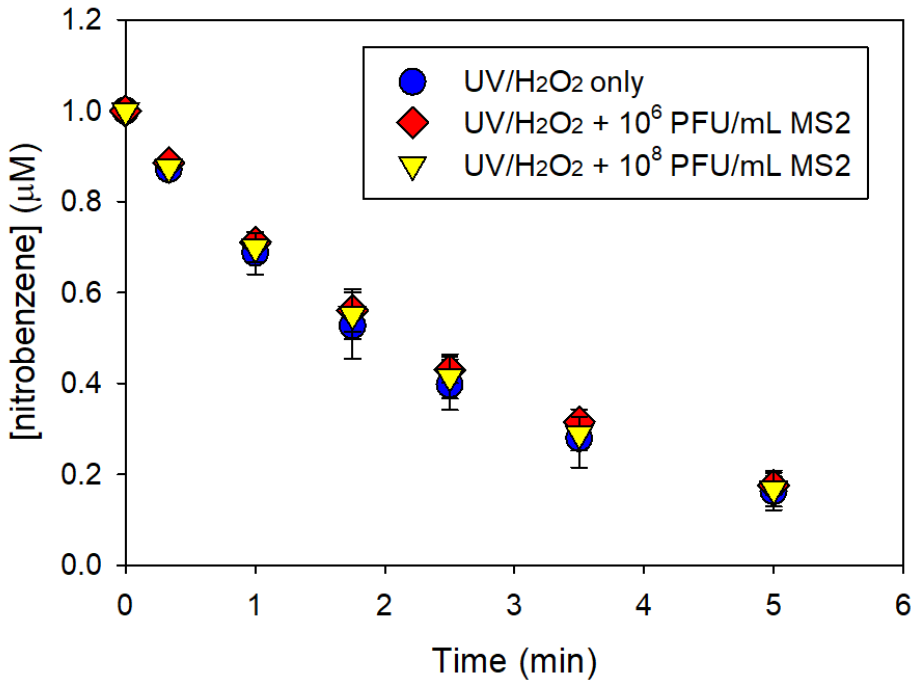

Figure S5.1. UV/H_2O_2 treatment of purified MS2 solutions using nitrobenzene as $HO^{\bullet}$ probe. Experiments were conducted by irradiation of $[H_2O_2]_0$ =1 mM with $[NB]_0$ = 1 μM, and [MS2] = 10^6 or 10^8 PFU/mL using a low pressure Hg lamp. Error bars represent one standard deviation about the mean of duplicate measurements.

References for Chapter 5

APHA/AWWA/WEF, 2005. APHA Standard Methods for the Examination of Water and Wastewater, Washington.

Barrette, W.C., Jr., Hannum, D.M., Wheeler, W.D. and Hurst, J.K., 1989. General mechanism for the bacterial toxicity of hypochlorous acid: abolition of ATP production. *Biochemistry* 28(23), 9172-9178. 10.1021/bi00449a032

Beck, N., Callahan, K., Nappier, S., Kim, H., Sobsey, M. and Meschke, J., 2009. Development of a spot-titer culture assay for quantifying bacteria and viral indicators. *Journal of Rapid Methods & Automation in Microbiology* 17(4), 455-464.

Blanch, E.W., Hecht, L., Syme, C.D., Volpetti, V., Lomonossoff, G.P., Nielsen, K. and Barron, L.D., 2002. Molecular structures of viruses from Raman optical activity. *Journal of general virology* 83(10), 2593-2600.

Bosch, A., 1998. Human enteric viruses in the water environment: a minireview. *Int Microbiol* 1(3), 191-196.

Casteel, M.J., Schmidt, C.E. and Sobsey, M.D., 2008. Chlorine disinfection of produce to inactivate hepatitis A virus and coliphage MS2. *International Journal of Food Microbiology* 125(3), 267-273. https://doi.org/10.1016/j.ijfoodmicro.2008.04.015

Cho, M., Chung, H., Choi, W. and Yoon, J., 2005. Different inactivation behaviors of MS-2 phage and Escherichia coli in TiO2 photocatalytic disinfection. *Applied and environmental microbiology* 71(1), 270-275.

Dawson, D., Paish, A., Staffell, L., Seymour, I. and Appleton, H., 2005. Survival of viruses on fresh produce, using MS2 as a surrogate for norovirus. *Journal of applied microbiology* 98(1), 203-209.

Facile, N., Barbeau, B., Prevost, M. and Koudjonou, B., 2000. Evaluating bacterial aerobic spores as a surrogate for Giardia and Cryptosporidium inactivation by ozone. *Water Research* 34(12), 3238-3246.

Forsyth, J.E., Zhou, P., Mao, Q., Asato, S.S., Meschke, J.S. and Dodd, M.C., 2013. Enhanced inactivation of Bacillus subtilis spores during solar photolysis of free available chlorine. *Environmental science & technology* 47(22), 12976-12984.

Furman, C.S. and Margerum, D.W., 1998. Mechanism of Chlorine Dioxide and Chlorate Ion Formation from the Reaction of Hypobromous Acid and Chlorite Ion. *Inorganic Chemistry* 37(17), 4321-4327. 10.1021/ic980262q

Golmohammadi, R., Valegård, K., Fridborg, K. and Liljas, L., 1993. The refined structure of bacteriophage MS2 at 2· 8 Å resolution. *Journal of molecular biology* 234(3), 620-639.

Grabow, W., 2001. Bacteriophages: update on application as models for viruses in water. *Water Sa* 27(2), 251-268.

Herath, G., Yamamoto, K. and Urase, T., 1999. Removal of viruses by microfiltration membranes at different solution environments. *Water Science and Technology* 40(4-5), 331-338.

Hu, J., Ong, S., Song, L., Feng, Y., Liu, W., Tan, T., Lee, L. and Ng, W., 2003. Removal of MS2 bacteriophage using membrane technologies. *Water Science and Technology* 47(12), 163-168.

Jacangelo, J.G., Adham, S.S. and Laîné, J.M., 1995. Mechanism of Cryptosporidium, Giardia, and MS2 virus removal by MF and UF. *Journal-American Water Works Association* 87(9), 107-121.

Keswick, B., Satterwhite, T.K., Johnson, P.C., DuPont, H.L., Secor, S.L., Bitsura, J.A., Gary, G.W. and Hoff, J.C., 1985. Inactivation of Norwalk virus in drinking water by chlorine. *Applied and Environmental Microbiology* 50(2), 261-264.

Kohn, T., Grandbois, M., McNeill, K. and Nelson, K.L., 2007. Association with Natural Organic Matter Enhances the Sunlight-Mediated Inactivation of MS2 Coliphage by Singlet Oxygen. *Environmental Science & Technology* 41(13), 4626-4632. 10.1021/es070295h

Kohn, T. and Nelson, K.L., 2007. Sunlight-mediated inactivation of MS2 coliphage via exogenous singlet oxygen produced by sensitizers in natural waters. *Environmental science & technology* 41(1), 192-197.

Lim, M.Y., Kim, J.-M. and Ko, G., 2010. Disinfection kinetics of murine norovirus using chlorine and chlorine dioxide. *Water Research* 44(10), 3243-3251. https://doi.org/10.1016/j.watres.2010.03.003

McDonnell, G. and Russell, A.D., 1999. Antiseptics and disinfectants: activity, action, and resistance. *Clin Microbiol Rev* 12(1), 147-179. 10.1128/cmr.12.1.147

Microbiology, A.S.G.o.H.R.W., 1991. Bacteriophages as model viruses in water quality controlag. *Water Research* 25(5), 529-545. https://doi.org/10.1016/0043-1354(91)90126-B

Morgan, M.S., Van Trieste, P.F., Garlick, S.M., Mahon, M.J. and Smith, A.L., 1988. Ultraviolet molar absorptivities of aqueous hydrogen peroxide and hydroperoxyl ion. *Analytica Chimica Acta* 215, 325-329. https://doi.org/10.1016/S0003-2670(00)85294-0

Panec, M. and Katz, D.S., 2006. Plaque assay protocol. *ASM MicrobeLibrary. Disponible at< Disponible at http://www.microbelibrary.org/component/resource/laboratory-test/3073-plaque-assay-protocols> Access on Jan* 15, 2017.

Pecson, B.M., Martin, L.V. and Kohn, T., 2009. Quantitative PCR for determining the infectivity of bacteriophage MS2 upon inactivation by heat, UV-B radiation, and singlet oxygen: advantages and limitations of an enzymatic treatment to reduce false-positive results. *Applied and environmental microbiology* 75(17), 5544-5554.

Shin, G.-A. and Sobsey, M.D., 2008. Inactivation of norovirus by chlorine disinfection of water. *Water Research* 42(17), 4562-4568. https://doi.org/10.1016/j.watres.2008.08.001

Sjogren, J.C. and Sierka, R.A., 1994. Inactivation of phage MS2 by iron-aided titanium dioxide photocatalysis. *Applied and Environmental Microbiology* 60(1), 344-347.

Sobsey, M.D., Hall, R.M. and Hazard, R.L., 1995. Comparative reductions of hepatitis A virus, enteroviruses and coliphage MS2 in miniature soil columns. *Water Science and Technology* 31(5-6), 203-209.

Sommer, R. and Cabaj, A., 1993. Evaluation of the efficiency of a UV plant for drinking water disinfection. *Water Science and Technology* 27(3-4), 357-362.

Thurston-Enriquez, J.A., Haas, C.N., Jacangelo, J., Riley, K. and Gerba, C.P., 2003. Inactivation of feline calicivirus and adenovirus type 40 by UV radiation. *Applied and Environmental Microbiology* 69(1), 577-582.

Chapter 6. GENERAL CONCLUSIONS

This dissertation conducted comprehensive investigation on utilizing some unconventional agents/catalysts to active H_2O_2 and FAC for generating reactive/radical species. Three novel processes, $O_2^{\bullet-}$/FAC, MeOx/H_2O_2 and MeOx/FAC, were studied in various aspects in their reaction kinetics, mechanisms, and efficiencies during water treatment of organic contaminant removal and/or microbial disinfection via chemical oxidation and/or surface adsorption. The major objectives included:

(i) to establish multiple fast and easy-to-operate approaches in producing $O_2^{\bullet-}$ stock via photochemical and non-photochamical methods

(ii) to systematically identify reactive/radical species being generated in the $O_2^{\bullet-}$/FAC process and to quantify their exposure under various reaction conditions, such as varying reaction pH, absolute dose of [$O_2^{\bullet-}$] and [FAC], [$O_2^{\bullet-}$]/[FAC] ratio, effect of water constituents, and different dosing appproaches (*pre-add dosing* and *post-add dosing*)

(iii) to evaluate the potential of applying the $O_2^{\bullet-}$/FAC process as a novel AOP, including disinfection byproduct measurements, cost evaluation, possible designs for practical implementation in water treatment

(iv) to systematically identify aqueous and/or surface-bounded reactive/radical species being generated in the MeOx/H_2O_2 and MeOx/FAC systems using multiple selected non-ferrous and non-cuprous minerals

(v) to assess the efficiencies of selected MeOx minerals on H_2O_2 and FAC decomposition as well as organic contaminant removal via catalytic reactions, redox reactions, or surface adsorption. Also, to evaluate their potentials in industrial and laboratory applications.

(vi) to investigate the efficacies of the MeOx/H_2O_2 and MeOx/FAC systems toward microorganisms inactivation under typical environmental conditions

$O_2^{\bullet-}$/FAC process:

Several photochemical and non-photochemical approaches were successfully established to generate sub-mM to mM-level of $O_2^{\bullet-}$ stock solutions with moderate stability under alkaline conditions, including KO_2 dissolution, UV irradiation of alkaline H_2O_2 at 254 nm or 222 nm, and ozone treatment of alkaline H_2O_2. These stocks were utilized to investigate the $O_2^{\bullet-}$/FAC process under various reaction conditions. Organic probe compound experiments have confirmed in situ generation of $HO^{\bullet}$ and RCS (including $ClO^{\bullet}$, $Cl^{\bullet}$, and/or $Cl_2^{\bullet-}$) during $O_2^{\bullet-}$/FAC reactions with radical exposures comparable to many currently applied AOPs in (waste)water treatment, such as UV/H_2O_2, O_3/H_2O_2, and UV/FAC. $O_2^{\bullet-}$/FAC treatment can be applied effectively in natural waters and SRNOM-amended artificial waters containing up to 5 mgC/L of DOC, though efficiency decreases with increasing DOC, due to scavenging of $HO^{\bullet}$ and RCS by DOM. This suggested the potential of applying $O_2^{\bullet-}$/FAC for contaminant removal in drinking water treatment or potable water reuse, which feed waters typically contain less than 5 mgC/L of DOC. Direct formation of halogen-containing DBPs – including chlorite, chlorate, bromate, perchlorate, THMs, and HAAs *during* $O_2^{\bullet-}$/FAC treatment is minimal, though THM and HAA formation was found to be moderately enhanced during *post-chlorination* of $O_2^{\bullet-}$/FAC-treated solutions.

The $O_2^{\bullet-}$/FAC process could potentially be useful in smaller-scale decentralized and point-of-use water treatments by generating $O_2^{\bullet-}$ stocks with small UV lamp array, and then relatively small volumes of $O_2^{\bullet-}$ stock solutions would need to be injected into the main flow of the water treatment facilities. It does not required to irradiate the whole water body for treatment like many of the currently applied UV-based AOPs, and hence it would need a much smaller lamp array, less associated capital costs, and have lower concern regarding UV light

transmission limitation. At current point, UV photolysis of alkaline H_2O_2 solution may be a more feasible way for stable $O_2^{\bullet-}$ stock generation . The stocks can be prepared by the mixture of H_2O_2 with NaOH or $Ca(OH)_2$, followed by UV irradiation. The resulted $O_2^{\bullet-}$ stocks can than be applied in three different scenarios, depending on the needs (*premix dosing* or *postmix dosing*). If the feed water already contains chlorine, then no chlorine or less amount of chlorine would be required for the *postmix dosing* treatment. The treatment can be applied in CSTRs or using static mixers or venturi mixers inside a pipe to ensure effective mixing, and the reaction reagents can be infused to the reactors (for CSTR), or at different locations of a pipeline (for PFR) for single or multiple-dosing application.

The findings reported in this study provide a foundation for further examining potential applications of $O_2^{\bullet-}$/FAC treatment. Additional works are required to fully evaluate opportunities for optimizing various aspects of this process – in particular, with respect to approaches for producing and stabilizing $O_2^{\bullet-}$ stocks, chemical usage and costs, implementation at scale, and predicting and monitoring process performance. Further refinement (if possible) on the kinetic model for $O_2^{\bullet-}$/FAC can also be beneficial in predicting organic contaminant removal during treatment in future works.

MeOx/H_2O_2 and MeOx/FAC processes:

Use of probe compounds and radical scavengers has suggested formation of reactive/radical species during the MeOx/H_2O_2 and MeOx/FAC reactions, including $^1O_2$, $O_2^{\bullet-}$, and potentially $HO^{\bullet}$, $Cl^{\bullet}$, $ClO^{\bullet}$, and $Cl_2^{\bullet-}$ either in aqueous phase or surface-bounded. Experiments using FFA probe and D_2O as reaction matrix indicate $^1O_2$ production in the presence of H_2O_2 with a-ZrO_2, m-ZrO_2 and CeO_2. In the MeOx/FAC systems, however, no clear evidence for $^1O_2$ production was observed. By detecting formaldehyde and acetone formation as reaction products in the presence of alcoholic radical scavengers (MeOH, iPrOH, and *t*-BuOH), minor $HO^{\bullet}$ was found to be generated in MeOx/H_2O_2 and MeOx/FAC systems. Two $O_2^{\bullet-}$ indicators (TNM and NBT) were used to identify aqueous and surface-bounded superoxide. Results indicated that a-ZrO_2+H_2O_2 could yield both aqueous and surface-bounded $O_2^{\bullet-}$, and m-ZrO_2+H_2O_2 primarily formed aqueous $O_2^{\bullet-}$. a-ZrO_2 possess high specific surface area (292 m^2/g) and can serve as a great choice of sorbent in removing organic pollutants and inorganic ions, while without generating many reactive/radical species leading to undesired DBP formation. CeO_2 can also caused rapid H_2O_2 and FAC decomposition (second to a-ZrO_2 among the MeOx tested in this study) accompanied by effective reactive/radical species production, which can be used to selectively degrade organic pollutants. Release of free and nano-scale metals during MeOx/H_2O_2 and MeOx/FAC treatment was found to be limited with no more than ~10 μg/L release throughout most of the conditions being tested.

Microbial inactivation experiments show that MeOx/H_2O_2 with a-ZrO_2, m-ZrO_2 and CeO_2 cause little treatment for *B. subtilis* spores. These minerals was also found can barely adsorb spores. MeOx/FAC with CeO_2 and TiO_2 facilitated spore inactivation compared to the FAC-only control experiment under the same reaction condition. Treatment of 0.1g/mL m-ZrO_2

and CeO_2 with 10mM H_2O_2 caused 3-log and 4.5-log of total MS2 losses primarily via chemical disinfection and with minor adsorption. Their disinfection efficiencies were consistent with their abilities in generating $^1O_2$. Dose of 0.1 g/mL a-ZrO_2, though not able to generate much $^1O_2$, achieved ~3.5-log of MS2 removal simply via adsorption within just 5 min. Despite the fact that a-ZrO_2 yielded less reactive species than other MeOx, its can be utilized in (waste)water treatment and laboratory use as a great adsorbent to remove water-borne pathogens like viruses and potentially some other microorganisms. CeO_2 was found to be the one most effective in treating MS2 via both chemical oxidation (primary) and adsorption (secondary). However, CeO_2 may result in higher change of DBP formation if used in water treatment as it can produce more reactive/radical oxidants in the presence of H_2O_2 and FAC. m-ZrO_2 was found to function in between a-ZrO_2 and CeO_2.

Findings in this study demonstrate the potentials for use of these less-explored MeOx in driving organic contaminant and microbial pathogen removal via degradation and/or adsorption, as well as in applications requiring removal of residual oxidants during or after conventional processes in (waste)water treatment. Activities of the MeOx systems were found sustained in terms of FFA degradation and formaldehyde formation over at least five treatment cycles, suggesting repeatedly use of these minerals or if appropriate recoveries can be performed. Further works can be focused on more systematic investigation for microorganism adsorption on these MeOx minerals. Other common water pathogens (i.e., *E. coli*) are also worthwhile to be included for assessing MeOx/H_2O_2 and MeOx/FAC treatment efficiencies. In addition, the study can later be extended to modeling of microorganism inactivation, so one can use it to predict microorganism inactivation under various reaction conditions.